Fakultät für
Mathematik, Informatik
und Naturwissenschaften

RWTH AACHEN UNIVERSITY

Exploring Cellular and Molecular Consequences of PROTAC-Mediated ASH2L Regulation in Mouse Embryonic Fibroblasts

Von der Fakultät für Mathematik, Informatik und Naturwissenschaften der RWTH Aachen University zur Erlangung des akademischen Grades einer

Doktorin der Naturwissenschaften genehmigte Dissertation

vorgelegt von

Roksaneh Sayadi Boroujeni, M.Sc.

aus

Abadan, Iran

Berichter: Univ.-Prof. Dr. rer. nat. Bernhard Lüscher

Univ.-Prof. Ivan Gesteira Costa Filho, Ph.D.

Tag der mündlichen Prüfung: 2024.11.20

Diese Dissertation ist auf den Internetseiten der Universitätsbibliothek verfügbar.

Parts of this thesis have been published as part of the following scientific articles:

Barsoum M.*, **Sayadi-Boroujeni R.***, Stenzel A. T., Bussmann P., Lüscher-Firzlaff J., Lüscher B. (2023) Sequential deregulation of histone marks, chromatin accessibility and gene expression in response to PROTAC-induced degradation of ASH2L. Scientific Reports 13(1), 22565.

Bochyńska, A.*, Stenzel, A. T.*, **Sayadi-Boroujeni, R.***, Kuo, C.-C., Barsoum, M., Liang, W., Bussmann, P., Costa, I. G., Lüscher-Firzlaff, J., & Lüscher, B. (2022). Induction of senescence upon loss of the Ash2l core subunit of H3K4 methyltransferase complexes. *Nucleic Acids Research*, 50(14), 7889-7905.

Barsoum M.*, Stenzel A.T.*, Bochynska A.*, Kuo C.-C.*, **Sayadi-Boroujeni R.**, Bussmann P., Lüscher-Firzlaff J., Costa I. G., Lüscher B. (2022). Loss of the Ash2l subunit of H3K4 methyltransferase complexes promotes chromtin compaction at promoters, *Scientific Reports* 12(1), 21506.

*Authors contributed equally as a first author

Work performed by others as well as contributions of collaborators as far as presented in this thesis is highlighted throughout the thesis and indicated at the appropriate locations.

Additional articles to which I contributed as a co-author are listed in the chapter 6.7.

Abstract

In this study, we utilized a PROTAC system (specifically dTAG) to achieve the rapid degradation of ASH2L, overcoming the limitations posed by its long half-life, which typically results in a slow decrease of the protein upon knockout. This approach harnesses the proteasome machinery of the cells to degrade the protein of interest through the ubiquitination of the ASH2L fusion protein. This process was facilitated by a heterobifunctional compound (called dTAG-13) binding to the E3 ligase substrate receptor, CRBN, and a degradable domain ($FKBP^{F36V}$) fused to ASH2L protein. This allowed us to observe the immediate and direct consequences of ASH2L loss in immortalized mouse embryonic fibroblasts (iMEFs).

Rapid degradation of ASH2L led to a significant inhibition of cell proliferation by day two of dTAG-13 treatment, with cells exhibiting compromised DNA synthesis and a tendency to accumulate in the G1 phase of the cell cycle one day post treatment. Restoration of the ASH2L-FKBP fusion protein reversed these effects, highlighting the essential role of ASH2L in cell cycle progression.

Following ASH2L degradation and ChIP-seq analysis, we observed a sequential depletion of H3K4me3, a histone mark associated with active promoters and deposited by the ASH2L-containing complex, KMT2. The half-life of H3K4me3 varied between different promoters, indicating differential sensitivity to ASH2L loss. Concurrently, there was an increase in H3K4me1 at promoters and a decrease at enhancers and intergenic regions, suggesting an accumulation of intermediate H3K4me3 demethylation products at promoters and redistribution of monomethylated marks at the rest of the genome, respectively. However, histone marks H3K27ac and H3K27me3, which are closely linked to H3K4 methylation, were affected with a considerable delay, indicating a downstream effect of ASH2L degradation.

Interestingly, nascent RNA transcription was not immediately affected by the loss of H3K4me3. However, further transcription analysis with more depth of sequencing will be needed to confirm the extent of the effect of immediate loss of ASH2L. Overall, these findings imply that the transcriptional machinery is buffered against rapid changes in histone methylation, maintaining transcriptional stability in the short term. However, overall RNA expression was deregulated at later stages post-ASH2L loss, demonstrating the eventual impact on gene expression.

Our findings highlight the ordered but relatively slow downstream effects of ASH2L loss, suggesting that the systems controlling gene transcription and chromatin dynamics are well-buffered. The rapid degradation of ASH2L initiates a cascade of events starting with H3K4me3 depletion, followed by H3K4me1 redistribution and H3K27ac reduction, delayed H3K27me3 accumulation, leading to changes in chromatin structure and transcriptional deregulation.

In conclusion, this study provides new insights into the role of ASH2L and the COMPASS/KMT2 complex in regulating histone modifications and gene expression. The PROTAC system proved to be a powerful tool for dissecting the immediate effects of protein loss, revealing the intricate and buffered nature of epigenetic regulation.

Zusammenfassung

In dieser Studie haben wir ein PROTAC-System (insbesondere dTAG) eingesetzt, um einen schnellen Abbau von ASH2L zu erreichen und so die Einschränkungen zu überwinden, die sich aus seiner langen Halbwertszeit ergeben, die normalerweise zu einem langsamen Rückgang des Proteins nach dem Knockout führt. Bei diesem Ansatz wird die Proteasom-Maschinerie der Zellen genutzt, um das betreffende Protein durch Ubiquitinierung des ASH2L-Fusionsproteins abzubauen. Dieser Prozess wurde durch eine heterobifunktionelle Verbindung (dTAG-13) erleichtert, die an den E3-Ligase-Substratrezeptor CRBN und eine mit dem ASH2L-Protein fusionierte abbaubare Domäne ($FKBP^{F36V}$) bindet. Dies ermöglichte es uns, die unmittelbaren und direkten Folgen des ASH2L-Verlusts in immortalisierten embryonalen Maus-Fibroblasten (iMEFs) zu beobachten.

Der rasche Abbau von ASH2L führte am zweiten Tag der dTAG-13-Behandlung zu einer erheblichen Hemmung der Zellproliferation, wobei die Zellen eine beeinträchtigte DNA-Synthese und eine Tendenz zur Akkumulation in der G1-Phase des Zellzyklus aufwiesen. Die Wiederherstellung des ASH2L-FKBP-Fusionsproteins kehrte diese Effekte um, was die wesentliche Rolle von ASH2L bei der Zellzyklusprogression unterstreicht.

Nach dem Abbau von ASH2L und der ChIP-seq-Analyse beobachteten wir eine sequenzielle Abnahme von H3K4me3, einer Histonmarkierung, die mit aktiven Promotoren assoziiert ist und durch den ASH2L-enthaltenden Komplex KMT2 abgelagert wird. Die Halbwertszeit von H3K4me3 variierte zwischen verschiedenen Promotoren, was auf eine unterschiedliche Empfindlichkeit gegenüber dem Verlust von ASH2L hinweist. Gleichzeitig gab es einen Anstieg von H3K4me1 an Promotoren und einen Rückgang an Enhancern und intergenen Regionen, was auf eine Anhäufung von H3K4me3-Demethylierungszwischenprodukten an Promotoren bzw. eine Umverteilung von monomethylierten Markierungen im restlichen Genom hindeutet. Die Histonmarkierungen H3K27ac und H3K27me3, die eng mit der H3K4-Methylierung verknüpft sind, waren jedoch mit erheblicher Verzögerung betroffen, was auf einen nachgeschalteten Effekt des ASH2L-Abbaus hinweist.

Interessanterweise war die Transkription der naszierenden RNA durch den Verlust von H3K4me3 nicht unmittelbar betroffen. Es sind jedoch weitere Transkriptionsanalysen mit einer tieferen Sequenzierung erforderlich, um das Ausmaß der Auswirkungen des unmittelbaren Verlusts von ASH2L zu bestätigen. Insgesamt deuten diese Ergebnisse darauf hin, dass die Transkriptionsmaschinerie gegen schnelle Veränderungen der Histonmethylierung gepuffert ist und die Transkriptionsstabilität kurzfristig aufrechterhält. Die gesamte RNA-Expression war jedoch in späteren Stadien nach dem Verlust von ASH2L dereguliert, was die letztendlichen Auswirkungen auf die Genexpression zeigt.

Unsere Ergebnisse heben die geordneten, aber relativ langsamen nachgelagerten Effekte des ASH2L-Verlusts hervor, was darauf hindeutet, dass die Systeme, die die Gen-Transkription und die Chromatindynamik steuern, gut gepuffert sind. Der rasche Abbau von ASH2L löst eine Kaskade von Ereignissen aus, beginnend mit dem Abbau von H3K4me3, gefolgt von der Umverteilung von H3K4me1 und der Reduktion von H3K27ac, einer verzögerten Akkumulation von H3K27me3, was letztlich zu Veränderungen in der Chromatinstruktur und zur Deregulierung der Transkription führt.

Zusammenfassend lässt sich sagen, dass diese Studie neue Erkenntnisse über die Rolle von ASH2L und dem COMPASS/KMT2-Komplex bei der Regulierung von Histonmodifikationen und der Genexpression liefert. Das PROTAC-System erwies sich als leistungsfähiges Instrument zur Untersuchung der unmittelbaren Auswirkungen des Proteinverlusts und enthüllte die komplizierte und gepufferte Natur der epigenetischen Regulierung.

Table of contents

1 Introduction

Nucleosomes are composed of 147 bp DNA sequence wrapped around a histone protein hetero-octamer. The octamer consists of two of each of the four histone protein subunits: H2A, H2B, H3, and H4. These structures have been identified as the primary entities responsible for condensing ~2-meter human DNA into a chromatin structure (Kornberg, 1974; Olins & Olins, 1974). This condensation process facilitates the efficient accommodation of DNA within the nucleus. However, it can potentially hinder DNA accessibility and suppress transcriptional activity (Lorch et al., 1987). As a result, epigenetic factors have evolved to regulate DNA accessibility and transcriptional processes without altering the underlying DNA sequence (Biel et al., 2005; Wolffe, 1994).

Various epigenetic mechanisms, including DNA methylation, nucleosome remodeling, non-coding RNAs, and post-translational modifications (PTMs) of histones, play a crucial role in different transcription factors and polymerases activity. The present dissertation aims to shed light on the dynamic regulation of histone post-translational modifications and their association with cell proliferation and gene regulation (Barsoum et al., 2022, 2023; Bochyńska et al., 2022).

1.1 Cellular Function and Gene Regulation by Histone Modifications

Epigenetics is a rapidly advancing field dedicated to the investigation of alterations to the chemical modifications of the genomic content of cells, all the while leaving the genetic code sequence intact. These changes often exhibit reversibility and can lead to changing modifications in various organismal systems, including development, memory, aging, and behavioral functions (Creighton et al., 2020; Isles, 2018; Maity et al., 2021; Osborne, 2017). Moreover, at a smaller scale, epigenetic control governs DNA-templated-associated molecular and cellular homeostasis during different developmental and growth stages, ultimately resulting in distinct organismal phenotypes without any alteration to the genotype (Biel et al., 2005).

A crucial element in this homeostasis process is the histone structure. The histones are primarily globular, allowing the highly conserved residues on the exposed tails to serve as substrates for various modifying enzymes (Biel et al., 2005). Among the array of epigenetic factors, the PTMs of histones have garnered significant attention. With over 400 different types of PTMs discovered so far (Cavalieri, 2021; Millán-Zambrano et al., 2022; Y. Zhao & Garcia, 2015), they stand as prominent regulators of gene expression. However, it's worth noting that the underlying mechanisms of how these modifications affect gene transcription are still not fully elucidated.

Histone PTMs are governed by an intricate network of signaling pathways involving distinct enzymes with specialized roles, categorized as writers, readers, and erasers (Bochyńska et al., 2018; Hyun et al., 2017; Millán-Zambrano et al., 2022; T. Zhang et al., 2015). Writers are responsible for adding specific PTMs, such as acetylation, methylation, phosphorylation, and ubiquitination, to histone proteins. Reader proteins, possessing specific domains, recognize and selectively bind to distinct histone PTMs. These readers decipher the histone code, facilitating the recruitment of proteins to precise chromatin regions. This process significantly impacts gene expression and related chromatin phenomena. Erasers, comprising enzymes, reverse PTMs introduced by writers, contributing to the dynamic chromatin landscape, and enabling gene expression regulation.

1.1.1 Histone 3 Lysine 4

The epigenetic mark denoted as histone 3 lysine 4 methylation (H3K4me) involves the addition of a methyl functional group to the fourth lysine residue of histone H3 at the ε-amine of the protruded N-terminal tail. The enzymes responsible for depositing lysine methylation at H3K4 are the SET1/MLL-COMPASS (complex proteins associated with Set1) histone methyltransferase complexes. These complexes consist of multiple catalytic subunits including MLL (Mixed-lineage leukemia) 1-4, SET1A, and B that work together with core subunits, namely WDR5, RBBP5, ASH2L, and a homodimer of DPY30. These components have been demonstrated to exhibit a high degree of evolutionary conservation from yeast to humans. The orthologs in yeast consist of: Cps30, Cps50, Cps60, and Cps25, respectively (Shilatifard, 2012; Takahashi et al., 2011). This methylation event can occur in mono-, di-, and tri-methylated states, each potentially exerting distinct functional effects contingent upon the genomic location (Dorighi et al., 2017), and the local level of modification expression (Pokholok et al., 2005; Schneider et al., 2004). Indeed, diverse methylated states of H3K4 have been demonstrated to be associated with gene transcription activity (Cheng et al., 2014; Hughes et al., 2020; Shilatifard, 2012; H. Wang et al., 2023).

1.1.1.1 Tri-methylation

H3K4me3 has been shown to be situated at active gene promoters, thus correlating with primed promoter and mostly active transcription in eukaryotes (Hu et al., 2023; Serra-Cardona et al., 2022; Shimoda et al., 2019; Sims et al., 2007). The deposition of this modification is primarily facilitated by the (lysine methyltransferase 2) KMT2 family (Figure 1). This enzymatic group comprises one catalytic subunit, four core components, and several additional factors that are believed to augment methyltransferase activity (Dou et al., 2006; P. Ernst & Vakoc, 2012; Patel et al., 2009). The complex components were reported to regulate transcription (Park et al., 2020), influence cell survival (W. L. Cai et al., 2022; Lüscher-Firzlaff et al., 2019; Z. Yang et al., 2014), impact pathogenesis (Batbayar et al., 2023; Shilatifard, 2012), modulate metabolism (Ali et al., 2014; Simboeck et al., 2013), and contribute to the stabilization/localization attributes of the KMT2 enzymes (Ma et al., 2022; L. Zhao et al., 2022). However, these findings are not surprising considering that active promoters possess H3K4me3, and thus its alterations will affect all cellular processes. It has been demonstrated that modification pattern breadth and intensity correlate with the state of the gene transcription (Beacon et al., 2021; Benayoun et al., 2014; K. Chen et al., 2015). The resulting H3K4me3 mark has been suggested to influence RNA polymerase II (RNA Pol II) activity, primarily during the pausing and elongation phase (Benayoun et al., 2014; Dorighi et al., 2017; Hoshii et al., 2022; Hu et al., 2023; H. Wang et al., 2023), rather than initiation (Ding et al., 2012). Moreover, it has been postulated that the WDR82 subunit of the Set1A complex (J.-H. Lee & Skalnik, 2008) exhibits the capacity to engage with the Ser5-phosphorylated (pS5) C-terminal domain (CTD) of RNA Pol II, but also playing a crucial role in facilitating the dephosphorylation of pS5 in association with a phosphatase (Landsverk et al., 2020, 2021). This intricate interaction is proposed to recruit the Set1A complex to transcription start sites (TSS) of actively transcribed genes (J.-H. Lee & Skalnik, 2008). Additionally, the collaborative action of WDR82, in conjunction with the PNUTS/PP1 complex (Landsverk et al., 2020), and ZC3H4 (Hughes et al., 2023) is posited to be involved in promoting transcription termination.

There are several protein domains (including PHD, chromo, and Tudor) considered to be potentially readers of the H3K4me3 mark (Vermeulen & Timmers, 2010). Amongst the proteins harboring these

domains, some are suggested to possess the ability to interpret the aforementioned histone mark and are known to be involved in transcriptional regulation. For example, TAF3 (TATA-Box binding protein associated factor 3), a subunit of the TFIID complex, recognizes the H3K4me3 mark through its PHD domain (Plant homoedomain) and subsequently recruits the TFIID complex to P53-regulated active genes (Lauberth et al., 2013; Vermeulen et al., 2007). A finding, however, that has not been reproduced (Hu et al., 2023). This complex is known to be responsible for recognizing core promoters and facilitating the assembly of the preinitiation complex (PIC) for RNA Pol II-mediated eukaryotic transcription (van Ingen et al., 2008). Furthermore, BPTF (Bromodomain PHD finger transcription factor), a constituent of the NURF (Nucleosome-remodeling factor) complex, has shown to exhibit binding preferences for H3K4me3, consequently earning recognition as a reader of this specific histone mark (H. Li et al., 2006; Ruthenburg et al., 2011; Sims et al., 2007; Wysocka et al., 2006). The NURF complex is proposed to be one of several ATP-dependent ISWI-associated protein complexes that remodel chromatin to facilitate the transcription process (Badenhorst et al., 2002). This could potentially contribute and support the association between H3K4me3 and chromatin organization (Barsoum et al., 2022). One of the other suggested reader proteins is PHF2 (PHD finger protein 2), described as a transcriptional activator through demethylating H3K9me2 (Wen et al., 2010), and H4K20me3 modifications (Stender et al., 2012) that are often associated with heterochromatin contents. The ING2 (Inhibitor of growth family member 2) protein family has also been observed to interact with H3K4me3. Their intricate association with HAT (Histone acetyl transferase) and HDAC (Histone deacetylase) enzymes can fine-tune the transcriptional activity either towards activation (Peña et al., 2006) or repression (X. Shi et al., 2006), respectively of promoters marked with H3K4me3. The CpG-binding CXXC zinc finger protein 1 (CFP1), a well-documented PHD-containing protein, represents another H3K4me3 reader element. It specifically binds to the unmethylated CpG regions at promoters, best described for CpG-island promoters (CGI). CFP1, regardless of its transcriptional activity regulates the global distribution of H3K4me3 in embryonic stem (ES) cells (Brown et al., 2017; Clouaire et al., 2012; Long, Blackledge, et al., 2013; van de Lagemaat et al., 2018). Among the readers containing PHD domains, there are also some demethylases, such as PHF8, which is an H3K9me1/2 demethylase (Feng et al., 2010; Fortschegger et al., 2010), and JARID1a, known as a H3K4me3 demethylase (Secombe & Eisenman, 2007). Another group of H3K4me3 readers consists of proteins containing chromo domains, such as the chromatin remodeling protein known as CHD1 (Chromodomain helicase DNA binding protein 1) (Flanagan et al., 2005; Sims et al., 2005, 2007). CHD1 exhibits a preference for binding to GC-rich active promoters, to preserve hyper-transcription and safeguard against double-strand DNA breaks (Bulut-Karslioglu et al., 2021). Additionally, another group of proteins containing Tandem Tudor domains also serves as H3K4me3 readers. For example, Spindlin1, a member of the Spin/Ssty family, functions as a reader of H3K4me3 and contributes to downstream gene transcription regulation (W. Wang et al., 2011; N. Yang et al., 2012; F. Zhao et al., 2020). Furthermore, SGF29 (SAGA complex associated factor 29), a constituent of the SAGA (Spt-Ada-Gcn5 acetyltransferase) complex, is also recognized for its recruitment by the H3K4me3 mark and its role in inducing acetylation, resulting in gene activation (Bian et al., 2011).

The maintenance of homeostasis for this epigenetic mark necessitates a delicate balance achieved through the action of counteracting enzymes responsible for demethylating the trimethylated lysine residue. This group of enzymes is commonly referred to as lysine demethylases (KDMs), also known as "erasers". The JARID1 (jumonji AT-rich interactive domain-1) family of proteins, which includes JARID1A/KDM5A, JARID1B/KDM5B, JARID1C/KDM5C, and JARID1D/KDM5D, (Secombe & Eisenman, 2007; G.-J. Yang et al., 2021) along with the JmjC domain-containing protein NO66 (also known as

MAPJD), have been identified as enzymes responsible for the demethylation of H3K4 (Højfeldt et al., 2013).

1.1.1.2 Di-methylation

Histone 3 lysine 4 di-methylation is an epigenetic mark that has been proposed to be intricately linked with transcriptional regulatory processes. It is deposited by the MLL1/2-COMPASS complexes (Figure 1), frequently observed at cis-regulatory regions of active genes, and is typically distributed in proximity to promoters that are enriched with H3K4me3 marks (Bernstein et al., 2005), more enriched at the 5' end of the transcribed region (Pekowska et al., 2010).

A limited subset of H3K4me3 reader proteins possesses reader domains for interpreting the H3K4me2 modification. Among them are certain subunits of COMPASS complexes, as well as others known to interact with chromatin remodelers and acetylase/deacetylases (Howe et al., 2017). SET3C, a histone deacetylase complex, is a potential reader of H3K4me2 and plays a crucial role in transcriptional memory. It forms a physical association with the enzyme responsible for depositing H3K4me2 (COMPASS) and participates in the maintenance of H3K4me2 inheritance following DNA replication through mitosis (Sump et al., 2022; Woo et al., 2017).

In addition to the demethylases commonly associated with both tri- and di-methylated lysine, LSD1 (Lysine-specific histone demethylase 1A, also referred to as KDM1A) displays a notable preference for demethylating di-methylated histones (Ciccone et al., 2009; Y. Shi et al., 2004).

1.1.1.3 Mono-methylation

H3K4me1 represents a histone modification that distinguishes itself from the di- and tri-methylated lysine 4 marks. It primarily associates with active enhancer regions, where it co-occurs with other histone marks including H3K27ac (Dorighi et al., 2017; Jang et al., 2017; Shlyueva et al., 2014). It is additionally recognized as a hallmark of poised chromatin regions, including promoter elements (Bae & Lesch, 2020). It has also been postulated that the presence of an enriched level of H3K4me1 at promoter positions is associated with gene repression (Cheng et al., 2014). The H3K4me1 mark is a product of methyltransferase activity of MLL3/4-COMPASS complexes (Figure 1A).

Certain interacting partners of H3K4me1 at enhancer regions have been identified in *in vitro* studies (Local et al., 2018). As for example, BAF45C, a constituent of BAF (BRG1/BRM-associated factor) remodeling complexes, has been shown to exhibit a preference for binding to H3K4me1 rather than H3K4me3 (Local et al., 2018). The same has been shown for cBAF preferentially binding to H3K4me1 at enhancer regions (Ahmad et al., 2024; Reddy & Workman, 2018). Another histone tail modification reader, the CW (Cys-Trp rich) domain-containing family, is noted for its selective binding preference for H3K4me1 over the di- and tri-methylated forms (Bril'kov et al., 2022). The CW domain is a zinc binding domain, with a motif length of 50- 60 residues including four conserved cysteine, and two to four conserved tryptophan residues (He et al., 2010). The CW domain family has also been investigated for its involvement in various complexes, including the MORC family of ATPase chromatin remodelers (Andrews et al., 2016; Y. Zhang et al., 2019). The MBT (malignant brain tumor) domain is present in some chromatin reader and organizer proteins. It exhibits its highest binding affinity for H3K4me1 mark, a property shared by the MBT domains found in both L(3)MBTL and CGI-72, allowing them to recognize H3K4me1 effectively over other modified histone (J. Kim et al., 2006). It has also been proposed that H3K4me1 interacts with the CoREST complex, which is a histone-

modifying complex known to engage with various histone-modifying enzymes, including HDACs, which potentially could explain the gene repressory effects of this mark at promoter regions (Perillo et al., 2020).

The mono-methyl group attached to H3K4 can be specifically removed by LSD1/KDM51A. Other members of the Jumonji family of histone demethylases, such as KDM5C/JARID1C, are able to remove mono- and di-methylated states from H3K4 (Dimitrova et al., 2015).

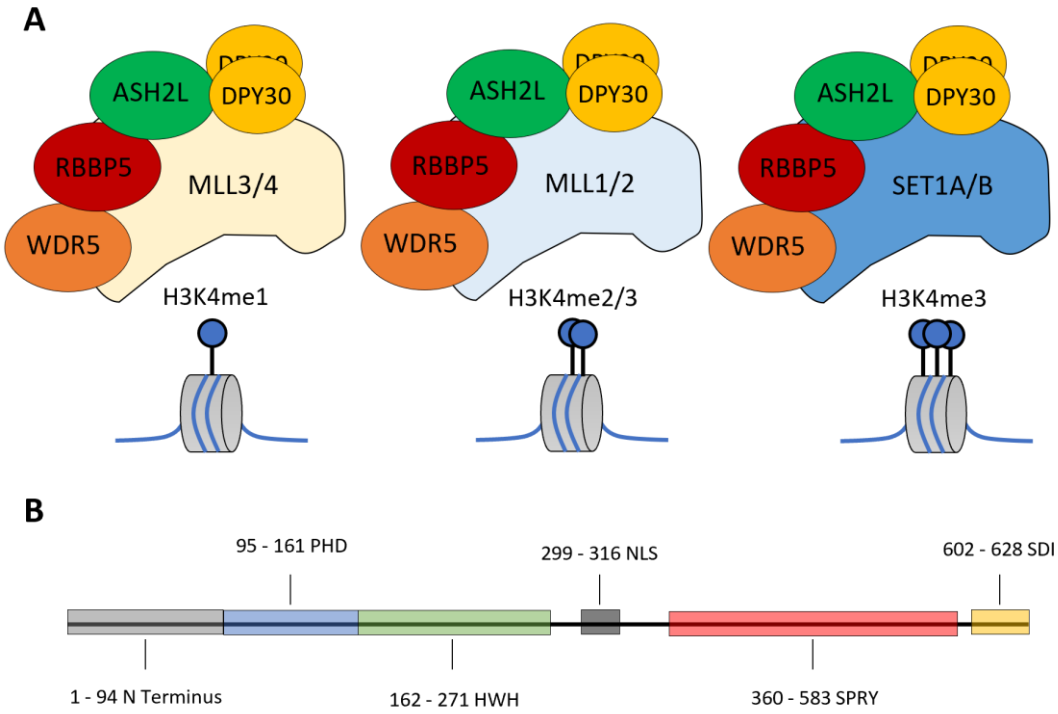

Figure 1: KMT2 Complex and ASH2L Schematic Depiction. (A) Different KMT2 Catalytic Subunits and Corresponding Deposited Histone Modifications. (B) ASH2L isoform 1 domain annotation. Derived from (Y. Chen et al., 2011).

1.1.2 Histone 3 Lysine 27

As discussed earlier, H3K4me3 and H3K4me1 are known to be associated with active promoters and enhancers, respectively. Simultaneously, other forms of H3K27 modifications (such as acetylation and trimethylation) have been shown to contribute to interact/co-occur at the sites of aforementioned histone marks. Studies have indicated the inducing role of H3K27ac at active promoters and enhancers, co-localizing with H3K4me3 and H3K4me1, respectively. Additionally, the suppressing role of H3K27me3 at bivalent or silent promoters, co-localizing with H3K4me3, and in the absence of an enriched level of H3K4me3, respectively. Bivalent promoters are the promoters at which both H3K4me3 and H3K27me3 marks are present. The occurrence of both marks in particular genomic areas, identified as bivalent regions, suggests a state of readiness for gene regulation. This means that genes can either be activated or suppressed depending on cellular signals and environmental stimuli. The interaction between H3K4me3 and H3K27me3 marks enables precise regulation of gene expression, underscoring the fluidity of chromatin regulation via histone modifications. Therefore, this panel of histone modifications has been vastly studied for their interaction with each other through co-occurrence or combined functional mechanisms (Beacon et al., 2021; Igolkina et al., 2019) in the era of gene regulation and chromatin organization.

1.1.2.1 Acetylation

The acetylation of lysine 27 on histone 3 is orchestrated by a diverse array of enzymes belonging to the GNAT (Gcn5-related N acetyltransferases) protein family, collectively known as lysine acetyltransferases (KATs). This group primarily encompasses proteins such as p300/CBP (CREB-binding protein) paralogues. Nevertheless, other complexes, such as GCN5 and PCAF, have also been implicated in facilitating this specific histone modification (Allis et al., 2007). H3K27ac, the resultant modification, has garnered significant attention due to its robust association with active gene transcription. This association is attributed to its pivotal role in mediating the binding of transcription factors (TF) and RNA Pol II (Miao et al., 2022; Weinert et al., 2018). Furthermore, it appears that the mere presence or TF-binding mediation of this mark at the gene promoter is sufficient to activate gene transcription (Hilton et al., 2015; Miao et al., 2022). Moreover, H3K27ac serves a second role as an enhancer mark, frequently co-occurring with H3K4me1 at active enhancer regions (Creyghton et al., 2010). This multifaceted modification plays a role in neutralizing the positive charge of lysine residues and thus reduces the overall positive charge of histone, thereby promoting the dissociation of histones from the negatively charged DNA strands. Consequently, it facilitates primarily opening of chromatin, which facilitates TF and Pol loading at the accessible promoters within the open chromatin regions (Y.-J. C. Chen et al., 2022; Igolkina et al., 2019).

The H3K27ac mark is associated inducers of gene transcription, mediated by interacting proteins or complexes. One such example is the Bromodomain-containing protein 4 (BRD4), which possesses the capability to recognize acetylated lysine residues on H3 and H4 proteins (Chiang, 2009) which is studied to interact with numerous transcription factors (Mann et al., 2021; Y. Zhang et al., 2017). NSD1 (Nuclear receptor-binding SET domain protein 1) is also acknowledged for its interaction with the H3K27ac mark, facilitating the recruitment of various chromatin modifiers to enhancer regions, thereby contributing to the preservation of enhancer transcription integrity (Fang et al., 2021). It has also been demonstrated that the SEC (Super Elongation Complex) interacts with the present H3K27ac mark at the promoter, mediated by the AFF4 transcription factor (Y. Gao et al., 2020). On the other hand, it has been shown that HMGN (High Mobility Group protein) preferentially binds to the H3K27ac region and maintains cell-type-specific chromatin organization, resulting in the stabilization of cell identity gene expression (S. Zhang et al., 2022).

The family of HDACs and the Sirtuin proteins, with more than 18 members are categorized as reader proteins with the ability to remove histone modifications, thus earning them the designation of "erasers" (Seto & Yoshida, 2014). The precise genomic localization of HDACs, much like other chromatin modifiers, relies on their interaction with a specific set of transcription factors or DNA-binding co-factors complexes, rather than being guided by sequence-specific DNA binding domains (X. Li et al., 2014). The HDACs are studied to be engaged in the regulation of fundamental cellular processes, including proliferation, cell cycle control, regeneration, apoptosis, and cellular differentiation (K. Wu et al., 2023). HDAC malfunction has been detected in both cancer cells and tumor tissues, rendering HDACs appealing candidates for exploring innovative approaches to combat cancer (Caslini et al., 2019; G. Li et al., 2020). Almost similar function applies to other species for example in *Drosophila*, NURF-55, a tryptophan-aspartic acid (WD) repeat protein, is linked to histone deacetylases, and is potentially serving as a central hub for assembling protein complexes engaged in chromatin regulation (Martínez-Balbás et al., 1998). Moreover in mammalians, both NURF and Trithorax exhibit strong associations with genes characterized by transcriptional pausing, which also exhibit a more pronounced upregulation in response to HDAC inhibition (Vaid et al., 2020).

Furthermore, HDAC3 is indispensable for recruiting NURF to the promoter region of the IL-1β gene, underscoring its role in the regulation of gene expression and chromatin dynamics (Ziesché et al., 2013). Additionally, the NuRD (Nucleosome remodeling and deacetylase) complex is a multi-protein complex that possesses two enzymatic functions: ATP-dependent chromatin remodeling and histone deacetylation. It initiates gene repression by deacetylating H3 lysine and depositing histone variants (Kraushaar et al., 2018; Reynolds et al., 2012) and can potentially result in facilitating PRC2-mediated H3K27me3 deposition (T. W. Kim et al., 2015).

1.1.2.2 Trimethylation

The polycomb repressor complex 2 (PRC2), known as the evolutionarily conserved polycomb group of proteins (PcG), play a crucial role in catalyzing the trimethylation of lysine 27 on the N-terminal tail of histone 3 (Boyer et al., 2006). This PRC2 complex comprises essential components, including EZH2, EED, SUZ12, RbAp48, along with auxiliary interactors like AEBP2, JARID2, and PCL1 (Y. Shi et al., 2017). The deposition of the H3K27me3 mark, as a result of PRC2 activity, leads to silencing of transcription through induced chromatin compaction (Margueron & Reinberg, 2011). Another potential methyltransferase for H3K27 is G9a, also known as EHMT2, which has been shown to catalyze the methylation of lysine 27 on histone H3 both *in vitro* and *in vivo* (H. Wu et al., 2011). Moreover, deposition of H2AK119ub (Histone H2A lysine 119 mono-ubiquitination) by PRC1 recruits PRC2 complexes, which in turn promotes the resulting-H3K27me3 interaction with PRC1. This interaction creates a feed-forward loop that spreads both repressive marks, H2AK119ub and H3K27me3, which eventually results in propagating the compacted chromatin (Margueron & Reinberg, 2011). H3K27me3 is a suppressive modification, typically linked to silenced enhancers and promoters. When it comes to promoters, it tends to be primarily deposited at regions rich in CG dinucleotides (Morey & Helin, 2010). It has been shown that EZH2 interacts directly with *de novo* DNA methyltransferases (DNMTs), and EZH2 plays a crucial role in preserving DNA methylation, particularly for certain promoter regions (Viré et al., 2006). DNA methylation, mediated by DNMTs, produces 5-methyl-cytosine (5mC) that form the methylated CpG islands, also known as repressing gene transcription parameter. In embryonic cells, PRC2 is attracted to unmethylated CpG islands, avoiding DNMT-mediated methylated regions. It has been studied, that removing DNA methylation allows H3K27me3 to spread, reducing PRC2 density at promoters and potentially activating transcription (King et al., 2016; Meehan & Pennings, 2017; Reddington et al., 2013; Uckelmann & Davidovich, 2021). Despite this, how PRC2 avoids methylated CpG islands remains unclear and often contradictory in literature. In summary, H3K27me3 and CpG methylation appear to be linked in several ways, including mutual antagonism, and correlation between CpG density and H3K27me3 modification.

There have been various reader proteins or complexes discovered for the H3K27me3 mark in various organisms, including both plants and animal cell models. Recent research suggests the existence of a plant-specific complex composed of EBS (Early bolting In short day), its homolog SHL (Short life), and EMF1 (Embryonic flower 1), which acts as a chromatin reader associated with Polycombs (Krause & Turck, 2018) in plants. These proteins are believed to possess the ability to interpret H3K27me3 through a BAH (bromo-adjacent homology) domain (Z. Yang et al., 2018). Furthermore, they contain a PHD domain with an extended C-terminal region that potentially recognizes H3K4me3, making them well-suited for identifying bivalent promoters. The evolutionarily conserved BAH domain is also found in some vertebrate-specific nuclear proteins, including BAHD1 (bromo adjacent homology

domain-containing protein 1). BAHD1 plays a role in gene silencing by facilitating the assembly of a scaffold for the formation of facultative heterochromatin (Bierne et al., 2009; D. Zhao et al., 2016). The PRC2 complex not only deposits the H3K27me3 mark but also serves as a chromatin reader. When it reads the product of PRC1, H2AK119ub, it enhances the propagation of PRC2 marks. However, when interacting with the MLL complex it prevents PRC2 from accessing the MLL-occupied regions (Uckelmann & Davidovich, 2021). EED is commonly recognized as a pivotal member of the PRC2 and serves as a chromatin remodeler. Intriguingly, it plays a dual and somewhat contradictory role in gene regulation, being associated with both gene repression and gene activation (M. Zhang et al., 2023).

1.2 ASH2L (Absent, Small, or Homeotic 2-Like) Trithorax Protein

1.2.1 A Trithorax Protein

Trithorax-group proteins (TrxG) are a group of proteins that play a role in gene expression activation or maintaining active gene expression (Kassis et al., 2017; Kingston & Tamkun, 2014). Based on their mechanism of action, they can be divided into three main functional groups. TrxG proteins can be involved in histone modifying complexes, such as ASH2L in KMT2/COMPASS complexes. They can also be members of chromatin remodelers, for example, CHD or SWI/SNF factors (Dorighi & Tamkun, 2013). Sometimes, they are also known to act as DNA-binding TrxG proteins as transcriptional activators by interacting with TrxG response elements (TREs) of DNA, or participating in the transcription machinery (Schuettengruber et al., 2007).

ASH2L is recognized as a crucial core member of the KMT2 enzymatic complex. The presence of ASH2L is essential for the histone methyltransferase (HMT) activity of the complex (Cao et al., 2010; Steward et al., 2006). Besides ASH2L, several other catalytic, core, and auxiliary proteins collaborate to constitute the functional form of the KMT2 complex. The catalytic components include MLL 1-4, SETD1A, and SETD1B, also known as KMT2 A, B, C, D, F, and G, respectively (Bögershausen et al., 2013). The core members are known to include WDR5, RBBP5, and a homodimer of DPY30, while a variable number of auxiliary members for this complex have been identified (Poreba et al., 2022).

ASH2L[1] is a nuclear protein that is ubiquitously expressed in different tissues. Different isoforms have been identified for this protein: isoform 1 with a length of 628 amino acid, and isoform 2, lacking amino acids 1-94 and 541-573 (Stoller et al., 2010; J. Wang et al., 2001). Additionally, a third isoform has also been suggested, with the missing amino acids in 1-94 position introduced in the protein databases such as UniProt. Isoform 1 seems to be the predominant protein found in different tissues and cell lines. The protein has been identified to consist of several functional domains in the following order from the N-terminus to the C-terminus: PHD (Plant Homeodomain), WH (Winged Helix domain), SPRY (SPla and the RYanodine Receptor), and SDI (Sdc1 DPY30 Interaction) domains, along with two intrinsically disordered regions (IDR), one at the N-terminal and one between the WH and SPRY domains (Figure 1B) (Y. Chen et al., 2011, 2012). That said, ASH2L interacts with other KMT2 members through the aforementioned domains, i.e. binding to the MLL-WDR5-RBBP5 complex through its SPRY interaction with the RBBP5 subunit, and then bringing the DPY30 homodimer to the

[1] Please note, wherever a human/general study is indicated, the protein term is in capital letters, otherwise the term is written in lowercase.

SDI C-terminal domain (Xue et al., 2019). It is also considered to regulate the stability and substrate specificity of the MLL complex through the SDI domain (Ma et al., 2022; L. Zhao et al., 2022), and IDRs (Y.-T. Lee et al., 2021).

In addition to the COMPASS components, a few more direct interactors for ASH2L have been proposed. It has been demonstrated that ASH2L, as an interactive cofactor, associates with the Ap2δ transcription factor and recruits HMT complexes to specific gene regions (Tan et al., 2008). Furthermore, it has been suggested that Ash2l may interact with the transactivation domain (TAD) of developmental transcription factor Tbx1, and its homozygous deletion leads to embryonic lethality in mice during gestation (Stoller et al., 2010). Additionally, ASH2L has been recognized as a direct interactor of the MYC oncoprotein, which also interacts with the p300/CBP acetyltransferase. The association of MYC with HMTs depends on the ASH2L interaction, and their interaction may regulate transcription by controlling H3K27 modification (Ullius et al., 2014). Moreover, Ash2l has been proposed to interact with Oct4 TAD domain to form an Oct4/Sox2/Nanog (OSN) complex at super enhancers, which can enhance enhancer activity and regulate the pluripotency network of cells (Tsai et al., 2019). Nevertheless, it is important to note that this is not a comprehensive list of all studied ASH2L interactions.

1.2.2 ASH2L as an Oncoprotein

The MLL1 gene is a proto-oncogene associated with various types of cancer when mutated (Yokoyama et al., 2004) as well as other KMT2 members described in a review study (Rao & Dou, 2015). ASH2L, as a core subunit of the KMT2 complexes and as an interactor of the MYC oncoprotein, is known to possess oncoprotein functions itself. ASH2L is implicated in various cancer diseases and disorders. It induces transformation when it cooperates with the Ha-RAS oncogene (Lüscher-Firzlaff et al., 2008). Additionally, targeting ASH2L expression, reduces the expression of estrogen receptor alpha target genes, leading to reduced proliferation and migration of endometrial cancer cells (Zeng et al., 2020). Recent studies have also shown that ASH2L might drive the expression of inflammatory genes, such as IL-1beta, in regulating the invasion and migration of triple-negative breast cancer cell lines (Batbayar et al., 2023). On the other hand, ASH2L KD in lymphoma and testicular cancer cell lines confers resistance to some genotoxic agents such as bleomycin, etoposide, and cisplatin, while its re-expression makes those cells sensitive again (Constantin & Widmann, 2020). As mentioned before, ASH2L is not only involved in cancers but its elevated level of expression is also involved in other types of disorders, such as diabetic endothelial dysfunction (Zhong, Dong, et al., 2023), fibrosis and inflammation in glucose-induced glomerular mesangial cells (Zhong et al., 2022), and diabetic nephropathy (Zhong, Hong, et al., 2023). However, it's not clear whether its role is through its methyltransferase activity within HMT complexes or beyond these complexes.

On the other hand, ASH2L is studied for its role in regulating the expression of pro-apoptotic target genes of the P53 tumor suppressor by controlling H3K4me3 and the formation of pre-initiation complexes at these promoters. When overexpressed, it induces the expression of these pro-apoptotic genes in response to chemotherapy agents (Mungamuri et al., 2015). Targeting Ash2l expression in neural progenitor cells reveals its role in brain development and cell proliferation by affecting H3K4me3 levels of Wnt-ß-catenin signaling genes and their expression (L. Li et al., 2019). Additionally, the disruption of Ash2l expression in the murine hematopoietic system results in the immediate loss of mature hematopoietic cells and, consequently, the death of the animal. The depletion of the protein leads to the reduction of global H3K4 methylation, disrupted gene

regulation, aberrant cell proliferation and differentiation dysregulation (Lüscher-Firzlaff et al., 2019). It has been demonstrated that Ash2l interacts with the pluripotency transcription factor (OSN) network and promotes the recruitment of this complex to super enhancers to activate them (Tsai et al., 2019). Furthermore, in its role as a transcriptional activator, it has been shown that Ash2l knockout in MEFs (Mouse Embryonic Fibroblasts) results in the global loss of H3K4 trimethylation, both globally and in promoter regions. This is followed by chromatin compaction and gene repression (Barsoum et al., 2022). The loss of the protein and the resulting H3K4me3 reduction induce cell proliferation cessation, leading to a senescence phenotype in the same cell system. This discovery has identified a set of downregulated genes proposed to be shared senescence markers in different induced senescence phenotypes (Bochyńska et al., 2022). Additionally Ash2l KD (Knock down) leads to an increased silent chromatin state enriched with H3K9 trimethylation (Wan et al., 2013).

1.3 PROTACs (PRoteolysis TArgeting Chimera) Technology

1.3.1 Proteasome Machinery

In general, two major cellular machineries exist within cells that mediate protein degradation: the ubiquitin-proteasome system (UPS) and lysosomes (X. J. Wang et al., 2013). Protein degradation through the UPS is initiated by the covalent addition of a 76-amino acid ubiquitin (Ub) protein, catalyzed by E1, E2, and E3 enzymes, to the ε-amino group of the side chain of a lysine residue of the substrate. It is worth to mention that poly-ubiquitination serves various functions in cellular processes (Damgaard, 2021). One of which is the recognition of the resulting polyubiquitin-tagged protein by the 26S proteasome machinery and being targeted for degradation (Ciechanover & Schwartz, 1998; Grice & Nathan, 2016). The transfer of ubiquitin to the target protein can occur in two ways: I) Transferred from E2 to E3 ubiquitin ligase, and then to the substrate protein, or II) directly from the E2 subunit in a complex with E3 ligase to the substrate protein (LeBlanc et al., 2021).

Within cellular systems, most cells contain one or two E1, numerous E2 enzymes, and multiple families of E3 ligases. This diversity enhances the specificity of substrate protein recognition (Hershko & Ciechanover, 1998). E3 ligases, characterized by their domains and ubiquitin transfer mechanisms, can be classified into three distinct families: RING (Really interesting new gene), HECT (Homologous to the E6AP carboxyl terminus), and RBR (RING-betweenRING-RING) (Q. Yang et al., 2021). Among these, the RING family stands out as the most abundant and diverse group of E3 ligases. The RING family encompasses various types of scaffolds, including monomeric RING, homodimer RING, heterodimeric RING, monomeric U-box (which is often considered a separate family, while sharing very similar 3D structure with RINGs), Cullin-RING, and multi-subunit RING scaffolds (Morreale & Walden, 2016). The Cullin-RING ligase (CRL) complex is composed of a Cullin scaffold with a RING-box protein attached to the N-terminus, and a substrate receptor connected to the Cullin scaffold via an adaptor protein at the C-terminus (Figure 2) (Petroski & Deshaies, 2005). To enhance the specificity of these scaffolds, numerous CRLs are expressed within and across different organisms, each recognizing specific groups of substrates.

Ubiquitination of the substrate protein occurs in various cell compartments, including the cytosol, nucleus, and even in specialized organelles like mitochondria (Y. Zhang et al., 2022). These ubiquitinated proteins are subsequently degraded by proteasomes in the cytosol. However, as reviews, several studies have provided evidences for the existence of a nuclear UPS (von Mikecz,

2006). Moreover, the identification of protein complexes that serve as export pathways for ubiquitinated nuclear proteins to transit to the cytosol represents an additional regulatory mechanism for the degradation of nuclear proteins (Hirayama et al., 2018).

1.3.2 Hijacking Cellular UPS in PROTAC Technology

To explore the functions of a specific gene, researchers have developed various genetic engineering methodologies that facilitate the analysis of phenotypes and characteristics resulting from the loss of function of that gene. For instance, these methodologies involve the application of different chemical mutagens, genome editing tools such as CRISPR/Cas, and TALEN for DNA engineering, and also RNAi methods to disrupt mRNA processes (Housden et al., 2017). However, it's important to note that these techniques primarily focus on DNA and mRNA, which may require time to manifest their effects on proteins, particularly those with longer half-lives. Consequently, for a more precise analysis of the functional studies related to the desired gene, targeted protein degradation (TPD) approaches currently hold greater intrigue (Sincere et al., 2023). Therefore, as previously demonstrated, the ASH2L protein, with a half-life exceeding 1 day, was considered a promising candidate for targeted manipulation using protein engineering approaches (Bochyńska, 2023; Bochyńska et al., 2022).

Not too long ago, researchers developed PROTACs (Proteolysis targeting chimera), which exploit the cellular proteasome machinery's functions to target specific proteins for degradation (Sakamoto et al., 2001). PROTACs are heterobifunctional small molecules composed of two binding ligands and a linker. These small molecules have the ability to bind to two different targets, one being E3 ligases, and the other being the protein of interest (POI). This binding brings them into proximity, leading to the ubiquitination and subsequent degradation of the targeted protein (Figure 2). This approach has been subsequently proven to be effective for studying loss of function in cellular and animal model systems (Guo et al., 2019).

Contrary to conventional protein inhibitors, non-covalent PROTACs exhibit a catalytic mechanism of action, allowing them to be recycled after inducing degradation. However, some PROTACs based on inhibitor molecules may employ different binding chemistry and have irreversible effects (Kiely-Collins et al., 2021).

PROTACs offer numerous advantages and are considered highly promising in pharmaceutical studies. They provide benefits such as affecting beyond enzymatic functions, degrading undruggable targets, extending their effective period, and consequently reducing the required dosage. These advantages render the PROTAC platform intriguing for future TPD medicines. To date, several PROTACs have entered clinical trials for various cancer treatments (Békés et al., 2022). While no PROTACs have received approval for clinical use, two of them have paved the way towards establishing trust in PROTAC's ability to meet safety and efficacy requirements for the approval processes (X. Gao et al., 2022; Hamilton et al., 2022).

1.3.3 The dTAG System

PROTACs are designed to target a variety of substrate receptor subunits within E3 ligase complexes. The dTAG-13 compound has been developed based on the binding properties of Cereblon (CRBN) and FK506-binding protein (FKBP) families (Nabet et al., 2018). The substrate receptor ligand moiety of this compound is designed after thalidomide, known as one of the class of immunomodulatory

drugs (IMiDs) (Ito et al., 2010; Marriott et al., 2001). On the other hand, the corresponding PROTAC compound in dTAG system includes a derivative of morpholine-containing ligand, Shield-1 (Shld1), that binds to FKBP12 (Banaszynski et al., 2006). However, in Nabet's study, the composite compound has been engineered to bind to the $FKBP^{F36V}$ mutant rather than the WT (Wild-type) version of this protein to enhance specificity and reduce endogenous protein interference. The mutant $FKBP12^{F36V}$ works as a binding domain that is fused to the N- or C-terminus of the POI. Among the compounds studied in this research, dTAG-13 demonstrated fast and efficient fusion protein degradation, achieving effective results with only a few hundred nanomolar concentrations in less than a couple of hours for *in cellulo* assays (Nabet et al., 2018).

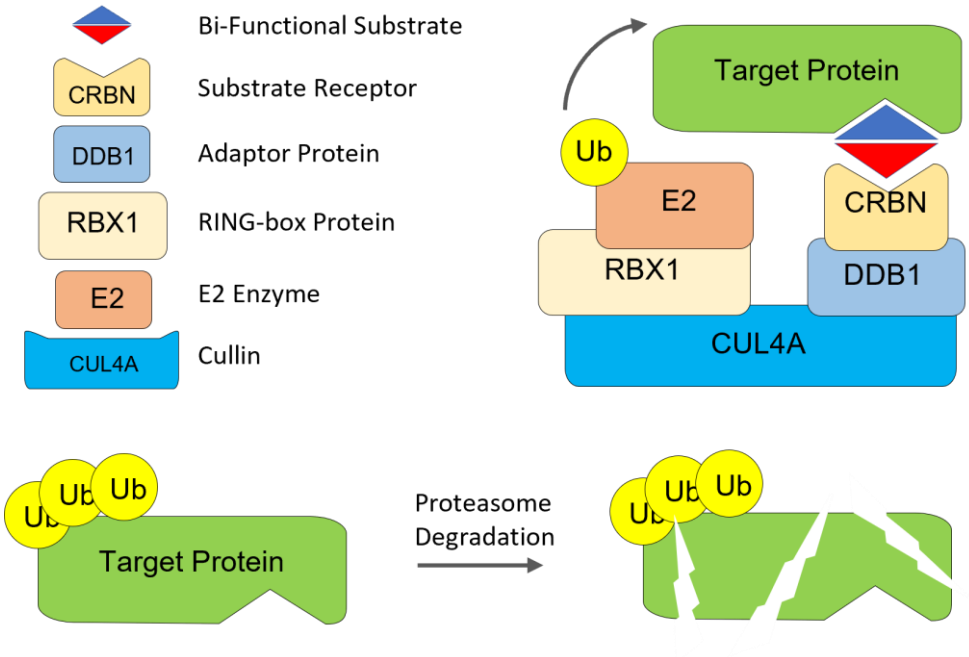

Figure 2: PROTACs- dTAG System Mechanism of Action. PROTACs are heterobifunctional small molecules composed of two binding ligands and a linker. PROTACs (in this dissertation, dTAG-13 compound) bind to two different targets through two functional moieties (Indicated as blue and red triangles). One moiety binds to the CRBN substrate receptor of the E3 ligases, and the other binds to degradable domain of the protein of interest (POI). This interaction brings the POI and E3 Ligase complex into proximity, leading to the ubiquitination and subsequent degradation of the targeted protein via proteasome machinery of the cell.

Up to now, three WRAD components (WDR5, RBBP5, and DPY30) along with SET1A and SET1B subunits have been targeted using PROTACs. One study demonstrates the development of several PROTACs that bind to CRBN and target WDR5 for various purposes, including cancer treatment and molecular biology research. The study revealed a global reduction in both H3K4me2 and genome-wide MLL occupation (D. Li et al., 2022). Additionally, dTAG-13 has also been introduced to the SET1A and SET1B subunits of KMT2 to uncover their connection with transcription termination at CGI-associated genic regions in mESCs (Hughes et al., 2023). The dTAG system has also been employed to target the RBBP5 and DPY30 core subunits of KMT2 complexes in mESCs, revealing their contributions to the deposition and removal of H3K4 methylation with subsequent consequences for transcriptional control (Hu et al., 2023; H. Wang et al., 2023).

Hence, a substantial body of evidence has emerged, establishing that PROTACs represent a promising avenue for epigenetic regulation. They enable the targeting of epigenetic modulators and proteins,

the development of dual-targeted PROTACs, and the achievement of highly specific degradation of histone-modifying enzymes (Webb et al., 2022).

1.3.3.1 Reversible dTAG-13-Induced Degradation

With all that said, the loss of function of POI may, under optimal conditions, produce certain phenotypic changes for tracking and analyzing. However, at times, it may only manifest as a slight perturbation of the system that must be carefully analyzed to distinguish it from artificial effects. To meticulously analyze the effects of the loss of ASH2L, this study has introduced a novel approach to reverse the impact of dTAG-13-induced ASH2L degradation. This allows the results to be confirmed in a reverse genetic manner. For this purpose, the study has utilized an analogue of the thalidomide family, which competes with dTAG-13 for binding to CRBN subunit. It has been demonstrated that lenalidomide and pomalidomide, two family members and analogues of thalidomide, exhibit a higher binding affinity to CRBN subunits than thalidomide itself (Ito & Handa, 2020). For this reason, lenalidomide has been selected for conducting reversal experiments to confirm the observed functions of ASH2L.

1.4 Aim of the Study

The objective of the current study is to elucidate the function of the ASH2L protein a core subunit of KMT2 complexes in immortalized MEF cells. Previous studies have demonstrated the role of *Ash2l* KO-driven H3K4me3 depletion on gene transcription, chromatin organization, and certain transcription-associated histone PTMs (Barsoum et al., 2022; Bochyńska et al., 2022). However, it has not been determined whether the observed consequences were directly impacted by Ash2l loss or more as results of secondary consequences followed by the loss of the protein. The previous studies have used tamoxifen-inducible Cre/ER system to induce the deletion of exon 4 of *Ash2l* genomic sequence in mouse embryo fibroblasts, which results in a slow decrease of Ash2l, taking up to 5 days for an efficient elimination of protein (measured by qualitative Western blotting).

To be able to address direct consequences, a system needed to be established that allows the rapid degradation of Ash2l. To achieve this, this study employed a rapidly responsive dTAG-13-inducible degradation system to target the $FKBP^{F36V}$-ASH2L fusion protein that was introduced into $Ash2l^{fl/fl}$ MEF cell lines. To achieve this, a lentiviral gene delivery system has been utilized with the aim to introduce the $FKBP^{F36V}$-ASH2L fusion construct into the murine cells. The engineered cells were subsequently dependent on the $FKBP^{F36V}$-ASH2L fusion protein for proliferation and further treated with 4-Hydroxytamoxifen (also known as HOT) to activate CRE/ER recombinase and induce endogenous *Ash2l* elimination. Such cells were obtained, and monoclonal lines established. These cells were then characterized for protein expression, histone modifications, gene expression, and cell physiology.

In summary, protein expression and cell characteristics were validated using qPCR and qualitative Western blotting. Subsequently, the cells were analyzed using immunofluorescent staining to confirm the correct cellular localization of the exogenous fusion protein within the nuclear compartment. The monoclonal cell lines were evaluated for the optimal dosage and time dependency of the dTAG-13 treatment, which was achieved and verified using Western blotting. Following the establishment of the experimental cell model system, the cellular properties, and phenotypes of the dTAG-13-induced KD cells in comparison to WT cells were measured. The cell

proliferation, the integrity of the cell cycle phase distribution, and DNA synthesis using flow cytometry analysis were assessed. Most of these experiments were conducted in a time course manner, which allowed this study to document the progression and the order of events at the cellular and molecular levels with higher resolution. These intervals were instrumental in contributing to the observed cellular and molecular phenotypes with each other. To investigate the effect of ASH2L on the WRAD components and the resulting H3K4me3, a time course blotting method was employed. Furthermore, several other transcription-associated histone PTMs, such as H3K4me1, H3K27ac, and H3K27me3, were analyzed to understand the impact of the loss of active KMT2 complexes on the transcription-associated PTM network. For obtaining high-resolution evidence of the deregulation of histone PTMs, a time course chromatin immunoprecipitation method followed by sequencing (ChIP-seq) was applied to gain a genome-wide view of the distribution of the aforementioned histone modifications. This allowed the study to track alterations at the gene-level resolution. Last but not least, a nascent-RNA sequencing method, using Click chemistry (Click-seq), was utilized to document alterations in gene transcription at the early time points following dTAG-13-induced ASH2L loss. In sum, these experiments aimed to unveil the contribution of ASH2L and its resulting HMT product, H3K4me3, to gene transcription and the regulation of other transcription-associated histone modification networks.

2 Material and Methods

The Material and Methods chapter is written according to the standard protocols generated and used in the Institute of Biochemistry and Molecular Biology, University Hospital of RWTH Aachen. In case of making any adjustments to the existing protocols or establishing new ones, the details are given. All experiments and analyses in this thesis were conducted by the author, otherwise, it is indicated.

2.1 Material

2.1.1 Oligonucleotides

Table 1. Oligonucleotides.

Primer Name	Sequence (5'-3')	Purpose
Nested PCR - DNA		
Outer-For	AGGCGCATAACGATACCACGAT	Loss of *Ash2l* Exon4- Genomic DNA
Outer-Rev	CCAATGTGAGGTAGTGCCGA	
Inner-For	CCGGAACCGAAGTTCCTATTCC	
Inner-Rev	ACTGATGGCGAGCTCAGACC	
RTqPCR - RNA		
Ex4.*Ash2l*-For	CCGCTGACACCTTTGGAATA	Loss of *Ash2l* Exon4- RNA
Ex4.*Ash2l*-Rev	TTGCTTCCGGAGAAAGTAGG	
Mm-*Gusb*-1-SG	QT00176715, QIAGEN	Normalizer
ChIPqPCR - DNA		
Atp9a-ChIP-For	GAATTGAGTAGAGCCTCCGAAC	Histone Marks Level Check at TSS
Atp9a-ChIP-Rev	GGTATCAGTGTAGGAAGGAGAGA	
Cdh3-ChIP-For	GTCCTGACCCGGATTGTTCC	Histone Marks Level Check at TSS
Cdh3-ChIP-Rev	CACAGCCCTAAGATTCCCCC	
Mga-ChIP-For	GGAGGGCGTCGCTTCAATAG	Histone Marks Level Check at TSS

Mga-ChIP-Rev	GAAGCTCTCTCTGCGGAACG		
Rab8a-UpTSS-For	CTTAACCCGCGCCACTTTTG	H3K4me3 Level Check at Upstream TSS	
Rab8a-UpTSS-Rev	AGGCGAAGCGCAGGAAGTA		
Rab8a-DownTSS-For	TGCAGACAGGGACATGCAG	H3K4me3 Level Check at Downstream TSS	
Rab8a-DownTSS-Rev	ACACAGAGAGTTGACAGGCG		
Rims2-ChIP-For	AACATTTCCCCGAGCGCA	Histone Marks Level Check at TSS	
Rims2-ChIP-Rev	CAATGGCCTTCAATCCGAGG		
Rspo2-ChIP-For	CGCGTCCACTCTCTTCTTGG	ASH2L Level Check at TSS	
Rspo2-ChIP-Rev	AGGCAGCGAGAAACTTCAGC		
Tbc1d1-ChIP-For	CTGTTGCTCGCCTGTGACTC	Histone Marks Level Check at TSS	
Tbc1d1-ChIP-Rev	CAGGAGTAGATGCCCTCCCT		
Zfp503-ChIP-For	CTCAGCTTGACCCCGAGAGA	Histone Marks Level Check at TSS	
Zfp503-ChIP-Rev	ATTTGCAACCCCTGCCTTCC		
CtrlNeg-Chr4-For	CAGCTTGGTTGAGGCATGAG	Gene Desert Region- Chromosome 4	
CtrlNeg-Chr4-Rev	AGGTTACCGCCATCCCA		
CtrlNeg-Chr12-For	AATGCTGGCTCTTCAGTACC	Gene Desert Region- Chromosome 12	
CtrlNeg-Chr12-Rev	CGTAGAGAGGGATATTGTCTTCA		
Plasmid Sanger-Sequencing Oligos			
pENTRfwd	AGTTACTTAAGCTCGGGC	Custom	pENTR1A-hASH2L-ΔTE
pENTattL2-rev	ACATCAGAGATTTTGAGACACG	Standard Primer	Sequencing

2.1.2 Plasmids

Table 2. Plasmids.

Plasmid Name	Resistance	Last Resort*	Comments
Entry Plasmids			
pENTR1A-hASH2L	Kanamycin	48,b2	Generated by Anja Redecker
pENTR1A-hASH2L-Nostop	Kanamycin	45,d9	Generated by Anja Redecker
pENTR1A-hASH2L-ΔTE	Kanamycin	53,a7	Generated in this study
Co-Transfection Plasmids			
pH2B-YFP	Kanamycin	5,g7	Generated by Dr. Juliane Lüscher
Destination Plasmids			
pLEX-305-N-dTAG	Ampicillin/Puromycin	53,b5	Addgene #91797
pLEX-305-C-dTAG	Ampicillin/Puromycin	53,b6	Addgene #91798
pLEX-305-N-dTAG-hASH2L-ΔTE-ΔBamHI	Ampicillin/Puromycin	53,d3	Generated in this study
pLEX-305-C-dTAG-hASH2L-Nostop	Ampicillin/Puromycin	53,b7	Generated in this study
Lentiviral Packaging			
pMDLg/pRRE	Ampicillin	26,f9	JF, Addgene #12251
pRSV-Rev	Ampicillin	26,g1	JF, Addgene #12253
pCMV-VSV-G	Ampicillin	33,g7	JF, Addgene #8452

* This refers to the repository of the Institute of Biochemistry and Molecular Biology

2.1.3 Antibodies

Table 3. Antibodies.

Antigen	Origin	Clonality	Co./Cat.No.	RRID Number	Purpose
Primary Antibodies					

Actin	Mouse	MC-C4	MP Biomedicals #691001/2	AB_2335304	WB
Ash2l	Rabbit	MC-D93F6	Cell Signaling #5019	AB_1950350	WB/IF
H3	Rabbit	PC	Abcam #ab1791	AB_302613	WB/ChIP
H3K4me1	Rabbit	PC	Abcam #ab8895	AB_306847	WB/ChIP
H3K4me3	Rabbit	PC	Abcam #ab8580	AB_306649	WB/ChIP
H3K27ac	Rabbit	PC	Abcam #ab4729	AB_2118291	WB/ChIP
H3K27me3	Rabbit	PC	Antibodies Online #ABIN6923144	-	WB/ChIP
H3K27me3	Rabbit	PC	Antibodies Online #ABIN6952339	-	WB/ChIP
HA	Rabbit	MC-C29F4	Cell Signaling #3724	AB_1549585	WB
HA	Mouse	MC-B1612	Covance/Biolegend	-	WB/ChIP/IF
IgG	Rabbit	PC	Diagenode #C01010080	AB_2722553	ChIP
Mll1-C Term	Rabbit	MC-D6G8N	Cell Signaling #14197	AB_2688010	WB
Myc	Rabbit	PC-N262	Santa Cruz #sc-764	AB_631276	WB
Rbbp5	Rabbit	PC	Bethyl #A300-109A	AB_210551	WB
γ-Tubulin	Mouse	MC-GTU88	Sigma-Aldrich #T5236	AB_532292	WB
Wdr5	Rabbit	PC	Bethyl #A302-429A	AB_1944302	WB
Secondary Antibodies					
Mouse IgG-HRP	Rat	PC	Jackson Immuno Res., 415-035-166	-	WB
Rabbit IgG-HRP	Goat	PC	Jackson Immuno Res., 111-035-144	-	WB
Mouse IgG AF488	Donkey	PC	Invitrogen #A21202	AB_141607	IF
Rabbit IgG AF488	Goat	PC	MolecularProbes #A11008	AB_143165	IF

2.1.4 Chemicals

Table 4. Chemicals.

Compound	Cat.No.	Company	CAS.No.	Formula
DAPI	6335.2	ROTH	28718-90-3	$C_{16}H_{17}Cl_2N_5$
dTAG-13	6605	TOCRIS	2064175-41-1	$C_{57}H_{68}N_4O_{15}$
Hoechst 33258	861405	Sigma-Aldrich	23491-45-4	$C_{25}H_{24}N_6O.3HCl.2H_2O$
(Z)-4-Hydroxytamoxifen	3412	TOCRIS	68047-06-3	$C_{26}H_{29}NO_2.1/4H_2O$
Lenalidomide	AB282488	Abcr	191732-72-6	$C_{13}H_{13}N_3O_3$
Puromycin-2HCl	A2856,0010	AppliChem	58-58-2	$C_{22}H_{29}N_7O_5.2HCl$
SUPERase•In™ RNase Inhibitor	AM2694	Invitrogen	-	-
TRIzol Reagent	FP312	ABP Biosciences	-	-
Vybrant™ DyeCycle™ Violet	V35003	Invitrogen	-	-

2.1.5 Enzymes

Table 5. Enzymes.

Name	Company	Cat.No.
AgeI-HF	New England Biolabs	R3552
BamHI-HF	New England Biolabs	R3136
BsrGI-HF	New England Biolabs	R3575
EcoRI-HF	New England Biolabs	R3101
EcoRV-HF	New England Biolabs	R3195
KpnI-HF	New England Biolabs	R3142

NcoI-HF	New England Biolabs	R3193
PvuI-HF	New England Biolabs	R3150
Tth111I	New England Biolabs	R0185
DNA Polymerase I, Large (Klenow) Fragment	New England Biolabs	M0210
T4 DNA Ligase	New England Biolabs	M0202

2.1.6 Kits & Reagents

Table 6. Kits and Reagents.

Name	Company	Cat.No.
Bioruptor® DNA QC kit	DIAGENODE	C40010002
ChIP-IT High Sensitivity®	ActiveMotif	53040
Click-iT™ EdU Alexa Fluor™ 488 Flow Cytometry Assay Kit	Invitrogen™	C10420
Click-iT™ Nascent RNA Capture Kit	Invitrogen™	C10365
eBioscience™ Foxp3/ Transcription Factor Staining Buffer Set	Invitrogen™	00-5523-00
Gateway™ LR Clonase™ Enzyme Mix	Invitrogen™	11791043
High Pure RNA Isolation Kit	Roche	11828665001
High Sensitivity D1000 Reagents	Agilent Technologies	5067- 5585
High Sensitivity D1000 ScreenTape	Agilent Technologies	5067- 5584
High Sensitivity DNA Kit	Agilent Technologies	5067-4626
NEBNext® Ultra™ II DNA Library Prep Kit for Illumina®	NewEngland/Biolabs	E7645
NextSeq 500/550 High Output Kit v2.5 (75 Cycles)	Illumina	20024906
NextSeq 500/550 Mid Output Kit v2.5 (150 Cycles)	Illumina	20024904
NucleoSpin™ DNA RapidLyse	MACHERY-NAGEL	15795412
NucleoSpin® Plasmid EasyPure	MACHERY-NAGEL	740727
Pierce™ BCA Protein Assay Kit	Thermo Scientific™	23227
Phusion® High-Fidelity DNA Polymerase	New England Biolabs	M0530
QIAquick PCR Purification Kit	QIAGEN	28104
QuantiNova SYBR Green PCR Kit	QIAGEN	208052
QuantiTect® Reverse Transcription Kit	QIAGEN	205311
Zymoclean Gel DNA Recovery Kit (uncapped)	Zymo Research	D4002

2.1.7 Bacterial Strain

Table 7. Bacterial Strain.

Name	Source	Genotype
E. coli One Shot™ Stbl3™	Invitrogen™	*F-mcrB mrrhsdS20(rB-, mB-) recA13 supE44 ara-14 galK2 lacY1 proA2 rpsL20(StrR) xyl-5 λ-leumtl-1*

2.1.8 FBS, Cell Lines, and Medium Culture

Table 8. FBS.

Name	Company	Cat.No.	Lot.No.

Fetal Bovine Serum (FBS)	Gibco™	10270-106	42G9377K

Table 9. Insect Cell Lines and Medium Culture.

Name	Origin	Tissue	Source	Description
S2R+	*Drosophila melanogaster*	Embryo	External: Kindly provided by Dr. Ekatarina Seib, Postdoc of Professor Thomas Klein's group. Institute of Genetics, University of Düsseldorf	Received at passage 19

Cell Culture Medium	Cat.No.	Cell Type	Company
Schneider's *Drosophila* Medium*	21720024	S2R+	Gibco™

*Approximately 50 mL was kindly provided by Dr. Ekatarina Seib, Prof. Klein research group, Institute of Genetics, University of Düsseldorf.

Table 10. Mouse Cell Lines and Medium Culture.

Name	Origin	Tissue	Genotype	Source	Description
Immortalized Mouse Embryonic Fibroblast *Ash2l* KO	E13.5 mouse embryo	Fibroblast	*Ash2l*$^{fl/fl}$; *CAGGCre_ER*	Internal Litter Mate Embryos (13.5 dpc) Strain 004682: The Jackson Laboratory	shRNA*p19ARF*/bsR 4-Hydroxytamoxifen (HOT) inducible conditional Knock Out

Name	Origin	Tissue	Genotype	Source	Description
Immortalized Mouse Embryonic Fibroblast *Ash2l* KO *ASH2L-FKBP*	E13.5 mouse embryo	Fibroblast	*Ash2l*$^{-/-}$; *CAGGCre_ER*	Internal: Generated in this study from iMEF cells	shRNA*p19ARF*/bsR N-*FKBP-ASH2L* /purR dTAG-13 Inducible KnockDown Isolated Monoclones: NB5-ND10-NG3
					shRNA*p19ARF*/bsR C-*FKBP-ASH2L* /purR dTAG-13 Inducible KnockDown Isolated Monoclones: CA1

Cell Culture Medium	Cat.No.	Cell Type	Company
DMEM, high glucose, GlutaMAX™	61965-026	MEF	Gibco™

Table 11. Human Cell Lines and Medium Culture.

Name	Origin	Tissue	Genotype	Source	Description	RRID Number
293T	Human	Epithelial-Like Kidney, Embryo	CAGGCre_ER	Internal	Contains SV40 T-antigen	CVCL_0063

Cell Culture Medium	Cat.No.	Cell Type	Company
DMEM, high glucose, GlutaMAX™ supplement, pyruvate	31966-021	HEK293T	Gibco™

2.2 Methods

2.2.1 Prokaryotic Cell Culture

LB-Agar plates: 1% (w/v) tryptone; 0.5% (w/v) yeast extract; 1% (w/v) NaCl; 1.5% (w/v) bacto agar
Antibiotic: 100 µg/mL ampicillin or 30 µg/mL kanamycin

LB (Luria-Bertani) medium: 1% (w/v) tryptone; 0.5% (w/v) yeast extract; 1% (w/v) NaCl
Antibiotic: 100 µg/mL ampicillin or 30 µg/mL kanamycin

SOB (Super Optimal Broth) medium: 2% (w/v) tryptone; 0.5% (w/v) yeast extract; 0.05% (w/v) NaCl

SOC (SOB with Catabolite repression): SOB; 20mM Glucose; 10 mM $MgCl_2$; 10 mM $MgSO_4$

2.2.1.1 Bacterial Cultivation

For bacteria, two forms of solid and liquid culture were used in this study. For solid culture, an LB-Agar plate containing the specific concentration of an antibiotic agent, corresponding to the bacterial plasmid, was used. Spread plates were incubated at 37 °C for overnight (~16h) until the single colonies were observable and ready for inoculation. LB medium containing the corresponding antibiotic was used for liquid culture of bacteria, and plasmid preparation (Mini/Maxi). Bacteria were grown in LB medium in a test tube or Erlenmeyer Flask at 37 °C in a shaker incubator at 160 round per minute (RPM). Bacteria were harvested once the turbidity of the culture reached 0.6 ptical density (OD) at 600 nm.

2.2.2 Eukaryotic Cell Culture

1X PBS (Phosphate Buffered Saline)
140 mM NaCl; 2.6 mM KCl; 2 mM Na_2HPO_4; 1.45 mM KH_2PO_4; pH 7.4

FBS (Fetal Bovine Serum), heat-inactivated (Gibco™)

Trypsin/EDTA (0.05 %) (TrypLE™ Express, phenol red Gibco™)

P/S (Penicillin 10,000 U/mL + Streptomycin 10 mg/mL) (Gibco™)

2.2.2.1 Drosophila Cells

Cultivation

Schneider's *Drosophila* Medium (Gibco™)

Drosophila S2R+ cell lines were cultivated in Schneider medium (kindly provided by Dr. Ekatarina Seib, Prof. Klein research group, Institute of Genetics, University of Düsseldorf) supplemented with 10% (v/v) FBS and 0.5% (v/v) P/S at 25°C. The semi-adherent cells were grown in T-75 flasks in 10 mL of medium. Passaging was performed every 3-5 days when the cells became over 90% confluent. To passage the cells, they were resuspended in the medium by pipetting up and down until they were all detached. Subsequently, a fraction of the cell suspension was transferred to a new T-75 flask with fresh medium, in a ratio dependent on the purpose of the experiment

Freezing and Thawing

Cryoconservation medium: 50% Schneider Medium; 40% heat-inactivated FBS; 10% DMSO

For long-term conservation cells were detached from a T-75 flask after reaching 80-90% confluency using pipetting and re-suspending cells. The cells were pelleted at 500xg for 3 min at 4 °C. The old medium was removed and a number of ~1 X 10^7 cells per mL was re-suspended in cryoconservation medium and transferred to a cryo-tube (Nalgene). Tubes were then stored at -80°C in a freezing container filled with isopropanol or a Styrofoam box for 3-5 days until they were transferred to -150 °C for long-term storage.

For thawing, the cryo-tubes were quickly half-thawed in a 37 °C water bath and promptly transferred into a 10 mL centrifuge tube containing a pre-warmed medium. The cells were pelleted at 500xg for 3 min at 4 °C. Then, the medium was discarded and the cells were re-suspended in the fresh, pre-warmed medium before being transferred to a new T-75 flask.

Seeding

The semi-adherent cells were detached by pipetting up and down. Then, the cell concentration of the suspension was determined using Trypan Blue Exclusion with a Neubauer cell chamber (Depth: 0,1 mm) using the following formula:

$$\frac{Viable\ cell\ count}{Square\ number} \times Dilution\ Factor \times Hemocytometer\ factor\ (10{,}000)\ \times currnt\ volume(ml) = viable\ cell\ yield$$

The required number of cells was then seeded or harvested dependent on the purpose and stage of the experiment.

2.2.2.2 Mouse Cells

DMEM (Dulbecco's Modified Eagle Medium), high Glucose, GlutaMAX™ (Gibco™)

Puromycin - Dihydrochloride BioChemica, 8 µg/mL (Applichem)

Cultivation

Immortalized Mouse Embryonic Fibroblast (iMEF, and iMEF dTAG clones) cells were cultured in DMEM supplemented with 10% (v/v) FBS and 1% P/S (v/v) (Full cell culture medium) at 37 °C in a humidified incubator at 5% CO_2. Cells were grown in different sizes of cell culture plates including 96-well, 24-well, 6-well, 6 cm, 10 cm, and 15 cm based on the purpose of the experiment. Cells were kept in the corresponding volume of medium corresponding to each plating area until they reached the desired confluency. For regular cell culture maintenance, cells were passaged every 2-4 days in a 1:3-1:5 ratio. For passaging, cells were first washed with 1X PBS and incubated in Trypsin/EDTA for <5 min in a 37 °C incubator until they were detached from the plate. Then, the trypsinization was stopped by adding 5-10 folds volume of fresh medium to the plate. Cells were then re-suspended in the medium and a fraction of the cell suspension was transferred to a new plate (the ratio was dependent on the purpose and time scale of the experiment/treatment). For harvesting, the cell suspension was centrifuged at 500xg, for 3 min at 4 °C and the pellet was processed accordingly to the desired experimental protocol. The stable iMEF single cells (referred to as iMEF dTAG clones), constitutively expressing ASH2L-FKBP were cultured in full medium supplemented with 8 µg/mL puromycin (Applichem) selection marker.

Freezing and Thawing

Cryoconservation medium: 90% heat-inactivated FBS; 10% DMSO

For long-term conservation cells were detached from a 10 cm plate after reaching 80-90% confluency using trypsinization. The cells were pelleted at 500xg for 3 min at 4 °C. The old medium was removed and the pellet was re-suspended in 1 mL of cryoconservation medium and transferred to a cryo-tube (Nalgene). Tubes were then stored at -80°C in a freezing container filled with isopropanol or a Styrofoam box for 3-5 days until it was further moved to -150 °C for long-term storage.

For thawing, the cryo-tubes were quickly half-thawed in a 37 °C water bath and promptly transferred into a 10 mL centrifuge tube containing a pre-warmed medium. The cells were pelleted at 500xg for 3 min at 4 °C. Then, the medium was discarded, and the cells were re-suspended in the fresh, pre-warmed medium before being transferred to a new 10 cm cell culture plate.

Seeding

Cell counting was performed with the CASY cell counter (OMNI Life Science) using a cell type-specific program. Cells were detached by trypsinization and re-suspended in a 10 mL medium. Then, a 50 µL of cell suspension was diluted in 10 mL (1:200 dilution) CASY ton prior to measurement. The diluted sample was then inverted gently and measured by the CASY machine.

The following CASY program was used for different iMEF/ iMEF dTAG Clones:

Table 12. CASY Cell Counting Programs.

Cell Line	Capillary	Program Number*
iMEF	1	19
iMEF – NG3	3	6

* The numbers are internally generated for different capillaries.

Isolation of Monoclonal Cell Lines

Untreated transduced iMEF cells from chapter 2.2.3.2 express both endogenous mAsh2l and exogenous hASH2L-FKBP. In order to eliminate the endogenous expression and pick cells with an equal level of exogenous protein expression, monoclonal isolation via a limiting dilution protocol was applied. Initially, transduced iMEF pools were treated with 5 nM of HOT for 3 days in order to excise the endogenous *Ash2l* exon 4 genomic sequence. The resulting treated KO pools were then suspended in a 1:2 dilution of fresh and conditioned iMEF medium supplemented with 8 µg/mL puromycin. The final concertation of 50 cells/10 mL was distributed into a 96-well plate (100 ul in each well) and stored for ~2 weeks to let the cells recover. The very first well was seeded with a higher number of cells, to aid in the focal adjustment of the microscope. The 96-well plate was checked every 3 – 4 days to monitor the growth of the recovered cells. The growing clones were then transferred into 48-well, 24-well, 6-well, and finally 10 cm plates. A fraction of cells was kept for expression analysis and the rest of the cells were cryoconserved at -150 °C. Isolated monoclonal cell cultures were checked for the deletion of exon 4 of the endogenous Ash2l KO on a genomic and protein level. As the second criterion, clones with an equal expression level of exogenous fusion protein ASH2L-FKBP were further selected. The final selected clones are as below:

Table 13. Isolated Monoclonal Cells.

Maternal iMEF Pool	Derived Monoclonal Cultures Used in This Study
iMEF NdTAG-hASH2L-FKBP	NB5, ND10, NG3
iMEF CdTAG-hASH2L-FKBP	CA1 (Isolated by Malte Benje)

2.2.2.3 Human Cells

DMEM (Dulbecco's Modified Eagle Medium), high Glucose, GlutaMAX™, + pyruvate (Gibco™)

Cultivation

HEK293T cells were cultured in DMEM supplemented with 10% (v/v) FBS and 1% P/S (v/v) (Full Cell Culture Medium) at 37 °C in a humidified incubator at 5% CO_2. Cells were grown in 10 cm plates with a 10 mL medium for transfection purposes. Cells were kept in culture until they reached the desired confluency. For regular cell culture maintenance, cells were passaged every 2-3 days at a 1:5 ratio. For passaging, cells were first washed with 1X PBS followed by the addition of Trypsin/EDTA to the plate. Cells were detached applying a few times shaking/tapping. Then, the trypsinization was stopped by adding 5-10 folds volume of fresh medium to the plate. Cells were then re-suspended in the medium and a fraction of the cell suspension was transferred to a new 10 cm plate (the ratio was dependent on the purpose and time scale of the experiment). For harvesting, the cell suspension was centrifuged at 500xg, for 3 min at 4 °C and the pellet was processed according to the specific experimental protocol.

Freezing and Thawing

Cryoconservation medium: 90% heat-inactivated FBS; 10% DMSO

For long-term conservation cells were detached from a 10 cm plate after reaching 80-90% confluency using trypsinization. The cells were pelleted at 500xg for 3 min at 4 °C. The old medium was removed and the pellet was re-suspended in 1 mL of cryoconservation medium and transferred to a cryo-tube (Nalgene). Tubes were then stored at -80°C in a freezing container filled with isopropanol or a Styrofoam box for 3-5 days until it was moved to -150 °C for long-term storage.

For thawing, the cryo-tubes were quickly half-thawed in a 37 °C water bath and promptly transferred into a 10 mL centrifuge tube containing a pre-warmed medium. The cells were pelleted at 500xg for 3 min at 4 °C. Then, the medium was discarded, and the cells were re-suspended in the fresh, pre-warmed medium before being transferred to a new 10 cm cell culture plate.

Seeding

Cell counting was performed with the CASY cell counter (OMNI Life Science) using a cell type-specific program. Cells were detached by trypsinization and re-suspended in a 10 mL medium. Then, 50 µL of cell suspension was diluted in 10 mL (1:200 dilution) CASY ton prior to measurement. The diluted sample was then inverted gently and measured by the CASY machine.

The following CASY program was used for HEK cells:

Cell Line	Capillary	Program Number*
HEK293T	1	6

* The numbers are internally generated for different capillaries.

2.2.3 Gene Delivery Experiments

2.2.3.1 Bacterial Transformation

For bacterial transformation, a conventional heat-shock protocol was used. Various amounts of plasmid DNA, depending on the purpose of the experiment (<50 ng for plasmid propagation, 10 µL of LR reaction, 10 µL ligation reaction) were mixed with 100 µL of chemically competent bacteria, which were thawed on ice shortly beforehand. The mixture was then incubated on ice for 30 min followed by a heat shock at 42 °C for exactly 45 sec. Transformed bacteria were subsequently chilled on ice for 2-5 min prior to the addition of 900 µL room-temperature SOC medium. The bacteria were then incubated at 37 °C for 1 h at a speed of 160 RPM. Next, the bacteria were spun down at 3000 RPM for 2 min to discard 90% of the supernatant. Subsequently, they were re-suspended in the ~100 µL of the residual medium and cultured using the spread plate method on agar plates supplemented with the appropriate amount of antibiotic (See chapter 2.2.1.1).

2.2.3.2 Calcium Phosphate Transfection

1X HBS buffer: 17 mM HEPES; 138 mM NaCl; 5 mM KCl; 0.71 mM Na_2HPO_4; pH 6.95

1X HEPES buffer: 10 mM HEPES; 142 mM NaCl; 6.7 mM KCl; pH 7.3

2.5 M $CaCl_2$

Transient Transfection- Overexpression in HEK293T Cells

HEK293T cells were seeded, and the transfection reaction was prepared according to the following table.

Cell Number	**Transfection Reaction per Sample**
7 – 8 x10^5 / 10 cm Plate	Σ20 µg Plasmid DNA (1:10 pH2B-YFP)*
1 day prior to the transfection reaction	950 µL 1X HBS Buffer
	50 µL 2.5 M $CaCl_2$

* Each reaction was co-transfected with 2 µg of H2B-YFP plasmid to estimate the transfection efficiency.

The next day after seeding the cells, a total of 20 µg of plasmid DNA(s) mixture was prepared and thoroughly mixed with 950 µL of 1X HBS buffer by vortexing. Then, 50 µL of 2.5 M $CaCl_2$ was added to the mixture while vortexing the tube. This solution was incubated at room temperature (RT) for 30 minutes. Later, it was distributed dropwise into the cell culture medium. The cell plate was swayed gently and incubated at 37 °C incubator for 6 – 8 hours. Cells were then checked under a bright field microscope to observe the formation of DNA-$CaPO_4$ precipitants around the cell membrane. Cells were then washed with 10 mL of pre-warmed 1X HEPES buffer for 10 min, and re-fed with 10 mL fresh medium per 10 cm culture dish. Plates were then incubated overnight – 24h and checked for green fluorescence of cell nuclei, originating from the co-transfected H2B-YFP control plasmid to evaluate the transfection efficiency. Plates with >90% of green nuclei were picked for the downstream experiments (expression analysis, and lentiviral vector production (Chapter 2.2.3.3)). The table below shows the plasmid types and ratios for different transfection experiments for the analysis of the specific protein expression levels.

Plasmid Mixture	Ratio Σ 20 µg	Harvesting Purpose
pH2B-YFP	2:20	Plasmid Expression Analysis
pLEX-305-N-dTAG	18:20	
pH2B-YFP	2:20	Plasmid Expression Analysis
pLEX-305-N-dTAG-hASH2L-ΔTE-ΔBamHI	18:20	
pH2B-YFP	2:20	Plasmid Expression Analysis
pLEX-305-C-dTAG-hASH2L-Nostop	18:20	

2.2.3.3 Lentiviral Vector Production, and Transduction

The whole procedure of the production and the work with lentiviruses in this chapter was done in the Safety Level 2 (S2) cell culture laboratory and stored there. After 2 – 3 passages, the cell cultures were considered free of transduced viruses and were transferred to the Safety Level 1 (S1) cell culture laboratory of the institute.

For lentiviral vector production, a third-generation packaging system was used. This system contains three helper plasmids (pMDLg/pRRE, pRSV-Rev, pCMV-VSV-G, please see the table below).

A total of 20 µg of a mixture of helper plasmids plus transfer plasmid (Plasmid of interest) was prepared according to the table below. An extra 1 µg of pH2B-YFP plasmid was added to the plasmid mixture, to estimate the transfection efficiency. Co-transfection was done as previously mentioned in chapter 2.2.3.2 according to the table below (Day 0).

Plasmid Mixture	Ratio Σ 21 µg	Function	Harvesting Purpose
pH2B-YFP	1:21	Control Plasmid	Lentiviral Production
pMDLg/pRRE	6:21	Packaging Plasmid	
pRSV-Rev	5:21	Packaging Plasmid	
pCMV-VSV-G	2:21	Envelop Plasmid	
pLEX-305-N-dTAG-hASH2L-ΔTE-ΔBamHI	7:21	Transfer Plasmid	
pH2B-YFP	1:21	Control Plasmid	Lentiviral Production
pMDLg/pRRE	6:21	Packaging Plasmid	
pRSV-Rev	5:21	Packaging Plasmid	
pCMV-VSV-G	2:21	Envelop Plasmid	
pLEX-305-C-dTAG-hASH2L-Nostop	7:21	Transfer Plasmid	

24h post-transection (Day 1) cells were checked for the green nuclear signal of the YFP plasmid. Passing the transfection efficiency threshold (>90%) they were cultured for another day to increase the viral titer. The next day (Day 2), the cell culture supernatant from HEK293T cells was collected and passed through a 0.45 µm PVDF filter. HEK293T cells were again fed with fresh medium and kept in the incubator for another day (Day 3) to produce a second round of viral particles. iMEF cells were seeded so that a confluency of ~40% was reached a day prior to the transduction. The virus-containing supernatant from day 2 was preferably used on the same day to transduce target iMEF cells. For this purpose, the filtered HEK293T supernatant (from Day 2) was diluted 1:2 with a fresh iMEF cell culture medium. To a final concentration of 8 µg/mL, Polybrene (neutralizing the charge

repulsion between packaged viral vectors and cell surface) was added to the diluted medium mixture and added to iMEF plates. After 6 – 8 hours of incubation, the medium on iMEF cells was refreshed until the next day to allow the cells to recover from the viral infection. On the next day (Day 3), the virus-containing medium from HEK293T cells was again collected and filtered through 0.45 µm PVDF filter, and again diluted 1:2 with fresh iMEF medium (containing 8 µg/mL Polybrene) and added to the corresponding iMEF plate. HEK293T cells were harvested for plasmid expression check. Transduced iMEF cells were then incubated for another 6 – 8 hours followed by a medium change for recovery and incubated overnight. The day after the 2nd transduction, iMEF cells were split at a 1:3 ratio and allowed to grow for another day. Subsequently, a plate of transduced and non-transduced (Control) iMEF cells were treated with 8 µg/mL of Puromycin (The selection marker within the transfer plasmid backbone). The next day the number of dead cells in both sample and control cells was evaluated under the microscope and the fresh medium supplemented with antibiotics was added to the plates. This medium change and antibiotic selection was continued until there were no more live cells visible in control plates (usually 2 – 4 days). The transduced iMEF pools were then further cultured for expression analysis, cryoconservation, and the generation of monoclonal cell cultures.

2.2.4 DNA-Related Experiments

2.2.4.1 Plasmid Propagation and Extraction

On a small scale, DNA plasmids were purified from 4 mL of bacterial culture using the NucleoSpin Plasmid EasyPure Mini Kit (Macherey Nagel) according to the manufacturer's instructions. On a large scale, DNA plasmids were purified from 300 ml bacterial culture using the NucleoBond® Xtra Maxi Kit (Macherey Nagel) according to the manufacturer's instructions. Generally, the integrity of the resulting plasmids was controlled by restriction digestion and if necessary, sequencing (chapter 2.2.4.2, and 2.2.4.8). The concentration and the purity of the plasmids were analyzed using the NanoDrop™ 1000 (Thermo Fisher Scientific).

2.2.4.2 Restriction Digestion

Restriction digests were performed according to the respective instruction from the manufacturer (NEB). To evaluate the overall integrity of a plasmid preparation, a reaction mixture with a final volume of 25 µL was prepared to contain 0.5 µL of the restriction enzyme and 0.5 – 1 µg of plasmid DNA. To generate fragments of plasmids for cloning purposes, a 50 µL reaction mixture was used containing 1 µL of the restriction enzyme and 1 – 3 µg of plasmid DNA. For double or multiple serial enzymatic digestions, the protocol from the Restriction Enzyme Single/Double Digestion – NEBcloner website (https://nebcloner.neb.com/#!/redigest) was applied. The digestion products were then analyzed using 0.7 – 2% agarose gel electrophoresis.

2.2.4.3 Gel Electrophoresis

1X TBE buffer: 89 mM Tris base (pH 8.0); 89 mM Boric Acid; 2 mM EDTA

6X Gel Loading Dye, Purple, NEB #B7024S

Agarose Low EEO (Sigma); 0.7-2% (w/v)

Ethidium Bromide: 0.5 µg/mL, Applichem

Molecular weight marker: GeneRuler™ 1 kb Plus DNA Ladder, MBI Fermentas

Agarose gel electrophoresis analyses were used to evaluate the Deoxyribonucleic Acid/Ribonucleic Acid (DNA/RNA) preparations for different purposes: restriction digest (chapter 2.2.4.2), PCR reaction (chapter 2.2.4.11), RNA extraction (chapter 2.2.5.1), and chromatin shearing (chapter 2.2.10.1) experiments. DNA/RNA samples were diluted 1:6 with 6X loading dye and loaded on an agarose gel (0.7 – 2%) supplemented with 0.5 µg/mL Ethidium Bromide. Gels were then run with 80 – 100 V for 30 – 45 min in 1X TBE buffer. The nucleic acids were then visualized on a UV Trans-Illuminator (E-BOX VX2, Peqlab, with λ=302 nm wavelength at 70% intensity).

2.2.4.4 Agarose Gel DNA Recovery

After agarose gel electrophoresis of DNA fragments from restriction digests, desired DNA fragments were excised from the agarose gel by a scalpel under UV light. Subsequently, the DNA was purified using the ZymoClean™ Gel DNA Recovery Kit (Zymo Research) according to the manufacturer's instructions. The DNA was eluted in 10 µL TE buffer and used for molecular cloning. This procedure was specifically performed on the pENTR1A-hASH2L plasmid, double-digested with EcoRV and Tth111I, to eliminate the excised interval fragment from the digestion reaction and avoid unwanted ligation.

2.2.4.5 Klenow-Mediated DNA End Repair

To allow a T4-Mediated Blunt End Ligation (chapter 2.2.4.7) of DNA fragments with overhanging ends, a treatment with the Klenow fragment of DNA Polymerase I was performed. The large (Klenow) fragment possesses 5' —> 3' polymerase and 3' —> 5' exonuclease activity, which blunts the overhanging ends resulting from restriction digestion. This end-repair reaction was performed according to the manufacturer's instructions in a total volume of 54 µL. This treatment was performed on gel-extracted pENTR1A-hASH2L plasmid, double-digested with EcoRV and Tth111I, in order to fill in the sticky ends of the Tth111I digestion reaction. This procedure was also performed on pLEX305-N-dTAG-hASH2L-ΔTE-ΔBamHI to destroy the BamHI site inside the vector backbone and generate an open reading frame of the gene cassette.

2.2.4.6 PCR Purification

A PCR purification kit was used to remove inhibitory components of the restriction digestion, like nucleotides, enzymes, and buffers, prior to the ligation with T4 ligase. This step was performed on the digested pLEX305-N-dTAG-hASH2L-ΔTE-ΔBamHI plasmid according to the manufacturer's instructions.

2.2.4.7 Blunt End Ligation

The T4-mediated blunt-end ligation reaction protocol was performed according to the manufacturer's instruction in a total volume of 20 µL. This procedure was performed on gel-extracted double-digested pENTR1A-hASH2L (EcoRV and Tth111I) with blunt ends. This method was also performed on the DNA fragment pLEX305-N-dTAG-hASH2L-ΔTE-ΔBamHI to religate the blunted BamHI sites. 100 ng of vector backbone was used for this reaction. It was then incubated at RT for 2

hours followed by heat inactivation at 65 °C for 10 min. 10 µL of the ligation reaction was subsequently used to transform 100 µL of *Stbl3* competent cells (chapter 2.2.3.1).

2.2.4.8 Gateway LR Reaction

A cloning method based on the sequence-specific recombination of the bacteriophage λ is called the "Gateway System" (Invitrogen). Specific attachment (att) sites are recombined by the recombinase enzymes BP clonase and LR clonase. AttB (Expression Vector) and attP (Donor Vector) sites are recombined by BP clonase to produce attL (Entry Vector) and attR (Destination Vector) sites, whereas the resulting attL and attR are recombined by the LR clonase which generates attB and attP sites. The sequence of interest is always between attB or attR arms, while the toxic negative selective ccdB cassette is located between attP and attR sites. In the LR reaction, the toxic cassette of ccdB (from Destination Vector, attR) is replaced with the gene of interest (from Entry Vector, attL). The LR reactions were performed overnight at 25 °C in a final volume of 10 µl reaction volume according to the manufacturer's instruction. The whole LR reaction was used to subsequently transform 100 µL competent Stbl3 bacteria (chapter 2.2.3.1). After plasmid preparation (chapter 2.2.4.1) the integrity of the Gateway expression constructs was controlled by restriction digest (chapters 2.2.4.2, and 2.2.4.3). Using this cloning method, it is not necessary to sequence the resulting constructs as the recombination reactions do not introduce sequence errors.

2.2.4.9 Plasmid Sequencing

The integrity of new vectors was controlled by Sanger Sequencing performed by Seqlab/Microsynth. For this, 1.2 µg of plasmids in a volume of 12 µl were analyzed using the standard primers provided by the company dependent on the plasmid backbone. If necessary, custom primers were directly ordered from and synthesized by Seqlab/Microsynth (chapter 2.1.1). The sequencing results were analyzed with the SnapGene software (Licensed Version).

2.2.4.10 Genomic DNA Extraction

Genomic DNA was extracted from iMEF cells using the NucleoSpin™ DNA RapidLyse (Macherey-Nagel™) kit according to the manufacturer's instructions. To assess the quality and quantity of the extracted DNA a NanoDrop 1000 Spectrophotometer was used.

2.2.4.11 Polymerase Chain Reaction

PCRs were performed to evaluate the genomic status of the Ash2l KO in iMEF and iMEF dTAG clones. The floxed exon 4 region was amplified using forward and reverse primers, with the Phusion® High-Fidelity DNA Polymerase (NEB) following the manufacturer's instructions, in a reaction volume of 25 µL. An amount of 50 ng of template DNA was included in each reaction. The PCR program was adjusted based on the polymerase instruction (see table below). The PCR product was analyzed via agarose gel electrophoresis.

For the nested PCR, the same polymerase and PCR program were used (see table below), but the template was a 1:10 dilution of the outer fragment PCR product.

Step	**Temperature**	**Time**
Initial Denaturation	98 °C	1 min

Amplification	98 °C	10 sec
30 Cycles	60 °C	15 sec
	72 °C	15 sec
Final Extension	72 °C	2 min
Hold	4 °C	Forever

2.2.5 RNA-Related Experiments

There were several experiments performed on RNA samples extracted from cell cultures: 1) To determine relative expression levels, total RNA was isolated followed by RT-qPCR measurements (chapter 2.2.5.3); 2) To assess newly synthesized RNA, a Click nascent RNA method was employed (chapter 2.2.10.2).

2.2.5.1 Total RNA Extraction

Total RNA was isolated from iMEF or iMEF dTAG clones using a High Pure RNA Isolation kit (Roche) according to the manufacturer's instruction. In case the isolated RNA would have to include also short RNA fragments, the TRIzol reagent from ABP Biosciences was used. Based on the sample volume, the RNA isolation with the TRIzol reagent was altered accordingly.

2.2.5.2 Complementary DNA (cDNA) Synthesis

For RT-qPCR, cDNA synthesis was performed on total RNA using the QuantiTect Reverse Transcription Kit (QIAGEN) according to the manufacturer's instructions.

2.2.5.3 Quantitative Polymerase Chain Reaction (qPCR)

For the determination of the relative expression of RNA transcripts and also for quantitative measurements of immune-precipitated chromatin fragments (chapter 2.2.10.1), qPCR reactions were performed using the QuantiNova SYBR Green PCR kit (QIAGEN) in a Rotor-Gene Q machine (QIAGEN).

The mouse GusB transcript level was used as a normalizer. The level of this transcript did not change regardless of the genotype, or the treatments of the cell lines used. Primers were either purchased from QIAGEN (QuantiTect Primer Assays) or designed using the NCBI primer designing tool. A primer efficiency test was done for each primer pair. Only those with an efficiency above 90 % were employed. The baseline threshold on the amplification plot was set at 0.01 to generate Ct values. The calculations of qPCR were done based on the $2^{\wedge -(\Delta Ct\text{-}Control\ -\ \Delta Ct\text{-}Test)}$ formula (Livak & Schmittgen, 2001).

In the qPCR reactions following chromatin-immunoprecipitation (chapter 2.2.10.1), input DNA (protein-digested total chromatin DNA) was used as a normalizer. Since the input DNA was diluted concerning the chromatin amount used for IP, this had to be taken into account while calculating the result of the experiment as % input.

Adjusted Input Ct = Input Ct - Log_2 (Dilution Factor)

In general, the qPCR reaction was prepared in 10 µL volume according to the following table:

Component	Vol. (µL)	Final Conc.	Comments
2X QuantiNova SYBR Green Master Mix	5	1X	
Forward & Reverse Primer Mix	1	1 µM	RTqPCR: 1:10 dilution of the QuantiTect Primer Assays ChIPqPCR: 10 µM stock solution
Template	2	-	RTqPCR; 1:3 – 1:5 diluted cDNA ChIPqPCR; 1:5 – 1:10 diluted IP-DNA or Input DNA
Nuclease-Free Water	1	-	

Two different sets of qPCR profiles were applied for the RTqPCR and ChIPqPCR reactions respectively:

Table 14. RNA RT-qPCR Profile.

RT-qPCR Profile	
Hold	Hold @ 95°C, 3min
Cycling (40 repeats)	Step 1: Hold @ 95°C, 10s
	Step 2: Hold @ 60°C, 10s
	Step 3: Hold @ 72°C, 10s, acquiring to Cycling A([Green])
Melt	Ramp from 57°C to 95°C
	Hold for 90s on the 1st step
	Hold for 5s for the following steps, acquiring to Melt A([Green])

Table 15. ChIPqPCR Profile.

ChIPqPCR Profile	
Hold	Hold @ 95°C, 2min
Cycling (40 repeats)	Step 1: Hold @ 95°C, 10s
	Step 2: Hold @ 61°C, 10s
	Step 3: Hold @ 72°C, 5s, acquiring to Cycling A([Green])
Melt	Ramp from 60°C to 95°C
	Hold for 90s on the 1st step
	Hold for 5s for the following steps, acquiring to Melt A([Green])

2.2.6 Protein-Related Experiments

Protein extraction from cell lysate was mainly done with the purpose of expression level measurements of protein upon different treatments.

2.2.6.1 Eukaryotic Cell Protein Lysate Preparation

RIPA Buffer: 10 mM Tris base, pH 7.4; 150 mM NaCl; 1% NP-40; 1% deoxycholate; 0.1% SDS

1% SDS Lysis Buffer: 10 mM Tris base, pH 8.0; 1% SDS; 1 mM EDTA

Protease Inhibitor Cocktail (PIC, Sigma): Contains AEBSF, Aprotinin, Bestatin, E-64d, Leupeptin, and Pepstatin A

Lysate preparation was performed on a cell culture sample. First, the cells were washed with 1X PBS to remove the old medium, then detached from the plate using trypsinization or resuspension. The cell pellet was then spun down using a centrifuge at 4°C, 500xg for 3-5 min. RIPA lysis buffer supplemented with 1X PIC was added to the cell pellet (100-300 µL RIPA based on the pellet size from a 10 cm plate). The pellet was pipetted up and down, and the mixture was incubated on ice for approximately 30 min. After the lysis reaction, the released DNA was sheared using a water bath sonicator at 70% amplitude for an overall time of 5 min with a 30s/30s pulse. The tubes were then centrifuged at 4°C for 30 min at 20,000xg, and the supernatant (lysate) was transferred into clean tubes. The total protein concentration of the lysates was measured using a Pierce™ BCA Protein Assay Kit according to the manufacturer's instructions. The lysates were then used for immuno-blotting of different proteins

2.2.6.2 Sodium Dodecyl-Sulfate Poly-Acrylamide Gel Electrophoresis (SDS-PAGE)

2X Sample Buffer (2X SB): 160 mM Tris-HCl, pH 6.8; 20% (v/v) glycerol; 10% (v/v) SDS; 0.5% bromophenol blue; 8% (v/v) β-mercaptoethanol

4X Sample Buffer (4X SB): 320 mM Tris-HCl, pH 6.8; 40% (v/v) glycerol; 8% (w/v) SDS; 0.5% bromophenol blue; 16% (v/v) β-mercaptoethanol

SDS Running Buffer: 25 mM Tris base, pH 8.3; 250 mM glycine; 0.1% (w/v) SDS

Protein Ladder VI: 10 - 245 kDa (AppliChem)

Proteins can be separated according to their molecular weight by denaturing, discontinuous SDS-PAGE. SDS_PAGE was performed using the Mini-PROTEAN Tetra Cell system (Bio-Rad). The gels consisted of a 5% polyacrylamide (PAA) stacking gel and for the separation gel, the PAA concertation varied from 7.5% to 20%, depending on the molecular weight of the proteins. The samples were mixed with 2X SB or 4X SB (depending on the volume limitation) to a final concentration of 1X SB and denatured at 95°C for 5 min. A protein size marker was used to allow the estimation of the molecular weight of the proteins. The gels were run at 150-200 V until the running front reached the end of the gel. The gels were immediately used for Western blotting (chapters 2.2.6.3-5).

2.2.6.3 Turbo-Western Blot

Semidry Transfer Buffer: 25 mM Tris base; 192 mM Glycine; 20% (v/v) Methanol

Amersham™ Protran® Western blotting membranes, nitrocellulose, 0.2 µm pore size (Cytiva)

Ponceau S Solution: 0.05% (w/v) Ponceau S; 1% (v/v) Acetic Acid

For the immunodetection of proteins with specific antibodies after SDS-PAGE (chapter 2.2.6.2), the proteins were typically transferred to nitrocellulose membranes using the semi-dry Western blotting technique. The gel, 12 transfer stacks, and the membrane were equilibrated in semidry transfer buffer for ~5 min. Afterward, everything was stacked from bottom (anode) to top (cathode) starting with 6 bottom stack pads, blotting membrane, gel, and another 6 stack pads on a Semidry blotting apparatus (Trans-Blot Turbo Transfer System, BIORAD). The transfer took place with High Molecular Weight (10 min, 1 A, 25 V) or Mixed Molecular Weight program (7 min, 1 A, 25 V) from the apparatus. Afterward, the loading equality and transfer efficiency was evaluated by staining the

membrane in Ponceau S solution under gentle rocking for ~5 min. The blot was further used for immunodetection of proteins and modifications via specific antibodies (chapter 2.2.6.5).

2.2.6.4 Tank-Western Blot

Histone Transfer Buffer: 48 mM Tris base pH 8.8 – 9.4; 39 mM Glycine; 20% Methanol

High Molecular Weight Transfer Buffer: 25 mM Tris base; 192 mM Glycine; 20% (v/v) Methanol

Whatman® Qualitative Filter Paper, Grade 3

In order to transfer proteins with high molecular weight and also histones with a higher pH transfer buffer system, a wet/tank blotting was performed. The tank blot was performed using the Mini Trans-Blot® Module (Bio-Rad). The two sponges, the gel, 6 filter papers, and the membrane were incubated in an ice-cold tank blotting transfer buffer for a few minutes. The blotting cassette was assembled from black to transparent side starting with a sponge, 3 filter papers, the gel, and the membrane, 3 filter papers, and a sponge. The cassette was then placed into the blotting chamber with black facing cathode. The frozen cooling element and a magnetic stirring were placed in the blotting chamber and the blotting chamber was filled with an ice-cold tank blotting transfer buffer. Then, the apparatus was placed in the cold room on a magnetic stirrer. While stirring, the transfer took place at 60 V for 3 h for histones and 90 V for 2 h for large proteins. Afterward, the transfer efficiency was evaluated by staining the membrane in Ponceau S solution under gentle rocking for 5 min. The blot was further used for immunodetection of proteins and modifications via specific antibodies.

2.2.6.5 Immuno-Detection

1X TBS: 50 mM Tris base, pH 7.5; 150 mM NaCl

1X TBS-T: 0.05% (v/v) Tween-20 in TBS

Blocking Solutions: 5% (w/v) non-fat dry milk in 1X TBS-T or 5% (w/v) BSA pH 7 in 1X TBS-T

Following Semidry or Tank Western blot (chapters 2.2.6.3-4), the transferred proteins or modifications were detected using specific antibodies. After Ponceau S staining, the blot was incubated in a blocking solution (according to the primary antibody datasheet), agitating at RT for 1 h to block nonspecific binding sites. The blocking solution was removed by washing three times with 1X TBS-T for 5 min each. Thereafter, the primary antibody was added to the membrane in a dilution specific to the antibody (according to the antibody datasheet) and incubated at 4°C, agitating overnight. The next morning, following the removal of the excess, unbound antibody, the membrane was washed three times in TBS-T for 5 min each. Thereafter, the secondary, HRP-coupled antibody was added to the membrane in a dilution specific to the antibody (against the primary antibody origin) and incubated at RT, agitating for 1 h. Again, to remove excess, unbound antibodies, the membrane was washed three times with 1X TBS-T for 5 min each. The membranes were developed using ECL solutions (SuperSignal™ West Pico PLUS Substrate or SuperSignal™ West Femto Maximum Sensitivity Substrate, Thermo Fisher Scientific) with the WesternBright Quantum HRP substrate (Advansta) and the Azure c600 (Azure Biosystems) for detection.

2.2.7 Cell-Related Experiments

Tissue culture was performed using cell lines from humans, mice, and insects. The experiments described in chapters 2.2.7.1 and 2.2.7.2 were mainly performed on mouse cell lines (iMEF and iMEF dTAG clones) and human cell lines (HEK293T). In all of the experiments, the confluency of cells was controlled to be between 70-80% at the time of harvesting (unless otherwise specified in detail).

2.2.7.1 Compounds Dose/Time Response Assessment

(Z)-4-Hydroxytamoxifen (Referred as HOT in this thesis) (TOCRIS): 5 nM in Ethanol

dTAG-13 (TOCRIS): 100 nM in Ethanol

Lenalidomide (Abcr): 50 µM in DMSO

To induce the *Ash2l* KO, a 3 – 7 day treatment with a final concentration of 5 nM HOT was performed. For KO assessment, cells were treated for 5 days unless otherwise described in detail. For transduced KO induction, transduced iMEF cells were treated for 3 days with 5 nM HOT and then prepared for monoclonal isolation (chapter 2.2.2.2).

The chemical compound dTAG-13 with a final concentration of 100 nM was used to induce the FKBP-ASH2L degradation in iMEF dTAG clones. The degradation dose/time dependency was confirmed via immune-detecting the fusion protein in gradient-treated/time-course samples. In long-term treatments, dTAG-13 was added every 24h to the cell culture dishes.

Lenalidomide was used as a competitive binding inhibitor for dTAG-13 in a final concentration of 50 µM (Otherwise, described in detail). In long-term treatments, lenalidomide was added every 48h to the cell culture dishes.

2.2.7.2 Cell Proliferation Assay

A cell proliferation assay was conducted in three biological replicates, each consisting of three technical replicates for iMEF and iMEF dTAG clones, to track the growth of cells and their response to dTAG-13 treatment. 5 x 104 cells were seeded in a 6-well plate, and they were treated that same day (Day 0). Trypsin was used to dissociate cells, which were then resuspended and counted using a CASY machine every three days unless otherwise specified (chapter 2.2.2.2). A splitting ratio of 1:2–1:3 was used for confluent cells, however, the same number of cells (1:1) were seeded back into treated wells. The growth pattern of the treated cells was then determined using the cell counts, which were multiplied by the splitting ratios.

2.2.8 Microscopy-Related Experiments

The general cellular morphology and growth patterns of all cell types were regularly examined using the Inverted Phase Contrast Microscope (Olympus CK30), after seeding, passaging, and treating the cells.

The transient transfection efficiency of HEK293T cells and the signal transmission of YFP expression (chapter 2.2.3.2) were examined using the EVOS® FL microscope through the GFP channel (470 nm excitation, 525 nm emission).

The fluorescent signal from immunofluorescent-stained samples was detected using the OLYMPUS IX50 Inverted Fluorescence Phase-Contrast Microscope (U_RFL_T Mercury Lamp). Images were acquired using the coupled XM10 camera and dedicated software cell-F (Olympus) with a customized acquisition system (same for all photos of the same experiment). A magnification of 60X objective (with a drop of Immersol™ 518F, ZEISS) and the universal condenser phase ring at position 5 were set for the imaging system. The DAPI signal was detected with the aid of UV light through the NU filter, and the AlexaFluor488 signal was measured through the WIBA filter. Exposure time was set to 50 msec for DAPI and 500 msec for AlexaFluor488. The brightness was adjusted to 50% for all images. Images were saved in TIF format with 72 dpi

2.2.8.1 Immuno-Fluorescent Staining

Fixing Solution: 4% Paraformaldehyde (PFA)

Permeabilization Solution: 0.2% Triton in 1X PBS

Blocking Solution/Antibody Diluent: 20% Horse Serum in 1X PBS

Nuclear Staining Solution: 1 µg/mL DAPI (ROTH)

Mounting Medium: 10% (w/v) Mowiol 4-88; 25% Glycerol; 0.2 M Tris Base pH 8.5; 2% (w/v) NaN_3

A number of 5-6 x 10^4 cells from the NG3 cells were seeded on each sterilized coverslip in a 12-well plate. The following day, the cells were washed three times with 1X PBS and then fixed with 600 µL of 4% PFA per well, which was incubated at RT for 20 min. After fixation, the cells were washed three times with 1X PBS and permeabilized by incubating with 500 µL of permeabilization solution at RT for 5 min. Cells were washed three times with 1X PBS, then blocked with 500 µL of blocking solution at 37 °C for 30 min before antibody staining. To do so, 60 µL of 1:100 diluted primary antibody was dropped onto a piece of Parafilm sheet, and the coverslips were then stored upside down on the respective drops of antibody at 37 °C in a moist chamber for 45 min. Afterward, the cells were washed three times with 1X PBS. A volume of 60 µL of a 1:1000 dilution of secondary antibody (against the origin of primary antibody) coupled with a fluorophore was added and incubated in a moist-dark chamber, in the cold room overnight. The cells were washed three times with 1X PBS and once with ddH_2O before the DNA was stained with 500 µL of 1 µg/mL DAPI (diluted in ddH_2O) at RT for 5 min. Finally, the coverslips were washed twice with ddH_2O and mounted onto a microscope slide with 10 µL Mowiol 4-88. The slides were stored horizontally at RT for 30 min and then transferred to 4 °C in the dark until microscopy.

2.2.9 FACS-Related Experiments

Fluorescence-activated cell sorting (FACS) experiment was done to analyze the cell cycle distribution and measure the DNA synthesis ability in treated iMEF dTAG clones. For FACS purposes, the cells were harvested at a final confluency of 50-60% (To avoid the major effect of the contact inhibition). The signal was acquired for 100,000 events per sample per experiment. The FACS Canto II (BD Bioscience, FACSDiva Software v9.0.1) machine is equipped with three Violet, Blue, and Red, with excitation wavelengths of 405, 488, and 633 nm, respectively. Output raw data was saved in FCS file format and analyzed with a licensed version of FlowJo software (BD Bioscience).

2.2.9.1 Cell Cycle Distribution Assay

Fixation/Permeabilization Concentrate (4X): Diluted 1:4 in Diluent solution.

Permeabilization Buffer (10X): Diluted 1:10 in ddH_2O.

In order to analyze the cell cycle distribution of WT and time-course treated iMEF dTAG clones, the eBioscience™ Foxp3/ Transcription Factor Staining Buffer Set (Invitrogen) in combination with Hoechst 33258 or Vybrant Dyecycle Violet dye was used. Treated cells were harvested by trypsinization and spun down at 500xg for 5 min at 4 °C. Cells were washed twice with 5 mL ice-cold 1X PBS at 500xg, for min at 4 °C. The pellet was then resuspended in 200 µL 1X PBS and 800 µL 1X Fixation/Permeabilization Buffer, vortexed thoroughly, and incubated for 15 min at RT, protected from light. Afterward, 2 mL of 1X Permeabilization buffer was added, and samples were directly centrifuged at 380xg for 3 min at RT. Cells were then resuspended in 1 mL ddH_2O with a final concentration of 1 µg/mL of Hoechst 33258, or 5 µM Vybrant Dyecycle Violet dye and incubated at 37 °C for 30 min. The cell suspension was then split into three parts and transferred to separate FACS tubes to generate three technical replicates for each biological replicate sample. Cells were then prepared for FACS counting. Hoechst/Violet signal was acquired in the Pacific Blue channel in a linear mode with a low speed. The percentage of the cell population in distinct phases of the cell cycle was determined using a manual gating method. G1 gate width was considered the same as G2 gate width (unconstrained), and the area under the curve was calculated as cell percentage.

2.2.9.2 EdU Incorporation Assay

1% Bovine Serum Albumin (BSA) in 1X Phosphate Buffered Saline (PBS), pH 7.1–pH 7.4

A Click-iT™ EdU Alexa Fluor™ 488 (AF488) Flow Cytometry Assay kit (Invitrogen) was used to analyze the DNA synthesis ability of WT and a time-course treated NG3 cells. The protocol was mainly followed as per the manufacturer's instruction, with one adjustment: the labeling with AF488-Conjugated EdU was done at a final concentration of 10 µM for 3 hours (3 hours before the harvesting time point). The DNA content was then stained using Vybrant Dyecycle Violet dye (at a final concentration of 5 µM) or Hoechst (diluted in ddH_2O with a final concentration of 1 µg/mL), and then incubated for 30 min at 37 °C. The samples signal was then acquired at a medium speed, with the following parameters:

Dye	Channel	Acquisition Mode
Hoechst 33258	Pacific Blue	Linear (Lin)
DyeCycle Violet	Pacific Blue	Linear (Lin)
AF488	FITC	Logarithmic (Log)

The percentage of FITC-Positive cells was determined using a manual gating method, with a threshold set above the FITC signal from non-EdU treated samples.

2.2.10 Next Generation Sequencing Experiments

Next generation sequencing (NGS) methods were applied to further delineate the effects of the corresponding treatment on a Genome-wide (GW) level in iMEF dTAG clones. The sequencing was

done in collaboration with the Interdisciplinary Center for Clinical Research (IZKF)-Genomic core facility. The following performed NGS experiments are described in detail.

2.2.10.1 Chromatin Immuno-Precipitation Followed by Sequencing (ChIP-seq)

Chromatin-Immunoprecipitation (ChIP) followed by sequencing was used to profile several transcription-associated histone modifications on a GW scale. For this purpose, the ChIP-IT High Sensitivity® kit (ActiveMotif) was used. The experiment was carried out according to the manufacturer's instructions with a few adjustments as follows: 1) For nuclei isolation, 60-70 strokes were applied using a 5 mL glass-dounce homogenizer with a tight (B) pestle. 2) The amount of chromatin used per IP was 30 µg and 100 µg for histone marks and ASH2L, respectively. 3) Chromatin shearing was conducted using the Bioruptor® Pico sonication device. 4) The sonication was performed on 300 µL of chromatin aliquot in a 1.5 mL Bioruptor® Pico microtube with a cap, for 4-5 rounds of 10 cycles (each cycle was 30s sonication/30s pause), until the majority of chromatin fragments were sheared down to ~200 bp. 5) Input DNA was precipitated using 2 µL of the carrier (provided and instructed by the kit) and the addition of 2 µL glycogen (20 mg/mL) (I observed that the reproducibility of the reaction and the quality of the precipitated input DNA noticeably improved).

ChIP-seq was performed in two biological replicates for WT and time-course treated ND10 (H3K4me3) and NG3 (H3K4me1, H3K4me2, H3K27ac, and H3K27me3) clones. Final Input and IPed DNA were sent to IZKF Genomic Core Facility for quality/quantity assessments. The concentration of samples was measured using the Quantus™ Fluorometer. Sample quality control/fragment size distribution was assessed using the Bioanalyzer system (Agilent). Samples were then indexed and adaptor-ligated using NEBNEXT Ultra II DNA Library Preparation Kit (NEB) according to the manufacturer's instructions. For all histone marks (except H3K27me3, known as broad histone mark) a ~350 bp (200 bp chromatin fragment size + 120 bp two adaptors size) size selection step was conducted prior to PCR library amplification. After PCR enrichment, samples were then PCR-cleaned up and prepared for launching on the sequencer platform. Samples were sequenced on a NextSeq 550 (Illumina) system using a NextSeq 500/550 High Output v2.5 (75 Cycles) cartridge (Single-End). The number of samples per cartridge was arranged in a way to provide a minimum of 40 – 50 M raw reads per ChIP sample.

2.2.10.2 Click-Based Nascent RNA Sequencing (Click-iT 3'mRNAseq)

In order to measure the alteration of nascent transcripts in ASH2L-depleted cells, the Click-iT RNAseq experiment was performed using the Click-iT™ Nascent RNA Capture Kit (Invitrogen). EU-modified nucleotide pulse labeling was done at a concentration of 0.2 mM for two hours (Minus/Plus one hour of the harvesting time-point). The experiment was conducted according to the manufacturer's instructions. After the final RNA pull-down, biotinylated RNAs were separated from the beads with the aid of the TRIzol reagent. Isolated RNA samples from two independent biological replicates were prepared and sent to the IZKF Genomic Core Facility. The concentration of samples was measured using the Quantus™ Fluorometer. Sample quality control/fragment size distribution was assessed using the Bioanalyzer system (Agilent). Isolated RNA samples with an RNA Integrity Number (RIN) higher than 9 were validated for further sequencing analysis. Construction of cDNA libraries from RNA samples was done using the Collibri™ 3´ mRNA Library Prep Kit (Invitrogen). Samples were sequenced on a NextSeq 550 (Illumina) system using a NextSeq 500/550 Mid Output v2.5 (75 Cycles)

cartridge (Single-End). The number of samples per cartridge was arranged in a way to provide a minimum of 20 M raw reads per 3'mRNAseq sample.

2.2.11 Statistical Analysis

Prism software (GraphPad) version 9 was used to perform the statistical analysis of the data. To evaluate the distribution of cells in different phases of the cell cycle between the control and treated groups, and to assess the null hypothesis in cell cycle analysis, a non-parametric Mann-Whitney test was used. The p-values 0.05 *, 0.01 **, 0.001 ***, and 0.0001 *** were used to calculate significance.

2.2.12 Bioinformatics Analysis

2.2.12.1 Computational NGS Data Analysis

Computational analysis was conducted by Dr. Mirna Barsoum to analyze the sequencing raw data. The ChIP-seq analysis involved four distinct steps: pre-processing, alignment, normalization, peak calling, and differential analysis. The demultiplexed raw FastQ files underwent quality control assessment using the MultiQC tool. To map the low-divergent sequences of the ChIP-seq data against mm9 mouse reference genome (H. Li & Durbin, 2009), the BWA software package was employed. Normalization was then performed by scaling the data to the lower depth sample within a consistent ChIP-seq dataset. The data was normalized to the lowest coverage in each comparison. The normalized data was then used as input for the differential analysis using Deseq2. Subsequently, the true peaks were identified using the MACS2 (Model-based Analysis of ChIP-seq) tool (Y. Zhang et al., 2008). Finally, a comparative analysis of the identified binding regions was conducted using the DESeq2 method (Love et al., 2014). The significance of the differential analysis was determined based on a false discovery rate smaller than 0.05.

Computational analysis for 3'mRNAseq and Click-RNAseq was conducted by Dr. Mirna Barsoum, involving a series of five essential steps: trimming, alignment, annotation, Spike-in normalization, and differential analysis. Initially, the reads were subjected to trimming using Trim-Galore, a powerful tool available at https://www.bioinformatics.babraham.ac.uk/projects/trim_galore/. After trimming, the reads were aligned to the mouse reference genome, with mm9 being used for 3'mRNAseq and later mm10 for Click-RNAseq, employing the STAR alignment software (Dobin et al., 2013). Subsequently, the aligned reads were assigned to the annotated genes within the respective reference genome using FeatureCounts (Liao et al., 2014). For normalization purposes, the Spike-in ERCC (External RNA Control Consortium, Invitrogen) counts were employed. Finally, the differential analysis was performed using Deseq2. For more information, please visit the M&M section of Barsoum et al., 2023.

2.2.12.2 Downstream NGS Data Analysis

The downstream analysis was performed on computationally generated data, curated by Dr. Mirna Barsoum, from Next-Generation Sequencing (NGS) experiments. The gene ontology (GO) term analysis was conducted using a functional enrichment web server (https://biit.cs.ut.ee/gprofiler/gost) (Raudvere et al., 2019) on a list of RefSeq IDs for the genes of interest. The enriched KEGG pathways were analyzed based on the Benjamini-Hochberg False

Discovery Rate (FDR) value with a threshold of 0.01. A transcription factor enrichment analysis was also performed using the Enrichr web-based tool based on the PWMs (Position Weight Matrix) of TRANSFAC and JASPAR datasets (https://maayanlab.cloud/Enrichr/) (E. Y. Chen et al., 2013). Gene names were used as input IDs, and only those transcription factors with an adjusted p-value less than 0.01 were selected for further analysis and plotting purposes. Additionally, a heatmap visualization approach was employed using the gplots package library, Heatmap2 function, within the RStudio environment (version 2023.3.0.386, R version 4.2.2) for the differentially analyzed data.

3 Results

In order to investigate the function of ASH2L as a core subunit of Histone 3 Lysine 4 methyltransferases, this study has utilized a rapidly-evolving PROTAC technology to implement a quick-acting targeted protein degradation method.

Numerous experiments were conducted throughout this study to elucidate diverse facets of the cellular and molecular functions of the ASH2L protein. The findings of these experiments were categorized into five main sections. The first section details the procedure of generating inducible KD cells utilizing dTAG degron system and expands on the isolation and confirmation of monoclonal cells expressing ASH2L-FKBP^{F36V} fusion protein. Furthermore, the second section describes the evaluation of the cellular and molecular phenotypes of the induced-KD cells. Whereas in the third section, the aim is to describe the NGS-based methodology used to investigate the role of ASH2L in maintaining epigenetic homeostasis in immortalized mouse embryonic fibroblast (iMEF $^{Ash2l\ -/-}$) cell lines. In the fourth section of the study, the author presents the findings related to transcription analysis and illustrates the key findings. Moving on to the fifth section, a comprehensive analysis is conducted to examine the correlation between the results obtained from various NGS methodologies.

3.1 Generation and Characterization of PROTAC-Induced ASH2L KD iMEF Cells

Ash2l, also referred to as Absent, Small, or Homeotic discs 2-like, is a trithorax-group protein member initially identified in *Drosophila*. It is known to play important roles in epigenetic regulation of gene expression and maintenance of cellular homeostasis in *Drosophila* (Ikegawa et al., 1999; Kennison, 1995; LaJeunesse & Shearn, 1995; Mazo et al., 1990) and mammalian cells (Dou et al., 2006; Steward et al., 2006; Stoller et al., 2010).

Ash2l together with SET1 family catalytic subunits and several essential core components, including WDR5, RBBP5, and a homodimer of DPY30, forms the KMT2 complexes (Steward et al., 2006). The so-called KMT2 complex is able to deposit a methyl functional group to the Lysine 4 residue at the N-terminal tail of the histone 3 protein present in the nucleosome structure predominantly located at promoter regions. The resulting H3K4me3 histone mark is known to be linked to active gene transcription (Bernstein et al., 2005; Lauberth et al., 2013).

Ash2l has been implicated in a variety of biological processes, including hematopoiesis, embryonic development, and cancer progression (T. J. Chen et al., 2022; Lüscher-Firzlaff et al., 2008; Lüscher-Firzlaff et al., 2019; Shah et al., 2019). However, the mechanism by which the disruption of Ash2l results in abnormal cell proliferation and oncogenesis is not yet fully comprehended.

In prior studies carried out in Prof. Lüscher's laboratory to investigate the function of Ash2l in various molecular and cellular aspects, a conditional KO system was employed to study the loss of function of

Ash2l in iMEF cells (Bochyńska, 2023; Liang, 2016). In this system, a steroid-like compound called 4-Hydroxytamoxifen (referred to as HOT system) was used to induce a recombination/excision reaction between two flanking floxed arms located around both sides of the *Ash2l* exon 4 genomic region. This reaction results in an RNA frameshift and gain of a nonsense mutation within the *Ash2l* locus, leading to no protein production. This was achieved with the assistance of a constitutively expressed Cre-ER fusion recombinase (Figure S1). After inducing the *Ash2l* KO, caused by deletion of *Ash2l* exon 4, cell proliferation ceased within 5 days, and global RNA transcription was deregulated. Additionally, the cells developed a flat and enlarged morphology and showed positive staining for beta-Galactosidase (beta-Gal), a known attribute of senescent cells (Bochyńska et al., 2022). Due to the extended half-life of the Ash2l protein, the investigation of the direct effects of Ash2l loss after a complete knockout was limited to a slow pace of 5 to 7 days. This duration of time could be confounded by other secondary and tertiary consequences of gradual protein loss, which may be difficult to disentangle.

Hence, the current study tried to elucidate the mechanism underlying ASH2L dysregulation utilizing a rapid and efficient PROTAC-inducible targeted protein degradation approach (referred to as the dTAG system) based on the previously established maternal HOT cell system. The dTAG system with the aim of targeted protein degradation was first described by Nabet and colleagues (Nabet et al., 2018). A PROTAC compound (dTAG-13 here) is a heterobifunctional compound that possesses two binding ligand sites connected by a linker molecule. It simultaneously binds to the $FKBP^{F36V}$ degradable domain (12-kDa cytosolic prolyl isomerase engineered variant) fused N-terminally/C-terminally to the human ASH2L protein, and the CRBN (Cereblon) receptor of an E3 ligase complex. This interaction facilitates the proximity of the ASH2L-$FKBP^{F36V}$ fusion protein to the ubiquitin ligase, resulting in the addition of ubiquitin molecules and guiding the fusion protein toward the proteasomal machinery for degradation (Figure 3).

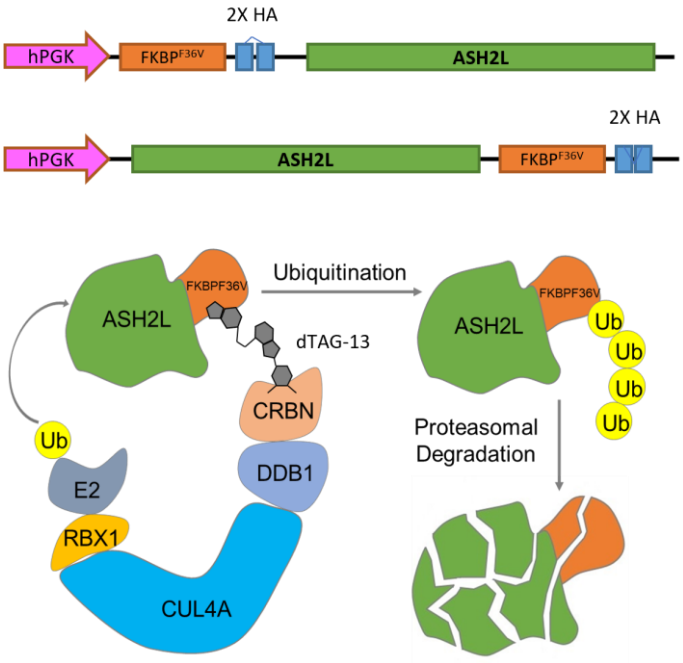

Figure 3: The Schematic of dTAG-13-Induced Degradation of ASH2L-$FKBP^{F36V}$. A thalidomide-derived heterobifunctional compound (dTAG-13) binds to the CRBN substrate receptor of the E3 ligase, connected through a linker to a degron domain of the ASH2L-FKBP fusion protein. This interaction brings the fusion

protein in proximity to the E3 ligase complex, resulting in the addition of the Ub group to the target protein and, eventually, its degradation facilitated by dTAG-13. Adapted from Nabet. et al. *Nat Chem Biol*, (2018).

As outlined in the Methods chapter, HEK293T cell lines were transfected with gateway amenable constructs containing a pLEX305 backbone that encodes for *ASH2L* tagged with *FKBP*^{F36V} at both the N- and C- terminal, in addition to lentiviral packaging vectors (2nd generation). The resulting lentiviral particles were utilized to transduce maternal iMEF cells (Bochyńska et al., 2022). Subsequently, iMEF cells expressing ASH2L-FKBP^{F36V} were selected for puromycin resistance, and the resulting transduced iMEF cell pools were evaluated for the expression of the fusion protein (86.5 KDa for N-terminal ASH2L-FKBP and 84 KDa for C-terminal ASH2L-FKBP) before monoclonal isolation was performed (data not shown).

3.1.1 Monoclonal Cell Lines Isolation, Validation, and dTAG-13 Induced Degradation

Single-cell clones were isolated from transduced pools under KO induction conditions. The recovered monoclonal cells (NB5, NG3, ND10; N-terminally tagged, and CA1; C-terminally tagged) were subsequently assessed for equal expression levels of exogenous fusion protein with the maternal endogenous Ash2l. The clones were additionally examined for the nuclear localization of the ASH2L-FKBP fusion protein, to validate their suitability for the study (Figure 4A, and B, and Figure S1). Additionally, it was confirmed, using a conventional nested PCR approach, that the single-cell clones efficiently lost their *Ash2l* exon 4 genomic locus (Figure S1).

Afterward, single-cell clones were treated with the dTAG-13 compound to evaluate its dose and time dependence. The treatment assay demonstrated very rapid and efficient induced degradation of the ASH2L-FKBP fusion protein with the final selected dose of 100 nM of dTAG-13 as early as half an hour (Figure 4). A western blot analysis was conducted on a dilution series of the cell lysate, which was estimated to have an ASH2L-FKBP KD efficiency of equal or greater than 99.9% in the isolated single-cell clones (Figure S2).

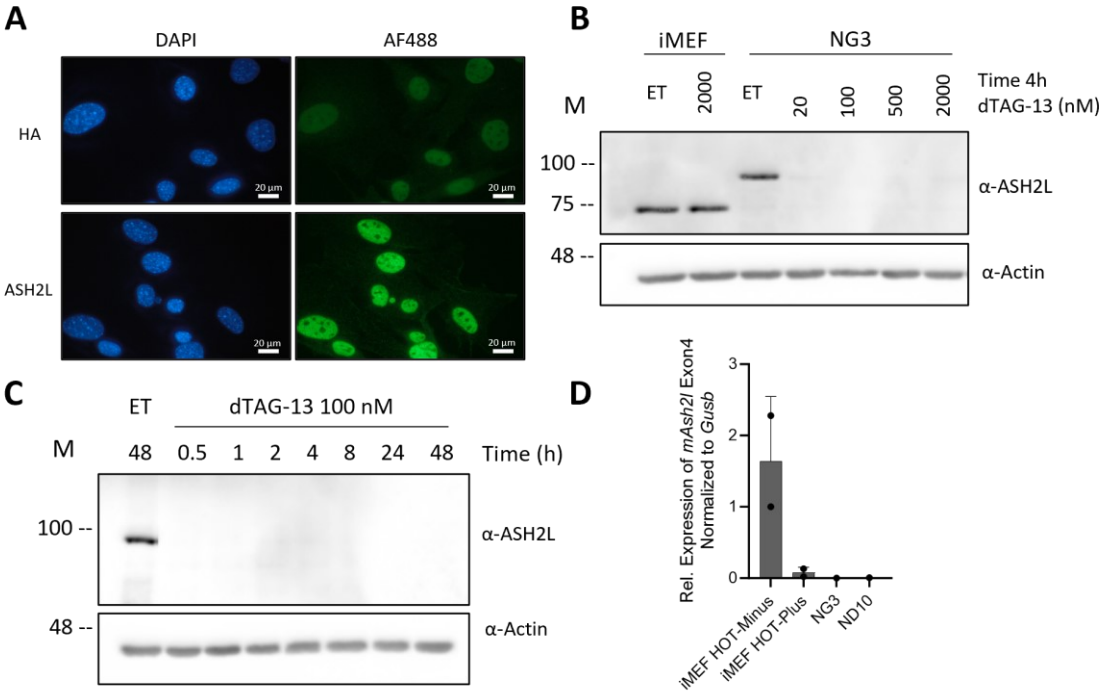

Figure 4: Validation of Isolated Monoclonal Cells. (A) The untreated NG3 clone was fixated with 4% PFA on a glass slide and stained with primary antibodies against HA and ASH2L. Nuclei were stained with DAPI, and the cells were visualized using DAPI and AF488 setups with fluorescent microscopy, as detailed in Chapter 2.6.8. The scale bar indicates 20 µm. (B) Cell lysates prepared from NG3 and maternal iMEF cells treated with dTAG-13 at serial concentrations, and with ethanol as the vehicle control, were used for western blotting. 20 µg of each lysate was loaded for analysis. Treatment was carried out for 4 hours in cell culture for each concentration. Actin served as an internal control, and an antibody against ASH2L was used for knockdown (KD) evaluation. (C) Cell lysates prepared from NG3 treated with 100 nM dTAG-13 and ethanol as the vehicle control were used for western blotting. Treatment was conducted in a time-course manner in cell culture. 20 µg of each lysate was loaded for analysis. Actin served as an internal control, and an antibody against ASH2L was used for KD evaluation. (D) Quantitative PCR was performed on RNA extracted from maternal iMEF treated with HOT and vehicle control, ND10, and NG3 clone. Primers detecting exon 4 of *Ash2l* mRNA was used for the reaction. The values were normalized to the determined housekeeping gene, *Gusb*. Two biological replicates, each performed in two technical replicates per reaction, were considered for the maternal iMEF cells. Bars indicate the standard deviation (SD) for the samples. All experiments were done by the author.

3.1.2 ASH2L-FKBP Expression Recovery with the Aid of Lenalidomide

The re-expression of knocked-down proteins is known as a valuable approach to study the dosage effect of protein expression and confirm the discovered roles of the KD protein. Several PROTACs (including dTAG-13) have been shown to be reversible in *in vivo* experiments and can be washed out from cells (Fischer et al., 2014; Kiely-Collins et al., 2021; Nabet et al., 2018). However, in the present study, the washout of dTAG-13 from iMEF cells was very slow as estimated from ASH2L-FKBP re-expression (data not shown). Therefore, this study took advantage of using lenalidomide that shares the properties of the dTAG-13 CRBN binding site (a Thalidomide-derivative). Thus, lenalidomide competes with dTAG-13 for binding to CRBN but does not interact with ASH2L-FKBP. As a consequence, ASH2L-FKBP expression recovered within one hour upon addition of 10 to 50 µM lenalidomide (Figure 5, and Figure S3).

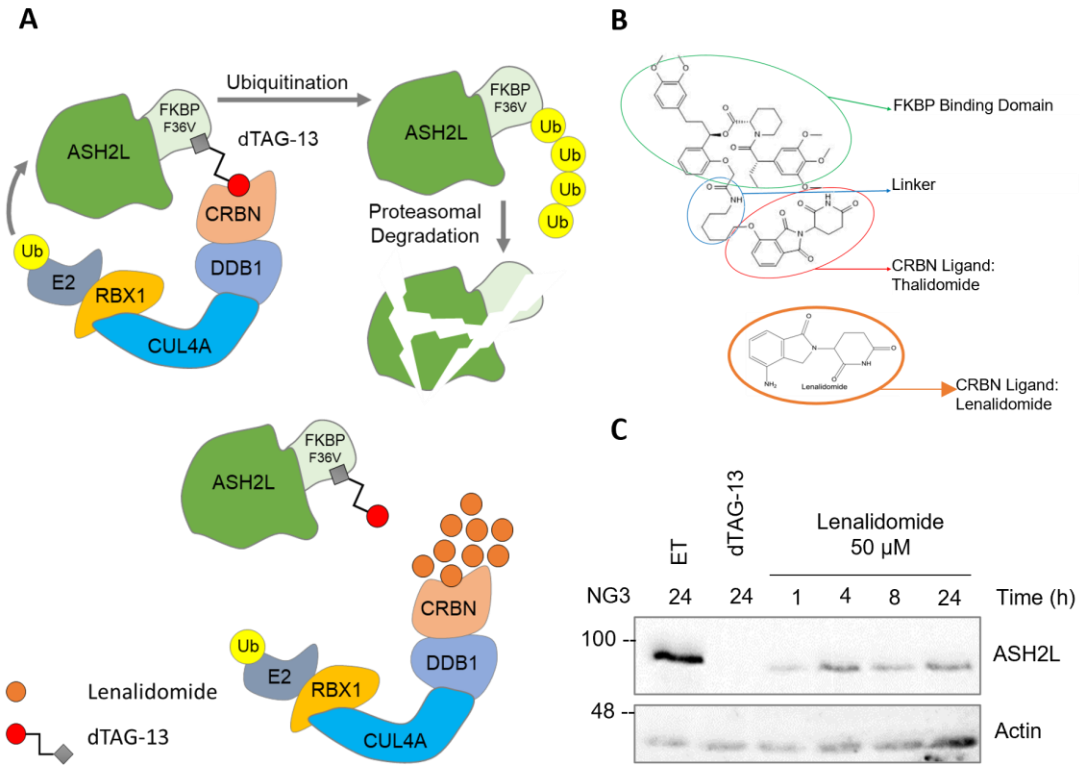

Figure 5: The Rescue of ASH2L-FKBPF36V Expression. (A) A schematic of lenalidomide's mechanism of action through competitive binding to the CRBN subunit of the E3 ligase complex. (B) Molecular structures of dTAG-13 and lenalidomide (a thalidomide derivative). (C) NG3 cells were treated for 24 hours with dTAG-13 or the vehicle control. Another set of dTAG-induced cells for 24h were further treated with 50 µM lenalidomide for 1, 4, 8, and 24 hours. Total cell lysates were used for western blotting. Actin detection served as a loading control, and an antibody against ASH2L was used to evaluate the re-expression of the fusion protein. 20 µg of each lysate was loaded for analysis. The experiment in panel C was done by the author.

3.2 The Effects of ASH2L Loss on Cell Biological Aspects of KD-Induced iMEF Single Cells

3.2.1 ASH2L Loss Impairs Cell Proliferation and DNA Synthesis Abilities in KD Clones

ASH2L is known to play a critical role in regulating gene expression during development and differentiation. Several studies have shown that the deregulation of ASH2L correlates with abnormal cell proliferation and cell cycle distribution in multiple cell types (Ali et al., 2014; Bochyńska et al., 2022; Campbell et al., 2019; L. Li et al., 2019; Lüscher-Firzlaff et al., 2019; Mohammadparast & Chang, 2022; Stoller et al., 2010; Z. Yang et al., 2014).

In previous studies, it was observed that *Ash2l* KO in iMEF cells stopped proliferation and induced cellular senescence five days after HOT treatment (Bochyńska, 2023; Bochyńska et al., 2022). In the current study however, it was demonstrated that the treatment of NG3 cells with 100 nM dTAG-13 resulted in a rapid and substantial inhibition of cell proliferation, with effects observed as early as two days after treatment, as depicted in Figure 6A. Interestingly, lenalidomide-induced re-expression of the ASH2L fusion protein reversed the effect of dTAG-13 treatment. Cells resumed proliferation within three days after treatment (from day 6 to day 9). Flow cytometry analysis was conducted to investigate cell cycle distribution (Appendix 1, and 2). The results showed a tendency to accumulation of cells in the G1 phase after day 1 of treatment, which increased slightly on days 2 and 3. Thus, this did not result in any specific cell cycle arrest, as shown in Figure 6B.

However, the reduction by half in the number of cells in S phase raised the question of whether the decrease of DNA synthesis is attributable to the loss of ASH2L before ceased proliferation. To investigate this possibility, a further analysis was performed using flow cytometry and staining for 5-ethynyl-2'-deoxyuridine (5-EdU) incorporated into the newly synthesized DNA. The results, depicted in Figure 6C, showed that the loss of ASH2L did not significantly affect DNA synthesis ability at 8h treatment, but a significant reduction was observed after 1 day of dTAG-13 treatment.

As demonstrated in this study for NG3 and other single-cell clones (Figure S4) and previously reported (Barsoum et al., 2023; Bochyńska et al., 2022), loss of ASH2L is associated with loss of cell proliferation. The dTAG-induced clones (also referred to as KD clones in this study) exhibit impaired DNA synthesis and tend to accumulate in the G1 phase. These effects can be reversed upon lenalidomide-induced restoration of the ASH2L-FKBP fusion protein (Figure S4).

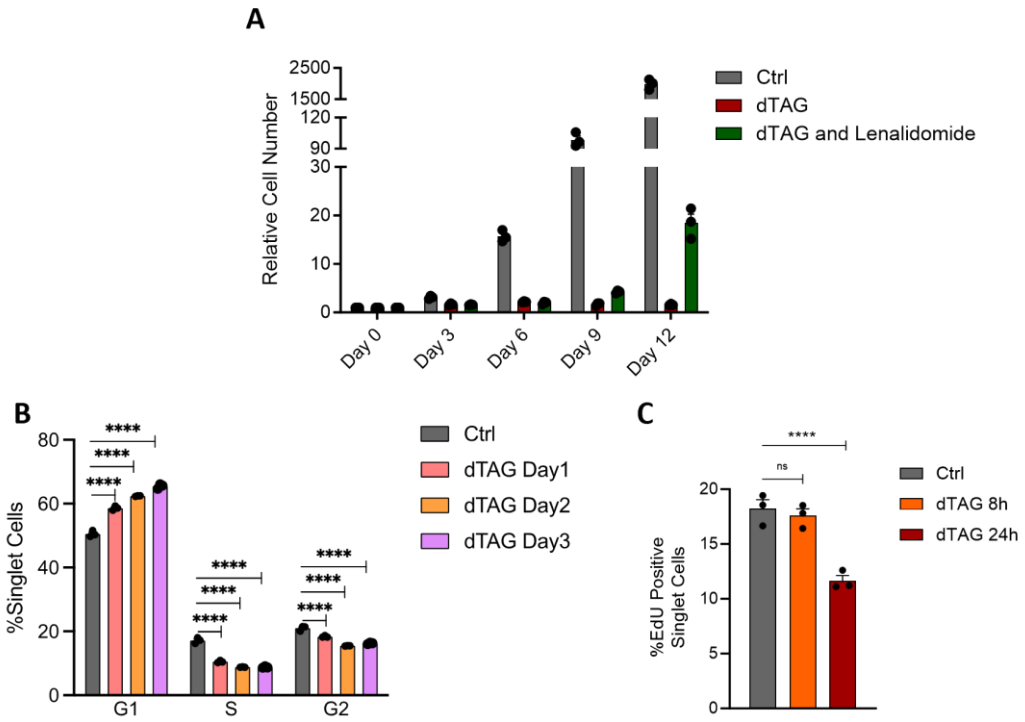

Figure 6: Loss of ASH2L Leads to Ceased Cell Proliferation and Impaired DNA Synthesis Ability. (A) NG3 cells were treated with the vehicle control or 100 nM dTAG-13 for a period of 12 days. Every 3rd day, the cells were detached, counted, and seeded back into the cell culture plates. A subset of cells was initially treated with dTAG-13 for 6 days, followed by 10 µM lenalidomide treatment for an additional 6 days. The experiment was performed in three biological replicates, with each replicate measured three times. Error bars indicate the SEM for the samples. (B) NG3 cells were treated with the vehicle control or 100 nM dTAG-13 for a time course of 1, 2, and 3 days. Cells were fixed and stained with DyeCycle Vybrant Violet. The cell cycle phase distribution histogram was obtained with FACS and analysed with FlowJo software. The experiment was performed in three biological replicates, each containing three technical measurements. Error bars indicate the SEM for samples. Significance was assessed using the Mann-Whitney test, and asterisks represent a p-Value < 0.0001 (****). (C) NG3 cells were treated with the vehicle control or 100 nM dTAG-13 for 8 and 24 hours. The cell culture was treated with 5-EdU for three hours according to chapter 2.6.9.2. The cells were then fixed and labelled with AF488 dye and stained with DyeCycle Vybrant Violet for DNA content. The reactions were then measured in three biological replicates, each containing three independent measurements using the FACS machine. Error bars indicate the SEM for the samples. Significance was assessed using the Mann-Whitney test, and asterisks represent a p-Value < 0.0001 (****), and "ns" indicates p-Value > 0.05. All the experiments were done by the author.

3.2.2 Loss of ASH2L Leads to a Global Deregulation of Transcription-Associated Histone Marks

ASH2L, a component of the KMT2 complex, is crucial for the deposition of the active promoter histone mark H3K4me3 (Shilatifard, 2012). As expected, the knockdown of ASH2L in NG3 cells resulted in a significant reduction in H3K4me3, indicating a 50% depletion of this histone mark after 2 hours treatment (Figure 7). However, upon treatment with lenalidomide, the recovery of lost H3K4me3 was slow (Figure S5). This suggests that the demethylation process is potentially facilitated by demethylase enzymes and occurs faster than the gain of enzymatic activity upon re-expression of the ASH2L-FKBP fusion protein. Conversely, the effect of ASH2L knockdown on declined H3K4me1 levels are slower and emerge at a later time point (Figure 7, Figure S5). This suggests that the loss of

the ASH2L component affects the catalytic activities of the KMT2 complexes at different levels, with the monomethyltransferase activity being less sensitive than the trimethyltransferase activity. This could also potentially be due to differences in their corresponding lysine demethylase activities.

Moreover, active genes are typically marked by both H3K4me3 and H3K27ac (Igolkina et al., 2019; Ullius et al., 2014; W. Zhao et al., 2021), with H3K27ac also being an "activating mark" found at enhancer regions that regulate gene expression (Creyghton et al., 2010; Dorighi et al., 2017). Subsequently, this mark appears to be affected by the loss of ASH2L at late time points (Figure 7).

On the other hand, H3K4me3 and H3K27me3 are two opposing histone modifications in gene regulation, where H3K4me3 is associated with active gene transcription and H3K27me3 with gene repression (Blanco et al., 2020). Interestingly, these two marks can coexist at certain genomic regions, forming a bivalent chromatin state. This bivalency has been observed in pluripotent stem cells, where genes important for differentiation are kept in a poised state until the cells receive appropriate differentiation signals (Bernstein et al., 2006; Blanco et al., 2020). However, no significant global change in the H3K27me3 level was observed within the experimental time frame (Figure 7).

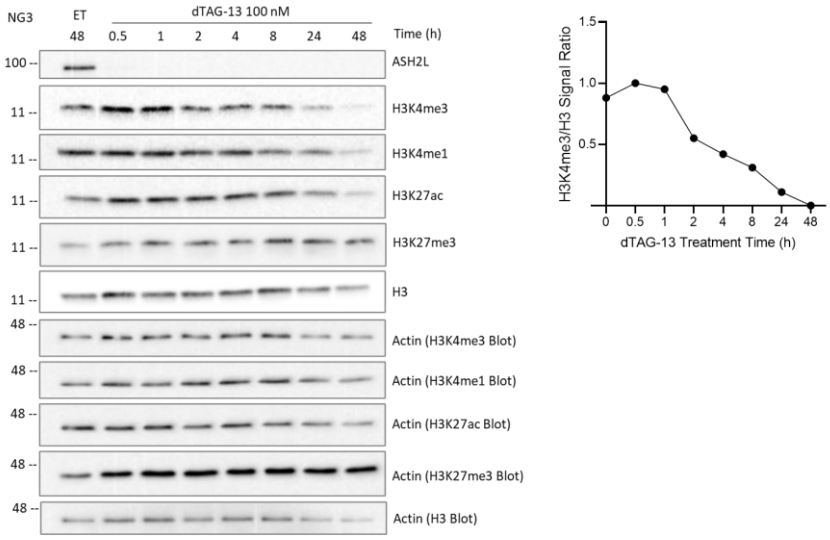

Figure 7: Deregulation of Transcription-Associated Histone Marks in Response to ASH2L. On the left panel: NG3 cells were treated over a time course with 100 nM dTAG-13 or the vehicle control for 48 hours. Total cell lysates were utilized for western blotting. Actin detection served as a cell lysate loading control, and an antibody against ASH2L was employed to assess the expression of the fusion protein. Antibodies against various histone modifications were used to determine the global levels of H3K4me3, H3K4me1, H3K27ac, and H3K27me3. H3 expression served as a histone loading control. 5 µg of each lysate was loaded for analysis. On the right panel: Quantification was applied to the H3K4me3 blot. The H3K4me3/H3 ratio was calculated based on the band intensities using Image J software. All the experiments were done by the author.

3.2.3 dTAG-13 Induced Degradation of ASH2L-FKBP Has A Slight Effect on ASH2L Interactors Protein Level

Utilizing a PROTAC system, a question arises as to whether ubiquitination can occur on POIs that are part of a complex.

It has been studied that the E2 ubiquitin ligase adds the Ubiquitin at approximately 46° (~4.5 nm) to another protein in its proximity, in a closed conformation (Branigan et al., 2020). However, the

distance between the ASH2L and SET subunit in the KMT2 complex has been calculated in the Cryo-EM structure to be about 21-30° (2-3 nm) (Y.-T. Lee et al., 2021). To address this, a blotting analysis was performed to detect alterations in the protein level of some of the main interactors of ASH2L, such as WRAD components. A slight decrease in the protein levels of Wdr5 and Rbbp5 was detected (Figure 8, Figure S6). However, this was mainly observed at later time points, which could be attributed to the overall adverse effects of ASH2L loss on the cell's total transcriptomic or proteomic content. The MYC oncogene has been reported to regulate gene expression by interacting with KMT2 components such as ASH2L (Ullius et al., 2014) and WDR5 (Thomas et al., 2015). However, Myc expression analysis revealed only a slight increase in the protein level (Figure S6), which is somewhat surprising knowing that the proliferation stops after 2 days treatment.

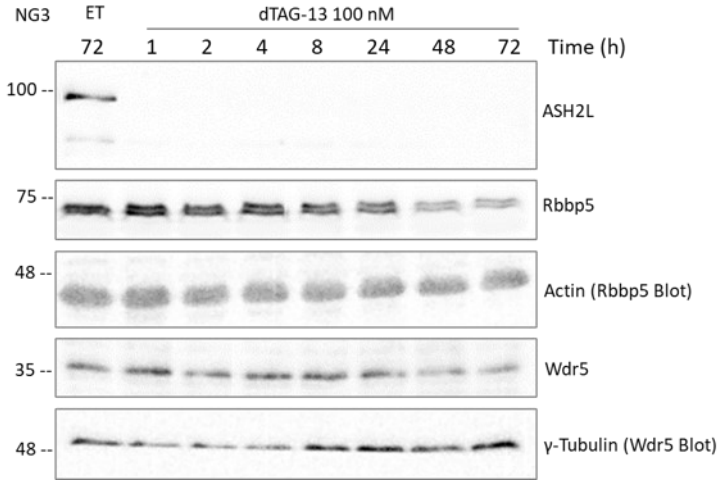

Figure 8: The Response of KMT2 Components Occurs Later Following dTAG-13 Treatment. NG3 cells were treated over a time course with 100 nM dTAG-13 or the vehicle control for 72 hours. Total cell lysates were utilized for western blotting. Actin detection served as a cell lysate loading control for Rbbp5 blot membrane. Tubulin detection served as a cell lysate loading control for Wdr5 blot membrane and an antibody against ASH2L was employed to assess the expression of the fusion protein. 20 µg of each lysate was loaded for analysis. All the experiments were done by the author.

3.3 ASH2L Loss Impacts Genome-Wide Distribution of Transcription-Associated Histone Marks

Epigenetic marks refer to modifications of DNA and histone proteins that do not alter the primary genetic sequence but have the ability to manage gene expression and impact various cellular processes. These marks include DNA methylation, histone modifications, and non-coding RNA molecules, all of which can impact gene expression in diverse ways. Understanding the mechanisms by which these marks are established and maintained is critical for understanding normal development and disease. This study aimed to investigate the changes in various histone marks in response to the loss of ASH2L over time in order to determine the sequence of events. In pursuit of this goal, the study utilized a ChIP-seq to examine and analyze the resulting changes.

3.3.1 ASH2L Induced-KD Leads to a Decrease of H3K4me3 at Promoters in NG3 Cells

H3K4me3 facilitates transcription by enabling the recruitment of proteins necessary for transcriptional initiation (Lauberth et al., 2013; van de Lagemaat et al., 2018). "Reader" proteins

recognize the H3K4me3 modification and assist in the recruitment of components of the transcriptional machinery to the promoters (Beacon et al., 2021; Nishioka et al., 2002; Vermeulen & Timmers, 2010).

To further investigate H3K4 methylation, ChIP-seq analysis targeting the H3K4me3 mark was performed in WT and dTAG-13 treated NG3 cells. A heatmap was generated to visualize the signal distribution 3 kb upstream and downstream of the TSS of all mm9 transcripts, which revealed a considerable decrease in the average signal intensity within the aforementioned window at 2 hours post-treatment (Figure 9A). The differential analysis identified 1067 (2h KD), 7249 (4h KD), 15373 (8h KD), and 16859 (16h KD) binding sites with Log2FC<-0.58, and FDR<0.05, which were designated as loss peaks and plotted in the depicted MA plots (Figure 9B, and Table S1). A notable variability was observed in the pace of H3K4me3 decrease at different promoters following the loss of ASH2L. The examination of the TSS region of the relatively slow promoters revealed a complete loss of ASH2L binding in a ChIPqPCR analysis (Figure S7A-B). This suggests that other mechanisms may be responsible for maintaining the H3K4me3 mark at these slow promoters, than the persistence of ASH2L binding after an induced KD.

A few gain peaks with a Log2FC>0.58, and FDR<0.05 were also observed at later time points, which could be separated in two groups (Table S2). The first small group comprised peaks that initially displayed a very low signal in IGV, mainly intergenic regions, potentially due to technical artifacts. The second smaller group consisted of peaks located at the gene body or promoter of highly enriched H3K4me3 genes (*Sfi1*, *Rn45s*) that also remained resistant to ASH2L loss within the examined time frame (Figure S7C).

A comparable ChIP-seq experiment was conducted in a time series and assessed the reproducibility of the data obtained from NG3 in the sister ND10 clone (Figure S8-10). However, owing to the low sequencing depth, the number of peaks and the resolution of the differential analysis are considerably lower than those of the NG3 experiment. Nevertheless, the overall results confirm the findings discussed subsequently (ND10 results shown in Figure S7-10).

3.3.1.1 Genomic Annotation of the Deregulated H3K4me3 Binding Sites

To investigate the genomic distribution of the altered binding sites, two categories of genomic locations were analysed: peaks within the 3 kb window upstream and downstream of the TSS, and peaks located elsewhere in the genome (also referred to as intergenic regions). Grouping the differential peaks based on their proximity to the TSS indicated that the majority of lost signals occurred within the TSS window, suggesting a significant role of ASH2L and resulting H3K4me3 in gene transcription. Conversely, a few gained peaks appeared to be randomly distributed in intergenic regions (Figure 10A).

3.3.1.2 Characterization of the H3K4me3 Altered Promoters

CGIs have been demonstrated to recruit TrxG and PxG (van de Lagemaat et al., 2018). A strong correlation between H3K4me3 and CpG density at promoter regions in human and mouse cells has also been suggested (Mikkelsen et al., 2007). CxxC zinc finger (ZF-CxxC) domain-containing proteins such as CFP1, MLL1, MLL2, KDM2A, and KDM2B are also known to bind to CGIs (Long, Blackledge, et al., 2013). Hence, the question arises as to how susceptible CpG-rich promoters are to the loss of ASH2L. To address this question, a comparison was made between promoters with altered H3K4me3

binding sites and annotated CpG-enriched promoters (enriched within 1 kb upstream and downstream of TSS). It has been postulated that approximately 70% of vertebrate promoters feature a CGI (Long, Sims, et al., 2013; Saxonov et al., 2006). Based on the annotation of CpG-enriched regions in mm9 curated by Dr. Mirna Barsoum, 12,595 promoters were identified to contain at least one CGI at 1 kb window of the TSS (Table S3). However, the total number of promoters in mm9 is 37,311. In other words, approximately 33% of all mm9 promoters were counted as CGI-associated promoters in mm9 genome. In order to investigate potential specific alterations in histone modification patterns at CGI-associated promoters during the brief modulation period of ASH2L, a comprehensive analysis was conducted involving the intersection of dysregulated promoters and those associated with CpG Islands. Somewhat unexpectedly, despite the previously established correlation between H3K4me3 and CGI-associated promoters (Mikkelsen et al., 2007), the proportion of CpG promoters affected by the loss of ASH2L did not exhibit any remarkable enrichment in H3K4me3-depleted promoter group. These observations indicate no noteworthy disparity in the susceptibility of CpG promoters, compared to other promoters, to H3K4me3 mark depletion following the loss of ASH2L (Figure 10B).

A GO Term and TF-enrichment analysis were conducted to uncover the functions and pathways associated with the H3K4me3 loss promoters. The enriched KEGG pathway observed in the analysis were consistent with the observed cell biological downstream effects of ASH2L loss, including cell cycle, cellular senescence, and DNA replication (Barsoum et al., 2023; Bochyńska et al., 2022) (Figure 10C). The analysis of transcription factor enrichment was performed on the list of the promoters that exhibit a depletion of the corresponding mark within 3 kb upstream and downstream of the TSS. The results confirmed the significant involvement of various transcription factors associated with cell cycle regulation and CGI-associated gene transcription, such as SP1 (Höller et al., 1988) and EGR1 (Zandarashvili et al., 2015) (Figure 10D). There has been a few studies indicating a probable gain of repressive DNA methylation at CGIs resulting from the loss of H3K4me3 (Balasubramanian et al., 2012; Zardo, 2021). However the gain of DNA methylation may not be sufficient to silence the respective promoter, given that these two transcription factors can bind to methylated CGIs and drive transcription (Huang et al., 1997; Kubosaki et al., 2009; Sun et al., 2019). It is important to note, since the TF binding information has been derived from public databases, compelling experimental data for their actual binding is lacking, and therefore it has to be further verified for drawing solid conclusion.

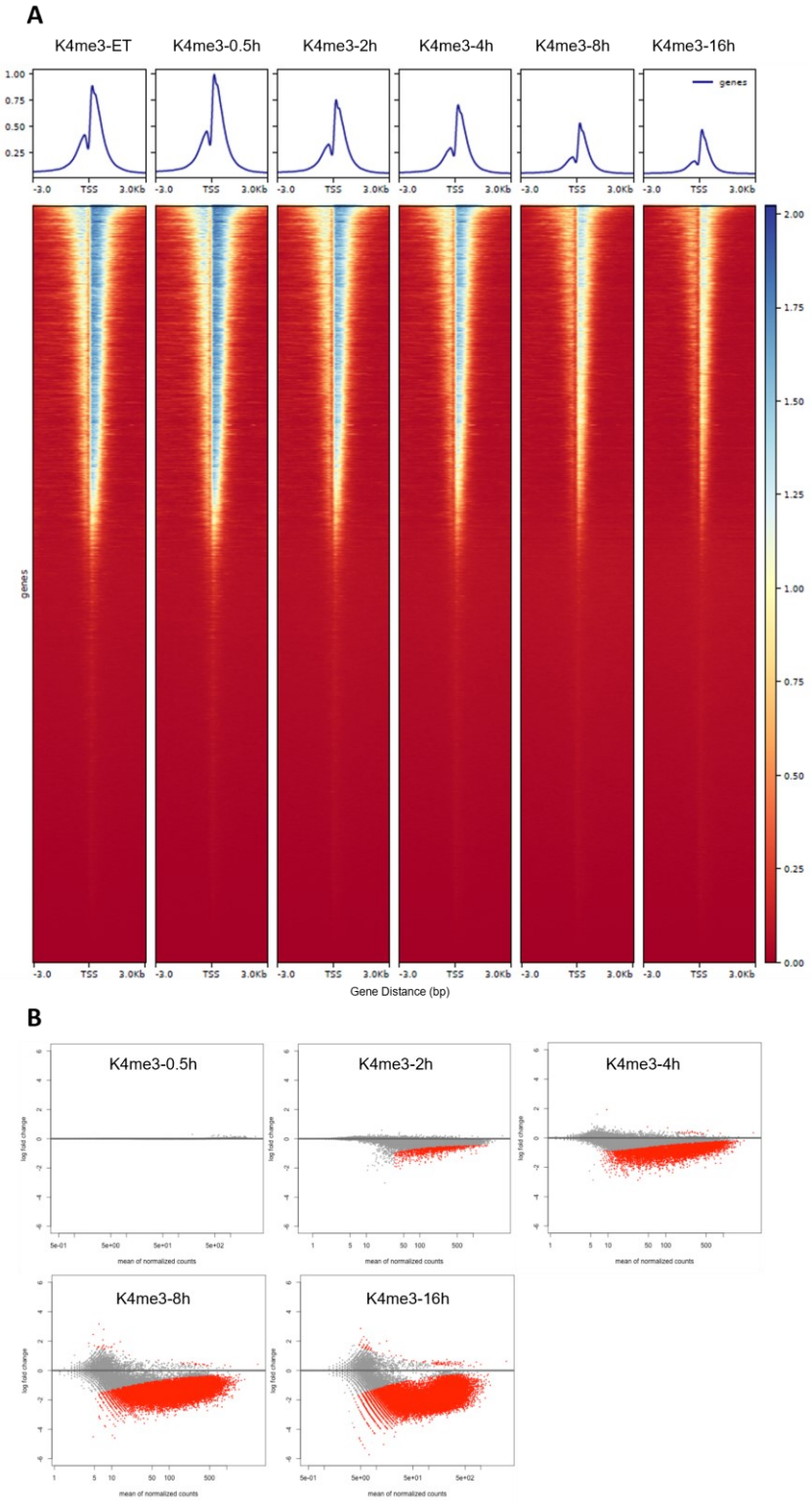

Figure 9: Loss of ASH2L Leads to Depletion of H3K4me3 at Promoter Regions. (A) NG3 cells were treated in a time-course manner with 100 nM dTAG-13 and subjected to chromatin immunoprecipitation using an H3K4me3 antibody, followed by sequencing (two technical replicates for each time point). The signal density (merged from two replicates and normalized to RPM), mapped against the mm9 reference genome, is represented as a heatmap in the figure. The distribution density is normalized between samples, demonstrating the signal within a 3 kb window around the TSS regions of all genes. (B) For the differential analysis performed on the deregulated peaks, an MA plot was generated (Y-axis: LogFC, X-axis: mean of normalized reads). Differential peaks meeting the parameters with FDR<0.05 are shown in red. The experimental procedure was done by the author, with computational analysis curated by Dr. Mirna Barsoum.

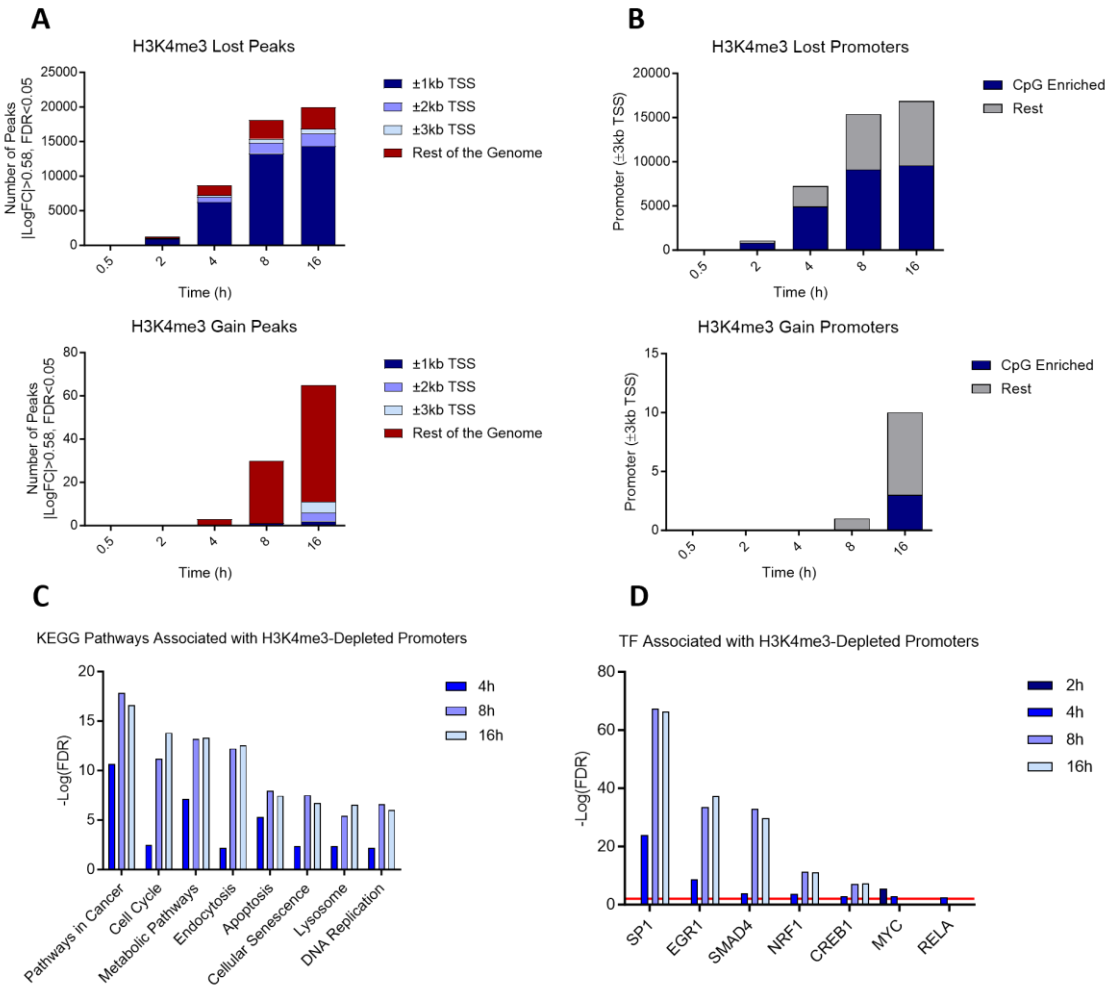

Figure 10: Genomic Distribution of H3K4me3-Depleted Peaks Enriches for Promoter Regions. (A) Annotated differential peaks from the ChIP-seq experiment were subjected to genomic distribution within windows of 1 kb, 2 kb, and 3 kb around the TSS, with another category for the 'rest of the genome'. (B) An intersection analysis was performed between the differentially annotated peaks within a 3 kb window of TSSs at each time point and CGI-associated promoters. The promoters were categorized as CpG Enriched and Rest. (C) KEGG Pathway analysis was performed on the annotated differentially peaks at different time points. The top-ranked most significant pathways were plotted, with the Y-axis representing the negative Log(FDR). (D) Promoters containing loss peaks (LogFC<-0.58 and FDR<0.05) within the 3 kb window of the TSS were subjected to TF analysis based on the JASPAR and TRANSFAC databases. Significance was set to FDR<0.01 and plotted for each time point. The differential analysis and annotation were curated by Dr. Mirna Barsoum. Distribution number plotting, CGI-promoter intersection, KEGG analysis, and TF binding site analysis were done by the author.

3.3.2 ASH2L Induced-KD Results in Accumulation of H3K4me1 Mark at Promoters and Loss of the Mark at Intergenic Regions as a Later Consequence

H3K4me1 is a histone modification that is predominantly associated with enhancers (Froimchuk et al., 2017). Its function lies in the regulation of gene expression by evicting the nucleosome at enhancer regions, thereby enabling the recruitment of transcriptional activators (Kang et al., 2021). However, H3K4me1 can also be found at promoters and may play a role in regulating the accessibility of chromatin and the recruitment of gene repressors (Bhagwat & Vakoc, 2014; Cheng et al., 2014). Overall, the precise role of H3K4me1 at promoters is still an active area of research and may vary

depending on the specific context and cell type. H3K4me1 is primarily deposited by the histone methyltransferase MLL3/4 complexes which comprise ASH2L as a core subunit (Figure 1).

In order to investigate the role of ASH2L in monomethyltransferase activity, a ChIP-seq experiment targeting H3K4me1 was conducted in both WT and dTAG-13 treated NG3 cells. The signal distribution at 3 kb upstream and downstream of the TSS of all mm9 transcripts was visualized using a heatmap, which revealed a noticeable increase in the average signal intensity within the aforementioned window at 4 hours post-treatment (Figure 11A). Differential analysis identified 26 (2h KD), 4270 (4h KD), 6905 (8h KD), and 9634 (16h KD) binding sites with Log2FC>0.58 and FDR<0.05, which were designated as gain peaks and plotted in the MA plots shown in Figure 11B (Table S4). On the other hand, there were 2, 256, 4031, and 4916 loss peaks identified at 2h, 4h, 8h, and 16h time points, respectively (Table S5). The genomic distribution of these differential peaks revealed that most of the gain peaks were concentrated at the defined promoter window, whereas the loss peaks were at intergenic regions (Figure 12A). It appears that the gain of the H3K4me1 mark at the promoters occurs faster and much stronger than the loss of the mark. This suggests that the accumulation of the H3K4me1 is an intermediate consequence of losing the dimethyl group of H3K4me3 in response to ASH2L loss, while the loss of this mark at intergenic regions is due to the loss of monomethyltransferase activity of the ASH2L-missing KMT2 complex. Nonetheless, H3K4me1 appears to be a more stable mark in response to ASH2L loss in the studied NG3 cells.

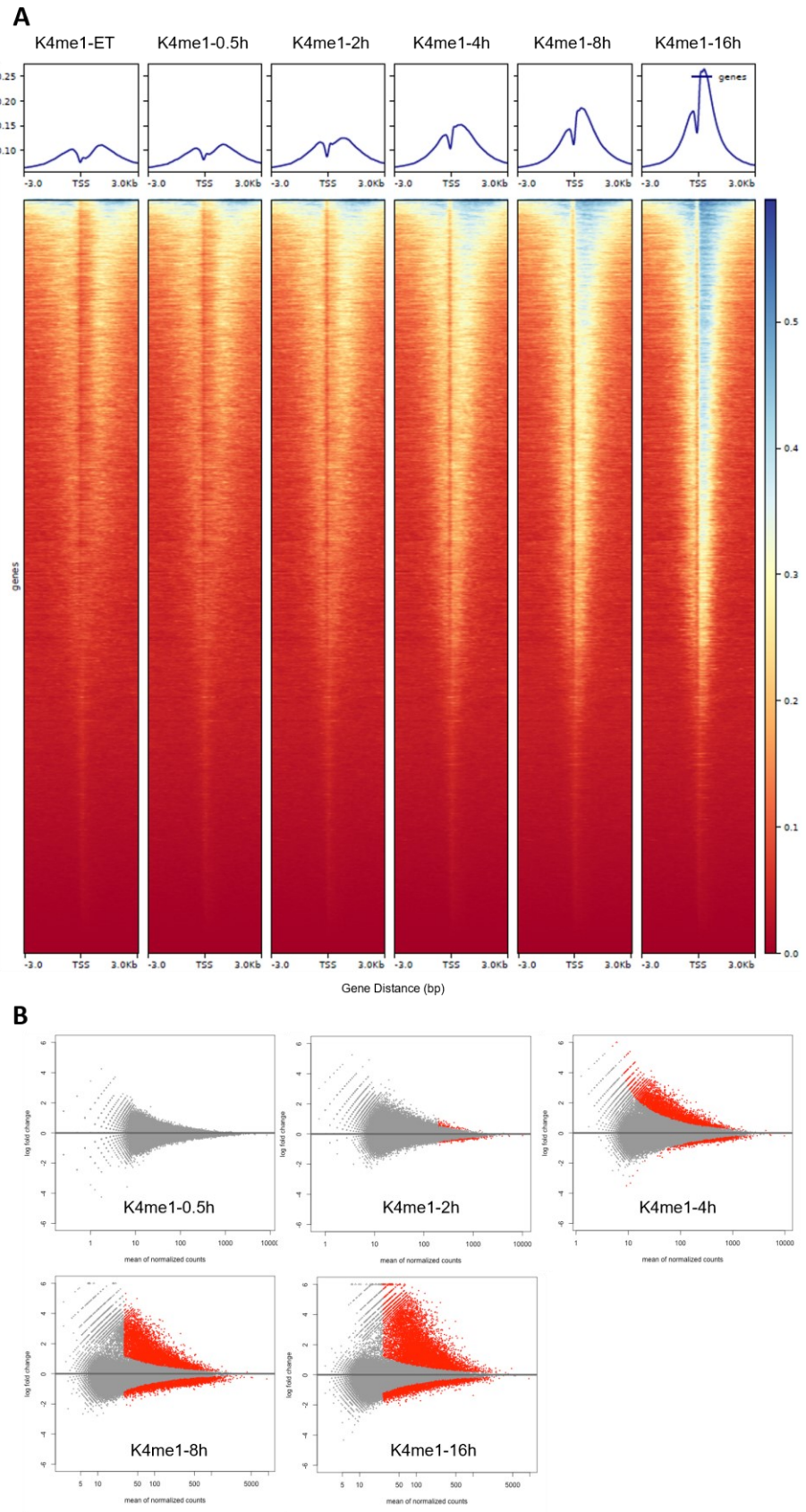

Figure 11: Loss of ASH2L Leads to Accumulation of H3K4me1 at Promoter Regions. (A) NG3 cells were treated in a time-course manner with 100 nM dTAG-13 and subjected to chromatin immunoprecipitation using an H3K4me1 antibody, followed by sequencing (two technical replicates for each time point). The signal density (merged from two replicates and normalized to RPM), mapped against the mm9 reference genome, is

represented as a heatmap in the figure. The distribution density is normalized between samples, demonstrating the signal within a 3 kb window around the TSS regions of all genes. (B) For the differential analysis performed on the deregulated peaks, an MA plot was generated (Y-axis: LogFC, X-axis: mean of normalized reads). Differential peaks meeting the parameters with FDR<0.05 are shown in red. The experimental procedure was done by the author, with computational analysis curated by Dr. Mirna Barsoum.

3.3.2.1 Characterization of the H3K4me1 Altered Promoters

Not exactly similar to the analysis of H3K4me3 lost promoters, the examination of H3K4me1 gained promoters revealed a notable proportion of CGI promoters (Figure 12B). Additionally, enrichment analysis of TFs further confirms that the same set of promoters are undergoing both loss of H3K4me3 and the gain of H3K4me1 marks and are being potentially regulated by a similar set of TFs involved in regulating cell cycle and CpG promoters (Figure 12C).

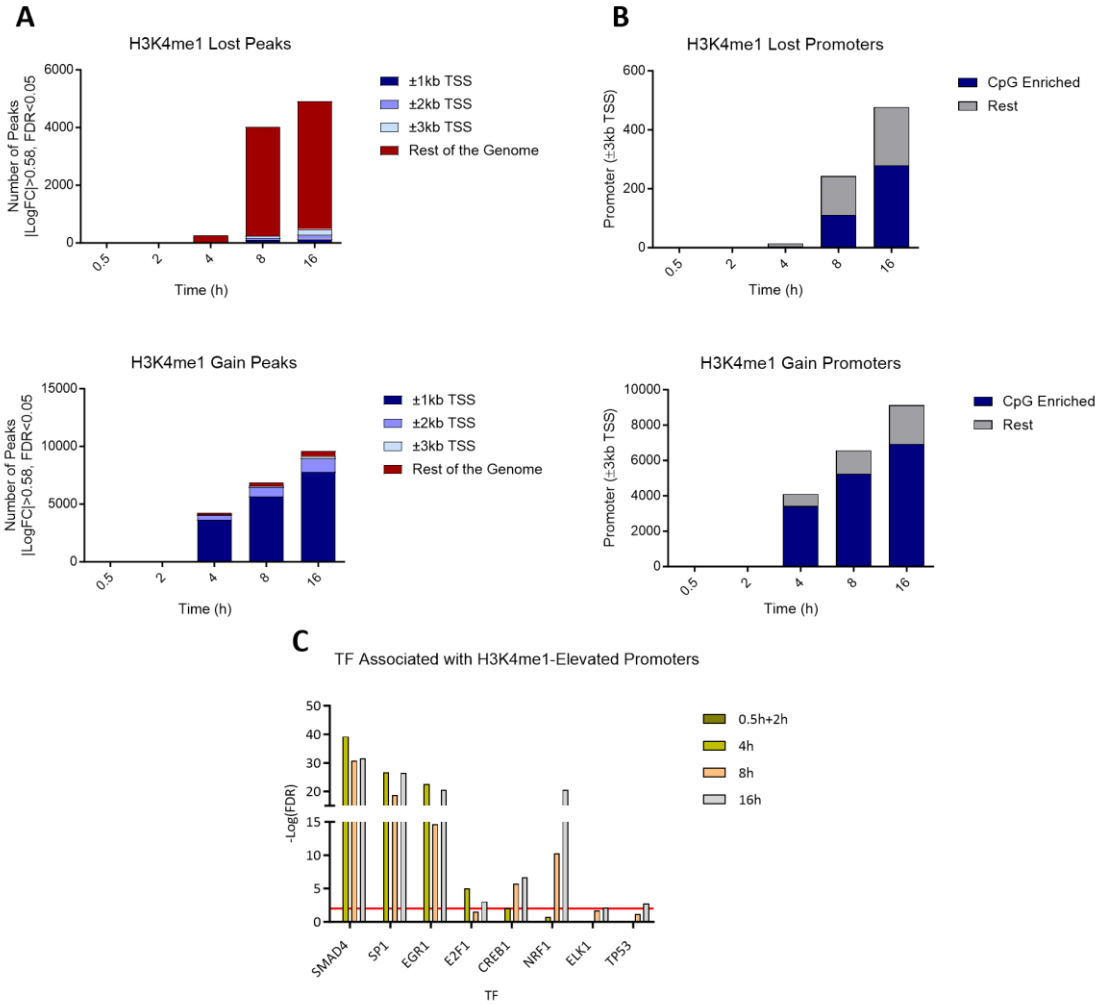

Figure 12: Genomic Distribution of H3K4me1-Elevated Peaks Enriches for Promoter Regions. (A) Annotated differential peaks from the ChIP-seq experiment were subjected to genomic distribution within windows of 1 kb, 2 kb, and 3 kb around the TSS, with another category for the 'rest of the genome'. (B) An intersection analysis was performed between the differentially annotated peaks within a 3 kb window of TSSs at each time point and CGI-associated promoters. The promoters were categorized as CpG Enriched and Rest. (C) Promoters containing loss peaks (LogFC>0.58 and FDR<0.05) within the 3 kb window of the TSS were subjected to TF analysis based on the JASPAR and TRANSFAC databases. Significance was set to FDR<0.01 and plotted for each

time point. The differential analysis and annotation were curated by Dr. Mirna Barsoum. Distribution number plotting, CGI-promoter intersection, and TF analysis were done by the author.

3.3.3 ASH2L KD Results in Loss of H3K27ac Mark at Promoters and Later Gain of the Mark at Intergenic Regions

The H3K27ac mark is a product of an acetyl group being deposited onto lysine 27 of histone 3 by HAT enzymes, including members of the p300/CBP coactivator family. Extensive research has demonstrated its association with active promoter/enhancer and open chromatin regions. It interacts with a diverse array of transcription factors, coactivators, and chromatin remodeling complexes, thereby playing a crucial role in gene expression regulation (Creyghton et al., 2010; J. Ernst et al., 2016; Igolkina et al., 2019). Studies have revealed that the rapid and dynamic acetylation of H3K4me3 enriched regions, facilitated by p300/CBP, is a widespread and evolutionarily conserved process essential for gene activation in eukaryotes (Crump et al., 2011). Additionally, proteins such as the SAGA coactivator complex (Bian et al., 2011), have been identified as capable of recognizing the H3K4me3 mark and mediating the deposition of the H3K27ac mark at H3K4me3-enriched regions. Therefore, an intriguing question arises regarding the influence of ASH2L loss on the dynamics of the H3K27ac mark at genomic loci, particularly focusing on promoters.

To explore the impact of ASH2L on HAT activity, a ChIP-seq experiment was performed targeting the H3K27ac mark genome-wide. This experiment involved WT and dTAG-13 treated NG3 cells (0.5h, 2h, 4h, 8h, 16h). The signal distribution within a region of 3 kb upstream and downstream of the TSS for all mm9 transcripts was analyzed and visualized using a heatmap. The results showed a clear depletion in the average signal intensity within this region, particularly at the 4-hour mark after treatment (Figure 13A).

The differential analysis conducted revealed the existence of distinct H3K27ac binding sites exhibiting significant alterations in their abundance subsequent to the knockdown of ASH2L at various time intervals. Specifically, a total of 1, 50, 668, 3767, and 6417 binding sites were identified as "loss peaks" at 0.5h, 2h, 4h, 8h, and 16h knockdown periods, respectively (Table S6). These assignments were based on predefined criteria, namely Log2FC<-0.58 and FDR<0.05. The loss peaks mentioned above have been graphically depicted in the MA plots featured in Figure 13B. Conversely, "gain peaks" were detected at 0.5h, 2h, 4h, 8h, and 16h time points, yielding 3, 0, 1, 8, and 360 instances, respectively (Table S7).

Through an analysis of the genomic distribution of these differential peaks, it was observed that a significant portion of the loss peaks, particularly at 4h, exhibited a distinct concentration within the defined promoter region. In contrast, the gain peaks were primarily situated in intergenic regions, with their prominence intensifying at a later time point (16h), as depicted in Figure 14A.

Additionally, it is worth noting that approximately one-third of the loss peaks were identified in intergenic regions, which could potentially be associated with enhancers. Interestingly, when examining the regions where H3K4me1 was depleted, an enrichment in the vicinity of intergenic regions was found during later time points (Figure 12A), which may also correspond to the same enhancer regions. Further validation using enhancer-associated histone marks such as H3K4me1 and H3K27ac will be necessary, as outlined in the study by Shlyueva et al. (Shlyueva et al., 2014). Moreover, the loss of H3K27ac at promoter regions can be attributed to a potential reduction in the HAT activity of the p300/CBP complex. Previous research has suggested a direct interaction between

the ASH2L and the MYC transcription factor, which in turn is considered to modulate the enzymatic activity of p300/CBP (Ullius et al., 2014).

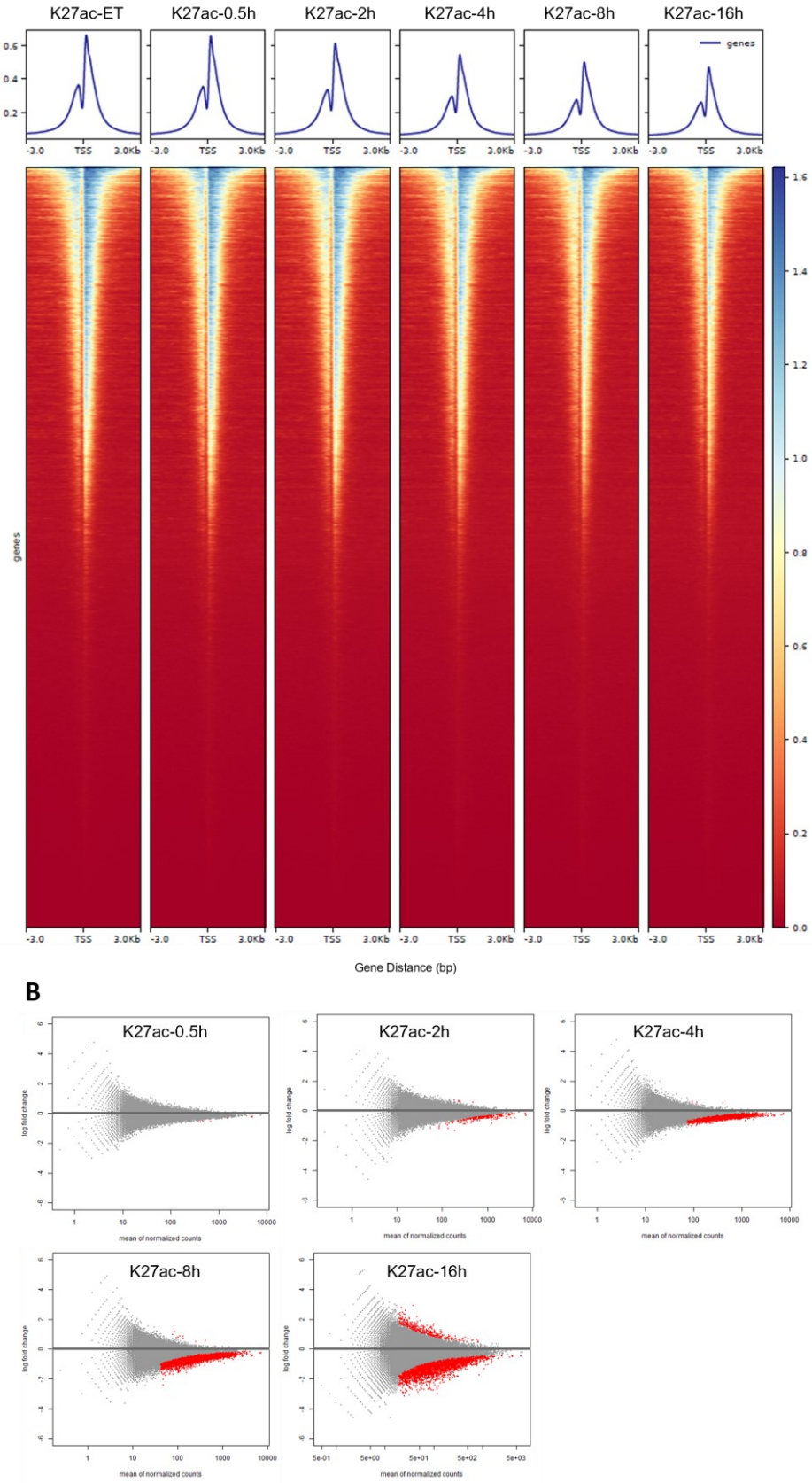

Figure 13: Loss of ASH2L Leads to Depletion of H3K27ac at Promoter Regions. (A) NG3 cells were treated in a time-course manner with 100 nM dTAG-13 and subjected to chromatin immunoprecipitation using an H3K27ac

antibody, followed by sequencing (two technical replicates for each time point). The signal density (merged from two replicates and normalized to RPM), mapped against the mm9 reference genome, is represented as a heatmap in the figure. The distribution density is normalized between samples, demonstrating the signal within a 3 kb window around the TSS regions of all genes. (B) For the differential analysis performed on the deregulated peaks, an MA plot was generated (Y-axis: LogFC, X-axis: mean of normalized reads). Differential peaks meeting the parameters with FDR<0.05 are shown in red. The experimental procedure was done by the author, with computational analysis curated by Dr. Mirna Barsoum.

3.3.3.1 Characterization of the H3K27ac Altered Promoters

The investigation into H3K27ac-lost promoters exhibited that the promoters experiencing a loss of H3K27ac mark at the TSS region are notably enriched with CpG islands (Figure 14B). Notably, a comparative analysis demonstrates that these same promoters experience loss of the H3K4me3 mark and acquisition of the H3K4me1 mark at the TSS regions. Moreover, the enrichment analysis of TFs further strengthens the evidence deregulated promoters undergo almost similar changes in transcription-associated histone marks, including the loss of H3K4me3, gain of H3K4me1, and subsequent loss of H3K27ac marks. These promoters are regulated by a similar set of potential TFs that are associated with the regulation of the cell cycle and CGI promoters (Figure 14C).

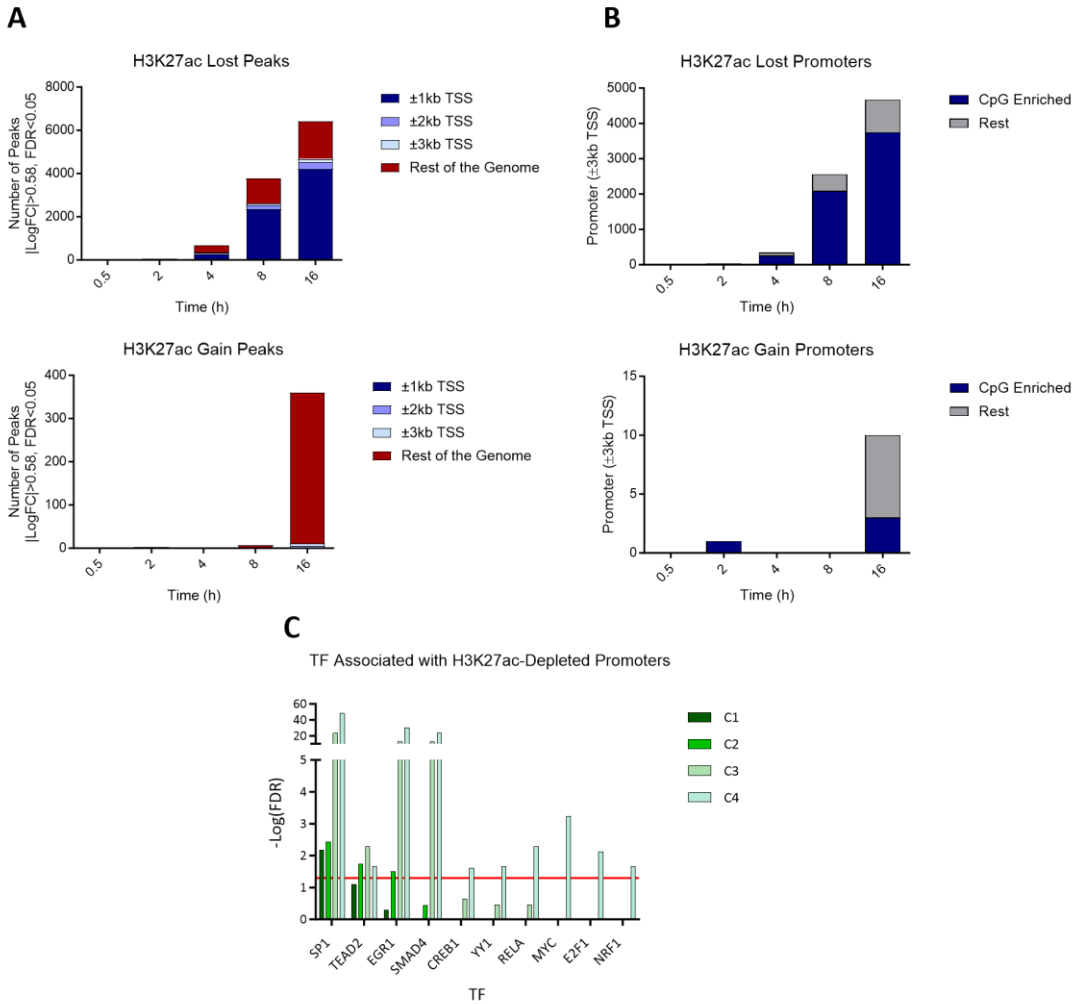

Figure 14: Genomic Distribution of H3K27ac-Depleted Peaks Enriches for Promoter Regions. (A) Annotated differential peaks from the ChIP-seq experiment were subjected to genomic distribution within windows of 1 kb, 2 kb, and 3 kb around the TSS, with another category for the 'rest of the genome'. (B) An intersection

analysis was performed between the differentially annotated peaks within a 3 kb window of TSSs at each time point and CGI-associated promoters. The promoters were categorized as CpG Enriched and Rest. (C) Promoters containing loss peaks (LogFC<-0.58 and FDR<0.05) within the 3 kb window of the TSS were subjected to TF analysis based on the JASPAR and TRANSFAC databases. Significance was set to FDR<0.01 and plotted for each time point. The differential analysis and annotation were curated by Dr. Mirna Barsoum. Distribution number plotting, CGI-promoter intersection, and TF analysis were done by the author.

3.3.4 ASH2L KD Results in Gradual Accumulation of H3K27me3 Mark at Promoters Regions

H3K27me3 is an epigenetic modification associated with the compaction of nucleosome structures. This mark is established through the enzymatic activity of the PRC2 (Boros et al., 2014). Extensive research has shown its involvement in promoting chromatin compaction specifically in heterochromatin regions, hence earning its reputation as a gene silencing marker (Y. Cai et al., 2021). Furthermore, the H3K27me3 mark has been implicated in DNA damage repair processes, particularly in the context of double-strand breaks (Wei et al., 2018).

Following the approach typically employed in other Histone Mark ChIP-seq experiments (0.5h, 2h, 4h, 8h, 16h), due to the limitations imposed by the low sequencing depth, the statistical significance of the observed changes in binding sites could not be determined (Figure S11 & S12). Instead, a noticeable tendency towards an increase in the intensity of this mark was observed specifically at the 16-hour time point. Consequently, in subsequent repetitions of the experiment, it was assumed that the alteration in this mark exhibits a gradual effect, leading to a focus on the 16-hour time point as the starting time point for further investigation of this mark.

To investigate the influence of ASH2L on the regulation of H3K27me3 and its potential crosstalk with H3K4me3, a ChIP-seq experiment targeting H3K27me3 was conducted. This experiment employed WT and dTAG-13 treated NG3 cells (for 16h, 24h, and 48h- similar to the sequence of observed cell phenotype events). The analysis focused on the distribution of signal within a genomic region spanning 3 kb upstream and downstream of the TSS for all transcripts. The results were visually represented using a heatmap (Figure 15A). The analysis revealed that only a small proportion of transcripts exhibited the presence of the H3K27me3 mark at the 3 kb TSS window. However, these transcripts displayed an initial increase followed by a depletion of this mark over the course of time at the TSS window. Furthermore, the differential analysis, as illustrated in MA plots, identified a total of 243, 556, and 623 gained H3K27me3 peaks upon induction of ASH2L KD at 16h, 24h, and 48h, respectively (Table S8). To determine altered binding sites, the criteria for other histone modifications were set as Log2FC>0.58 and FDR<0.05 (Table S9). Interestingly, 18 peaks demonstrated a loss of occupancy for H3K27me3 at 48h in dTAG-13 treated NG3 cells (Figure 15B).

GW annotation of the significant differential peaks, showed that the majority of the gained peaks are enriched around the TSS regions, while the very low number of the lost peaks at 48h, are randomly distributed throughout the genome (Figure 15C). However, there is a small proportion of promoters that have gained H3K27me3 at 24h and lost the mark at 48h. Upon closer examination of these promoters, it became evident that the promoters showing a gain of the mark at 24h but not at later time points are indeed still considered gained compared to control sample (Figure S12). However, it is possible that the observed discrepancies in significance could be attributed to variations in the resolution of the sequenced samples.

3.3.4.1 Characterization of the H3K27me3 Altered Promoters

The examination of H3K27me3-altered promoter, focusing on the enrichment of CpG islands, unveiled that promoters exhibiting a gain in response to ASH2L loss were predominantly enriched with CpG regions. In contrast, only a limited number of promoters displaying a loss of the mark exhibited sparse enrichment in CpG regions (Figure 15D). This finding aligns with previous studies suggesting that CpG methylation functions as a constraint on PRC2-mediated H3K27me3 histone mark deposition, as there exists a mutual antagonism between H3K27me3 and DNA methylation (Manzo et al., 2017).

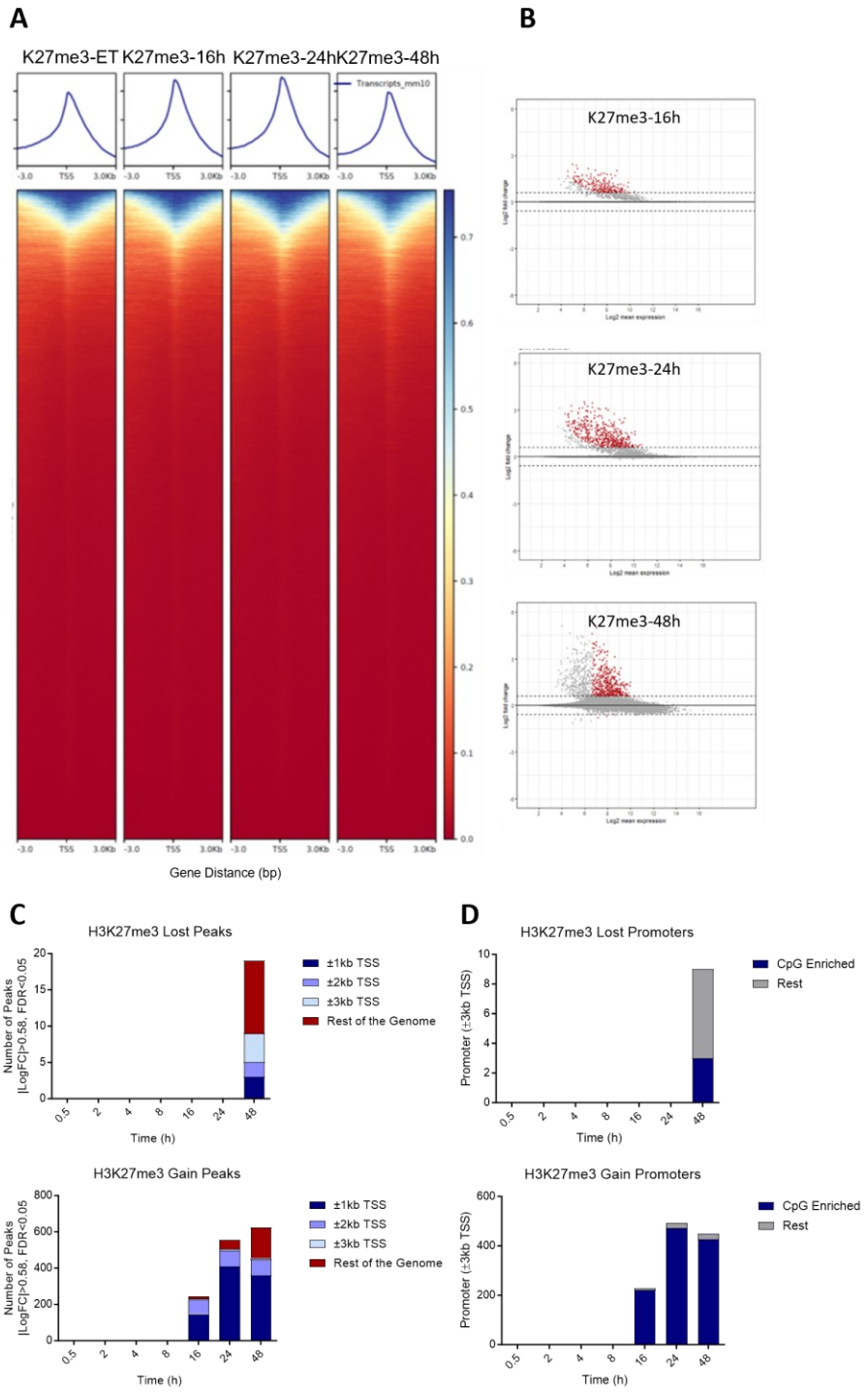

Figure 15: Loss of ASH2L Leads to Accumulation of H3K27me3 at Promoter Regions. (A) NG3 cells were treated in a time-course manner with 100 nM dTAG-13 and subjected to chromatin immunoprecipitation using an H3K27me3 antibody, followed by sequencing (two technical replicates for each time point). The signal density (merged from two replicates and normalized to RPM), mapped against the mm10[2] reference genome, is represented as a heatmap in the figure. The distribution density is normalized between samples, demonstrating the signal within a 3 kb window around the TSS regions of all genes. (B) For the differential analysis performed on the deregulated peaks, an MA plot was generated (Y-axis: LogFC, X-axis: mean of normalized reads). Differential peaks meeting the parameters with FDR<0.05 are shown in red. (C) Annotated differential peaks from the ChIP-seq experiment were subjected to genomic distribution within windows of 1 kb, 2 kb, and 3 kb around the TSS, with another category for the 'rest of the genome'. (D) An intersection analysis was performed between the differentially annotated peaks within a 3 kb window of TSSs at each time point and CGI-associated promoters. The promoters were categorized as CpG Enriched and Rest. The experimental procedure was done by the author, with computational analysis, differential analysis and annotation curated by Dr. Mirna Barsoum. Distribution number plotting, CGI-promoter intersection, and TF analysis were done by the author.

3.4 Loss of ASH2L Results in Transcriptional Deregulation

Through extensive ChIP-seq analysis, it has been observed that the H3K4me3 mark exhibits a concentrated distribution within the vicinity of TSS of actively expressed genes, thereby suggesting a robust correlation with transcriptional activation (Beacon et al., 2021; J. Ernst et al., 2016; Gatchalian et al., 2016; Millán-Zambrano et al., 2022). Conversely, the interaction between KMT2 components and various transcriptional co-activators provides compelling evidence supporting the instructive role of H3K4me3 in the process of gene activation (Lauberth et al., 2013; Nishioka et al., 2002). In line with the proposal that H3K4me3 serves as a marker for active promoters, it has been observed that the TFIID subunit TAF3 selectively interacts with H3K4me3. This interaction not only enhances the stability of the pre-initiation complex involving RNA Pol II but also facilitates the process of transcription, thereby promoting gene expression (van Ingen et al., 2008; Vermeulen et al., 2007). Furthermore, a group of additional proteins, often characterized by the presence of PHD zinc finger or Tudor motifs, exhibit interactions with H3K4me3. Notably, certain proteins such as NURF and BPTF, among others, have been specifically implicated in the process of gene activation. Their involvement suggests a broader regulatory network where H3K4me3 serves as a key player in orchestrating gene expression dynamics (Ruthenburg et al., 2011; Wysocka et al., 2006). Nevertheless, a definitive causal relationship between the presence of H3K4me3 and gene activation remains elusive.

RNA sequencing (RNA-seq) and Click nascent RNA sequencing (Click-seq) techniques were employed to analyze the transcriptomic landscape and identify specific alterations in gene expression profiles resulting from ASH2L loss. RNA-seq has been performed and extensively discussed in Alexander Tobias Stenzel's doctoral dissertation submitted to the faculty of Biology at the RWTH University of Aachen (2023), however, a brief comparison will be made to some of the analysis conducted in this study. It was utilized to capture global gene expression patterns, shedding light on the transcriptional changes associated with ASH2L loss. Click-RNAseq, on the other hand, performed in this study,

[2] Since the second set of H3K27me3 ChIP-seq was performed later during the project, mm10 was used as reference genome based on the Genome Reference Consortium recommendations.

enabled a more precise identification and quantification of nascent transcripts, providing insights into the dynamic transcriptional events occurring in the absence of ASH2L while excluding the influence of long-lived transcripts.

NG3 cells, namely WT and dTAG-13 treated cell culture, at 24-hour, 48-hour, and 72-hour time points were set for RNA-seq analysis. The results revealed a significant alteration in the expression pattern of numerous genes (Figure S13A). At 24 hours, 1865 genes were found to be downregulated, whereas 469 genes were upregulated. At 48 hours, the downregulated genes increased to 2425, while the upregulated genes reached 1830. Finally, at 72 hours, the downregulated genes further rose to 4153, while the upregulated genes amounted to 940 (Figure S13B).

However, initial considerations suggested that the downregulation of genes may be potentially masked by the prolonged half-life of certain RNA transcripts. Therefore, in order to mitigate this masking effect, RNA-seq analysis was exclusively conducted at later time points. Additionally, to investigate the immediate impact of ASH2L loss, Click-seq was employed, utilizing NG3 WT and dTAG-13 treated clones at 4h and 8h intervals. Surprisingly, the Click-seq results revealed a small number of genes showing significant deregulation upon ASH2L loss ($|Log2FC|>0.58$, $FDR<0.05$). Specifically, at the 4h time point, 40 genes were found to be upregulated and 48 genes were downregulated. At the 8h time point, the numbers increased to 80 upregulated genes and 124 downregulated genes (Figure 16A-B). Although somewhat unexpected, these findings still support the notion of gene upregulation as an immediate effect of ASH2L loss. It is important to note that the low sequencing depth obtained in this analysis may affect the significance assessment of some truly deregulated genes. Therefore, the actual number of deregulated genes may be higher than reported in this analysis.

Based on extensive previous experimental studies, it is generally expected that the loss of ASH2L would primarily result in gene downregulation. However, the analysis conducted in this study, considering the calculated average of nascent RNA base mean and Log2FC, indicates a stronger impact of ASH2L loss on the immediate upregulation of genes after 4h upon loss of ASH2L. The average Log2FC for upregulated genes exceeds 4, while downregulated genes exhibit an average Log2FC below 0.25, with the average base mean remaining relatively consistent. Notably, this disparity between upregulated and downregulated genes at the 8h time point diminishes, suggesting the activation of stress-response signaling pathway genes at earlier time points, 4h here (Figure 16C). To gain further insights, a GO term analysis was performed on the deregulated genes at the 4h time point (Figure S13C). This analysis revealed an enrichment of cellular component terms associated with the ubiquitin ligase complex, which may be attributed to the involvement of dTAG-13 targeting the CRBN-Cullin-RING ubiquitin E3 ligase. To confirm this effect, maternal iMEF cells (lacking the ASH2L-FKBP fusion insert) treated with dTAG-13 for the same time point is required. On the other hand, the deregulated genes at the 8h time point exhibited significant enrichment for snRNP binding (Figure S13C), providing potential support for the involvement of ASH2L in splicing reactions, as previously suggested by Sims et al., specifically implicating the engagement of H3K4me3 in pre-mRNA splicing (Sims et al., 2007).

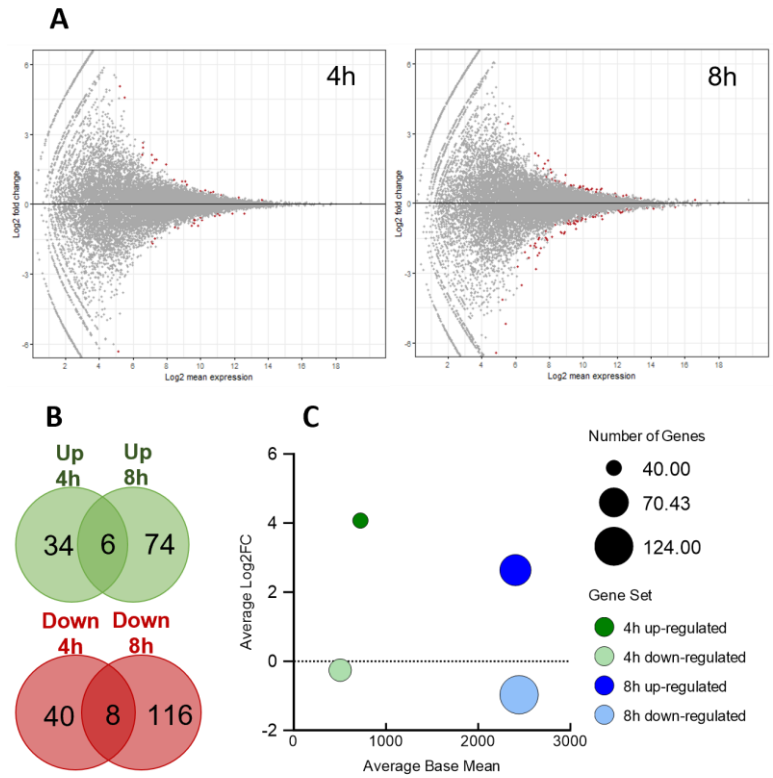

Figure 16: Loss of ASH2L Results in Nascent RNA Transcriptional Deregulation. (A) NG3 cells treated with 100 nM dTAG-13 for 4h and 8h were subjected to Click-seq (two technical replicates for each time point). For the differential analysis performed on the deregulated genes, an MA plot was generated (Y-axis: Log2FC, X-axis: Log2 mean expression). Differentially expressed genes meeting the parameters |Log2FC|>0.58 and FDR<0.05 are shown in red. (B) Venn diagram demonstrating the comparative analysis between significantly up- and down-regulated genes at different time points. (C) A bubble chart including three variables of gene number (size of bubbles), average base mean (X-axis), and Average Log2FC (Y-axis), depicts the effect of ASH2L loss on the deregulated nascent RNA at 4h and 8h time points. The experimental procedure was conducted by the author, with computational analysis, differential analysis, and annotation curated by Dr. Mirna Barsoum.

3.5 Perturbation of Molecular Homeostasis Induced by ASH2L Loss

ASH2L has been recognized as a transcriptional cofactor involved in epigenetic-mediated gene regulation. However, the precise mechanism underlying this regulatory function remains elusive. Interestingly, ASH2L exhibits a higher basal expression in RNAseq results compared to the SET-containing catalytic subunits of the KMT2 enzymes, suggesting potential additional functions beyond just participating in KMT2 complexes. To elucidate the intricate dynamics at play, time course experiments with short intervals were performed, allowing for the discrimination between the effects stemming from ASH2L deregulation and consequent dysregulation of epigenetic marks. In the subsequent analysis, the sequential dysregulation of histone modifications associated with transcription is examined. These findings are then integrated with the results pertaining to transcriptional regulation. This comprehensive approach aims to unravel the mechanism through which ASH2L orchestrates and maintains the molecular homeostasis critical for cellular function.

3.5.1 Unraveling an Orderly Pattern of Histone Modifications Deregulation Upon Loss of ASH2L

As the consequences of ASH2L loss unfold over time, a cascade of changes in histone modifications became evident. Specifically, there is a loss of H3K4me3, a gain of H3K4me1, a loss of H3K27ac, and subsequently, a later gain of H3K27me3 (Figure 17A). To understand the dynamics of these histone modification changes at specific promoters, a comparative analysis of significantly deregulated promoters within a 3-kilobase region of the TSS was performed. For this purpose, the overlap between three groups of differential binding sites from the promoters with lost H3K4me3, gained H3K4me1, and lost H3K27ac was examined (Figure 17B). The inclusion of early time point H3K27me3 ChIP-seq data was omitted due to the limited number of significantly altered binding sites identified within the investigated time frame. The analysis uncovers a prominent initial overlap between the loss of H3K4me3 and the gain of H3K4me1 at the 4-hour time point. This observation suggests the possibility of gradual accumulation of residual methyl groups remaining as a result of the demethylation process (Figure S14). However, at this early time point, the overlap between H3K4me1 gain and H3K27ac loss is not significant. Interestingly, as time progresses, there is a notable increase in the overlap among all three histone modifications at promoters, which became even more pronounced at the 8h and 16h time points. This analysis confirms that primarily the same promoters experience these changes in histone modifications. Furthermore, it establishes the sequential order of events, starting with the loss of H3K4me3, followed by the accumulation of H3K4me1, and finally the depletion of H3K27ac at the promoter region.

A detailed examination of the turnover dynamics of promoters that have experienced a loss of H3K4me3 after 2 hours provides further evidence that the majority of fast-responding (affected at 2h or earlier) promoters exhibiting H3K4me3 loss follow a consistent pattern of histone modification alterations (gain of K4me1 at 2h, loss of K27ac at 4h, and gain of H3K27me3 later than 16h). Notably, these promoters also demonstrate a subsequent decrease in DNA accessibility, which becomes evident starting from the 4h time point (Stenzel, 2024). Overall, these findings provide valuable insights into the temporal dynamics of histone modification changes and highlight the coordinated and sequential alterations occurring at specific promoters upon ASH2L loss.

As presented earlier, the gain of H3K27me3 was observed as later consequence of ASH2L loss. The question arose as to whether the promoters gaining H3K27me3 had already lost their H3K4me3, and if so, how quickly this transition occurred. To address this, a comparative analysis was performed between promoters that gained H3K27me3 and promoters that had lost H3K4me3 at earlier time points. The comparative analysis revealed that the majority of promoters that gained H3K27me3 at 16h had already lost their H3K4me3 marks at the 4h time point (Figure 17C). This suggests that the gain of H3K27me3 is not directly associated with the loss of H3K4me3.

On the other hand, previous studies have established that H3K27ac and H3K27me3 marks are mutually exclusive (Katoh et al., 2018; Pasini et al., 2010). Therefore, it was expected that promoters gaining H3K27me3 would show a concurrent loss of the H3K27ac mark. However, when an intersection comparison was performed, it was observed that as the loss of the K27ac mark progressed, the overlap with gained K27me3 increased but did not reach complete concurrence (Figure 17D). This finding suggests two possibilities. Firstly, it is possible that the dynamic process of gaining H3K27me3 is relatively slow and requires a longer time frame to fully manifest. This implies that the deposition of H3K27me3 might take more time to occur robustly at all relevant promoters

following ASH2L loss. Alternatively, it is plausible that there is still remaining H3K27ac present, which hinders the deposition of methylation at this position. This suggests the existence of a regulatory mechanism or a subset of promoters where the presence of H3K27ac may interfere with the establishment of further H3K27me3 mark.

These findings highlight the complex interplay between histone modifications and suggest that the gain of H3K27me3 upon ASH2L loss is not directly dependent on the loss of H3K4me3. Additionally, the incomplete overlap between the loss of H3K27ac and the gained H3K27me3 raises intriguing questions about the precise mechanisms underlying the establishment and maintenance of these histone marks. Further investigations are warranted to unravel the dynamics and interrelationships of these epigenetic modifications in the context of ASH2L loss.

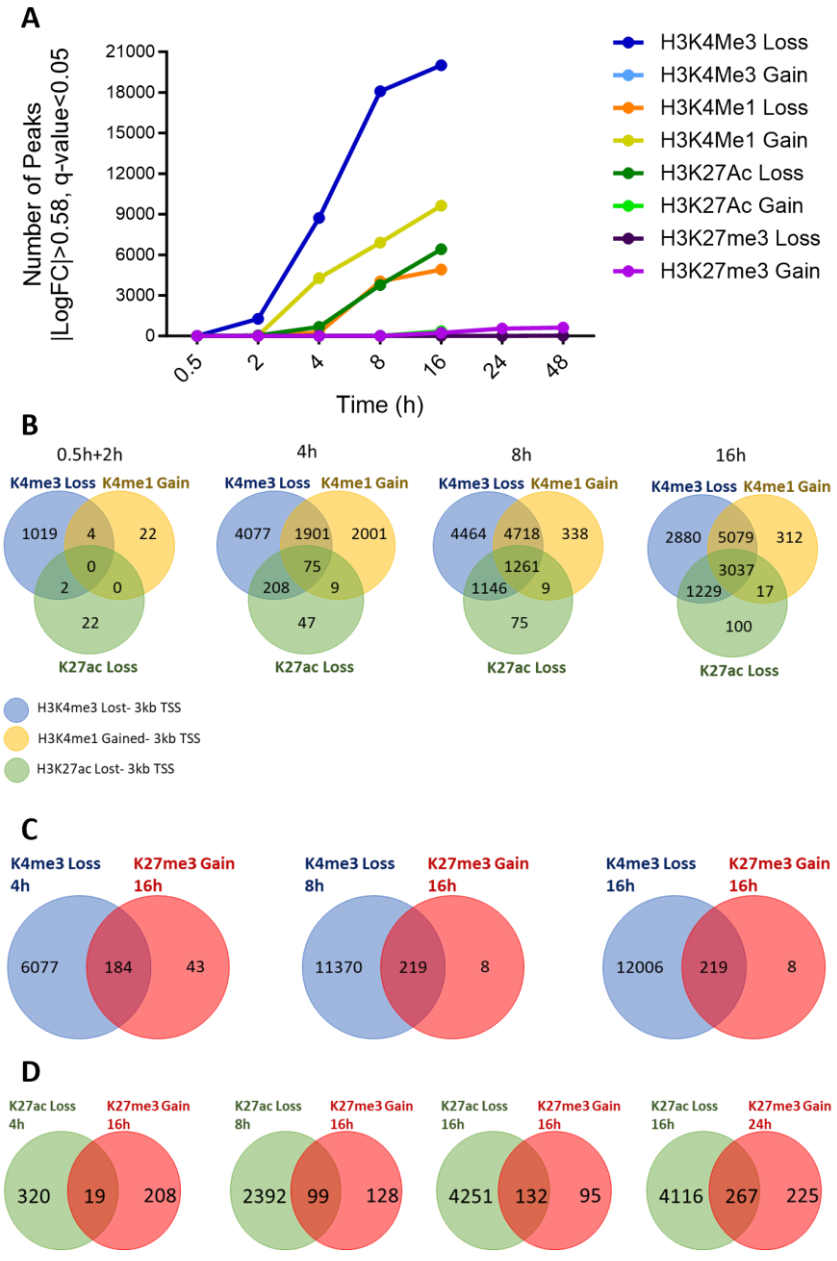

Figure 17: Sequential Deregulation of Histone Marks in Response to ASH2L Loss. (A) Differentially analyzed peaks within a 3 kb window of the transcription start site (TSS), obtained from various ChIP-seq data, were plotted at each time point. (B) Venn diagram demonstrating the intersection between gained and lost promoters of different histone modifications at different time points. (C) Comparative analysis of K4me3 lost

promoters at 4h, 8h, and 16h with K27me3 gain promoters at the 16h time point. Similar result were obtained when K27me3 gain promoters at 24h were used for this intersection (data not shown here). (D) Comparative analysis between K27ac lost promoters and K27me3 gain promoters. Computational analysis, differential analysis, and annotation were curated by Dr. Mirna Barsoum. Plotting and intersection analysis were performed by the author.

3.5.2 Disruption of Gene Expression Equilibrium Following ASH2L Loss

The loss of ASH2L, which leads to the depletion of H3K4me3, a well-established active gene histone mark, is expected to result in the loss of target gene transcription. However, the causal relationship between this histone mark and gene transcription remains incompletely understood. As discussed in chapter 3.4, a significant number of genes experience a disruption in their expression equilibrium upon the loss of ASH2L followed by dTAG-13 treatment in the NG3 cells. The observed deregulation of gene expression is likely attributed to the loss of ASH2L alone, as there is minimal alteration detected in the expression profiles of other KMT2 components (Figure 8) and H3K4me3 readers and writers (Figure S6, and Figure S15) at the respective time point (4h, and 8h). However, the mRNAseq assessment was conducted at later time points (24h, 48h, and 72h), which could be influenced by secondary and tertiary effects arising from ASH2L loss rather than its immediate effects. Moreover, the presence of long-lived RNA transcripts can obscure their true expression levels during statistical analysis, thereby potentially masking their deregulation. Nevertheless, this subsequent transcriptional analysis can be compared with later time points of different histone modification ChIP-seq analysis to elucidate the correlation between consequent histone modification changes and gene deregulation.

A comparative analysis was performed to investigate the relationship between different histone modification alterations and downregulated genes at various time points. The results reveal that gene transcription dependency is predominantly associated with the H3K4me3 mark, as a significant overlap is observed between downregulated genes and promoters exhibiting depleted H3K4me3 (Figure S16A). In contrast, the intersection between downregulated genes and H3K27ac lost promoters is relatively smaller (Figure S16B). Interestingly, the overlap between downregulated genes and H3K27me3 gained promoters is found to be the smallest (Figure S16C). This finding is somewhat unexpected, considering that H3K27me3 is commonly associated with gene silencing. However, it is possible that these promoters are still undergoing transcriptional activity and have not yet fully transitioned to a silent state. These results highlight the significance of the H3K4me3 mark in gene transcription regulation and suggest that additional factors and mechanisms may contribute to the observed downregulation of gene expression upon ASH2L loss.

To explore the dynamics of histone modifications at a set of altered genes, a comprehensive analysis of two groups was conducted: cell cycle regulatory key factors and previously described senescence-associated M genes (Bochyńska et al., 2022). The results were visualized using a heatmap analysis to depict the differential changes in histone modifications. For the cell cycle-associated genes (Figure S17A), we observed a clear transcriptional depletion accompanied by early and significant alterations in H3K4me3 levels at their 3Kb TSS regions. In contrast, the loss of H3K27ac at these promoters occurred at a slower rate. Notably, a significant or apparent gain of H3K27me3 at these promoters was not observed (Data not visualized). These findings highlight a distinct pattern of histone modification dynamics linked to the transcriptional regulation of cell cycle regulatory genes, with a prominent role for H3K4me3 and a delayed or limited involvement of H3K27ac and H3K27me3 in this

process. It was further performed a similar analysis for the senescence-associated M gene subsets, and the results (Figure S17B) aligned with the orderly pattern of ASH2L loss consequences discussed in chapter 3.5.1. These consistent findings across different gene groups provide further support for the specific and consistent effects of ASH2L loss on transcription-associated histone modifications and gene expression regulation.

In order to investigate the causal relationship between the loss of H3K4me3 and transcriptional depletion, a comparison between downregulated nascent RNA and H3K4me3-depleted promoters was conducted. Surprisingly, the intersection analysis between Click-seq at 4h and H3K4me3-depleted promoters at 2h revealed no overlap, suggesting that the transcriptional depletion is not directly associated with loss of H3K4me3 during this early time frame (Figure S18A). Even at later time points of H3K4me3 ChIP-seq, the intersection between Click-seq and H3K4me3-depleted promoters was substantially smaller than anticipated. However, a comparative analysis of Click-seq at 8h demonstrated some overlap with H3K4me3-depleted promoters from earlier time points (Figure S18B). These observations suggest that the immediate deregulation of gene transcription is primarily dependent on ASH2L separate function itself rather than the presence of the H3K4me3 mark at the promoters. However, at later time points, the changes in transcriptional activity appear to be more influenced by the status of H3K4me3 at the promoter region.

These observations suggest that the immediate deregulation of gene transcription is primarily driven by the loss of ASH2L itself, indicating that ASH2L may have separate functions beyond its role in maintaining the H3K4me3 mark at promoters. This implies that ASH2L may directly interact with transcriptional machinery or regulatory elements to modulate gene expression independent of H3K4me3. The absence of overlap between Click-seq at 4h and H3K4me3-depleted promoters at earlier time points further supports this notion. However, as the time progresses, the changes in transcriptional activity become more dependent on the status of H3K4me3 at the promoter region. This suggests that although the immediate effects of ASH2L loss on gene transcription may not rely solely on H3K4me3, the presence or absence of this histone mark at the promoter region starts to play a more significant role in modulating the expression of other groups of genes over time. Overall, these findings highlight the complex interplay between ASH2L, H3K4me3, and gene transcription. While ASH2L loss appears to have an immediate impact on gene expression independent of H3K4me3, the long-term changes in transcriptional activity involve a more intricate relationship with the presence or absence of H3K4me3 at the promoter region. Further studies are needed to elucidate the underlying mechanisms and molecular interactions involved in these dynamic processes.

4 Discussion

ASH2L is a crucial core member of the KMT2 enzymatic complex, essential for its histone HMT activity (Cao et al., 2010; Steward et al., 2006). It consists of core subunits such as: WDR5, RBBP5, and a DPY30 homodimer, along with various auxiliary proteins (Poreba et al., 2022). These components regulate transcription, influence cell survival, impact pathogenesis, modulate metabolism, and contribute to the stabilization/localization of KMT2 enzymes (Ali et al., 2014; Batbayar et al., 2023; W. L. Cai et al., 2022; Lüscher-Firzlaff et al., 2019; Ma et al., 2022; Park et al., 2020; Shilatifard, 2012; Simboeck et al., 2013; Z. Yang et al., 2014; L. Zhao et al., 2022). Homozygous deletion of *Ash2l* leads to embryonic lethality in mice during gestation (Stoller et al., 2010).

In line with previous study observations (Bochyńska et al., 2022), the complete inhibition of proliferation and cell cycle progression becomes evident upon the rapid loss of the ASH2L-FKBP fusion protein in the dTAG-induced KD iMEF clones. Additionally, the KD clones exhibit compromised DNA synthesis capacity and a tendency to accumulate in the G1 phase. However, they remain arrested throughout the cell cycle phases. Encouragingly, these effects can be reversed through the restoration of the ASH2L-FKBP fusion protein, induced by lenalidomide (Figure 5, and Figure S3). However, the effect on cell proliferation was discussed to be slower growth upon the inhibition of WDR5 in Li et al., 2022 and KD of DPY30 and RBBP5 in Wang et al., 2023 in mESC, but not ceased. This difference could be attributed to variations in cell type (for e.g. mESC vs MEF) or the intensity of the influential role of other involved factors in cell cycle orchestration, such as demethylases (Haines et al., 2018; Qu et al., 2023; Tumber et al., 2017). Additionally, as discussed in chapter 3.5.1, it could be that a certain remaining level of H3K4me3 and H3K27ac is sufficient to keep the transcription process ongoing, although it has been demonstrated that KMT2-associated transcription regulation is tightly dependent on the dynamic levels of H3K4methyl PTMs (Soares et al., 2017).

As pointed earlier, PROTACs have been applied to target three WRAD components (WDR5, RBBP5, and DPY30), in conjunction with SET1A and SET1B subunits. This approach has facilitated the examination of COMPASS/KMT2 complexes and their functionalities at an unprecedented level of detail, as evidenced by recent studies (Hu et al., 2023; Hughes et al., 2023; D. Li et al., 2022; H. Wang et al., 2023). Additionally, considerable evidence supports the promise of PROTACs for epigenetic regulation, allowing the targeted degradation of epigenetic modulators, the development of dual-targeted PROTACs (D. Li et al., 2022), and achieving highly specific degradation of histone-modifying enzymes (Webb et al., 2022). The significance of targeting WRAD lies in the pivotal and expansive role played by these complexes, responsible for the modification of both promoters and enhancers through H3K4me3 and H3K4me1, respectively. Given their close association with gene expression, characterized by a rapid and dynamic regulatory process, the rapid efficacy of the PROTACs system becomes crucial for effective interpretation. The current study is the first instance of applying this system to specifically target the ASH2L-FKBP fusion protein within MEF$^{Ash2l-/-}$ clones (NB5, ND10, and NG3). Similar to other studies, the targeted proteins exhibited a notable loss, occurring within a short timeframe. This loss was observed in less than half an hour (current study) to within a couple of hours (evident in other studies) following treatment with PROTAC compounds (refer to Figure 4, and Figure S2). This rapid and efficient degradation underscores the precision of the PROTAC system in orchestrating the removal of the specified WRAD components. Additionally, it is noteworthy that during KD treatment, the other WRAD components showed minimal impact, as illustrated in Figure 8, and Figure S6. This specific response emphasizes the selectivity of the treatment, as it predominantly influences the intended target proteins without significantly affecting the broader WRAD complex components, thereby allowing the study of the individual partners separately.

ASH2L as a member of the COMPASS complex, plays a crucial role in the deposition of different forms of methylated lysine in histone 3 (Klonou et al., 2021). Specifically, H3K4me3 and me2 which are primarily associated with promoters, and me1, which is linked to enhancers. In line with recent studies (Bochyńska et al., 2022; Chen Taylor, 2022; Barsoum et al., 2022; Zhu et al., 2023), the loss of ASH2L demonstrated here leads to global depletion (Figure 7, and Figure S5) and GW reduction of H3K4me3 signals at gene promoters (Figure 9-10, Appendix 3). However, when targeting other WRAD components via PROTACs, a distinct pace of H3K4me3 depletion was observed in Wang 2023, while the depletion pace observed in the current study aligns better with findings from Hu 2023

work. As mentioned earlier, the variation could be stemmed from difference in cell type and the proportional expression and role of KMT2 counterparts, such as demethylases.

On the other hand, the regulatory pattern of H3K4me1 displayed a distinct response following the loss of ASH2L, showing global depletion at the 24-hour time point (Figure 7, and Figure S5), while revealing a notable increase in modification over promoter regions and a corresponding decrease at intergenic regions in the time course ChIP-seq (Figure S12). In contrast, the findings in Wang et al., 2023 indicate an overall reduction in this modification on a GW scale throughout the observed time course, extending up to 48 hours. Notably, in the study by Hu et al., 2022 there was an initial accumulation of H3K4me1 across the genome until 6 hours, followed by a subsequent depletion of this mark after 12 hours. The comparative analysis reveals a notable initial convergence between the decline in H3K4me3 and the increase in H3K4me1 at the promoter regions. This finding implies the potential gradual accumulation of residual methyl groups, persisting as a consequence of the demethylation process (Figure S14). It is also known that the KMT2 complex catalytic subunits possess basal monomethylation activity even without ASH2L composition. This could serve as an additional reason for the persistence of monomethylation at a genome-wide level, while trimethylation is hindered due to the absence of the ASH2L member (Cao et al., 2010; Steward et al., 2006). However, the experimental setup of the current study does not provide a clear distinction to definitively conclude this determination.

Although the association of H3K27ac and H3K4me3 with active gene promoters has been suggested previously, a comprehensive study analyzing the mechanism and causal interplay between these two marks is missing. The current study has included the analysis of H3K27ac as one of the histone marks in the transcription associated PTM panels. It was observed that fairly early after the loss of H3K4me3 and gain of H3K4me1 at promoters, the H3K27ac mark started to disappear (Figure 13, and Appendix 3). While this crosstalk investigation is absent in recent PROTACs-targeted WRAD studies, some primary reports have suggested that H3K27ac is an upstream epigenetic mark that promotes H3K4me3 upregulation, but not the other way around (W. Zhao et al., 2021). Additionally, Ash2l is studied for its interaction with Oct4 stemness factors to facilitate a super-enhancer-driven pluripotency network. This interaction involves recruiting p300/CBP and Chd7 to catalyze H3K27ac, contributing to resultant gene regulation (Tsai et al., 2019). On the other side, the oncoprotein MYC has been introduced as a direct interactor of ASH2L within cells. Although MYC does not regulate the methyltransferase activity of the ASH2L-related complex, it was suggested to stimulate the demethylation and acetylation of H3K27 (Ullius et al., 2014). Additionally, there has also been an association of KMT2 complexes with H3K27 demethylases, specifically UTX and JMJD3, and their involvement in HOX gene regulation and development (Agger et al., 2007). The last two pieces of evidence may support the idea that COMPASS components orchestrate the deposition of acetyl groups on the demethylated H3K27, contributing to the loss of H3K27ac upon the loss of H3K4me3 resulting from ASH2L KD.

The crosstalk between H3K4me3 and H3K27me3 involves a dynamic interplay that regulates gene expression and chromatin structure. It is noteworthy that these two marks can coexist at specific genomic sites, generating a bivalent chromatin state (Bernstein et al., 2006; Blanco et al., 2020). Additionally, it has been demonstrated that H3K4me3 is suggested to counteract the repressive H3K27me3 histone mark (Liu et al., 2016); however, whether it acts through counteraction or contributes to bivalency is not elucidated. The current study comprehensively analyzed the time course response of the H3K27me3 mark in response to ASH2L loss, revealing a very delayed

accumulation (Figure 15, Figure 17A, and Figure S12). Additionally, the examination indicated that most promoters that acquired H3K27me3 at 16 hours had already experienced a loss of their H3K4me3 marks by the 4-hour time point (Figure 17C-D). This implies that the acquisition of H3K27me3 is not directly linked to the loss of H3K4me3. This issue was not addressed in any of the PROTACs-targeted WRAD studies and therefore needs further investigation to discover the regulatory networks applied on PRC2, possibly by the role of ASH2L or the KMT2 complex. On a second layer, this could be a result of the deregulation of acetylation, which is proven to be in a dynamic balance with its counterpart trimethyl, over-occupying the lysine 27 of histone 3 (Lavarone et al., 2019).

The repeatedly observed distribution of H3K4me3 signals over TSS through ChIP-seq experiments has led to the assumption of a potential connection between this PTM and transcription regulation (Ng et al., 2003; Santos-Rosa et al., 2002; Schneider et al., 2004). Since H3K4me3 is known to recruit both positive and negative transcriptional cofactors to gene promoters (Buratowski & Kim, 2011), the role of H3K4me3 at promoters is a subject of debate. For instance, certain KMT2 complexes form associations with the C-terminal domain of RNA Pol II, thereby presumed to enhance the recruitment of these complexes to transcribed genes (Hughes et al., 2023; J.-H. Lee & Skalnik, 2008; Tan et al., 2008). It has been documented that the PHD finger of TAF3, a subunit of the general transcription factor complex TFIID, reads H3K4me3. This has led to the proposition that H3K4me3 assists in recruiting the RNA Pol II complex (Lauberth et al., 2013; van Ingen et al., 2008; Vermeulen et al., 2007). This notion is supported by the discovery that promoting H3K4me3 using a dCas9 system was adequate to induce gene expression (Cano-Rodriguez et al., 2016; W. Zhao et al., 2021). Confirming the transcriptional dependency on H3K4me3 mark, over 80% of the downregulated genes upon loss of ASH2L exhibited intersection with the H3K4me3 lost promoters at 16h (Figure S16A) (Bochyńska et al., 2022; Hu et al., 2023; D. Li et al., 2022; Lüscher-Firzlaff et al., 2019; H. Wang et al., 2023; Z. Yang et al., 2014). There were also upregulated genes that did not show a clear correlation but generally exhibited the same tendency towards the redistribution of the PTMs, albeit not as high as the downregulated gene number (Data not shown) (Bochyńska et al., 2022; Hu et al., 2023). However, the study by Wang et al. did not show any upregulated genes after 24h of DPY30/RBBP5 induced KD, which differed from both the current study and the one published by Hu et al. 2023.

Despite numerous studies attempting to clarify the correlation or causality between H3K4me3 PTM and gene regulation, this matter remains partially understood. In the current study it has been demonstrated that at promoter regions, the 5' signals are typically weaker than the 3' signals, and the immediate vicinity of the TSS shows a valley in the distributed signal (Figure S10B-C). This region, also known as the nucleosome-free region (NFR), is accessible in ATAC experiments and is around the same region that exhibits ASH2L-FKBP binding sites (Barsoum et al., 2023). This could potentially indicate the interaction of ASH2L/KMT2 components with the residing RNA Pol II at active gene promoters. Consistent with this proposal, the interaction of RNA Pol II and the WDR82 component of the KMT2 complex has been studied. However, the biphasic distribution of the signal is still visible for WDR82-containing ZC3H4 complex ChIP plots, although lower compared to the depth of the valley for H3K4me3 (Hughes et al., 2023). Interestingly, the distribution patterns of other PROTACs-targeted WRAD components, such as DPY30 and RBBP5, have been demonstrated to be similar to that of ASH2L (Barsoum et al., 2023; Hu et al., 2023; H. Wang et al., 2023). Consistently, this pattern aligns with the integrator complex subunit 11 (INTS11), which facilitates the eviction of the paused Pol II (Hu et al., 2023) and also TAF3 and TAF1, PIC components, distribution pattern at TSS (Hu et al.,

2023). This supports the idea that transcriptional activity may be in a feedback interaction with H3K4me3 distribution at promoter regions, required and resulted by active transcription (Howe et al., 2017; Hughes et al., 2023; Okitsu et al., 2010).

To examine the connection between H3K4me3 loss and transcriptional depletion, we compared downregulated nascent RNA with H3K4me3 depleted promoters. Surprisingly, at the 4h time point, there was no significant overlap, suggesting that early transcriptional depletion is not directly linked to H3K4me3 loss, consistent with Click-seq results and a modest decline in Pol II occupancy at promoters observed in another study (Figure S18) (Hu et al., 2023). A further comparison at the 8h time point in the current study also revealed a small overlap (Figure S19).

In conclusion, current study's exploration into the rapid degradation of ASH2L facilitated by PROTACs, as suggested in the proposed descriptive model for the regulatory network modulated by ASH2L (Figure 18), reveals a sequential shift in a panel of transcription-associated histone marks. It initiates with the initial decline in H3K4me3, followed by a series of events involving the gain and loss of H3K4me1 at promoters and enhancers, respectively, succeeded by a simultaneous reduction in H3K27ac at both these regulatory regions. Additionally, a delayed decrease in chromatin accessibility ensues, resulting in a less structured nucleosomal organization, specifically at promoters (Barsoum et al., 2022), with minimal impact on H3K27me3. This emphasizes the rapid degradation of ASH2L as the primary event, while subsequent chromatin-associated processes and the regulation of gene expression exhibit a more gradual pace. This observation suggests the presence of a robust buffering mechanism within the system, potentially including different layers of epigenetic factors or resilient chromatin architecture properties. Moreover, distinct thresholds associated with various histone modifications may contribute to shaping the loading and activity of RNA polymerase II. Overall, this framework lays the groundwork for further intricate investigations aimed at elucidating the multifaceted functions of COMPASS/KMT2 complexes.

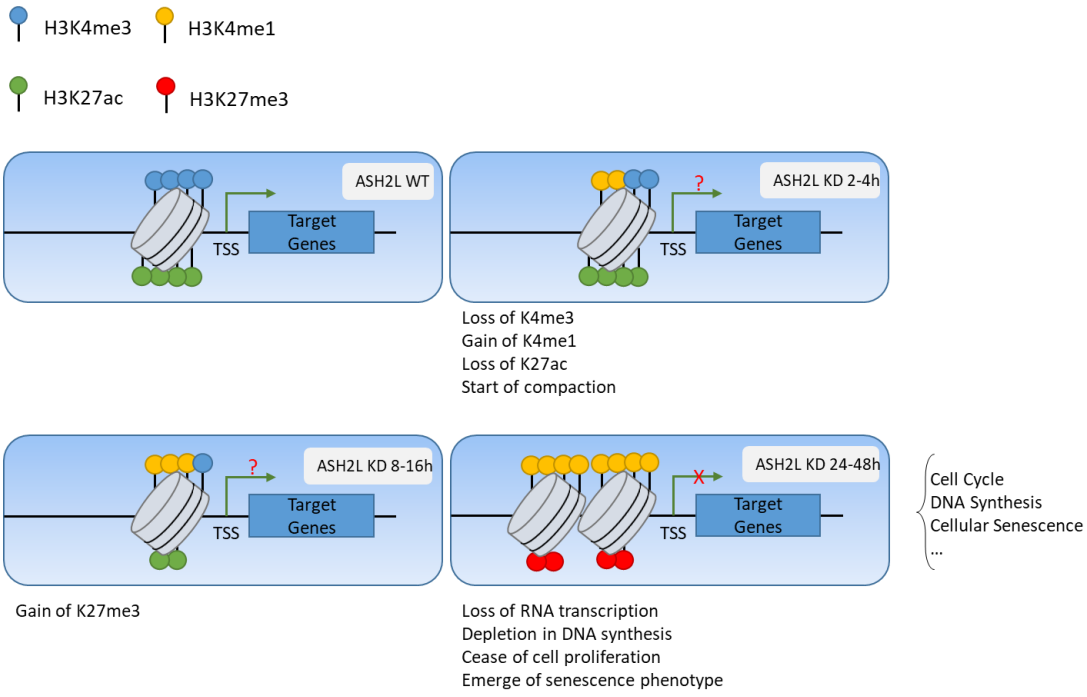

Figure 18: A Descriptive Model Suggested for the Regulatory Network Modulated by ASH2L.

4.1 Outlook

In the current study, it has been demonstrated that the use of dTAG-13 leads to an immediate loss of the ASH2L-FKBP fusion protein in immortalized MEF cells. This initiates a sequential series of cellular and molecular events in the KD cell lines, some of which have been shown to be reversible by using lenalidomide, a competitor compound that counteracts dTAG-13 biding to CRBN receptor of E3 ligase. The order of epigenomic deregulation, confirmed by ChIP-seq, primarily begins with the loss of H3K4me3, followed by the gain of H3K4me1, loss of H3K27ac, and a delayed gain of H3K27me3. However, the causal relationship of this apparent order is not very clear. The advantage of utilizing lenalidomide could verify the reversible order of events in a backward orientation, confirming the regulatory sequence of this network.

Moreover, specific inhibitors targeting KDMs could be employed to address the pure function of the loss of ASH2L separately from its KMT2-HMT enzymatic activity. This approach could shed light on the transactivational role of the ASH2L protein and its potential functional role of its direct DNA binding domains present in the protein sequence.

Furthermore, a thorough investigation into the ASH2L-specific transcriptional regulatory network could be conducted by performing RNA Pol II or nascent RNA run-on sequencing methods. Since H3K4me3 has also been implicated in alternative splicing of transcripts, addressing such questions with the help of Bulk-RNAseq would be of interest.

5 References

Agger, K., Cloos, P. A. C., Christensen, J., Pasini, D., Rose, S., Rappsilber, J., Issaeva, I., Canaani, E., Salcini, A. E., & Helin, K. (2007). UTX and JMJD3 are histone H3K27 demethylases involved in HOX gene regulation and development. *Nature*, *449*(7163), 731–734. https://doi.org/10.1038/nature06145

Ahmad, K., Brahma, S., & Henikoff, S. (2024). Epigenetic pioneering by SWI/SNF family remodelers. *Molecular Cell*, *84*(2), 194–201. https://doi.org/10.1016/j.molcel.2023.10.045

Ali, A., Veeranki, S. N., & Tyagi, S. (2014). A SET-domain-independent role of WRAD complex in cell-cycle regulatory function of mixed lineage leukemia. *Nucleic Acids Research*, *42*(12), 7611–7624. https://doi.org/10.1093/nar/gku458

Allis, C. D., Berger, S. L., Cote, J., Dent, S., Jenuwien, T., Kouzarides, T., Pillus, L., Reinberg, D., Shi, Y., Shiekhattar, R., Shilatifard, A., Workman, J., & Zhang, Y. (2007). New Nomenclature for Chromatin-Modifying Enzymes. *Cell*, *131*(4), 633–636. https://doi.org/https://doi.org/10.1016/j.cell.2007.10.039

Andrews, F. H., Tong, Q., Sullivan, K. D., Cornett, E. M., Zhang, Y., Ali, M., Ahn, J., Pandey, A., Guo, A. H., Strahl, B. D., Costello, J. C., Espinosa, J. M., Rothbart, S. B., & Kutateladze, T. G. (2016). Multivalent Chromatin Engagement and Inter-domain Crosstalk Regulate MORC3 ATPase. *Cell Reports*, *16*(12), 3195–3207. https://doi.org/10.1016/j.celrep.2016.08.050

Badenhorst, P., Voas, M., Rebay, I., & Wu, C. (2002). Biological functions of the ISWI chromatin remodeling complex NURF. *Genes & Development*, *16*(24), 3186–3198. https://doi.org/10.1101/gad.1032202

Bae, S., & Lesch, B. J. (2020). H3K4me1 Distribution Predicts Transcription State and Poising at Promoters. *Frontiers in Cell and Developmental Biology*, *8*, 289. https://doi.org/10.3389/fcell.2020.00289

Balasubramanian, D., Akhtar-Zaidi, B., Song, L., Bartels, C. F., Veigl, M., Beard, L., Myeroff, L., Guda, K., Lutterbaugh, J., Willis, J., Crawford, G. E., Markowitz, S. D., & Scacheri, P. C. (2012). H3K4me3 inversely correlates with DNA methylation at a large class of non-CpG-island-containing start sites. *Genome Medicine*, *4*(5), 47. https://doi.org/10.1186/gm346

Banaszynski, L. A., Chen, L., Maynard-Smith, L. A., Ooi, A. G. L., & Wandless, T. J. (2006). A Rapid, Reversible, and Tunable Method to Regulate Protein Function in Living Cells Using Synthetic Small Molecules. *Cell*, *126*(5), 995–1004. https://doi.org/10.1016/j.cell.2006.07.025

Barsoum, M., Sayadi-Boroujeni, R., Stenzel, A. T., Bussmann, P., Lüscher-Firzlaff, J., & Lüscher, B. (2023). Sequential deregulation of histone marks, chromatin accessibility and gene expression in response to PROTAC-induced degradation of ASH2L. *Scientific Reports*, *13*(1), 22565. https://doi.org/10.1038/s41598-023-49284-x

Barsoum, M., Stenzel, A. T., Bochyńska, A., Kuo, C.-C., Tsompanidis, A., Sayadi-Boroujeni, R., Bussmann, P., Lüscher-Firzlaff, J., Costa, I. G., & Lüscher, B. (2022). Loss of the Ash2l subunit of histone H3K4 methyltransferase complexes reduces chromatin accessibility at promoters. *Scientific Reports*, *12*(1), 21506. https://doi.org/10.1038/s41598-022-25881-0

Batbayar, G., Ishimura, A., Lyu, H., Wanna-udom, S., Meguro-Horike, M., Terashima, M., Horike, S., Takino, T., & Suzuki, T. (2023). ASH2L, a COMPASS core subunit, is involved in the cell invasion and migration of triple-negative breast cancer cells through the epigenetic control of histone H3 lysine 4 methylation. *Biochemical and Biophysical Research Communications*, *669*, 19–29. https://doi.org/https://doi.org/10.1016/j.bbrc.2023.05.061

Beacon, T. H., Delcuve, G. P., López, C., Nardocci, G., Kovalchuk, I., van Wijnen, A. J., & Davie, J. R. (2021). The dynamic broad epigenetic (H3K4me3, H3K27ac) domain as a mark of essential genes. *Clinical Epigenetics*, *13*(1), 138. https://doi.org/10.1186/s13148-021-01126-1

Békés, M., Langley, D. R., & Crews, C. M. (2022). PROTAC targeted protein degraders: the past is prologue. *Nature Reviews Drug Discovery*, *21*(3), 181–200. https://doi.org/10.1038/s41573-021-00371-6

Benayoun, B. A., Pollina, E. A., Ucar, D., Mahmoudi, S., Karra, K., Wong, E. D., Devarajan, K., Daugherty, A. C., Kundaje, A. B., Mancini, E., Hitz, B. C., Gupta, R., Rando, T. A., Baker, J. C., Snyder, M. P., Cherry, J. M., & Brunet, A. (2014). H3K4me3 breadth is linked to cell identity and transcriptional consistency. *Cell*, *158*(3), 673–688. https://doi.org/10.1016/j.cell.2014.06.027

Bernstein, B. E., Kamal, M., Lindblad-Toh, K., Bekiranov, S., Bailey, D. K., Huebert, D. J., McMahon, S., Karlsson, E. K., Kulbokas III, E. J., Gingeras, T. R., Schreiber, S. L., & Lander, E. S. (2005). Genomic Maps and Comparative Analysis of Histone Modifications in Human and Mouse. *Cell*, *120*(2), 169–181. https://doi.org/10.1016/j.cell.2005.01.001

Bernstein, B. E., Mikkelsen, T. S., Xie, X., Kamal, M., Huebert, D. J., Cuff, J., Fry, B., Meissner, A., Wernig, M., Plath, K., Jaenisch, R., Wagschal, A., Feil, R., Schreiber, S. L., & Lander, E. S. (2006). A bivalent chromatin structure marks key developmental genes in embryonic stem cells. *Cell*, *125*(2), 315–326. https://doi.org/10.1016/j.cell.2006.02.041

Bhagwat, A. S., & Vakoc, C. R. (2014). A New Bump in the Epigenetic Landscape. *Molecular Cell*, *53*(6), 857–858. https://doi.org/https://doi.org/10.1016/j.molcel.2014.03.001

Bian, C., Xu, C., Ruan, J., Lee, K. K., Burke, T. L., Tempel, W., Barsyte, D., Li, J., Wu, M., Zhou, B. O., Fleharty, B. E., Paulson, A., Allali-Hassani, A., Zhou, J.-Q., Mer, G., Grant, P. A., Workman, J. L., Zang, J., & Min, J. (2011). Sgf29 binds histone H3K4me2/3 and is required for SAGA complex recruitment and histone H3 acetylation. *The EMBO Journal*, *30*(14), 2829–2842. https://doi.org/https://doi.org/10.1038/emboj.2011.193

Biel, M., Wascholowski, V., & Giannis, A. (2005). Epigenetics--an epicenter of gene regulation: histones and histone-modifying enzymes. *Angewandte Chemie (International Ed. in English)*, *44*(21), 3186–3216. https://doi.org/10.1002/anie.200461346

Bierne, H., Tham, T. N., Batsche, E., Dumay, A., Leguillou, M., Kernéis-Golsteyn, S., Regnault, B., Seeler, J. S., Muchardt, C., Feunteun, J., & Cossart, P. (2009). Human BAHD1 promotes heterochromatic gene silencing. *Proceedings of the National Academy of Sciences of the United States of America*, *106*(33), 13826–13831. https://doi.org/10.1073/pnas.0901259106

Blanco, E., González-Ramírez, M., Alcaine-Colet, A., Aranda, S., & Di Croce, L. (2020). The Bivalent Genome: Characterization, Structure, and Regulation. *Trends in Genetics*, *36*(2), 118–131. https://doi.org/10.1016/j.tig.2019.11.004

Bochyńska, A. (2023). *The Trithorax protein Ash2l in the control of gene transcription in Mouse embryonic fibroblasts*. RWTH Aachen.

Bochyńska, A., Lüscher-Firzlaff, J., & Lüscher, B. (2018). Modes of Interaction of KMT2 Histone H3 Lysine 4 Methyltransferase/COMPASS Complexes with Chromatin. *Cells*, *7*(3). https://doi.org/10.3390/cells7030017

Bochyńska, A., Stenzel, A. T., Boroujeni, R. S., Kuo, C.-C., Barsoum, M., Liang, W., Bussmann, P., Costa, I. G., Lüscher-Firzlaff, J., & Lüscher, B. (2022). Induction of senescence upon loss of the Ash2l core subunit of H3K4 methyltransferase complexes. *Nucleic Acids Research*, gkac591. https://doi.org/10.1093/nar/gkac591

Bögershausen, N., Bruford, E., & Wollnik, B. (2013). Skirting the pitfalls: a clear-cut nomenclature for H3K4 methyltransferases. *Clinical Genetics*, *83*(3), 212–214. https://doi.org/10.1111/cge.12050

Boros, J., Arnoult, N., Stroobant, V., Collet, J.-F., & Decottignies, A. (2014). Polycomb repressive complex 2 and H3K27me3 cooperate with H3K9 methylation to maintain heterochromatin protein 1α at chromatin. *Molecular and Cellular Biology*, *34*(19), 3662–3674. https://doi.org/10.1128/MCB.00205-14

Boyer, L. A., Plath, K., Zeitlinger, J., Brambrink, T., Medeiros, L. A., Lee, T. I., Levine, S. S., Wernig, M., Tajonar, A., Ray, M. K., Bell, G. W., Otte, A. P., Vidal, M., Gifford, D. K., Young, R. A., & Jaenisch, R. (2006). Polycomb complexes repress developmental regulators in murine embryonic stem cells. *Nature*, *441*(7091), 349–353. https://doi.org/10.1038/nature04733

Branigan, E., Carlos Penedo, J., & Hay, R. T. (2020). Ubiquitin transfer by a RING E3 ligase occurs from a closed E2~ubiquitin conformation. *Nature Communications*, *11*(1), 2846. https://doi.org/10.1038/s41467-020-16666-y

Bril'kov, M. S., Dobrovolska, O., Ødegård-Fougner, Ø., Turcu, D. C., Strømland, Ø., Underhaug, J., Aasland, R., & Halskau, Ø. (2022). Binding Specificity of ASHH2 CW Domain Toward H3K4me1 Ligand Is Coupled to Its Structural Stability Through Its α1-Helix . In *Frontiers in Molecular Biosciences* (Vol. 9). https://www.frontiersin.org/articles/10.3389/fmolb.2022.763750

Brown, D. A., Di Cerbo, V., Feldmann, A., Ahn, J., Ito, S., Blackledge, N. P., Nakayama, M., McClellan, M., Dimitrova, E., Turberfield, A. H., Long, H. K., King, H. W., Kriaucionis, S., Schermelleh, L., Kutateladze, T. G., Koseki, H., & Klose, R. J. (2017). The SET1 Complex Selects Actively Transcribed Target Genes via Multivalent Interaction with CpG Island Chromatin. *Cell Reports*, *20*(10), 2313–2327. https://doi.org/https://doi.org/10.1016/j.celrep.2017.08.030

Bulut-Karslioglu, A., Jin, H., Kim, Y.-K., Cho, B., Guzman-Ayala, M., Williamson, A. J. K., Hejna, M., Stötzel, M., Whetton, A. D., Song, J. S., & Ramalho-Santos, M. (2021). Chd1 protects genome integrity at promoters to sustain hypertranscription in embryonic stem cells. *Nature Communications*, *12*(1), 4859. https://doi.org/10.1038/s41467-021-25088-3

Buratowski, S., & Kim, T. (2011). The role of cotranscriptional histone methylations. *Cold Spring Harbor Symposia on Quantitative Biology*, sqb-2010.

Cai, W. L., Chen, J. F.-Y., Chen, H., Wingrove, E., Kurley, S. J., Chan, L. H., Zhang, M., Arnal-Estape, A., Zhao, M., Balabaki, A., Li, W., Yu, X., Krop, E. D., Dou, Y., Liu, Y., Jin, J., Westbrook, T. F., Nguyen, D. X., & Yan, Q. (2022). Human WDR5 promotes breast cancer growth and metastasis via KMT2-independent translation regulation. *ELife*, *11*, e78163. https://doi.org/10.7554/eLife.78163

Cai, Y., Zhang, Y., Loh, Y. P., Tng, J. Q., Lim, M. C., Cao, Z., Raju, A., Lieberman Aiden, E., Li, S., Manikandan, L., Tergaonkar, V., Tucker-Kellogg, G., & Fullwood, M. J. (2021). H3K27me3-rich genomic regions can function as silencers to repress gene expression via chromatin interactions. *Nature Communications*, *12*(1), 719. https://doi.org/10.1038/s41467-021-20940-y

Campbell, S. A., McDonald, C. L., Krentz, N. A. J., Lynn, F. C., & Hoffman, B. G. (2019). TrxG Complex Catalytic and Non-catalytic Activity Play Distinct Roles in Pancreas Progenitor Specification and Differentiation. *Cell Reports*, *28*(7), 1830-1844.e6. https://doi.org/https://doi.org/10.1016/j.celrep.2019.07.035

Cano-Rodriguez, D., Gjaltema, R. A. F., Jilderda, L. J., Jellema, P., Dokter-Fokkens, J., Ruiters, M. H. J., & Rots, M. G. (2016). Writing of H3K4Me3 overcomes epigenetic silencing in a sustained but context-dependent manner. *Nature Communications*, *7*(1), 12284. https://doi.org/10.1038/ncomms12284

Cao, F., Chen, Y., Cierpicki, T., Liu, Y., Basrur, V., Lei, M., & Dou, Y. (2010). An Ash2L/RbBP5 Heterodimer Stimulates the MLL1 Methyltransferase Activity through Coordinated Substrate Interactions with the MLL1 SET Domain. *PLOS ONE*, *5*(11), e14102. https://doi.org/10.1371/journal.pone.0014102

Caslini, C., Hong, S., Ban, Y. J., Chen, X. S., & Ince, T. A. (2019). HDAC7 regulates histone 3 lysine 27 acetylation and transcriptional activity at super-enhancer-associated genes in breast cancer stem cells. *Oncogene*, *38*(39), 6599–6614. https://doi.org/10.1038/s41388-019-0897-0

Cavalieri, V. (2021). The Expanding Constellation of Histone Post-Translational Modifications in the Epigenetic Landscape. In *Genes* (Vol. 12, Issue 10). https://doi.org/10.3390/genes12101596

Chen, E. Y., Tan, C. M., Kou, Y., Duan, Q., Wang, Z., Meirelles, G. V., Clark, N. R., & Ma'ayan, A. (2013). Enrichr: interactive and collaborative HTML5 gene list enrichment analysis tool. *BMC Bioinformatics*, *14*(1), 128. https://doi.org/10.1186/1471-2105-14-128

Chen, K., Chen, Z., Wu, D., Zhang, L., Lin, X., Su, J., Rodriguez, B., Xi, Y., Xia, Z., Chen, X., Shi, X., Wang, Q., & Li, W. (2015). Broad H3K4me3 is associated with increased transcription elongation and enhancer activity at tumor-suppressor genes. *Nature Genetics*, *47*(10), 1149–1157. https://doi.org/10.1038/ng.3385

Chen, T. J., Bridges, C. S., Puppi, M., & Lacorazza, D. (2022). ASH2L Regulates Genes Involved in the Survival of Leukemic T Cells through a Loci-Specific H3K4me3 Landscape and Leukemogenesis Via Direct Gene Regulation. *Blood*, *140*(Supplement 1), 3048. https://doi.org/10.1182/blood-2022-167476

Chen, Y.-J. C., Koutelou, E., & Dent, S. Y. R. (2022). Now open: Evolving insights to the roles of lysine acetylation in chromatin organization and function. *Molecular Cell*, *82*(4), 716–727. https://doi.org/10.1016/j.molcel.2021.12.004

Chen, Y., Cao, F., Wan, B., Dou, Y., & Lei, M. (2012). Structure of the SPRY domain of human Ash2L and its interactions with RbBP5 and DPY30. *Cell Research*, *22*(3), 598–602. https://doi.org/10.1038/cr.2012.9

Chen, Y., Wan, B., Wang, K. C., Cao, F., Yang, Y., Protacio, A., Dou, Y., Chang, H. Y., & Lei, M. (2011). Crystal structure of the N-terminal region of human Ash2L shows a winged-helix motif involved in DNA binding. *EMBO Reports*, *12*(8), 797–803. https://doi.org/https://doi.org/10.1038/embor.2011.101

Cheng, J., Blum, R., Bowman, C., Hu, D., Shilatifard, A., Shen, S., & Dynlacht, B. D. (2014). A Role for H3K4 Monomethylation in Gene Repression and Partitioning of Chromatin Readers. *Molecular Cell*, *53*(6), 979–992. https://doi.org/https://doi.org/10.1016/j.molcel.2014.02.032

Chiang, C.-M. (2009). Brd4 engagement from chromatin targeting to transcriptional regulation: selective contact with acetylated histone H3 and H4. *F1000 Biology Reports*, *1*, 98. https://doi.org/10.3410/B1-98

Ciccone, D. N., Su, H., Hevi, S., Gay, F., Lei, H., Bajko, J., Xu, G., Li, E., & Chen, T. (2009). KDM1B is a histone H3K4 demethylase required to establish maternal genomic imprints. *Nature*, *461*(7262), 415–418. https://doi.org/10.1038/nature08315

Ciechanover, A., & Schwartz, A. L. (1998). The ubiquitin-proteasome pathway: the complexity and myriad functions of proteins death. *Proceedings of the National Academy of Sciences of the United States of America*, *95*(6), 2727–2730. https://doi.org/10.1073/pnas.95.6.2727

Clouaire, T., Webb, S., Skene, P., Illingworth, R., Kerr, A., Andrews, R., Lee, J.-H., Skalnik, D., & Bird, A. (2012). Cfp1 integrates both CpG content and gene activity for accurate H3K4me3 deposition in embryonic stem cells. *Genes & Development*, *26*(15), 1714–1728. https://doi.org/10.1101/gad.194209.112

Constantin, D., & Widmann, C. (2020). ASH2L drives proliferation and sensitivity to bleomycin and other genotoxins in Hodgkin's lymphoma and testicular cancer cells. *Cell Death & Disease*, *11*(11), 1019. https://doi.org/10.1038/s41419-020-03231-0

Creighton, S. D., Stefanelli, G., Reda, A., & Zovkic, I. B. (2020). Epigenetic Mechanisms of Learning and Memory: Implications for Aging. *International Journal of Molecular Sciences*, *21*(18). https://doi.org/10.3390/ijms21186918

Creyghton, M. P., Cheng, A. W., Welstead, G. G., Kooistra, T., Carey, B. W., Steine, E. J., Hanna, J., Lodato, M. A., Frampton, G. M., Sharp, P. A., Boyer, L. A., Young, R. A., & Jaenisch, R. (2010). Histone H3K27ac separates active from poised enhancers and predicts developmental state. *Proceedings of the National Academy of Sciences*, *107*(50), 21931–21936. https://doi.org/10.1073/pnas.1016071107

Crump, N. T., Hazzalin, C. A., Bowers, E. M., Alani, R. M., Cole, P. A., & Mahadevan, L. C. (2011). Dynamic acetylation of all lysine-4 trimethylated histone H3 is evolutionarily conserved and mediated by p300/CBP. *Proceedings of the National Academy of Sciences of the United States of America*, *108*(19), 7814–7819. https://doi.org/10.1073/pnas.1100099108

Damgaard, R. B. (2021). The ubiquitin system: from cell signalling to disease biology and new therapeutic opportunities. *Cell Death & Differentiation*, *28*(2), 423–426. https://doi.org/10.1038/s41418-020-00703-w

Dimitrova, E., Turberfield, A. H., & Klose, R. J. (2015). Histone demethylases in chromatin biology and beyond. *EMBO Reports*, *16*(12), 1620–1639. https://doi.org/10.15252/embr.201541113

Ding, Y., Ndamukong, I., Xu, Z., Lapko, H., Fromm, M., & Avramova, Z. (2012). ATX1-generated H3K4me3 is required for efficient elongation of transcription, not initiation, at ATX1-regulated genes. *PLoS Genetics*, *8*(12), e1003111. https://doi.org/10.1371/journal.pgen.1003111

Dobin, A., Davis, C. A., Schlesinger, F., Drenkow, J., Zaleski, C., Jha, S., Batut, P., Chaisson, M., &

Gingeras, T. R. (2013). STAR: ultrafast universal RNA-seq aligner. *Bioinformatics (Oxford, England)*, *29*(1), 15–21. https://doi.org/10.1093/bioinformatics/bts635

Dorighi, K. M., Swigut, T., Henriques, T., Bhanu, N. V, Scruggs, B. S., Nady, N., Still, C. D. 2nd, Garcia, B. A., Adelman, K., & Wysocka, J. (2017). Mll3 and Mll4 Facilitate Enhancer RNA Synthesis and Transcription from Promoters Independently of H3K4 Monomethylation. *Molecular Cell*, *66*(4), 568-576.e4. https://doi.org/10.1016/j.molcel.2017.04.018

Dorighi, K. M., & Tamkun, J. W. (2013). The trithorax group proteins Kismet and ASH1 promote H3K36 dimethylation to counteract Polycomb group repression in Drosophila. *Development (Cambridge, England)*, *140*(20), 4182–4192. https://doi.org/10.1242/dev.095786

Dou, Y., Milne, T. A., Ruthenburg, A. J., Lee, S., Lee, J. W., Verdine, G. L., Allis, C. D., & Roeder, R. G. (2006). Regulation of MLL1 H3K4 methyltransferase activity by its core components. *Nature Structural & Molecular Biology*, *13*(8), 713–719. https://doi.org/10.1038/nsmb1128

Ernst, J., Melnikov, A., Zhang, X., Wang, L., Rogov, P., Mikkelsen, T. S., & Kellis, M. (2016). Genome-scale high-resolution mapping of activating and repressive nucleotides in regulatory regions. *Nature Biotechnology*, *34*(11), 1180–1190. https://doi.org/10.1038/nbt.3678

Ernst, P., & Vakoc, C. R. (2012). WRAD: enabler of the SET1-family of H3K4 methyltransferases. *Briefings in Functional Genomics*, *11*(3), 217–226. https://doi.org/10.1093/bfgp/els017

Fang, Y., Tang, Y., Zhang, Y., Pan, Y., Jia, J., Sun, Z., Zeng, W., Chen, J., Yuan, Y., & Fang, D. (2021). The H3K36me2 methyltransferase NSD1 modulates H3K27ac at active enhancers to safeguard gene expression. *Nucleic Acids Research*, *49*(11), 6281–6295. https://doi.org/10.1093/nar/gkab473

Fischer, E. S., Böhm, K., Lydeard, J. R., Yang, H., Stadler, M. B., Cavadini, S., Nagel, J., Serluca, F., Acker, V., Lingaraju, G. M., Tichkule, R. B., Schebesta, M., Forrester, W. C., Schirle, M., Hassiepen, U., Ottl, J., Hild, M., Beckwith, R. E. J., Harper, J. W., … Thomä, N. H. (2014). Structure of the DDB1–CRBN E3 ubiquitin ligase in complex with thalidomide. *Nature*, *512*(7512), 49–53. https://doi.org/10.1038/nature13527

Flanagan, J. F., Mi, L.-Z., Chruszcz, M., Cymborowski, M., Clines, K. L., Kim, Y., Minor, W., Rastinejad, F., & Khorasanizadeh, S. (2005). Double chromodomains cooperate to recognize the methylated histone H3 tail. *Nature*, *438*(7071), 1181–1185. https://doi.org/10.1038/nature04290

Froimchuk, E., Jang, Y., & Ge, K. (2017). Histone H3 lysine 4 methyltransferase KMT2D. *Gene*, *627*, 337–342. https://doi.org/https://doi.org/10.1016/j.gene.2017.06.056

Gao, X., Burris III, H. A., Vuky, J., Dreicer, R., Sartor, A. O., Sternberg, C. N., Percent, I. J., Hussain, M. H. A., Rezazadeh Kalebasty, A., Shen, J., Heath, E. I., Abesada-Terk, G., Gandhi, S. G., McKean, M., Lu, H., Berghorn, E., Gedrich, R., Chirnomas, S. D., Vogelzang, N. J., & Petrylak, D. P. (2022). Phase 1/2 study of ARV-110, an androgen receptor (AR) PROTAC degrader, in metastatic castration-resistant prostate cancer (mCRPC). *Journal of Clinical Oncology*, *40*(6_suppl), 17. https://doi.org/10.1200/JCO.2022.40.6_suppl.017

Gao, Y., Chen, L., Han, Y., Wu, F., Yang, W.-S., Zhang, Z., Huo, T., Zhu, Y., Yu, C., Kim, H., Lee, M., Tang, Z., Phillips, K., He, B., Jung, S. Y., Song, Y., Zhu, B., Xu, R.-M., & Feng, Q. (2020). Acetylation of histone H3K27 signals the transcriptional elongation for estrogen receptor alpha. *Communications Biology*, *3*(1), 165. https://doi.org/10.1038/s42003-020-0898-0

Gatchalian, J., Gallardo, C. M., Shinsky, S. A., Ospina, R. R., Liendo, A. M., Krajewski, K., Klein, B. J., Andrews, F. H., Strahl, B. D., M van Wely, K. H., & Kutateladze, T. G. (2016). Chromatin condensation and recruitment of PHD finger proteins to histone H3K4me3 are mutually exclusive. *Nucleic Acids Research*, *44*(13), 6102–6112. https://doi.org/10.1093/nar/gkw193

Grice, G. L., & Nathan, J. A. (2016). The recognition of ubiquitinated proteins by the proteasome. *Cellular and Molecular Life Sciences : CMLS*, *73*(18), 3497–3506. https://doi.org/10.1007/s00018-016-2255-5

Guo, J., Liu, J., & Wei, W. (2019). Degrading proteins in animals: "PROTAC"tion goes in vivo. *Cell Research*, *29*(3), 179–180. https://doi.org/10.1038/s41422-019-0144-9

Haines, R. R., Barwick, B. G., Scharer, C. D., Majumder, P., Randall, T. D., & Boss, J. M. (2018). The Histone Demethylase LSD1 Regulates B Cell Proliferation and Plasmablast Differentiation. *The Journal of Immunology*, *201*(9), 2799–2811. https://doi.org/10.4049/jimmunol.1800952

Hamilton, E. P., Schott, A. F., Nanda, R., Lu, H., Keung, C. F., Gedrich, R., Parameswaran, J., Han, H. S., & Hurvitz, S. A. (2022). ARV-471, an estrogen receptor (ER) PROTAC degrader, combined with palbociclib in advanced ER+/human epidermal growth factor receptor 2–negative (HER2-) breast cancer: Phase 1b cohort (part C) of a phase 1/2 study. *Journal of Clinical Oncology*, *40*(16_suppl), TPS1120–TPS1120. https://doi.org/10.1200/JCO.2022.40.16_suppl.TPS1120

He, F., Umehara, T., Saito, K., Harada, T., Watanabe, S., Yabuki, T., Kigawa, T., Takahashi, M., Kuwasako, K., Tsuda, K., Matsuda, T., Aoki, M., Seki, E., Kobayashi, N., Güntert, P., Yokoyama, S., & Muto, Y. (2010). Structural Insight into the Zinc Finger CW Domain as a Histone Modification Reader. *Structure*, *18*(9), 1127–1139. https://doi.org/https://doi.org/10.1016/j.str.2010.06.012

Hershko, A., & Ciechanover, A. (1998). The ubiquitin system. *Annual Review of Biochemistry*, *67*, 425–479. https://doi.org/10.1146/annurev.biochem.67.1.425

Hilton, I. B., D'Ippolito, A. M., Vockley, C. M., Thakore, P. I., Crawford, G. E., Reddy, T. E., & Gersbach, C. A. (2015). Epigenome editing by a CRISPR-Cas9-based acetyltransferase activates genes from promoters and enhancers. *Nature Biotechnology*, *33*(5), 510–517. https://doi.org/10.1038/nbt.3199

Hirayama, S., Sugihara, M., Morito, D., Iemura, S., Natsume, T., Murata, S., & Nagata, K. (2018). Nuclear export of ubiquitinated proteins via the UBIN-POST system. *Proceedings of the National Academy of Sciences*, *115*(18), E4199–E4208. https://doi.org/10.1073/pnas.1711017115

Højfeldt, J. W., Agger, K., & Helin, K. (2013). Histone lysine demethylases as targets for anticancer therapy. *Nature Reviews. Drug Discovery*, *12*(12), 917–930. https://doi.org/10.1038/nrd4154

Höller, M., Westin, G., Jiricny, J., & Schaffner, W. (1988). Sp1 transcription factor binds DNA and activates transcription even when the binding site is CpG methylated. *Genes & Development*, *2*(9), 1127–1135. https://doi.org/10.1101/gad.2.9.1127

Hoshii, T., Perlee, S., Kikuchi, S., Rahmutulla, B., Fukuyo, M., Masuda, T., Ohtsuki, S., Soga, T., Nabet, B., & Kaneda, A. (2022). SETD1A regulates transcriptional pause release of heme biosynthesis genes in leukemia. *Cell Reports*, *41*(9), 111727. https://doi.org/10.1016/j.celrep.2022.111727

Housden, B. E., Muhar, M., Gemberling, M., Gersbach, C. A., Stainier, D. Y. R., Seydoux, G., Mohr, S. E., Zuber, J., & Perrimon, N. (2017). Loss-of-function genetic tools for animal models: cross-species and cross-platform differences. *Nature Reviews. Genetics*, *18*(1), 24–40. https://doi.org/10.1038/nrg.2016.118

Howe, F. S., Fischl, H., Murray, S. C., & Mellor, J. (2017). Is H3K4me3 instructive for transcription activation? *BioEssays*, *39*(1), e201600095. https://doi.org/https://doi.org/10.1002/bies.201600095

Hu, S., Song, A., Peng, L., Tang, N., Qiao, Z., Wang, Z., Lan, F., & Chen, F. X. (2023). H3K4me2/3 modulate the stability of RNA polymerase II pausing. *Cell Research*, *33*(5), 403–406. https://doi.org/10.1038/s41422-023-00794-3

Huang, R. P., Fan, Y., Ni, Z., Mercola, D., & Adamson, E. D. (1997). Reciprocal modulation between Sp1 and Egr-1. *Journal of Cellular Biochemistry*, *66*(4), 489–499.

Hughes, A. L., Kelley, J. R., & Klose, R. J. (2020). Understanding the interplay between CpG island-associated gene promoters and H3K4 methylation. *Biochimica et Biophysica Acta (BBA) - Gene Regulatory Mechanisms*, *1863*(8), 194567. https://doi.org/https://doi.org/10.1016/j.bbagrm.2020.194567

Hughes, A. L., Szczurek, A. T., Kelley, J. R., Lastuvkova, A., Turberfield, A. H., Dimitrova, E., Blackledge, N. P., & Klose, R. J. (2023). A CpG island-encoded mechanism protects genes from premature transcription termination. *Nature Communications*, *14*(1), 726. https://doi.org/10.1038/s41467-023-36236-2

Hyun, K., Jeon, J., Park, K., & Kim, J. (2017). Writing, erasing and reading histone lysine methylations. *Experimental & Molecular Medicine*, *49*(4), e324–e324. https://doi.org/10.1038/emm.2017.11

Igolkina, A. A., Zinkevich, A., Karandasheva, K. O., Popov, A. A., Selifanova, M. V, Nikolaeva, D., Tkachev, V., Penzar, D., Nikitin, D. M., & Buzdin, A. (2019). H3K4me3, H3K9ac, H3K27ac, H3K27me3 and H3K9me3 Histone Tags Suggest Distinct Regulatory Evolution of Open and Condensed Chromatin Landmarks. *Cells*, *8*(9), 1034. https://doi.org/10.3390/cells8091034

Ikegawa, S., Isomura, M., Koshizuka, Y., & Nakamura, Y. (1999). Cloning and characterization of ASH2L and Ash2l, human and mouse homologs of the Drosophila ash2 gene. *Cytogenetics and Cell Genetics*, *84*(3–4), 167–172. https://doi.org/10.1159/000015248

Isles, A. R. (2018). Epigenetics, chromatin and brain development and function. *Brain and Neuroscience Advances*, *2*, 2398212818812011. https://doi.org/10.1177/2398212818812011

Ito, T., Ando, H., Suzuki, T., Ogura, T., Hotta, K., Imamura, Y., Yamaguchi, Y., & Handa, H. (2010). Identification of a primary target of thalidomide teratogenicity. *Science (New York, N.Y.)*, *327*(5971), 1345–1350. https://doi.org/10.1126/science.1177319

Ito, T., & Handa, H. (2020). Molecular mechanisms of thalidomide and its derivatives. *Proceedings of the Japan Academy. Series B, Physical and Biological Sciences*, *96*(6), 189–203. https://doi.org/10.2183/pjab.96.016

Jang, Y., Wang, C., Zhuang, L., Liu, C., & Ge, K. (2017). H3K4 Methyltransferase Activity Is Required for MLL4 Protein Stability. *Journal of Molecular Biology*, *429*(13), 2046–2054. https://doi.org/https://doi.org/10.1016/j.jmb.2016.12.016

Kang, Y., Kim, Y. W., Kang, J., & Kim, A. (2021). Histone H3K4me1 and H3K27ac play roles in nucleosome eviction and eRNA transcription, respectively, at enhancers. *FASEB Journal : Official Publication of the Federation of American Societies for Experimental Biology*, *35*(8), e21781. https://doi.org/10.1096/fj.202100488R

Kassis, J. A., Kennison, J. A., & Tamkun, J. W. (2017). Polycomb and Trithorax Group Genes in Drosophila. *Genetics*, *206*(4), 1699–1725. https://doi.org/10.1534/genetics.115.185116

Katoh, N., Kuroda, K., Tomikawa, J., Ogata-Kawata, H., Ozaki, R., Ochiai, A., Kitade, M., Takeda, S., Nakabayashi, K., & Hata, K. (2018). Reciprocal changes of H3K27ac and H3K27me3 at the promoter regions of the critical genes for endometrial decidualization. *Epigenomics*, *10*(9), 1243–1257. https://doi.org/10.2217/epi-2018-0006

Kennison, J. A. (1995). The Polycomb and trithorax group proteins of Drosophila: trans-regulators of homeotic gene function. *Annual Review of Genetics*, *29*, 289–303. https://doi.org/10.1146/annurev.ge.29.120195.001445

Kiely-Collins, H., Winter, G. E., & Bernardes, G. J. L. (2021). The role of reversible and irreversible

covalent chemistry in targeted protein degradation. *Cell Chemical Biology*, *28*(7), 952–968. https://doi.org/https://doi.org/10.1016/j.chembiol.2021.03.005

Kim, J., Daniel, J., Espejo, A., Lake, A., Krishna, M., Xia, L., Zhang, Y., & Bedford, M. T. (2006). Tudor, MBT and chromo domains gauge the degree of lysine methylation. *EMBO Reports*, *7*(4), 397–403. https://doi.org/10.1038/sj.embor.7400625

Kim, T. W., Kang, B.-H., Jang, H., Kwak, S., Shin, J., Kim, H., Lee, S.-E., Lee, S.-M., Lee, J.-H., Kim, J.-H., Kim, S.-Y., Cho, E.-J., Kim, J. H., Park, K. S., Che, J.-H., Han, D. W., Kang, M. J., Yi, E. C., & Youn, H.-D. (2015). Ctbp2 Modulates NuRD-Mediated Deacetylation of H3K27 and Facilitates PRC2-Mediated H3K27me3 in Active Embryonic Stem Cell Genes During Exit from Pluripotency. *Stem Cells (Dayton, Ohio)*, *33*(8), 2442–2455. https://doi.org/10.1002/stem.2046

King, A. D., Huang, K., Rubbi, L., Liu, S., Wang, C.-Y., Wang, Y., Pellegrini, M., & Fan, G. (2016). Reversible Regulation of Promoter and Enhancer Histone Landscape by DNA Methylation in Mouse Embryonic Stem Cells. *Cell Reports*, *17*(1), 289–302. https://doi.org/10.1016/j.celrep.2016.08.083

Kingston, R. E., & Tamkun, J. W. (2014). Transcriptional regulation by trithorax-group proteins. *Cold Spring Harbor Perspectives in Biology*, *6*(10), a019349. https://doi.org/10.1101/cshperspect.a019349

Kornberg, R. D. (1974). Chromatin structure: a repeating unit of histones and DNA. *Science (New York, N.Y.)*, *184*(4139), 868–871. https://doi.org/10.1126/science.184.4139.868

Krause, K., & Turck, F. (2018). Plant H3K27me3 has finally found its readers. *Nature Genetics*, *50*(9), 1206–1208. https://doi.org/10.1038/s41588-018-0201-1

Kraushaar, D. C., Chen, Z., Tang, Q., Cui, K., Zhang, J., & Zhao, K. (2018). The gene repressor complex NuRD interacts with the histone variant H3.3 at promoters of active genes. *Genome Research*, *28*(11), 1646–1655. https://doi.org/10.1101/gr.236224.118

Kubosaki, A., Tomaru, Y., Tagami, M., Arner, E., Miura, H., Suzuki, T., Suzuki, M., Suzuki, H., & Hayashizaki, Y. (2009). Genome-wide investigation of in vivo EGR-1 binding sites in monocytic differentiation. *Genome Biology*, *10*(4), R41. https://doi.org/10.1186/gb-2009-10-4-r41

LaJeunesse, D., & Shearn, A. (1995). Trans-regulation of thoracic homeotic selector genes of the Antennapedia and bithorax complexes by the trithorax group genes: absent, small, and homeotic discs 1 and 2. *Mechanisms of Development*, *53*(1), 123–139. https://doi.org/10.1016/0925-4773(95)00430-0

Landsverk, H. B., Sandquist, L. E., Bay, L. T. E., Steurer, B., Campsteijn, C., Landsverk, O. J. B., Marteijn, J. A., Petermann, E., Trinkle-Mulcahy, L., & Syljuåsen, R. G. (2020). WDR82/PNUTS-PP1 Prevents Transcription-Replication Conflicts by Promoting RNA Polymerase II Degradation on Chromatin. *Cell Reports*, *33*(9), 108469. https://doi.org/https://doi.org/10.1016/j.celrep.2020.108469

Landsverk, H. B., Sandquist, L. E., Bay, L. T. E., & Syljuåsen, R. G. (2021). New link between the RNA polymerase II-CTD and replication stress. *Molecular & Cellular Oncology*, *8*(3), 1910008. https://doi.org/10.1080/23723556.2021.1910008

Lauberth, S. M., Nakayama, T., Wu, X., Ferris, A. L., Tang, Z., Hughes, S. H., & Roeder, R. G. (2013). H3K4me3 Interactions with TAF3 Regulate Preinitiation Complex Assembly and Selective Gene Activation. *Cell*, *152*(5), 1021–1036. https://doi.org/10.1016/j.cell.2013.01.052

Lavarone, E., Barbieri, C. M., & Pasini, D. (2019). Dissecting the role of H3K27 acetylation and methylation in PRC2 mediated control of cellular identity. *Nature Communications*, *10*(1), 1679. https://doi.org/10.1038/s41467-019-09624-w

LeBlanc, N., Mallette, E., & Zhang, W. (2021). Targeted modulation of E3 ligases using engineered ubiquitin variants. *The FEBS Journal*, *288*(7), 2143–2165. https://doi.org/10.1111/febs.15536

Lee, J.-H., & Skalnik, D. G. (2008). Wdr82 is a C-terminal domain-binding protein that recruits the Setd1A Histone H3-Lys4 methyltransferase complex to transcription start sites of transcribed human genes. *Molecular and Cellular Biology*, *28*(2), 609–618. https://doi.org/10.1128/MCB.01356-07

Lee, Y.-T., Ayoub, A., Park, S.-H., Sha, L., Xu, J., Mao, F., Zheng, W., Zhang, Y., Cho, U.-S., & Dou, Y. (2021). Mechanism for DPY30 and ASH2L intrinsically disordered regions to modulate the MLL/SET1 activity on chromatin. *Nature Communications*, *12*(1), 2953. https://doi.org/10.1038/s41467-021-23268-9

Li, D., Yu, X., Kottur, J., Gong, W., Zhang, Z., Storey, A. J., Tsai, Y.-H., Uryu, H., Shen, Y., Byrum, S. D., Edmondson, R. D., Mackintosh, S. G., Cai, L., Liu, Z., Aggarwal, A. K., Tackett, A. J., Liu, J., Jin, J., & Wang, G. G. (2022). Discovery of a dual WDR5 and Ikaros PROTAC degrader as an anti-cancer therapeutic. *Oncogene*, *41*(24), 3328–3340. https://doi.org/10.1038/s41388-022-02340-8

Li, G., Tian, Y., & Zhu, W.-G. (2020). The Roles of Histone Deacetylases and Their Inhibitors in Cancer Therapy . In *Frontiers in Cell and Developmental Biology* (Vol. 8). https://www.frontiersin.org/articles/10.3389/fcell.2020.576946

Li, H., & Durbin, R. (2009). Fast and accurate short read alignment with Burrows–Wheeler transform. *Bioinformatics*, *25*(14), 1754–1760. https://doi.org/10.1093/bioinformatics/btp324

Li, H., Ilin, S., Wang, W., Duncan, E. M., Wysocka, J., Allis, C. D., & Patel, D. J. (2006). Molecular basis for site-specific read-out of histone H3K4me3 by the BPTF PHD finger of NURF. *Nature*, *442*(7098), 91–95. https://doi.org/10.1038/nature04802

Li, L., Ruan, X., Wen, C., Chen, P., Liu, W., Zhu, L., Xiang, P., Zhang, X., Wei, Q., Hou, L., Yin, B., Yuan, J., Qiang, B., Shu, P., & Peng, X. (2019). The COMPASS Family Protein ASH2L Mediates Corticogenesis via Transcriptional Regulation of Wnt Signaling. *Cell Reports*, *28*(3), 698-711.e5. https://doi.org/https://doi.org/10.1016/j.celrep.2019.06.055

Li, X., Yang, H., Huang, S., & Qiu, Y. (2014). Histone Deacetylase 1 and p300 Can Directly Associate with Chromatin and Compete for Binding in a Mutually Exclusive Manner. *PLOS ONE*, *9*(4), e94523. https://doi.org/10.1371/journal.pone.0094523

Liang, W. (2016). *The functional role of Ash2l in mouse liver and embryonic fibroblasts using a conditional knockout model*. RWTH Aachen.

Liao, Y., Smyth, G. K., & Shi, W. (2014). featureCounts: an efficient general purpose program for assigning sequence reads to genomic features. *Bioinformatics*, *30*(7), 923–930. https://doi.org/10.1093/bioinformatics/btt656

Liu, X., Wang, C., Liu, W., Li, J., Li, C., Kou, X., Chen, J., Zhao, Y., Gao, H., Wang, H., Zhang, Y., Gao, Y., & Gao, S. (2016). Distinct features of H3K4me3 and H3K27me3 chromatin domains in pre-implantation embryos. *Nature*, *537*(7621), 558–562. https://doi.org/10.1038/nature19362

Livak, K. J., & Schmittgen, T. D. (2001). Analysis of relative gene expression data using real-time quantitative PCR and the 2(-Delta Delta C(T)) Method. *Methods (San Diego, Calif.)*, *25*(4), 402–408. https://doi.org/10.1006/meth.2001.1262

Local, A., Huang, H., Albuquerque, C. P., Singh, N., Lee, A. Y., Wang, W., Wang, C., Hsia, J. E., Shiau, A. K., Ge, K., Corbett, K. D., Wang, D., Zhou, H., & Ren, B. (2018). Identification of H3K4me1-associated proteins at mammalian enhancers. *Nature Genetics*, *50*(1), 73–82. https://doi.org/10.1038/s41588-017-0015-6

Long, H. K., Blackledge, N. P., & Klose, R. J. (2013). ZF-CxxC domain-containing proteins, CpG islands and the chromatin connection. *Biochemical Society Transactions*, *41*(3), 727–740. https://doi.org/10.1042/BST20130028

Long, H. K., Sims, D., Heger, A., Blackledge, N. P., Kutter, C., Wright, M. L., Grützner, F., Odom, D. T., Patient, R., Ponting, C. P., & Klose, R. J. (2013). Epigenetic conservation at gene regulatory elements revealed by non-methylated DNA profiling in seven vertebrates. *ELife*, *2*, e00348. https://doi.org/10.7554/eLife.00348

Lorch, Y., LaPointe, J. W., & Kornberg, R. D. (1987). Nucleosomes inhibit the initiation of transcription but allow chain elongation with the displacement of histones. *Cell*, *49*(2), 203–210. https://doi.org/10.1016/0092-8674(87)90561-7

Love, M. I., Huber, W., & Anders, S. (2014). Moderated estimation of fold change and dispersion for RNA-seq data with DESeq2. *Genome Biology*, *15*(12), 550. https://doi.org/10.1186/s13059-014-0550-8

Lüscher-Firzlaff, J., Chatain, N., Kuo, C.-C., Braunschweig, T., Bochyńska, A., Ullius, A., Denecke, B., Costa, I. G., Koschmieder, S., & Lüscher, B. (2019). Hematopoietic stem and progenitor cell proliferation and differentiation requires the trithorax protein Ash2l. *Scientific Reports*, *9*(1), 8262. https://doi.org/10.1038/s41598-019-44720-3

Lüscher-Firzlaff, J., Gawlista, I., Vervoorts, J., Kapelle, K., Braunschweig, T., Walsemann, G., Rodgarkia-Schamberger, C., Schuchlautz, H., Dreschers, S., Kremmer, E., Lilischkis, R., Cerni, C., Wellmann, A., & Lüscher, B. (2008). The Human Trithorax Protein hASH2 Functions as an Oncoprotein. *Cancer Research*, *68*(3), 749–758. https://doi.org/10.1158/0008-5472.CAN-07-3158

Ma, M., Zhou, J., Ma, Z., Chen, H., Li, L., Hou, L., Yin, B., Qiang, B., Shu, P., & Peng, X. (2022). The Ash2l SDI Domain Is Required to Maintain the Stability and Binding of DPY30. In *Cells* (Vol. 11, Issue 9). https://doi.org/10.3390/cells11091450

Maity, S., Farrell, K., Navabpour, S., Narayanan, S. N., & Jarome, T. J. (2021). Epigenetic Mechanisms in Memory and Cognitive Decline Associated with Aging and Alzheimer's Disease. *International Journal of Molecular Sciences*, *22*(22). https://doi.org/10.3390/ijms222212280

Mann, M., Roberts, D. S., Zhu, Y., Li, Y., Zhou, J., Ge, Y., & Brasier, A. R. (2021). Discovery of RSV-Induced BRD4 Protein Interactions Using Native Immunoprecipitation and Parallel Accumulation-Serial Fragmentation (PASEF) Mass Spectrometry. *Viruses*, *13*(3). https://doi.org/10.3390/v13030454

Manzo, M., Wirz, J., Ambrosi, C., Villaseñor, R., Roschitzki, B., & Baubec, T. (2017). Isoform-specific localization of DNMT3A regulates DNA methylation fidelity at bivalent CpG islands. *The EMBO Journal*, *36*(23), 3421–3434. https://doi.org/10.15252/embj.201797038

Margueron, R., & Reinberg, D. (2011). The Polycomb complex PRC2 and its mark in life. *Nature*, *469*(7330), 343–349. https://doi.org/10.1038/nature09784

Marriott, J. B., Muller, G., Stirling, D., & Dalgleish, A. G. (2001). Immunotherapeutic and antitumour potential of thalidomide analogues. *Expert Opinion on Biological Therapy*, *1*(4), 675–682. https://doi.org/10.1517/14712598.1.4.675

Martínez-Balbás, M. A., Tsukiyama, T., Gdula, D., & Wu, C. (1998). Drosophila NURF-55, a WD repeat protein involved in histone metabolism. *Proceedings of the National Academy of Sciences of the United States of America*, *95*(1), 132–137. https://doi.org/10.1073/pnas.95.1.132

Mazo, A. M., Huang, D. H., Mozer, B. A., & Dawid, I. B. (1990). The trithorax gene, a trans-acting

regulator of the bithorax complex in Drosophila, encodes a protein with zinc-binding domains. *Proceedings of the National Academy of Sciences of the United States of America*, *87*(6), 2112–2116. https://doi.org/10.1073/pnas.87.6.2112

Meehan, R. R., & Pennings, S. (2017). Shoring up DNA methylation and H3K27me3 domain demarcation at developmental genes. *The EMBO Journal*, *36*(23), 3407–3408. https://doi.org/10.15252/embj.201798498

Miao, L., Tang, Y., Bonneau, A. R., Chan, S. H., Kojima, M. L., Pownall, M. E., Vejnar, C. E., Gao, F., Krishnaswamy, S., Hendry, C. E., & Giraldez, A. J. (2022). The landscape of pioneer factor activity reveals the mechanisms of chromatin reprogramming and genome activation. *Molecular Cell*, *82*(5), 986-1002.e9. https://doi.org/10.1016/j.molcel.2022.01.024

Mikkelsen, T. S., Ku, M., Jaffe, D. B., Issac, B., Lieberman, E., Giannoukos, G., Alvarez, P., Brockman, W., Kim, T.-K., Koche, R. P., Lee, W., Mendenhall, E., O'Donovan, A., Presser, A., Russ, C., Xie, X., Meissner, A., Wernig, M., Jaenisch, R., … Bernstein, B. E. (2007). Genome-wide maps of chromatin state in pluripotent and lineage-committed cells. *Nature*, *448*(7153), 553–560. https://doi.org/10.1038/nature06008

Millán-Zambrano, G., Burton, A., Bannister, A. J., & Schneider, R. (2022). Histone post-translational modifications — cause and consequence of genome function. *Nature Reviews Genetics*, *23*(9), 563–580. https://doi.org/10.1038/s41576-022-00468-7

Mohammadparast, S., & Chang, C. (2022). Ash2l, an obligatory component of H3K4 methylation complexes, regulates neural crest development. *Developmental Biology*, *492*, 14–24. https://doi.org/10.1016/j.ydbio.2022.09.008

Morey, L., & Helin, K. (2010). Polycomb group protein-mediated repression of transcription. *Trends in Biochemical Sciences*, *35*(6), 323–332. https://doi.org/10.1016/j.tibs.2010.02.009

Morreale, F. E., & Walden, H. (2016). Types of Ubiquitin Ligases. *Cell*, *165*(1), 248-248.e1. https://doi.org/10.1016/j.cell.2016.03.003

Mungamuri, S. K., Wang, S., Manfredi, J. J., Gu, W., & Aaronson, S. A. (2015). Ash2L enables P53-dependent apoptosis by favoring stable transcription pre-initiation complex formation on its pro-apoptotic target promoters. *Oncogene*, *34*(19), 2461–2470. https://doi.org/10.1038/onc.2014.198

Nabet, B., Roberts, J. M., Buckley, D. L., Paulk, J., Dastjerdi, S., Yang, A., Leggett, A. L., Erb, M. A., Lawlor, M. A., Souza, A., Scott, T. G., Vittori, S., Perry, J. A., Qi, J., Winter, G. E., Wong, K.-K., Gray, N. S., & Bradner, J. E. (2018). The dTAG system for immediate and target-specific protein degradation. *Nature Chemical Biology*, *14*(5), 431–441. https://doi.org/10.1038/s41589-018-0021-8

Ng, H. H., Robert, F., Young, R. A., & Struhl, K. (2003). Targeted recruitment of Set1 histone methylase by elongating Pol II provides a localized mark and memory of recent transcriptional activity. *Molecular Cell*, *11*(3), 709–719. https://doi.org/10.1016/s1097-2765(03)00092-3

Nishioka, K., Chuikov, S., Sarma, K., Erdjument-Bromage, H., Allis, C. D., Tempst, P., & Reinberg, D. (2002). Set9, a novel histone H3 methyltransferase that facilitates transcription by precluding histone tail modifications required for heterochromatin formation. *Genes & Development*, *16*(4), 479–489. https://doi.org/10.1101/gad.967202

Okitsu, C. Y., Hsieh, J. C. F., & Hsieh, C.-L. (2010). Transcriptional activity affects the H3K4me3 level and distribution in the coding region. *Molecular and Cellular Biology*, *30*(12), 2933–2946. https://doi.org/10.1128/MCB.01478-09

Olins, A. L., & Olins, D. E. (1974). Spheroid chromatin units (v bodies). *Science (New York, N.Y.)*, *183*(4122), 330–332. https://doi.org/10.1126/science.183.4122.330

Osborne, A. (2017). The role of epigenetics in human evolution. *Bioscience Horizons: The International Journal of Student Research*, *10*, hzx007. https://doi.org/10.1093/biohorizons/hzx007

Park, K., Kim, J.-A., & Kim, J. (2020). Transcriptional regulation by the KMT2 histone H3K4 methyltransferases. *Biochimica et Biophysica Acta (BBA) - Gene Regulatory Mechanisms*, *1863*(7), 194545. https://doi.org/https://doi.org/10.1016/j.bbagrm.2020.194545

Pasini, D., Malatesta, M., Jung, H. R., Walfridsson, J., Willer, A., Olsson, L., Skotte, J., Wutz, A., Porse, B., Jensen, O. N., & Helin, K. (2010). Characterization of an antagonistic switch between histone H3 lysine 27 methylation and acetylation in the transcriptional regulation of Polycomb group target genes. *Nucleic Acids Research*, *38*(15), 4958–4969. https://doi.org/10.1093/nar/gkq244

Patel, A., Dharmarajan, V., Vought, V. E., & Cosgrove, M. S. (2009). On the mechanism of multiple lysine methylation by the human mixed lineage leukemia protein-1 (MLL1) core complex. *The Journal of Biological Chemistry*, *284*(36), 24242–24256. https://doi.org/10.1074/jbc.M109.014498

Pekowska, A., Benoukraf, T., Ferrier, P., & Spicuglia, S. (2010). A unique H3K4me2 profile marks tissue-specific gene regulation. *Genome Research*, *20*(11), 1493–1502. https://doi.org/10.1101/gr.109389.110

Peña, P. V, Davrazou, F., Shi, X., Walter, K. L., Verkhusha, V. V, Gozani, O., Zhao, R., & Kutateladze, T. G. (2006). Molecular mechanism of histone H3K4me3 recognition by plant homeodomain of ING2. *Nature*, *442*(7098), 100–103. https://doi.org/10.1038/nature04814

Perillo, B., Tramontano, A., Pezone, A., & Migliaccio, A. (2020). LSD1: more than demethylation of histone lysine residues. *Experimental & Molecular Medicine*, *52*(12), 1936–1947. https://doi.org/10.1038/s12276-020-00542-2

Petroski, M. D., & Deshaies, R. J. (2005). Function and regulation of cullin–RING ubiquitin ligases. *Nature Reviews Molecular Cell Biology*, *6*(1), 9–20. https://doi.org/10.1038/nrm1547

Pokholok, D. K., Harbison, C. T., Levine, S., Cole, M., Hannett, N. M., Lee, T. I., Bell, G. W., Walker, K., Rolfe, P. A., Herbolsheimer, E., Zeitlinger, J., Lewitter, F., Gifford, D. K., & Young, R. A. (2005). Genome-wide map of nucleosome acetylation and methylation in yeast. *Cell*, *122*(4), 517–527. https://doi.org/10.1016/j.cell.2005.06.026

Poreba, E., Lesniewicz, K., & Durzynska, J. (2022). Histone–lysine N-methyltransferase 2 (KMT2) complexes – a new perspective. *Mutation Research/Reviews in Mutation Research*, *790*, 108443. https://doi.org/https://doi.org/10.1016/j.mrrev.2022.108443

Qu, L., Yin, T., Zhao, Y., Lv, W., Liu, Z., Chen, C., Liu, K., Shan, S., Zhou, R., Li, X., & Dong, H. (2023). Histone demethylases in the regulation of immunity and inflammation. *Cell Death Discovery*, *9*(1), 188. https://doi.org/10.1038/s41420-023-01489-9

Rao, R. C., & Dou, Y. (2015). Hijacked in cancer: the KMT2 (MLL) family of methyltransferases. *Nature Reviews. Cancer*, *15*(6), 334–346. https://doi.org/10.1038/nrc3929

Raudvere, U., Kolberg, L., Kuzmin, I., Arak, T., Adler, P., Peterson, H., & Vilo, J. (2019). g:Profiler: a web server for functional enrichment analysis and conversions of gene lists (2019 update). *Nucleic Acids Research*, *47*(W1), W191–W198. https://doi.org/10.1093/nar/gkz369

Reddington, J. P., Perricone, S. M., Nestor, C. E., Reichmann, J., Youngson, N. A., Suzuki, M., Reinhardt, D., Dunican, D. S., Prendergast, J. G., Mjoseng, H., Ramsahoye, B. H., Whitelaw, E.,

Greally, J. M., Adams, I. R., Bickmore, W. A., & Meehan, R. R. (2013). Redistribution of H3K27me3 upon DNA hypomethylation results in de-repression of Polycomb target genes. *Genome Biology*, *14*(3), R25. https://doi.org/10.1186/gb-2013-14-3-r25

Reddy, D., & Workman, J. L. (2018). Targeting BAF-perturbed cancers. *Nature Cell Biology*, *20*(12), 1332–1333. https://doi.org/10.1038/s41556-018-0246-5

Reynolds, N., Salmon-Divon, M., Dvinge, H., Hynes-Allen, A., Balasooriya, G., Leaford, D., Behrens, A., Bertone, P., & Hendrich, B. (2012). NuRD-mediated deacetylation of H3K27 facilitates recruitment of Polycomb Repressive Complex 2 to direct gene repression. *The EMBO Journal*, *31*(3), 593–605. https://doi.org/10.1038/emboj.2011.431

Ruthenburg, A. J., Li, H., Milne, T. A., Dewell, S., McGinty, R. K., Yuen, M., Ueberheide, B., Dou, Y., Muir, T. W., Patel, D. J., & Allis, C. D. (2011). Recognition of a mononucleosomal histone modification pattern by BPTF via multivalent interactions. *Cell*, *145*(5), 692–706. https://doi.org/10.1016/j.cell.2011.03.053

Sakamoto, K. M., Kim, K. B., Kumagai, A., Mercurio, F., Crews, C. M., & Deshaies, R. J. (2001). Protacs: Chimeric molecules that target proteins to the Skp1–Cullin–F box complex for ubiquitination and degradation. *Proceedings of the National Academy of Sciences*, *98*(15), 8554–8559. https://doi.org/10.1073/pnas.141230798

Santos-Rosa, H., Schneider, R., Bannister, A. J., Sherriff, J., Bernstein, B. E., Emre, N. C. T., Schreiber, S. L., Mellor, J., & Kouzarides, T. (2002). Active genes are tri-methylated at K4 of histone H3. *Nature*, *419*(6905), 407–411. https://doi.org/10.1038/nature01080

Saxonov, S., Berg, P., & Brutlag, D. L. (2006). A genome-wide analysis of CpG dinucleotides in the human genome distinguishes two distinct classes of promoters. *Proceedings of the National Academy of Sciences of the United States of America*, *103*(5), 1412–1417. https://doi.org/10.1073/pnas.0510310103

Schneider, R., Bannister, A. J., Myers, F. A., Thorne, A. W., Crane-Robinson, C., & Kouzarides, T. (2004). Histone H3 lysine 4 methylation patterns in higher eukaryotic genes. *Nature Cell Biology*, *6*(1), 73–77. https://doi.org/10.1038/ncb1076

Schuettengruber, B., Chourrout, D., Vervoort, M., Leblanc, B., & Cavalli, G. (2007). Genome Regulation by Polycomb and Trithorax Proteins. *Cell*, *128*(4), 735–745. https://doi.org/10.1016/j.cell.2007.02.009

Secombe, J., & Eisenman, R. N. (2007). The function and regulation of the JARID1 family of histone H3 lysine 4 demethylases: the Myc connection. *Cell Cycle (Georgetown, Tex.)*, *6*(11), 1324–1328. https://doi.org/10.4161/cc.6.11.4269

Serra-Cardona, A., Duan, S., Yu, C., & Zhang, Z. (2022). H3K4me3 recognition by the COMPASS complex facilitates the restoration of this histone mark following DNA replication. *Science Advances*, *8*(18), eabm6246. https://doi.org/10.1126/sciadv.abm6246

Seto, E., & Yoshida, M. (2014). Erasers of histone acetylation: the histone deacetylase enzymes. *Cold Spring Harbor Perspectives in Biology*, *6*(4), a018713. https://doi.org/10.1101/cshperspect.a018713

Shah, K. K., Whitaker, R. H., Busby, T., Hu, J., Shi, B., Wang, Z., Zang, C., Placzek, W. J., & Jiang, H. (2019). Specific inhibition of DPY30 activity by ASH2L-derived peptides suppresses blood cancer cell growth. *Experimental Cell Research*, *382*(2), 111485. https://doi.org/https://doi.org/10.1016/j.yexcr.2019.06.030

Shi, X., Hong, T., Walter, K. L., Ewalt, M., Michishita, E., Hung, T., Carney, D., Peña, P., Lan, F., Kaadige,

M. R., Lacoste, N., Cayrou, C., Davrazou, F., Saha, A., Cairns, B. R., Ayer, D. E., Kutateladze, T. G., Shi, Y., Côté, J., … Gozani, O. (2006). ING2 PHD domain links histone H3 lysine 4 methylation to active gene repression. *Nature*, *442*(7098), 96–99. https://doi.org/10.1038/nature04835

Shi, Y., Lan, F., Matson, C., Mulligan, P., Whetstine, J. R., Cole, P. A., Casero, R. A., & Shi, Y. (2004). Histone demethylation mediated by the nuclear amine oxidase homolog LSD1. *Cell*, *119*(7), 941–953. https://doi.org/10.1016/j.cell.2004.12.012

Shi, Y., Wang, X., Zhuang, Y., Jiang, Y., Melcher, K., & Xu, H. E. (2017). Structure of the PRC2 complex and application to drug discovery. *Acta Pharmacologica Sinica*, *38*(7), 963–976. https://doi.org/10.1038/aps.2017.7

Shilatifard, A. (2012). The COMPASS family of histone H3K4 methylases: mechanisms of regulation in development and disease pathogenesis. *Annual Review of Biochemistry*, *81*, 65–95. https://doi.org/10.1146/annurev-biochem-051710-134100

Shimoda, H., Doi, S., Nakashima, A., Sasaki, K., Doi, T., & Masaki, T. (2019). Inhibition of the H3K4 methyltransferase MLL1/WDR5 complex attenuates renal senescence in ischemia reperfusion mice by reduction of p16(INK4a). *Kidney International*, *96*(5), 1162–1175. https://doi.org/10.1016/j.kint.2019.06.021

Shlyueva, D., Stampfel, G., & Stark, A. (2014). Transcriptional enhancers: from properties to genome-wide predictions. *Nature Reviews Genetics*, *15*(4), 272–286. https://doi.org/10.1038/nrg3682

Simboeck, E., Gutierrez, A., Cozzuto, L., Beringer, M., Caizzi, L., Keyes, W. M., & Di Croce, L. (2013). DPY30 regulates pathways in cellular senescence through ID protein expression. *The EMBO Journal*, *32*(16), 2217–2230. https://doi.org/10.1038/emboj.2013.159

Sims, R. J. 3rd, Chen, C.-F., Santos-Rosa, H., Kouzarides, T., Patel, S. S., & Reinberg, D. (2005). Human but not yeast CHD1 binds directly and selectively to histone H3 methylated at lysine 4 via its tandem chromodomains. *The Journal of Biological Chemistry*, *280*(51), 41789–41792. https://doi.org/10.1074/jbc.C500395200

Sims, R. J. 3rd, Millhouse, S., Chen, C.-F., Lewis, B. A., Erdjument-Bromage, H., Tempst, P., Manley, J. L., & Reinberg, D. (2007). Recognition of trimethylated histone H3 lysine 4 facilitates the recruitment of transcription postinitiation factors and pre-mRNA splicing. *Molecular Cell*, *28*(4), 665–676. https://doi.org/10.1016/j.molcel.2007.11.010

Sincere, N. I., Anand, K., Ashique, S., Yang, J., & You, C. (2023). PROTACs: Emerging Targeted Protein Degradation Approaches for Advanced Druggable Strategies. *Molecules (Basel, Switzerland)*, *28*(10). https://doi.org/10.3390/molecules28104014

Soares, L. M., He, P. C., Chun, Y., Suh, H., Kim, T., & Buratowski, S. (2017). Determinants of Histone H3K4 Methylation Patterns. *Molecular Cell*, *68*(4), 773-785.e6. https://doi.org/https://doi.org/10.1016/j.molcel.2017.10.013

Stender, J. D., Pascual, G., Liu, W., Kaikkonen, M. U., Do, K., Spann, N. J., Boutros, M., Perrimon, N., Rosenfeld, M. G., & Glass, C. K. (2012). Control of proinflammatory gene programs by regulated trimethylation and demethylation of histone H4K20. *Molecular Cell*, *48*(1), 28–38. https://doi.org/10.1016/j.molcel.2012.07.020

Stenzel, A. (2024). *Analysis of a senescence phenotype and changes of the chromatin landscape after a loss of ASH2L in mouse embryonic fibroblast systems*. RWTH Aachen University.

Steward, M. M., Lee, J.-S., O'Donovan, A., Wyatt, M., Bernstein, B. E., & Shilatifard, A. (2006). Molecular regulation of H3K4 trimethylation by ASH2L, a shared subunit of MLL complexes. *Nature Structural & Molecular Biology*, *13*(9), 852–854. https://doi.org/10.1038/nsmb1131

Stoller, J. Z., Huang, L., Tan, C. C., Huang, F., Zhou, D. D., Yang, J., Gelb, B. D., & Epstein, J. A. (2010). Ash2l interacts with Tbx1 and is required during early embryogenesis. *Experimental Biology and Medicine (Maywood, N.J.)*, *235*(5), 569–576. https://doi.org/10.1258/ebm.2010.009318

Sump, B., Brickner, D. G., D'Urso, A., Kim, S. H., & Brickner, J. H. (2022). Mitotically heritable, RNA polymerase II-independent H3K4 dimethylation stimulates INO1 transcriptional memory. *ELife*, *11*. https://doi.org/10.7554/eLife.77646

Sun, Z., Xu, X., He, J., Murray, A., Sun, M.-A., Wei, X., Wang, X., McCoig, E., Xie, E., Jiang, X., Li, L., Zhu, J., Chen, J., Morozov, A., Pickrell, A. M., Theus, M. H., & Xie, H. (2019). EGR1 recruits TET1 to shape the brain methylome during development and upon neuronal activity. *Nature Communications*, *10*(1), 3892. https://doi.org/10.1038/s41467-019-11905-3

Takahashi, Y., Westfield, G. H., Oleskie, A. N., Trievel, R. C., Shilatifard, A., & Skiniotis, G. (2011). Structural analysis of the core COMPASS family of histone H3K4 methylases from yeast to human. *Proceedings of the National Academy of Sciences of the United States of America*, *108*(51), 20526–20531. https://doi.org/10.1073/pnas.1109360108

Tan, C. C., Sindhu, K. V, Li, S., Nishio, H., Stoller, J. Z., Oishi, K., Puttreddy, S., Lee, T. J., Epstein, J. A., Walsh, M. J., & Gelb, B. D. (2008). Transcription factor Ap2δ associates with Ash2l and ALR, a trithorax family histone methyltransferase, to activate Hoxc8 transcription. *Proceedings of the National Academy of Sciences*, *105*(21), 7472–7477. https://doi.org/10.1073/pnas.0711896105

Thomas, L. R., Wang, Q., Grieb, B. C., Phan, J., Foshage, A. M., Sun, Q., Olejniczak, E. T., Clark, T., Dey, S., Lorey, S., Alicie, B., Howard, G. C., Cawthon, B., Ess, K. C., Eischen, C. M., Zhao, Z., Fesik, S. W., & Tansey, W. P. (2015). Interaction with WDR5 Promotes Target Gene Recognition and Tumorigenesis by MYC. *Molecular Cell*, *58*(3), 440–452. https://doi.org/10.1016/j.molcel.2015.02.028

Tsai, P.-H., Chien, Y., Wang, M.-L., Hsu, C.-H., Laurent, B., Chou, S.-J., Chang, W.-C., Chien, C.-S., Li, H.-Y., Lee, H.-C., Huo, T.-I., Hung, J.-H., Chen, C.-H., & Chiou, S.-H. (2019). Ash2l interacts with Oct4-stemness circuitry to promote super-enhancer-driven pluripotency network. *Nucleic Acids Research*, *47*(19), 10115–10133. https://doi.org/10.1093/nar/gkz801

Tumber, A., Nuzzi, A., Hookway, E. S., Hatch, S. B., Velupillai, S., Johansson, C., Kawamura, A., Savitsky, P., Yapp, C., Szykowska, A., Wu, N., Bountra, C., Strain-Damerell, C., Burgess-Brown, N. A., Ruda, G. F., Fedorov, O., Munro, S., England, K. S., Nowak, R. P., … Brennan, P. E. (2017). Potent and Selective KDM5 Inhibitor Stops Cellular Demethylation of H3K4me3 at Transcription Start Sites and Proliferation of MM1S Myeloma Cells. *Cell Chemical Biology*, *24*(3), 371–380. https://doi.org/10.1016/j.chembiol.2017.02.006

Uckelmann, M., & Davidovich, C. (2021). Not just a writer: PRC2 as a chromatin reader. *Biochemical Society Transactions*, *49*(3), 1159–1170. https://doi.org/10.1042/BST20200728

Ullius, A. (2014). *The trithorax protein ASH2L in MYC-dependent transcriptional regulation and in liver tumorigenesis*. RWTH Aachen.

Ullius, A., Lüscher-Firzlaff, J., Costa, I. G., Walsemann, G., Forst, A. H., Gusmao, E. G., Kapelle, K., Kleine, H., Kremmer, E., Vervoorts, J., & Lüscher, B. (2014). The interaction of MYC with the trithorax protein ASH2L promotes gene transcription by regulating H3K27 modification. *Nucleic Acids Research*, *42*(11), 6901–6920. https://doi.org/10.1093/nar/gku312

Vaid, R., Wen, J., & Mannervik, M. (2020). Release of promoter-proximal paused Pol II in response to histone deacetylase inhibition. *Nucleic Acids Research*, *48*(9), 4877–4890. https://doi.org/10.1093/nar/gkaa234

van de Lagemaat, L. N., Flenley, M., Lynch, M. D., Garrick, D., Tomlinson, S. R., Kranc, K. R., &

Vernimmen, D. (2018). CpG binding protein (CFP1) occupies open chromatin regions of active genes, including enhancers and non-CpG islands. *Epigenetics & Chromatin*, *11*(1), 59. https://doi.org/10.1186/s13072-018-0230-0

van Ingen, H., van Schaik, F. M. A., Wienk, H., Ballering, J., Rehmann, H., Dechesne, A. C., Kruijzer, J. A. W., Liskamp, R. M. J., Timmers, H. T. M., & Boelens, R. (2008). Structural insight into the recognition of the H3K4me3 mark by the TFIID subunit TAF3. *Structure (London, England : 1993)*, *16*(8), 1245–1256. https://doi.org/10.1016/j.str.2008.04.015

Vermeulen, M., Mulder, K. W., Denissov, S., Pijnappel, W. W. M. P., van Schaik, F. M. A., Varier, R. A., Baltissen, M. P. A., Stunnenberg, H. G., Mann, M., & Timmers, H. T. M. (2007). Selective anchoring of TFIID to nucleosomes by trimethylation of histone H3 lysine 4. *Cell*, *131*(1), 58–69. https://doi.org/10.1016/j.cell.2007.08.016

Vermeulen, M., & Timmers, H. T. M. (2010). Grasping trimethylation of histone H3 at lysine 4. *Epigenomics*, *2*(3), 395–406. https://doi.org/10.2217/epi.10.11

Viré, E., Brenner, C., Deplus, R., Blanchon, L., Fraga, M., Didelot, C., Morey, L., Van Eynde, A., Bernard, D., Vanderwinden, J.-M., Bollen, M., Esteller, M., Di Croce, L., de Launoit, Y., & Fuks, F. (2006). The Polycomb group protein EZH2 directly controls DNA methylation. *Nature*, *439*(7078), 871–874. https://doi.org/10.1038/nature04431

von Mikecz, A. (2006). The nuclear ubiquitin-proteasome system. *Journal of Cell Science*, *119*(10), 1977–1984. https://doi.org/10.1242/jcs.03008

Wan, M., Liang, J., Xiong, Y., Shi, F., Zhang, Y., Lu, W., He, Q., Yang, D., Chen, R., Liu, D., Barton, M., & Songyang, Z. (2013). The trithorax group protein Ash2l is essential for pluripotency and maintaining open chromatin in embryonic stem cells. *The Journal of Biological Chemistry*, *288*(7), 5039–5048. https://doi.org/10.1074/jbc.M112.424515

Wang, H., Fan, Z., Shliaha, P. V, Miele, M., Hendrickson, R. C., Jiang, X., & Helin, K. (2023). H3K4me3 regulates RNA polymerase II promoter-proximal pause-release. *Nature*, *615*(7951), 339–348. https://doi.org/10.1038/s41586-023-05780-8

Wang, J., Zhou, Y., Yin, B., Du, G., Huang, X., Li, G., Shen, Y., Yuan, J., & Qiang, B. (2001). ASH2L: alternative splicing and downregulation during induced megakaryocytic differentiation of multipotential leukemia cell lines. *Journal of Molecular Medicine (Berlin, Germany)*, *79*(7), 399–405. https://doi.org/10.1007/s001090100222

Wang, W., Chen, Z., Mao, Z., Zhang, H., Ding, X., Chen, S., Zhang, X., Xu, R., & Zhu, B. (2011). Nucleolar protein Spindlin1 recognizes H3K4 methylation and stimulates the expression of rRNA genes. *EMBO Reports*, *12*(11), 1160–1166. https://doi.org/10.1038/embor.2011.184

Wang, X. J., Yu, J., Wong, S. H., Cheng, A. S. L., Chan, F. K. L., Ng, S. S. M., Cho, C. H., Sung, J. J. Y., & Wu, W. K. K. (2013). A novel crosstalk between two major protein degradation systems. *Autophagy*, *9*(10), 1500–1508. https://doi.org/10.4161/auto.25573

Webb, T., Craigon, C., & Ciulli, A. (2022). Targeting epigenetic modulators using PROTAC degraders: Current status and future perspective. *Bioorganic & Medicinal Chemistry Letters*, *63*, 128653. https://doi.org/https://doi.org/10.1016/j.bmcl.2022.128653

Wei, S., Li, C., Yin, Z., Wen, J., Meng, H., Xue, L., & Wang, J. (2018). Histone methylation in DNA repair and clinical practice: new findings during the past 5-years. *Journal of Cancer*, *9*(12), 2072–2081. https://doi.org/10.7150/jca.23427

Weinert, B. T., Narita, T., Satpathy, S., Srinivasan, B., Hansen, B. K., Schölz, C., Hamilton, W. B., Zucconi, B. E., Wang, W. W., Liu, W. R., Brickman, J. M., Kesicki, E. A., Lai, A., Bromberg, K. D.,

Cole, P. A., & Choudhary, C. (2018). Time-Resolved Analysis Reveals Rapid Dynamics and Broad Scope of the CBP/p300 Acetylome. *Cell*, *174*(1), 231-244.e12. https://doi.org/10.1016/j.cell.2018.04.033

Wen, H., Li, J., Song, T., Lu, M., Kan, P.-Y., Lee, M. G., Sha, B., & Shi, X. (2010). Recognition of histone H3K4 trimethylation by the plant homeodomain of PHF2 modulates histone demethylation. *The Journal of Biological Chemistry*, *285*(13), 9322–9326. https://doi.org/10.1074/jbc.C109.097667

Wolffe, A. P. (1994). Nucleosome positioning and modification: chromatin structures that potentiate transcription. *Trends in Biochemical Sciences*, *19*(6), 240–244. https://doi.org/10.1016/0968-0004(94)90148-1

Woo, H., Dam Ha, S., Lee, S. B., Buratowski, S., & Kim, T. (2017). Modulation of gene expression dynamics by co-transcriptional histone methylations. *Experimental & Molecular Medicine*, *49*(4), e326–e326. https://doi.org/10.1038/emm.2017.19

Wu, H., Chen, X., Xiong, J., Li, Y., Li, H., Ding, X., Liu, S., Chen, S., Gao, S., & Zhu, B. (2011). Histone methyltransferase G9a contributes to H3K27 methylation in vivo. In *Cell research* (Vol. 21, Issue 2, pp. 365–367). https://doi.org/10.1038/cr.2010.157

Wu, K., Fan, D., Zhao, H., Liu, Z., Hou, Z., Tao, W., Yu, G., Yuan, S., Zhu, X., Kang, M., Tian, Y., Chen, Z.-J., Liu, J., & Gao, L. (2023). Dynamics of histone acetylation during human early embryogenesis. *Cell Discovery*, *9*(1), 29. https://doi.org/10.1038/s41421-022-00514-y

Wysocka, J., Swigut, T., Xiao, H., Milne, T. A., Kwon, S. Y., Landry, J., Kauer, M., Tackett, A. J., Chait, B. T., Badenhorst, P., Wu, C., & Allis, C. D. (2006). A PHD finger of NURF couples histone H3 lysine 4 trimethylation with chromatin remodelling. *Nature*, *442*(7098), 86–90. https://doi.org/10.1038/nature04815

Xue, H., Yao, T., Cao, M., Zhu, G., Li, Y., Yuan, G., Chen, Y., Lei, M., & Huang, J. (2019). Structural basis of nucleosome recognition and modification by MLL methyltransferases. *Nature*, *573*(7774), 445–449. https://doi.org/10.1038/s41586-019-1528-1

Yang, G.-J., Zhu, M.-H., Lu, X.-J., Liu, Y.-J., Lu, J.-F., Leung, C.-H., Ma, D.-L., & Chen, J. (2021). The emerging role of KDM5A in human cancer. *Journal of Hematology & Oncology*, *14*(1), 30. https://doi.org/10.1186/s13045-021-01041-1

Yang, N., Wang, W., Wang, Y., Wang, M., Zhao, Q., Rao, Z., Zhu, B., & Xu, R.-M. (2012). Distinct mode of methylated lysine-4 of histone H3 recognition by tandem tudor-like domains of Spindlin1. *Proceedings of the National Academy of Sciences of the United States of America*, *109*(44), 17954–17959. https://doi.org/10.1073/pnas.1208517109

Yang, Q., Zhao, J., Chen, D., & Wang, Y. (2021). E3 ubiquitin ligases: styles, structures and functions. *Molecular Biomedicine*, *2*(1), 23. https://doi.org/10.1186/s43556-021-00043-2

Yang, Z., Augustin, J., Chang, C., Hu, J., Shah, K., Chang, C.-W., Townes, T., & Jiang, H. (2014). The DPY30 subunit in SET1/MLL complexes regulates the proliferation and differentiation of hematopoietic progenitor cells. *Blood*, *124*(13), 2025–2033. https://doi.org/10.1182/blood-2014-01-549220

Yang, Z., Qian, S., Scheid, R. N., Lu, L., Chen, X., Liu, R., Du, X., Lv, X., Boersma, M. D., Scalf, M., Smith, L. M., Denu, J. M., Du, J., & Zhong, X. (2018). EBS is a bivalent histone reader that regulates floral phase transition in Arabidopsis. *Nature Genetics*, *50*(9), 1247–1253. https://doi.org/10.1038/s41588-018-0187-8

Yokoyama, A., Wang, Z., Wysocka, J., Sanyal, M., Aufiero, D. J., Kitabayashi, I., Herr, W., & Cleary, M.

L. (2004). Leukemia proto-oncoprotein MLL forms a SET1-like histone methyltransferase complex with menin to regulate Hox gene expression. *Molecular and Cellular Biology*, *24*(13), 5639–5649. https://doi.org/10.1128/MCB.24.13.5639-5649.2004

Zardo, G. (2021). The Role of H3K4 Trimethylation in CpG Islands Hypermethylation in Cancer. *Biomolecules*, *11*(2). https://doi.org/10.3390/biom11020143

Zeng, K., Wu, Y., Wang, C., Wang, S., Sun, H., Zou, R., Sun, G., Song, H., Liu, W., Sun, N., Wei, S., Liu, W., Su, Y., Zhou, T., Zhang, Y., & Zhao, Y. (2020). ASH2L is involved in promotion of endometrial cancer progression via upregulation of PAX2 transcription. *Cancer Science*, *111*(6), 2062–2077. https://doi.org/https://doi.org/10.1111/cas.14413

Zhang, M., Li, J., Wang, Q., Urabe, G., Tang, R., Huang, Y., Mosquera, J. V., Kent, K. C., Wang, B., Miller, C. L., & Guo, L.-W. (2023). Gene-repressing epigenetic reader EED unexpectedly enhances cyclinD1 gene activation. *Molecular Therapy - Nucleic Acids*, *31*, 717–729. https://doi.org/https://doi.org/10.1016/j.omtn.2023.02.024

Zhang, S., Postnikov, Y., Lobanov, A., Furusawa, T., Deng, T., & Bustin, M. (2022). H3K27ac nucleosomes facilitate HMGN localization at regulatory sites to modulate chromatin binding of transcription factors. *Communications Biology*, *5*(1), 159. https://doi.org/10.1038/s42003-022-03099-0

Zhang, T., Cooper, S., & Brockdorff, N. (2015). The interplay of histone modifications – writers that read. *EMBO Reports*, *16*(11), 1467–1481. https://doi.org/https://doi.org/10.15252/embr.201540945

Zhang, Y., Karmon, O., Das, K., Wiener, R., Lehming, N., & Pines, O. (2022). Ubiquitination Occurs in the Mitochondrial Matrix by Eclipsed Targeted Components of the Ubiquitination Machinery. *Cells*, *11*(24). https://doi.org/10.3390/cells11244109

Zhang, Y., Klein, B. J., Cox, K. L., Bertulat, B., Tencer, A. H., Holden, M. R., Wright, G. M., Black, J., Cardoso, M. C., Poirier, M. G., & Kutateladze, T. G. (2019). Mechanism for autoinhibition and activation of the MORC3 ATPase. *Proceedings of the National Academy of Sciences*, *116*(13), 6111–6119. https://doi.org/10.1073/pnas.1819524116

Zhang, Y., Liu, T., Meyer, C. A., Eeckhoute, J., Johnson, D. S., Bernstein, B. E., Nusbaum, C., Myers, R. M., Brown, M., Li, W., & Liu, X. S. (2008). Model-based Analysis of ChIP-Seq (MACS). *Genome Biology*, *9*(9), R137. https://doi.org/10.1186/gb-2008-9-9-r137

Zhang, Y., Sun, H., Zhang, J., Brasier, A. R., & Zhao, Y. (2017). Quantitative Assessment of the Effects of Trypsin Digestion Methods on Affinity Purification–Mass Spectrometry-based Protein–Protein Interaction Analysis. *Journal of Proteome Research*, *16*(8), 3068–3082. https://doi.org/10.1021/acs.jproteome.7b00432

Zhao, D., Zhang, X., Guan, H., Xiong, X., Shi, X., Deng, H., & Li, H. (2016). The BAH domain of BAHD1 is a histone H3K27me3 reader. In *Protein & cell* (Vol. 7, Issue 3, pp. 222–226). https://doi.org/10.1007/s13238-016-0243-z

Zhao, F., Liu, Y., Su, X., Lee, J.-E., Song, Y., Wang, D., Ge, K., Gao, J., Zhang, M. Q., & Li, H. (2020). Molecular basis for histone H3 "K4me3-K9me3/2" methylation pattern readout by Spindlin1. *The Journal of Biological Chemistry*, *295*(49), 16877–16887. https://doi.org/10.1074/jbc.RA120.013649

Zhao, L., Huang, N., Mencius, J., Li, Y., Xu, Y., Zheng, Y., He, W., Li, N., Zheng, J., Zhuang, M., Quan, S., & Chen, Y. (2022). DPY30 acts as an ASH2L-specific stabilizer to stimulate the enzyme activity of MLL family methyltransferases on different substrates. *IScience*, *25*(9), 104948. https://doi.org/https://doi.org/10.1016/j.isci.2022.104948

Zhao, W., Xu, Y., Wang, Y., Gao, D., King, J., Xu, Y., & Liang, F.-S. (2021). Investigating crosstalk between H3K27 acetylation and H3K4 trimethylation in CRISPR/dCas-based epigenome editing and gene activation. *Scientific Reports*, *11*(1), 15912. https://doi.org/10.1038/s41598-021-95398-5

Zhao, Y., & Garcia, B. A. (2015). Comprehensive Catalog of Currently Documented Histone Modifications. *Cold Spring Harbor Perspectives in Biology*, *7*(9), a025064. https://doi.org/10.1101/cshperspect.a025064

Zhong, W., Dong, Y.-J., Hong, C., Li, Y.-H., Xiao, C.-X., Liu, X.-H., & Chang, J. (2023). ASH2L upregulation contributes to diabetic endothelial dysfunction in mice through STEAP4-mediated copper uptake. *Acta Pharmacologica Sinica*. https://doi.org/10.1038/s41401-023-01174-8

Zhong, W., Hong, C., Dong, Y., Li, Y., Xiao, C., & Liu, X. (2022). ASH2L Aggravates Fibrosis and Inflammation through HIPK2 in High Glucose-Induced Glomerular Mesangial Cells. *Genes*, *13*(12). https://doi.org/10.3390/genes13122244

Zhong, W., Hong, C., Zhang, Y., Li, Y., Xiao, C., & Liu, X. (2023). ASH2L-mediated H3K4me3 drives diabetic nephropathy through HIPK2 and Notch1 pathway. *Translational Research : The Journal of Laboratory and Clinical Medicine*. https://doi.org/10.1016/j.trsl.2023.10.002

Ziesché, E., Kettner-Buhrow, D., Weber, A., Wittwer, T., Jurida, L., Soelch, J., Müller, H., Newel, D., Kronich, P., Schneider, H., Dittrich-Breiholz, O., Bhaskara, S., Hiebert, S. W., Hottiger, M. O., Li, H., Burstein, E., Schmitz, M. L., & Kracht, M. (2013). The coactivator role of histone deacetylase 3 in IL-1-signaling involves deacetylation of p65 NF-κB. *Nucleic Acids Research*, *41*(1), 90–109. https://doi.org/10.1093/nar/gks916

6 Appendix

6.1 Supplementary Figures

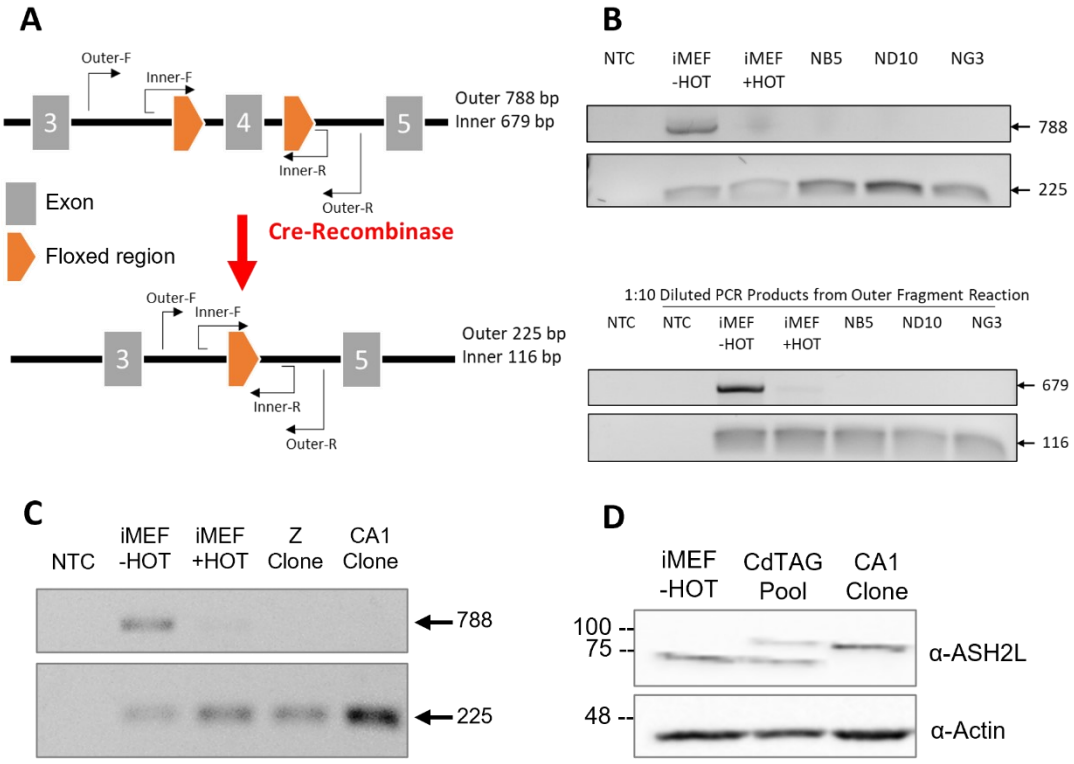

Figure S1: HOT-induced Ash2l recombination leads to the KO of the endogenous *Ash2l* gene. (A) A schematic of the genomic arrangement of floxed Exon 4 of the *Ash2l* gene, and the expected length of the nested PCR products, is indicated. (B) Verified nested PCR products on genomic DNA extracted from N-terminal clones, loaded on a 1% agarose gel, were visualized with Ethidium bromide. Maternal iMEF cells treated with 5 nM HOT, and ethanol served as the positive and negative controls, respectively. Distilled water was used as a no-template control for the PCR reaction. (C) Verified outer fragment PCR products on genomic DNA extracted from C-terminal clones, loaded on a 1% agarose gel, were visualized with Ethidium bromide. Maternal iMEF cells treated with 5 nM HOT, and ethanol served as the positive and negative controls, respectively. Distilled water was used as a no-template control for the PCR reaction. (D) Cell lysates prepared from CdTAG pool, CA1 isolated clone and maternal iMEF cells were used for western blotting. 20 µg of each lysate was loaded for analysis. Actin served as an internal control, and an antibody against ASH2L was used for fusion protein expression evaluation. Experiment A, and B, were done by the author. Experiment C, and D were generated by Malte Benje.

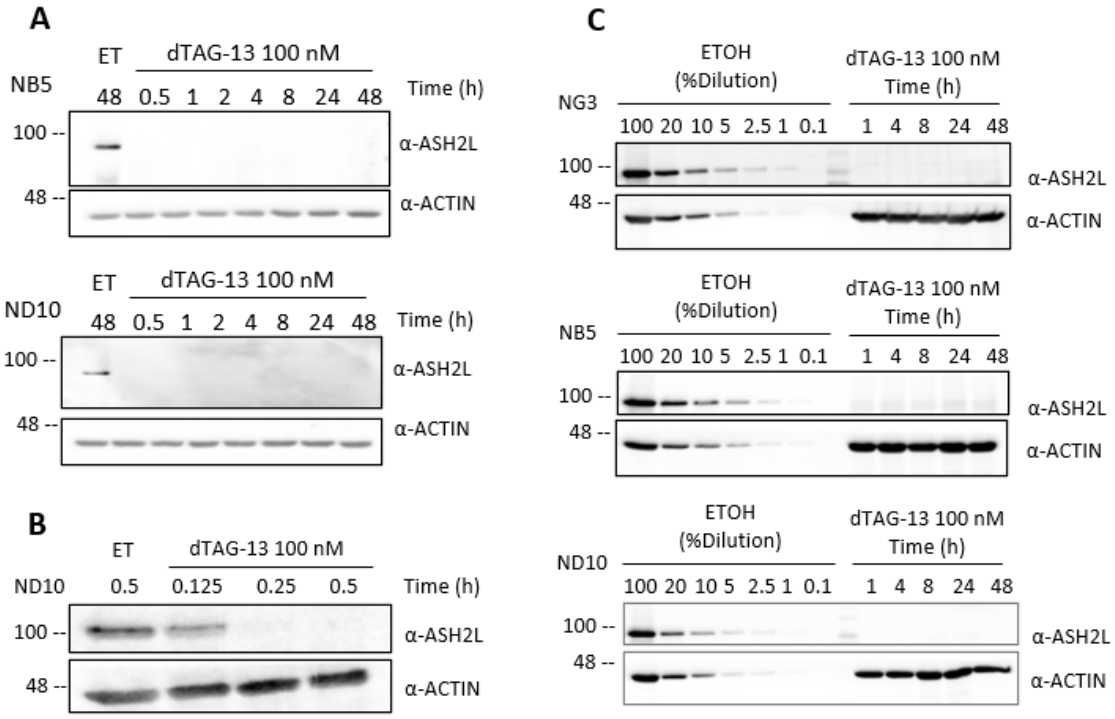

Figure S2: dTAG-13 Treatment Leads to an Almost Complete Knockdown (KD) of the ASH2L Fusion Protein. (A) Cell lysates prepared from single-cell clones treated with 100 nM dTAG-13 and ethanol as the vehicle control were used for western blotting. Treatment was conducted in a time-course manner in cell culture, with 20 µg of each lysate loaded for analysis. Actin served as an internal control, and an antibody against ASH2L was used for KD evaluation. (B) A similar western blot to panel A was performed for the ND10 clone, curated at very early time points. (C) Serial dilutions of the untreated cell lysate of different clones were prepared and run next to the treated time-course lysate samples. The KD efficiency in the time-course sample was compared to the serially diluted samples of the untreated lysates. All experiments were conducted by the author.

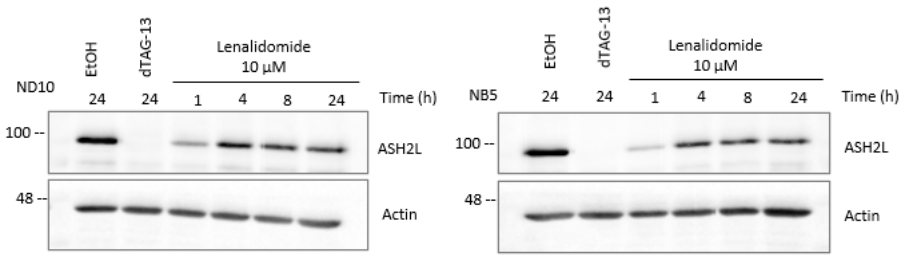

Figure S3: The Recovery of ASH2L Fusion Protein with the Aid of Lenalidomide. ND10 and NB5 clones were treated for 24 hours with dTAG-13 or the vehicle control. Another set of 24h-KD cells were further treated with 10 µM lenalidomide for 1, 4, 8, and 24 hours. Total cell lysates were used for western blotting. Actin detection served as a loading control, and an antibody against ASH2L was used to evaluate the re-expression of the fusion protein. 20 µg of each lysate was loaded for analysis. The experiments were done by the author.

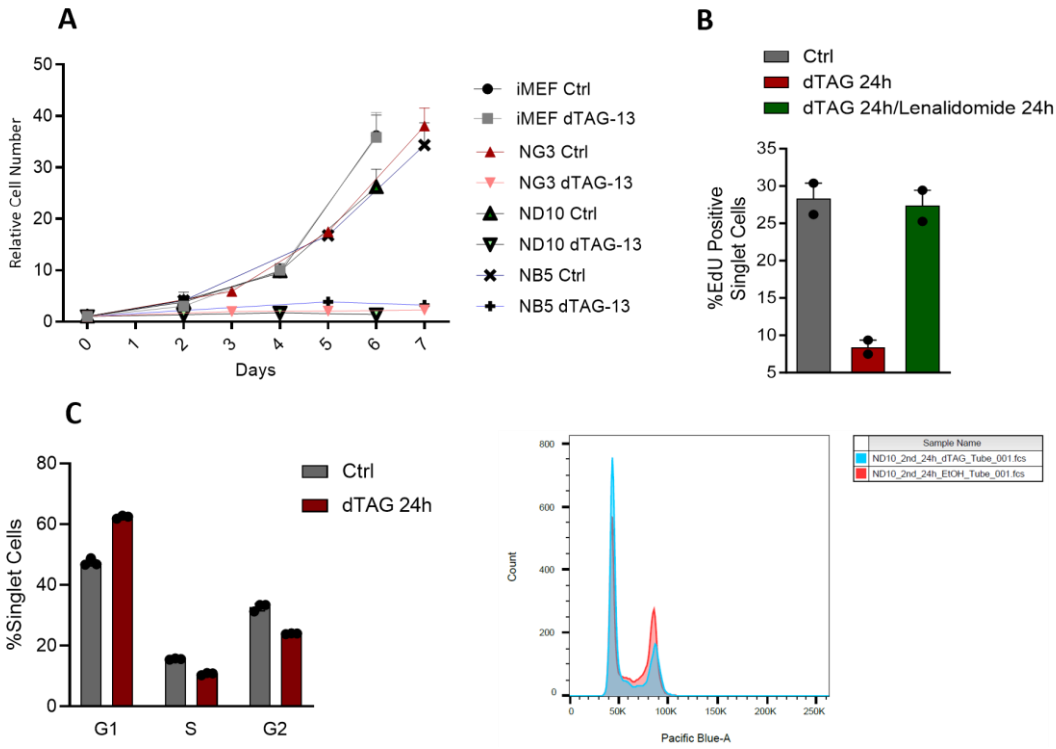

Figure S4: dTAG-13 Treatment Leads to Ceased Cell Proliferation in All Single Cell Clones. (A) All N-terminal monoclonals and iMEF cells were treated with the vehicle control or 100 nM dTAG-13 for a period of up to 7 days. Every 2/3rd day, the cells were detached, counted, and then seeded back into the cell culture plates under the respective treatment conditions. The experiment was performed in three biological replicates, with each replicate measured three times. Error bars indicate the SEM for the samples. (B) NG3 cells were treated with the vehicle control or 100 nM dTAG-13 for 24 hours. The cell culture was treated with 5-EdU for three hours, as described in chapter 2.6.9.2. The cells were then fixed, labeled with AF488 dye, and stained with Hoechst 33258 for DNA content. It is important to note that the BD FACS Canto II machine with a 405 nm Violet laser theoretically has excitation <5%. Therefore, in some other experiments (Figure 4), DyeCycle Vybrant Violet was replaced for DNA content staining. The reactions were measured in two biological replicates, each containing three independent measurements using the FACS machine. Error bars indicate the SD for the samples. (C) On the left panel: ND10 cells were treated with the vehicle control or 100 nM dTAG-13 for 24 hours. Cells were fixed and stained with Hoechst 33258. The cell cycle phase distribution histogram was obtained with FACS and analyzed using FlowJo software. The experiment was performed as one biological replicate, containing three technical measurements. Error bars indicate the SD for the sample. On the right panel: the overlay of the ND10 histogram at 24 hours treated with the vehicle control (red) and dTAG-13 (blue) is shown. All experiments were done by the author.

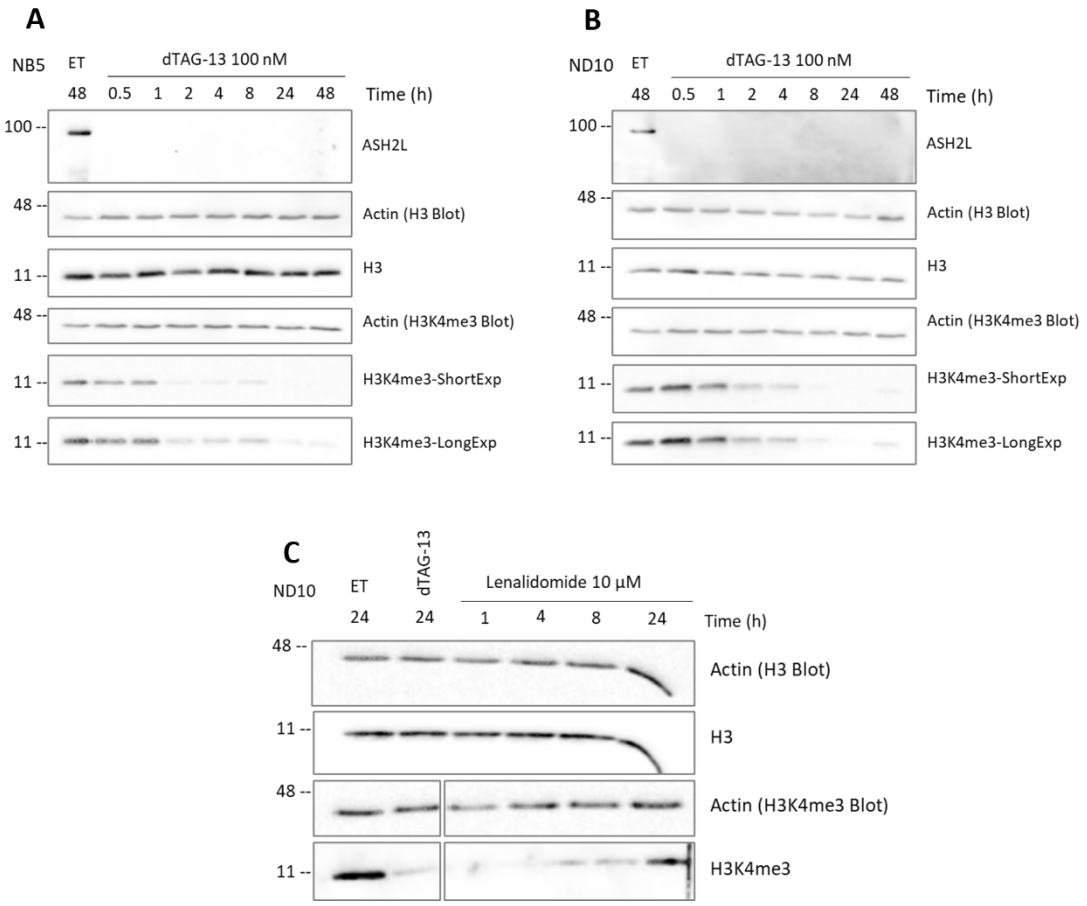

Figure S5: Disruption and Recovery of H3K4me3 Mark in Reaction to ASH2L Loss and Re-expression. NB5 (A) and ND10 (B) cells were subjected to a time course treatment with 100 nM dTAG-13 or the vehicle control for 48 hours. Total cell lysates were used for western blotting. Actin detection served as a cell lysate loading control, and an antibody against ASH2L was employed to assess the expression of the fusion protein. Antibodies against H3K4me3 were used to evaluate the global expression of this histone modification. H3 expression served as a histone loading control. 5 µg of each lysate was loaded for analysis. (C) ND10 cells treated for 24 hours with the vehicle control and 100 nM dTAG-13 were subjected to western blotting. A parallel set of 24-hour dTAG-treated cells was further treated with 10 µM lenalidomide to assess the re-expression of the H3K4me3 histone mark in a time-course manner. Actin detection served as a cell lysate loading control. Antibodies against H3K4me3 were used to evaluate the global expression of this histone modification, and H3 expression served as a histone loading control. 5 µg of each lysate was loaded for analysis. All experiments were done by the author.

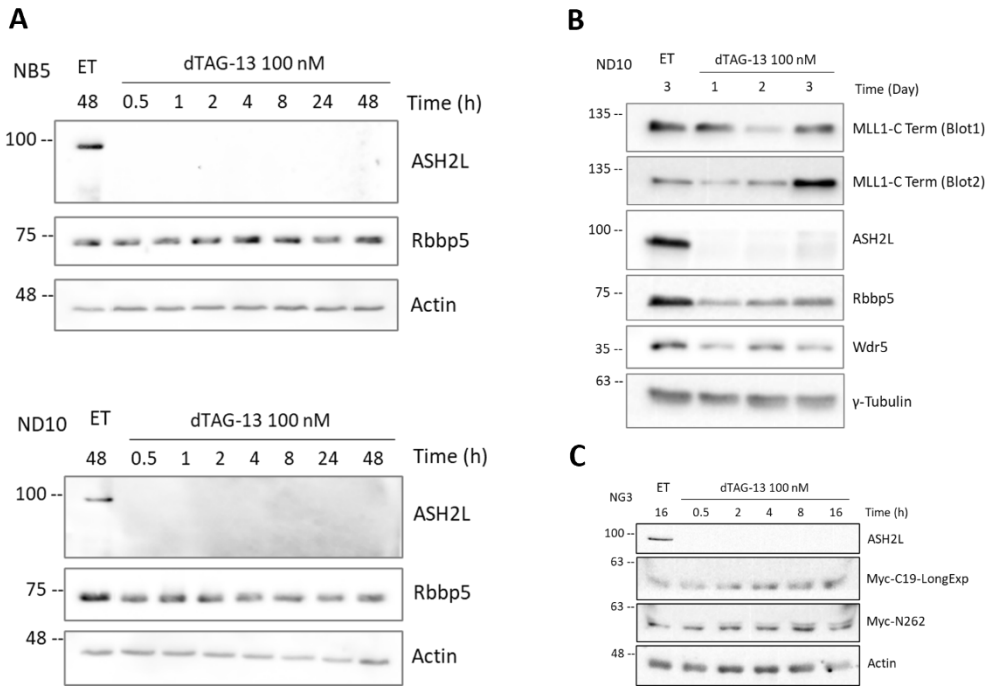

Figure S6: KMT2 Components Exhibit Slight Deregulation Upon dTAG-13 Treatment. (A) NB5 (Top Blot) and ND10 (Below Blot) cells underwent a time course treatment with 100 nM dTAG-13 or the vehicle control for 48 hours. Total cell lysates were used for western blotting. Actin detection served as a cell lysate loading control for the Rbbp5 blot membrane. An antibody against ASH2L was utilized to assess the expression of the fusion protein. 20 µg of each lysate was loaded for analysis. (B) ND10 cells were treated over a time course with 100 nM dTAG-13 or the vehicle control for 3 days. Tubulin detection served as a cell lysate loading control for the Wdr5 blot membrane. An antibody against ASH2L was employed to assess the expression of the fusion protein. An antibody against MLL1-C-terminal was used to detect the expression of the MLL subunit. The transfer of the large MLL protein was performed using Towbin buffer (25 mM Tris, 192 mM glycine, 20% (v/v) methanol, pH 8.3); however, it was not very efficient, as the protein remaining on the Coomassie staining of the gel showed uneven protein transfer for the region of interest. Therefore, two different blotting membranes were probed for the same protein. 40 µg of each lysate was loaded for analysis. (C) NG3 cells were treated over a time course with 100 nM dTAG-13 or the vehicle control for 16 hours. Total cell lysates were used for western blotting. Actin detection served as a cell lysate loading control. An antibody against ASH2L was employed to assess the expression of the fusion protein. Two different antibodies against Myc protein were used on two different blotting membranes. Myc-C19 exhibited a very weak signal and therefore was exposed for longer than 3 minutes to present a visible band on the membrane. 20 µg of each lysate was loaded for analysis. All experiments were conducted by the author.

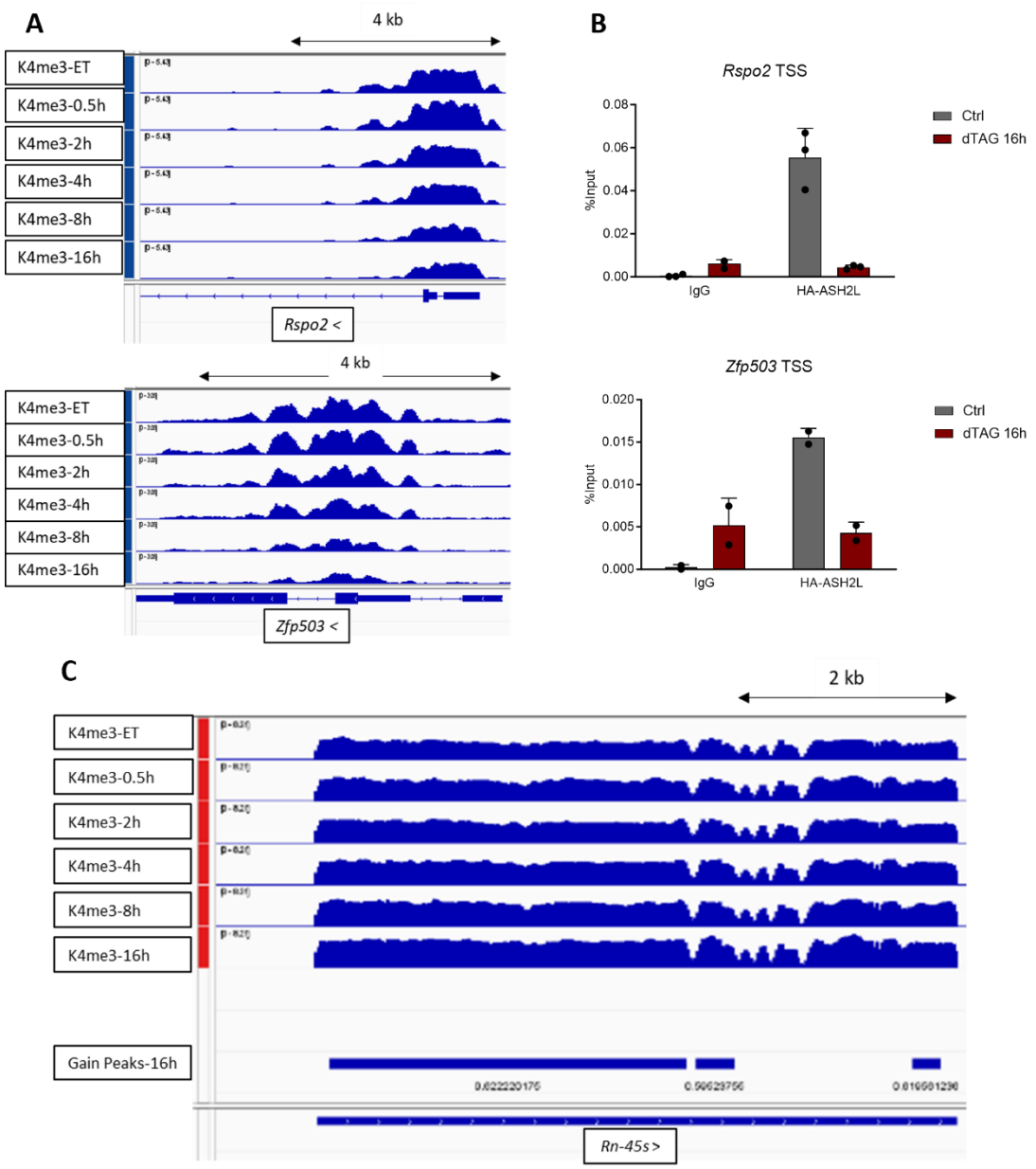

Figure S7: H3K4me3 is Deregulated at Promoter Regions in Response to ASH2L Loss. (A) The IGV genomic view depicts the H3K4me3 signal intensity from the BigWig files (group-scaled) for the NG3 H3K4me3-ChIPseq at different time points, at two different gene TSSs, *Rspo2* and *Zfp503*. (B) ChIP-qPCR demonstrates the ASH2L enrichment level at the TSS of the *Rspo2* and *Zfp503* genes after 16 hours of treatment with vehicle control and 100 nM dTAG-13. IgG enrichment was used as a background control. (C) The genomic view shows the gained H3K4me3 signals at the *Rn-45s* TSS region. BigWig files are group-scaled. The experimental procedure of H3K4me3 and ASH2L ChIP-seq and ChIP-qPCR was done by the author. The computational analysis of the data was curated by Dr. Mirna Barsoum.

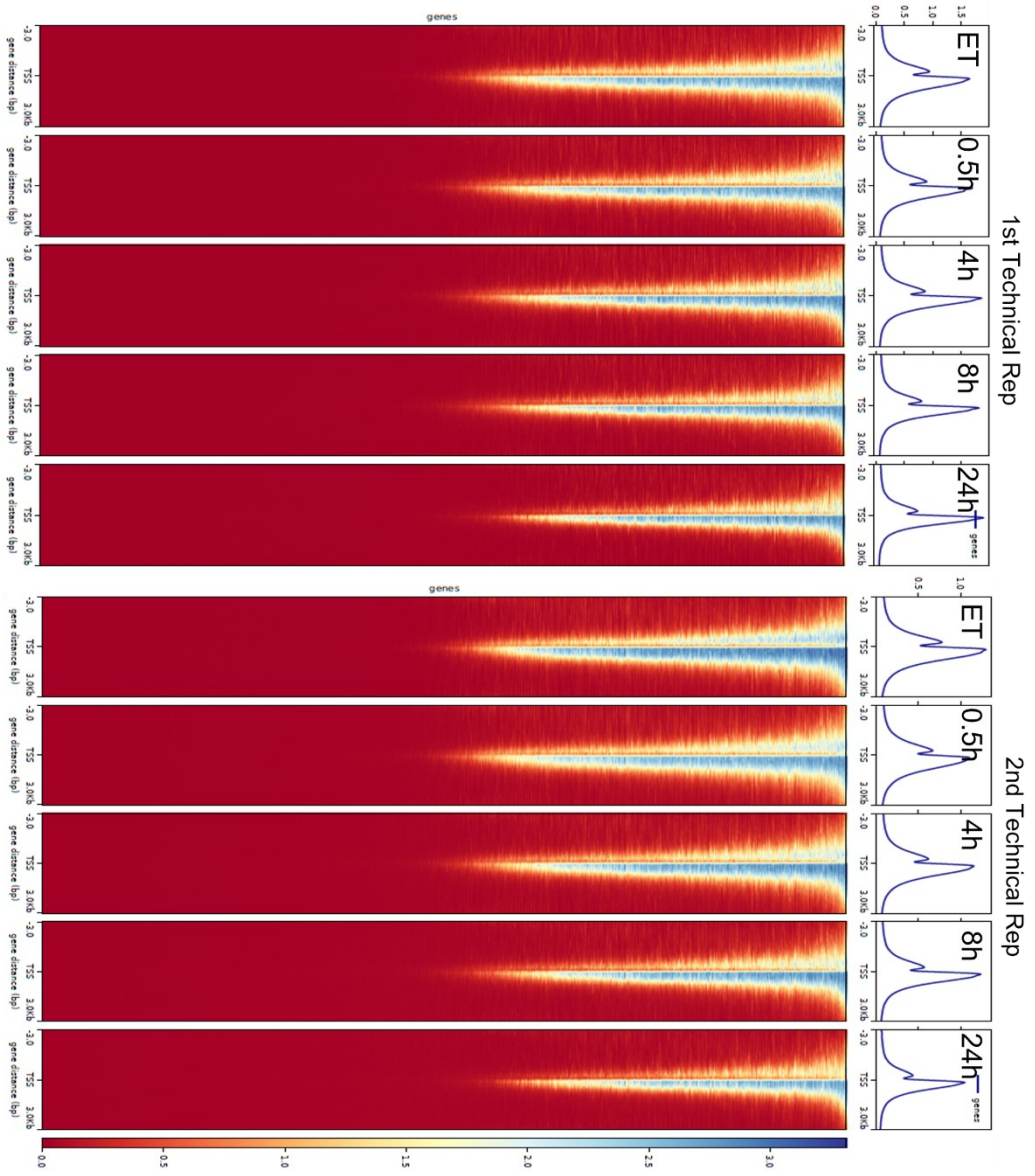

Figure S8: Loss of ASH2L Leads to Depletion of H3K4me3 at Promoter Regions. (A) ND10 cells were treated in a time-course manner with 100 nM dTAG-13 and subjected to chromatin immunoprecipitation using an H3K4me3 antibody, followed by sequencing (two technical replicates for each time point). The signal density, mapped against the mm9 reference genome, is represented as a heatmap around all mm9 transcripts in the figure. The distribution density is normalized between samples, demonstrating the signal within a 3 Kb window around the TSS regions of all genes.The experimental procedure was done by the author, with computational analysis curated by Dr. Mirna Barsoum.

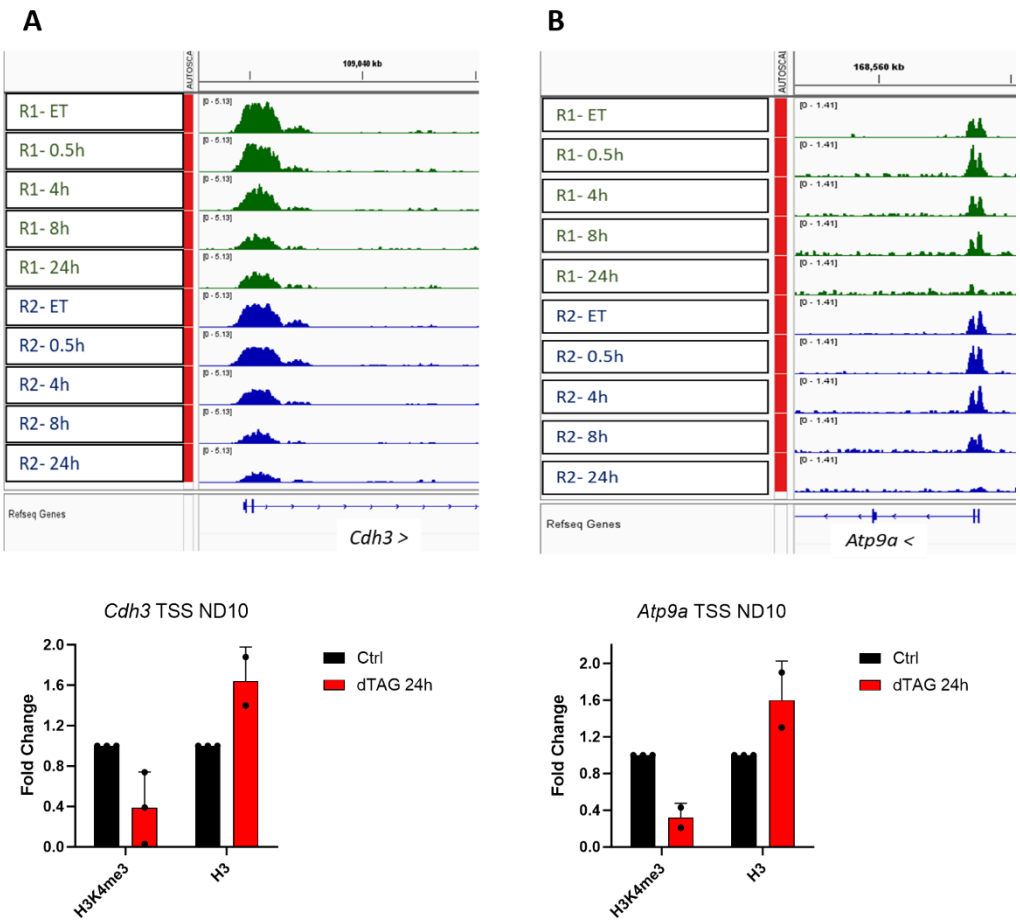

Figure S9: H3K4me3 and H3 are Deregulated at Promoter Regions in Response to ASH2L Loss. (A) The IGV genomic view depicts the H3K4me3 signal intensity from the BigWig files (group-scaled) for the ND10 H3K4me3-ChIPseq at 24h at the *Cdh3* TSS. Lower panel, ChIP-qPCR demonstrates the H3K4me3 and H3 enrichment level at the TSS of the *Cdh3* promoter after 24 hours of treatment with vehicle control and 100 nM dTAG-13. IgG enrichment was used as a background control (Not shown). Error bar shows the ±SEM for two replicates. (B) Same as panel B for *Atp8a* promoter. BigWig files are group-scaled. The experimental procedure of H3K4me3 and H3 ChIP-seq and ChIP-qPCR was done by the author. The computational analysis of the data was curated by Dr. Mirna Barsoum.

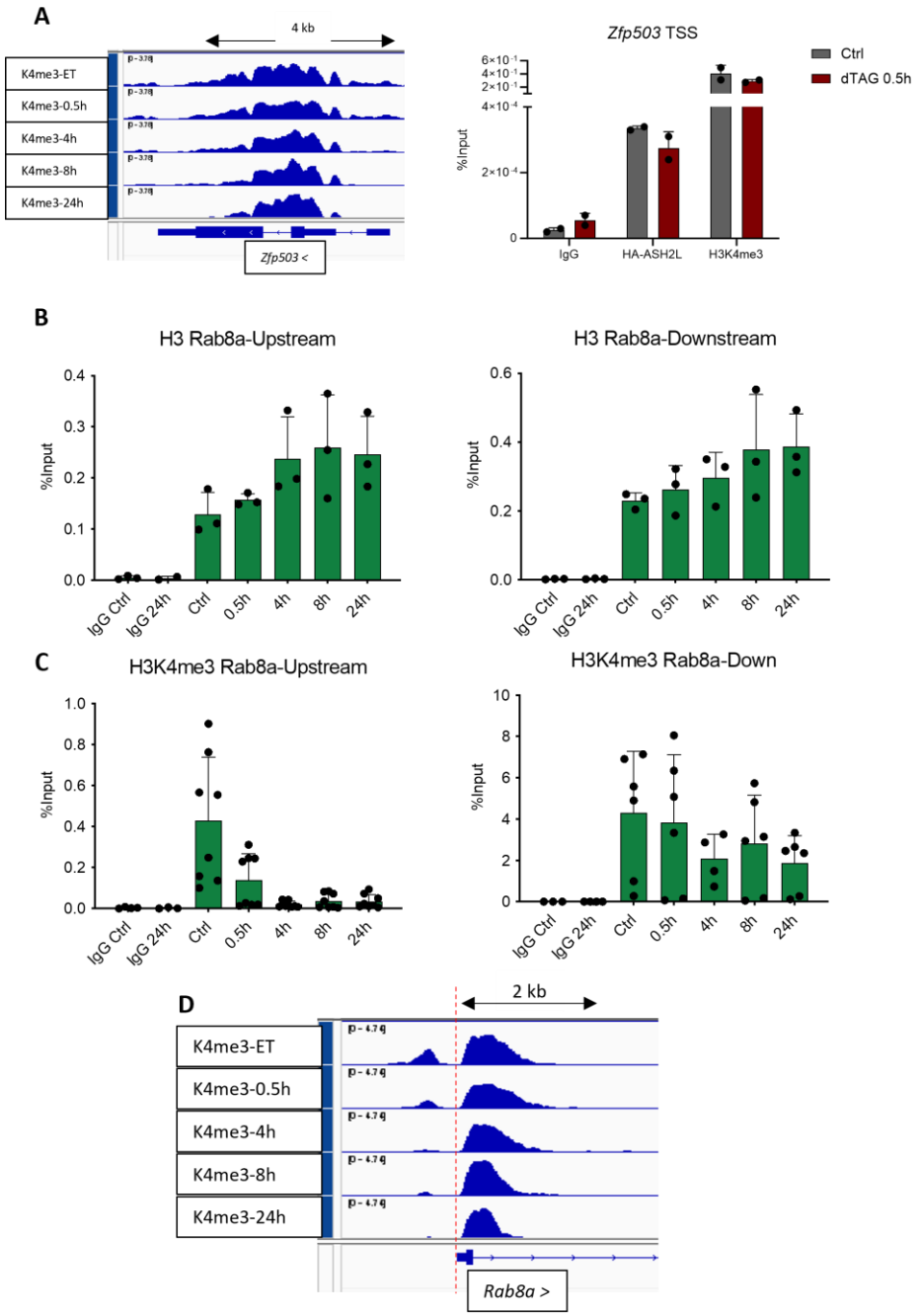

Figure S10: H3K4me3 Response to ASH2L Loss is Dependent on the Location Around TSS. (A) The IGV genomic view depicts the H3K4me3 signal intensity from the BigWig files (group-scaled) for the ND10 H3K4me3-ChIPseq at different time points at the *Zfp503* TSS. Right panel, ChIP-qPCR demonstrates the H3K4me3, H3, and HA-ASH2L enrichment level at the TSS of the *Zfp503* promoter after 0.5 hour of treatment with vehicle control and 100 nM dTAG-13. IgG enrichment was used as a background control. Error bar shows the ±SEM for two replicates. (B) ChIP-qPCR demonstrates the H3 enrichment level at the upstream and downstream of TSS of the *Rab8a* promoter in a time course treatment with vehicle control and 100 nM dTAG-13. IgG enrichment was used as a background control. Error bar shows the ±SEM for 3 replicates. (C) (B) ChIP-qPCR demonstrates the H3K4me3 enrichment level at the upstream and downstream of TSS of the *Rab8a* promoter in a time course treatment with vehicle control and 100 nM dTAG-13. IgG enrichment was used as a background control. Error bar shows the ±SEM for 4-7 replicates. (D) The genomic view depicts the H3K4me3 signal intensity from the BigWig files (group-scaled) for the ND10 H3K4me3-ChIPseq at different time points at the *Rab8a* TSS. H3K4me3, H3, and HA-ASH2L and ChIP-qPCR was done by the author. The computational analysis of the data was curated by Dr. Mirna Barsoum.

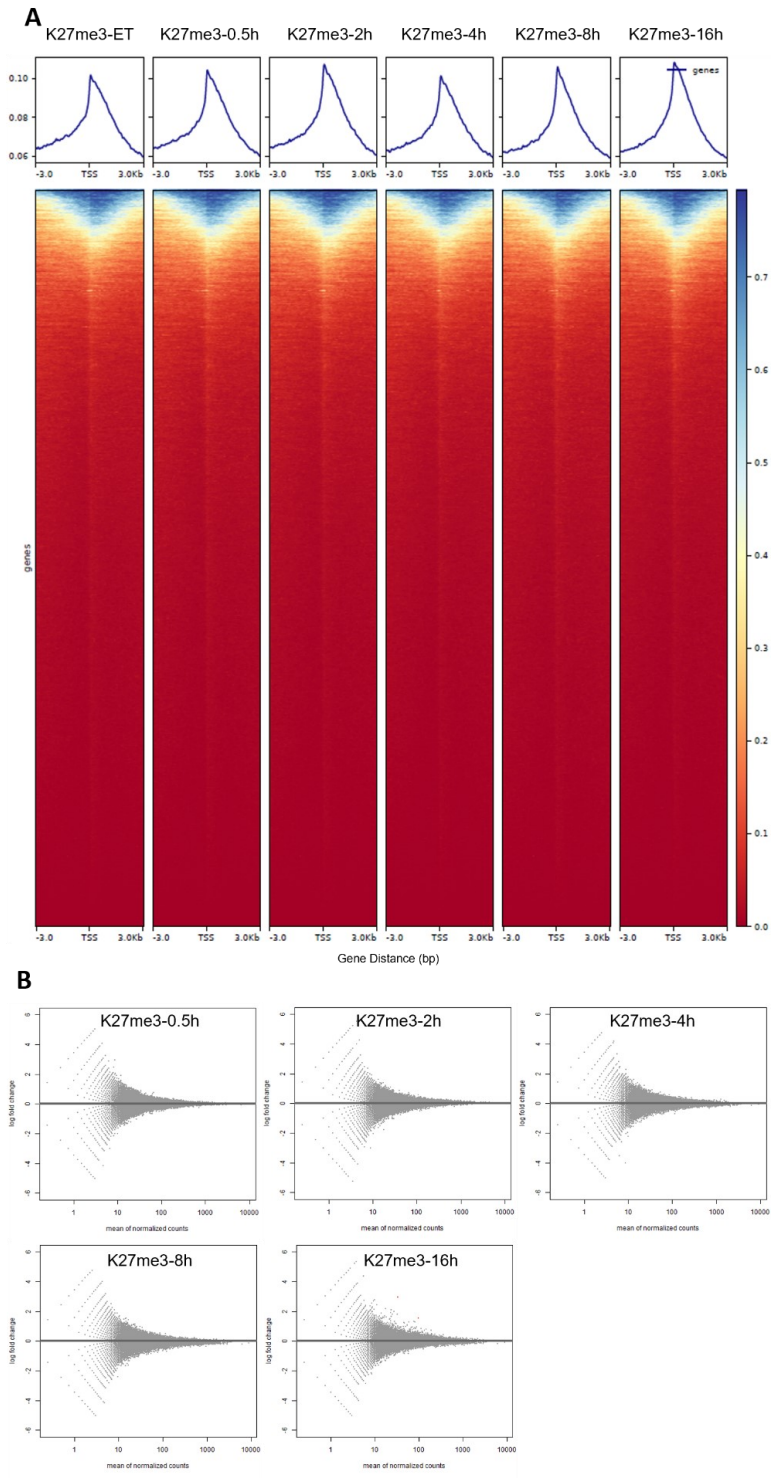

Figure S11: H3K27me3 ChIP-seq Attempt Resulted in Insufficient Sequencing Depth and Therefore Resolution. (A) NG3 cells were treated in a time-course manner with 100 nM dTAG-13 and subjected to chromatin immunoprecipitation using an H3K27me3 antibody, followed by sequencing (two technical replicates for each time point). The signal density, mapped against the mm9 reference genome, is represented as a heatmap around all mm9 transcripts in the figure. The distribution density is normalized between samples, demonstrating the signal within a 3 kb window around the TSS regions of all genes. (B) For the differential analysis performed on the deregulated peaks, an MA plot was generated (Y-axis: LogFC, X-axis: mean of normalized reads). Differential peaks meeting the parameters with FDR<0.05 are shown in red. The experimental procedure was done by the author, with computational analysis curated by Dr. Mirna Barsoum.

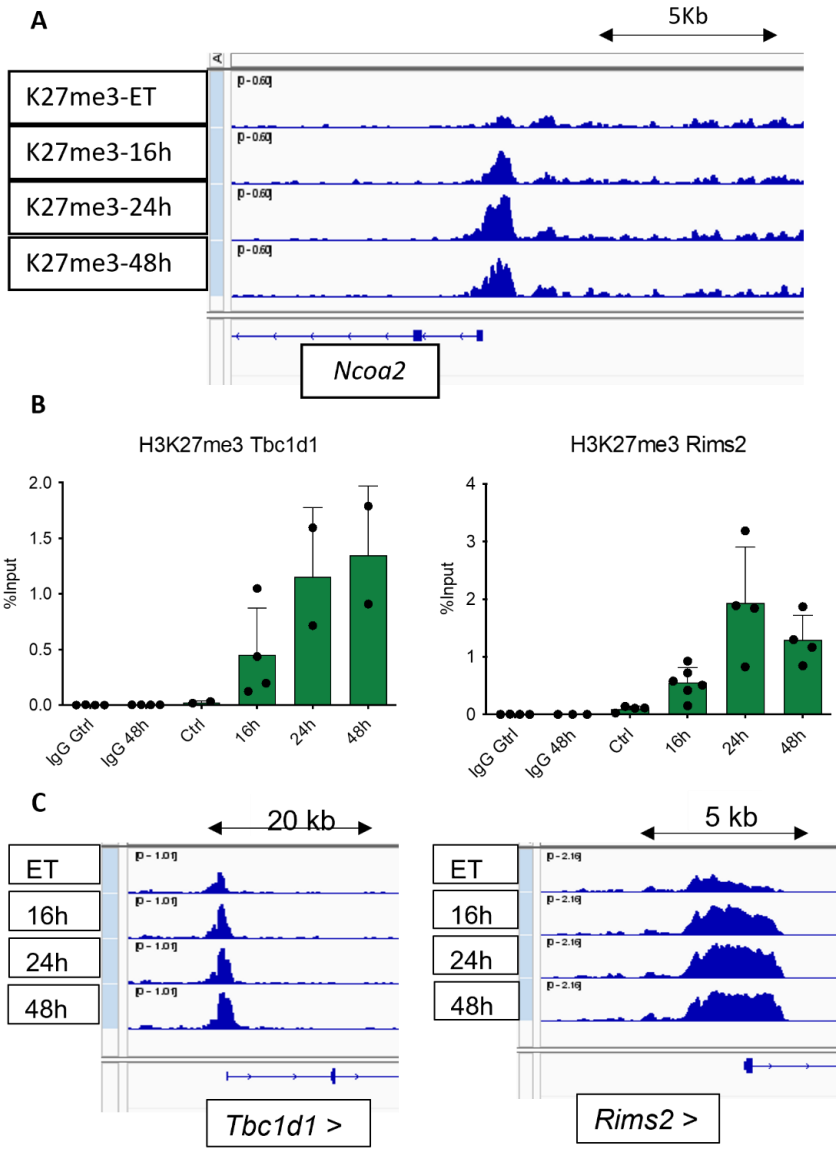

Figure S12: H3K27me3 is Accumulated d at Promoter Regions in Response to ASH2L Loss. (A) The IGV genomic view depicts the H3K27me3 signal intensity from the BigWig files (group-scaled) for the NG3 H3K27me3-ChIPseq at 16h, 24h, and 48h at the *Ncoa2* TSS. (B) ChIP-qPCR demonstrates the H3K27me3 enrichment level at the TSS of the *Tbc1d1* and *Rims2* promoters at different time points of treatment with vehicle control and 100 nM dTAG-13. IgG enrichment was used as a background control. Error bar shows the ±SEM for 2-6 replicates. (C) The IGV genomic view depicts the H3K27me3 signal intensity from the BigWig files (group-scaled) for the NG3 H3K27me3-ChIPseq at 16h, 24h, and 48h at the *Tbc1d1* and *Rims2* TSS. The experimental procedure of H3K27me3 ChIP-seq and ChIP-qPCR was done by the author. The computational analysis of the data was curated by Dr. Mirna Barsoum.

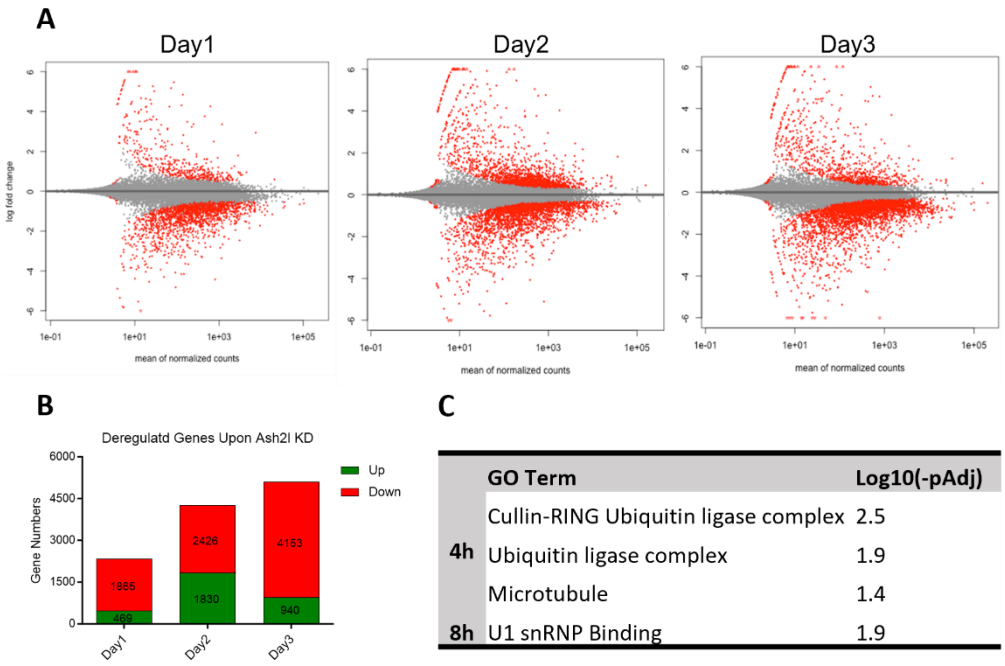

C

	GO Term	Log10(-pAdj)
4h	Cullin-RING Ubiquitin ligase complex	2.5
	Ubiquitin ligase complex	1.9
	Microtubule	1.4
8h	U1 snRNP Binding	1.9

Figure S13: Loss of ASH2L Results in RNA Transcriptional Deregulation. (A) NG3 cells treated with 100 nM dTAG-13 for 24h, 48h, and 72h were subjected to RNA-seq (three technical replicates for each time point). For the differential analysis performed on the deregulated genes, an MA plot was generated (Y-axis: Log2FC, X-axis: mean of normalized counts). Differentially expressed genes meeting the parameters |Log2FC|>0.58 and FDR<0.05 are shown in red. (B) The number of significantly deregulated genes at each time points were plotted. (C) A GO analysis performed by gProfiler2, for significantly down regulated genes obtained from Click-seq, demonstrating the molecular terms associated with the deregulated genes. The experimental procedure of RNA-seq was conducted by Alexander Stenzel, with computational analysis, differential analysis, and annotation curated by Dr. Mirna Barsoum. The GO term analysis was done by Author.

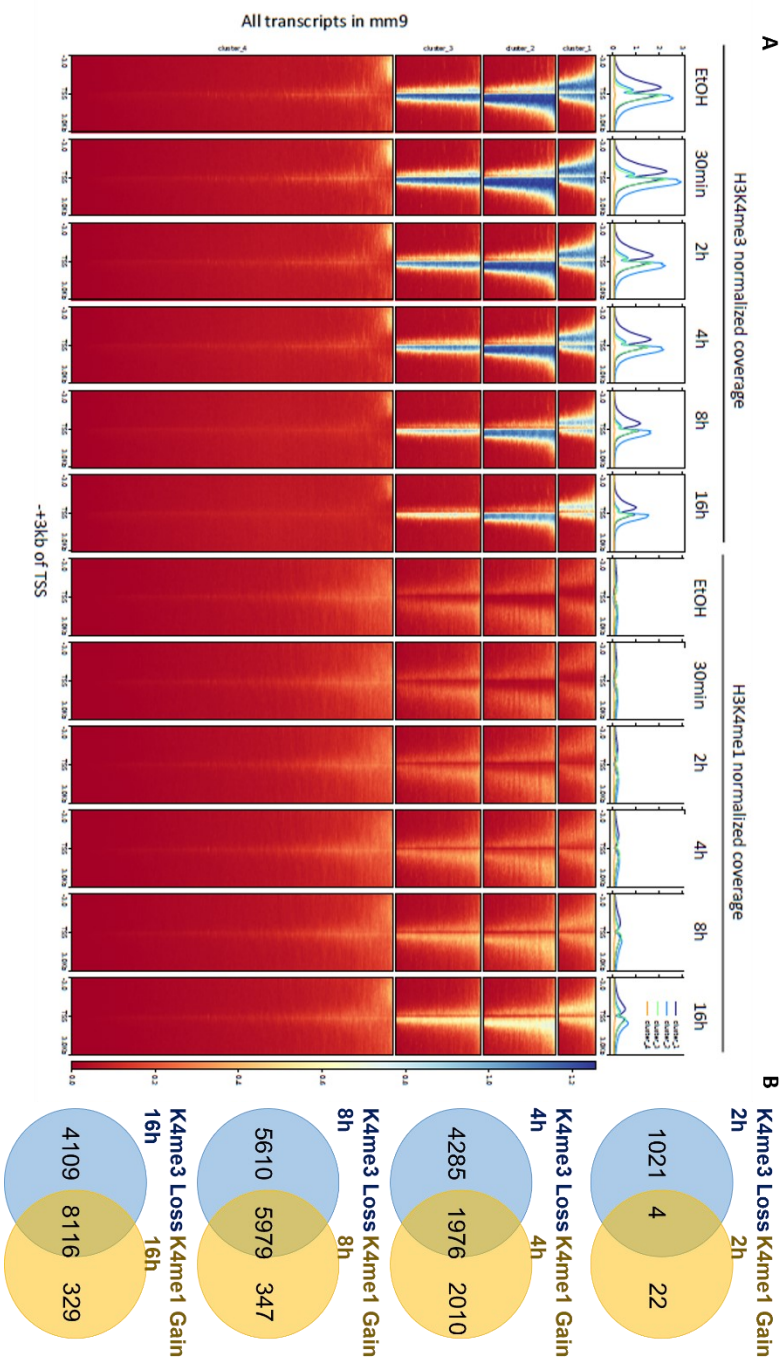

Figure S14: **H3K4me1 Accumulation is Potentially a Result of H3K4me3 Loss at Promoters**. (A) NG3 cells were treated in a time-course manner with 100 nM dTAG-13 and subjected to chromatin immunoprecipitation using an H3K4me3 and H3K4me1 antibody, followed by sequencing (two technical replicates for each time point). The signal density, mapped against the mm9 reference genome, is represented as a heatmap around all mm9 transcripts in the figure. The distribution density is normalized between samples, demonstrating the signal within a 3 kb window around the TSS regions of all genes. The signal density was clustered based on K-means for different transcripts in mm9 reference genome (B) The differential peaks meeting the parameters |LogFC|>0.58 and FDR<0.05 were annotated to gene promoters. An intersection was ran between the significant-deregulated promoter and the overlap was demonstrated by Venn diagram. The experimental procedure, and the intersection analysis was done by the author, with computational analysis curated by Dr. Mirna Barsoum.

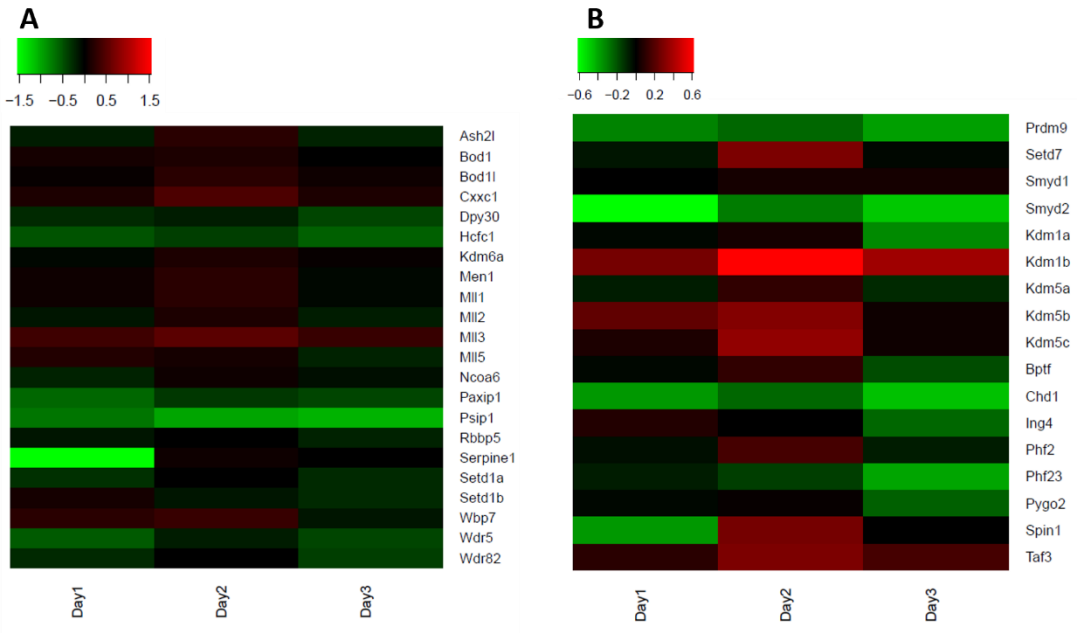

Figure S15: The Transcription of KMT2 Components and H3K4me3 Readers and Writers, does not Exhibit a Prominent Alteration. (A) A heatmap plot generated from Log2FC values extracted from differential gene expression analysis for the genes involved in COMPASS complex. The plots were drawn using gplots data visualization package through R Studio interface. (B) A heatmap plot generated from Log2FC values extracted from differential gene expression analysis for the genes involved in H3K4me3 deposition, erasing and reading. The plots were drawn using gplots data visualization package through R Studio interface. The experimental procedure was done by Alexander Stenzel, and the heatmap generation was done by the author, with computational analysis curated by Dr. Mirna Barsoum.

Figure S16: The Deregulation of Histone PTMs is Associated with RNA Transcription Level at Later Time points. (A) An intersection analysis between the significantly downregulated RNA at 24h, 48h, and 72h (Log2FC<-0.58, FDR<0.05) obtained from RNA-seq experiment performed by Alexander Stenzel was performed with significant (Log2FC<-58, FDR<0.05) H3K4me3-depleted promoters at 16h obtained from ChIP-seq experiment in NG3. The overlap was based on gene name and showed in Venn diagrams. (B) An intersection analysis between the significantly downregulated RNA at 24h, 48h, and 72h (Log2FC<-0.58, FDR<0.05) obtained from RNA-seq experiment performed by Alexander Stenzel was performed with significant (Log2FC<-0.58, FDR<0.05) H3K27ac-depleted promoters at 16h obtained from ChIP-seq experiment in NG3. The overlap was based on gene name and showed in Venn diagrams. (C) An intersection analysis between the significantly downregulated RNA at 24h, 48h, and 72h (Log2FC<-0.58, FDR<0.05) obtained from RNA-seq experiment performed by Alexander Stenzel was performed with significant (Log2FC<58, FDR<0.05) H3K27me3-elevated promoters at 16h obtained from ChIP-seq experiment in NG3. The overlap was based on gene name and showed in Venn diagrams. The experimental procedure of Histone PTM ChIP-seq, and the intersection analysis was done by the author. The RNA-seq experiment was done by Alexander Stenzel, with computational analysis of all NGS data curated by Dr. Mirna Barsoum.

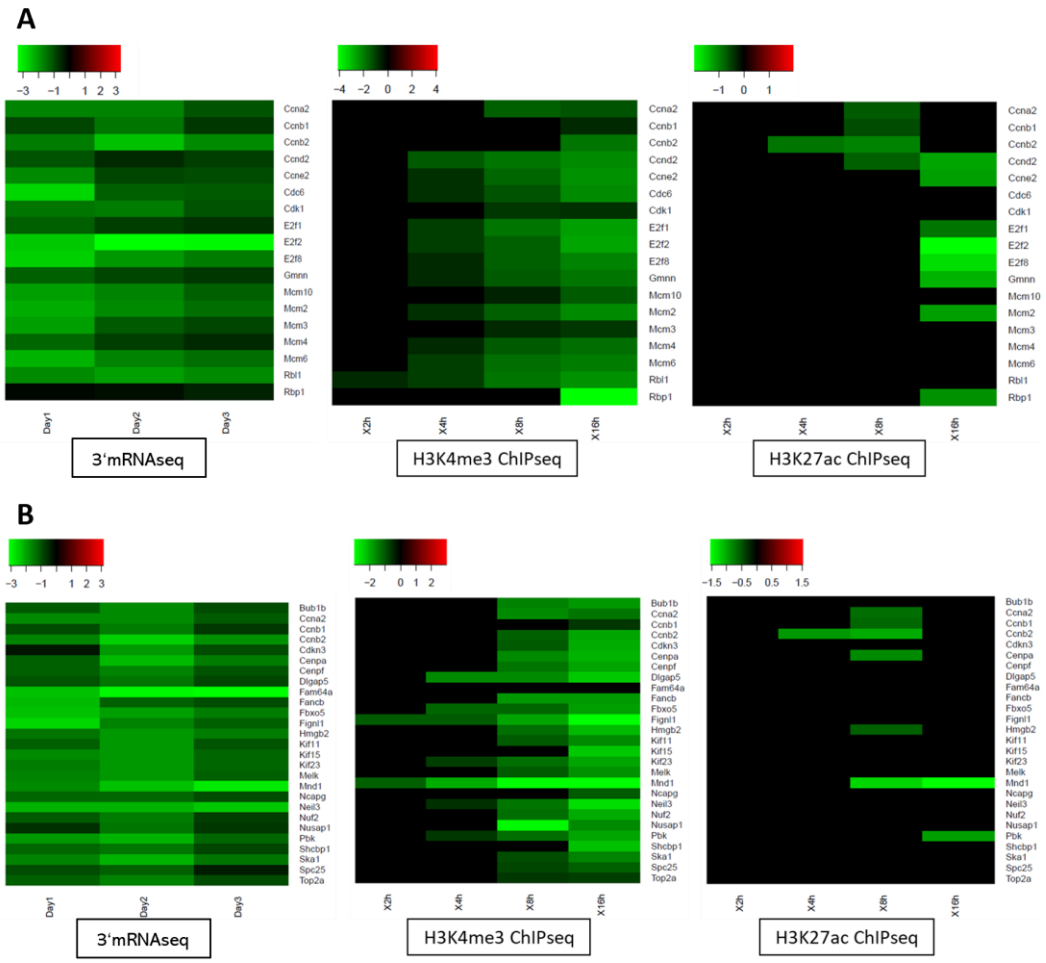

Figure S17: The Transcription Deregulation of Different Set of Genes is Associated with H3k4me3 and H3K27ac Signal Status at Their Promoters. (A) A heatmap plot (left) generated from Log2FC values extracted from differential gene expression analysis for the genes involved in cell cycle regulation. A heatmap plot (middle) generated from Log2FC values extracted from significantly deregulated H3K4me3 peaks at 3Kb window of TSS of the corresponding genes. A heatmap plot (right) generated from Log2FC values extracted from significantly deregulated H3K27ac peaks at 3Kb window of TSS of the corresponding genes. The plots were drawn using gplots data visualization package through R Studio interface. (B) A heatmap plot (left) generated from Log2FC values extracted from differential gene expression analysis for the genes involved in senescence (M genes). A heatmap plot (middle) generated from Log2FC values extracted from significantly deregulated H3K4me3 peaks at 3Kb window of TSS of the corresponding genes. A heatmap plot (right) generated from Log2FC values extracted from significantly deregulated H3K27ac peaks at 3Kb window of TSS of the corresponding genes. The plots were drawn using gplots data visualization package through R Studio interface. The experimental procedure of RNA-seq was done by Alexander Stenzel. The H3K4me3 and H3K27ac ChIP-seq experimental work, plus the heatmap generation was done by the author. All the computational analysis was curated by Dr. Mirna Barsoum.

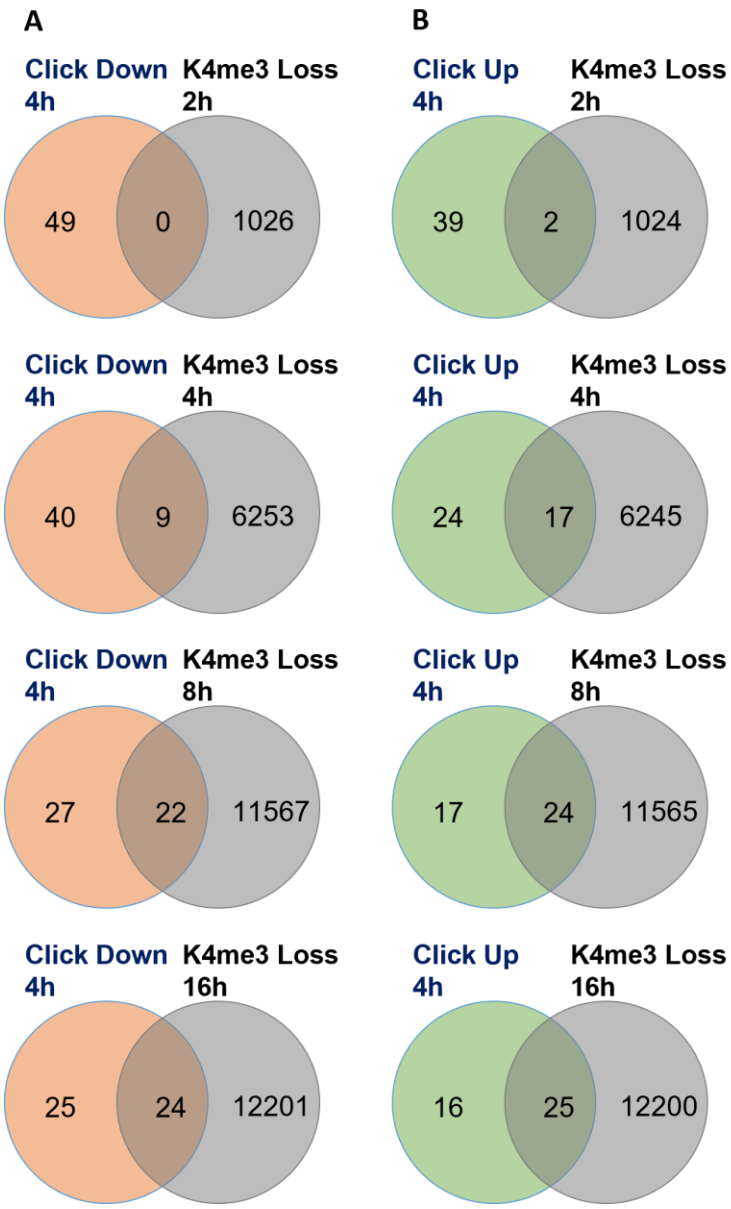

Figure S18: The Loss of H3K4me3 Does Not Seem to be the Driver of Loss of Transcription of Deregulated Nascent RNAs. (A) An intersection analysis between the significantly downregulated nascent RNA at 4h (Log2FC<-0.58, FDR<0.05) obtained from Click-seq experiment was performed with H3K4me3-depleted promoters obtained from ChIP-seq experiment in NG3. The overlap was based on gene name and showed in Venn diagrams. (B) An intersection analysis between the significantly upregulated nascent RNA at 4h (Log2FC>0.58, FDR<0.05) obtained from Click-seq experiment was performed with H3K4me3-depleted promoters obtained from ChIP-seq experiment in NG3. The overlap was based on gene name and showed in Venn diagrams. The experimental procedure, and the intersection analysis was done by the author, with computational analysis curated by Dr. Mirna Barsoum.

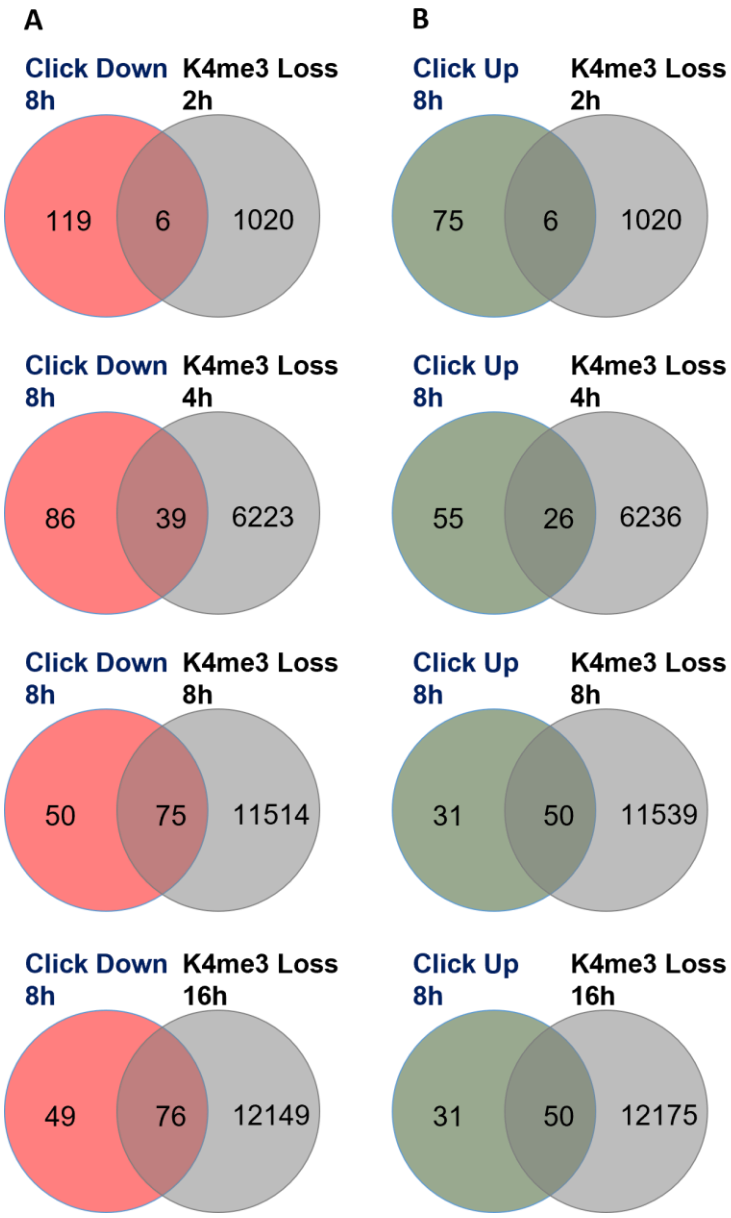

Figure S19: The Loss of H3K4me3 Does Not Seem to be the Driver of Loss of Transcription of Deregulated Nascent RNAs. (A) An intersection analysis between the significantly downregulated nascent RNA at 8h (Log2FC<-0.58, FDR<0.05) obtained from Click-seq experiment was performed with H3K4me3-depleted promoters obtained from ChIP-seq experiment in NG3. The overlap was based on gene name and showed in Venn diagrams. (B) An intersection analysis between the significantly upregulated nascent RNA at 8h (Log2FC>0.58, FDR<0.05) obtained from Click-seq experiment was performed with H3K4me3-depleted promoters obtained from ChIP-seq experiment in NG3. The overlap was based on gene name and showed in Venn diagrams. The experimental procedure, and the intersection analysis was done by the author, with computational analysis curated by Dr. Mirna Barsoum.

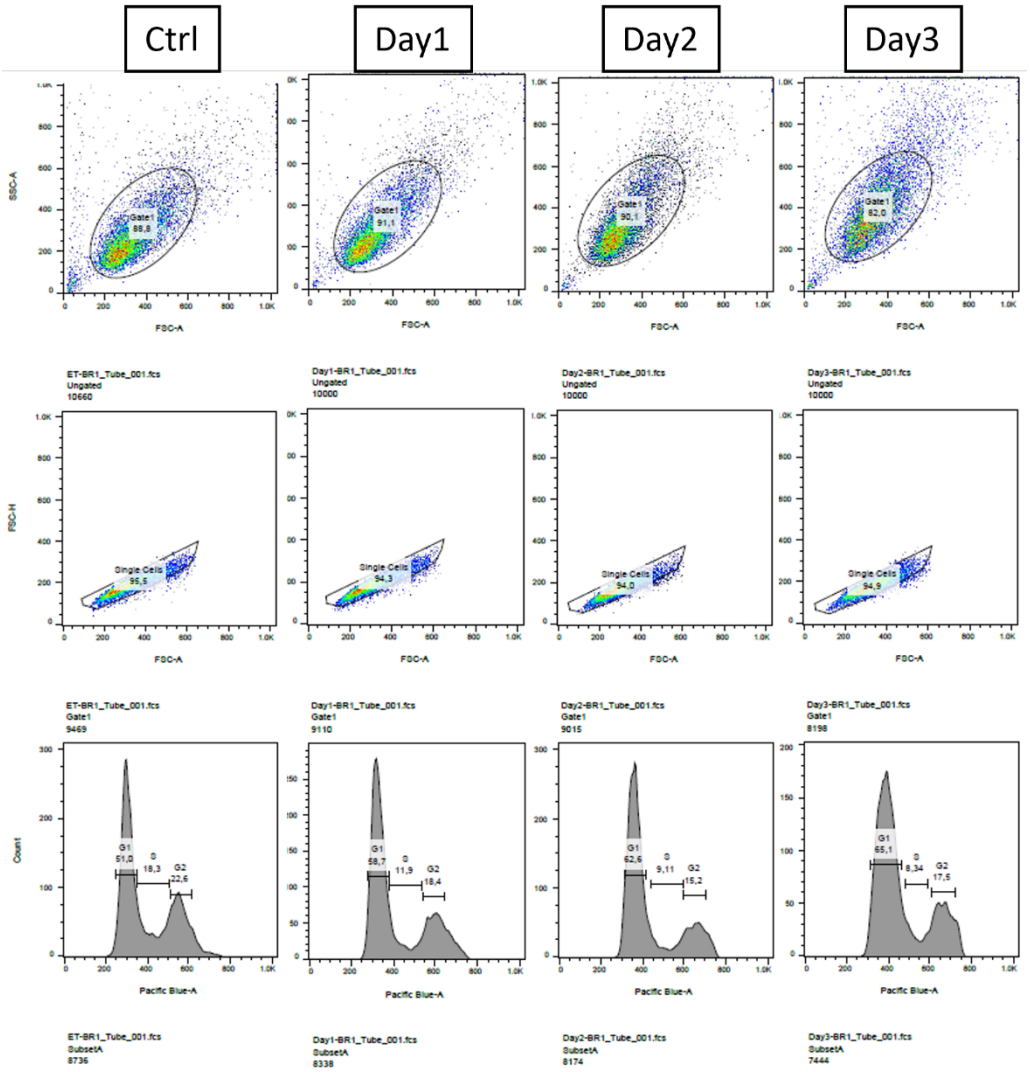

Appendix 1: Flowcytometery plots extracted from FlowJo. Support for cell phase analysis demonstrated in Figure 4B.

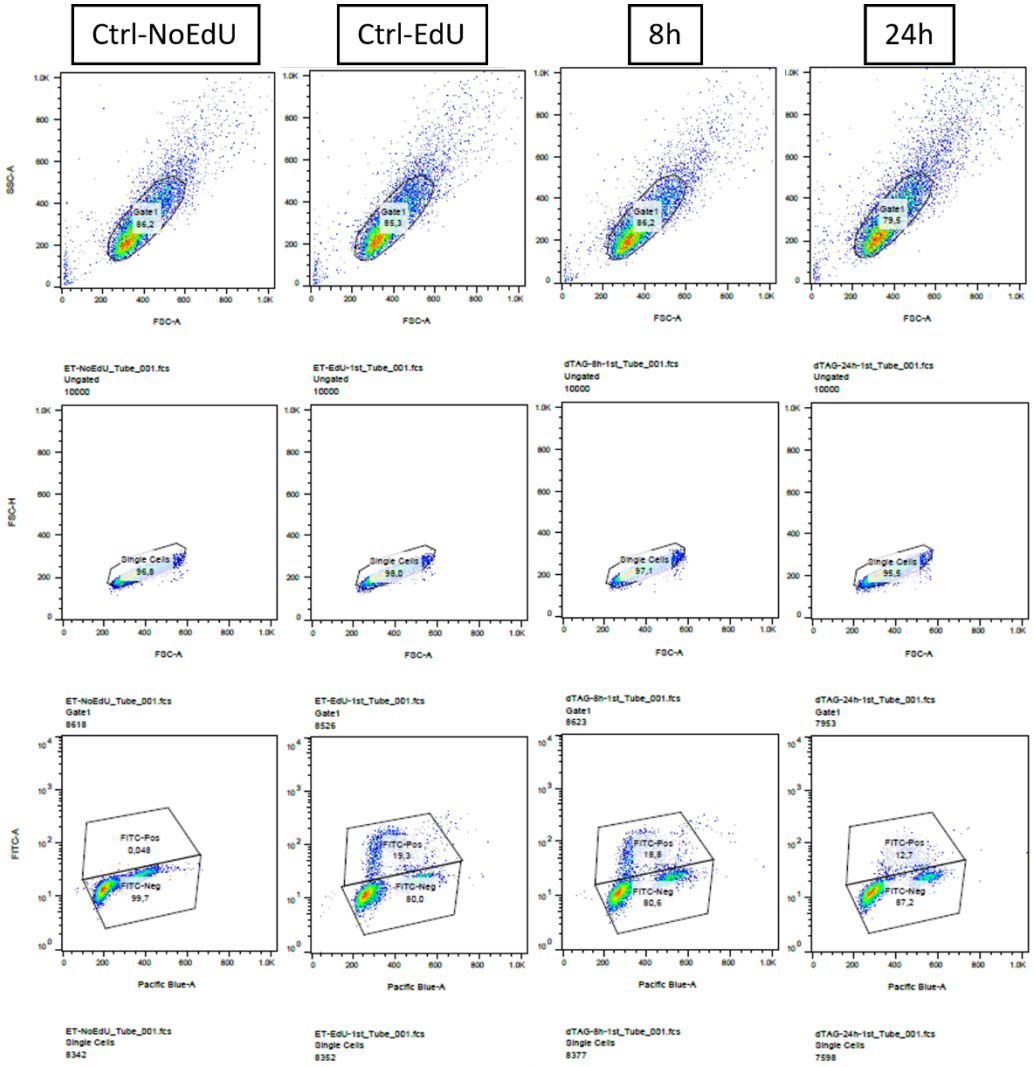

Appendix 2: Flowcytometery plots extracted from FlowJo. Support for DNA synthesis analysis demonstrated in Figure 4C.

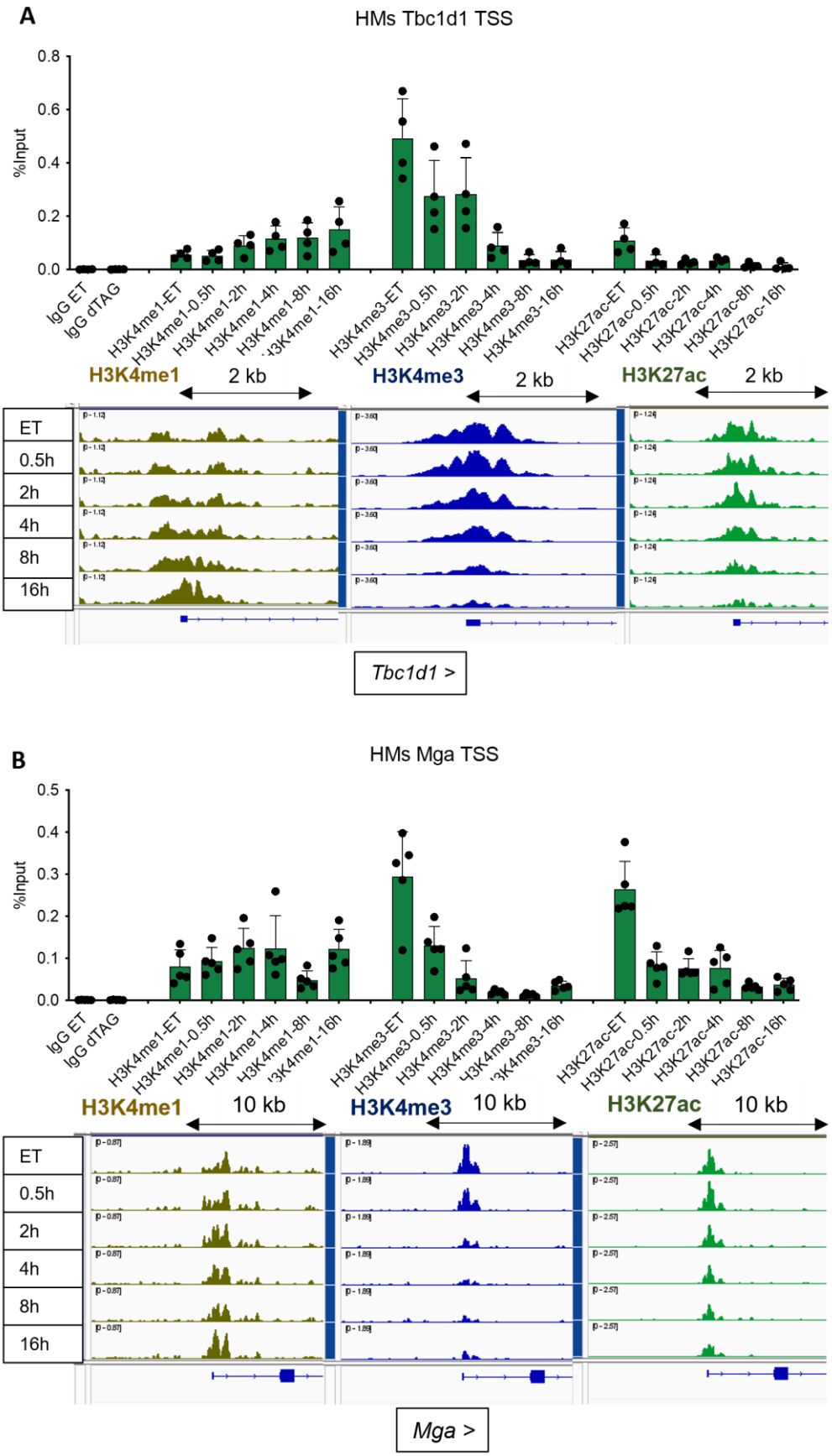

Appendix 3: Confirmatory ChIP-qPCR for the performed ChIP-seq experiments in NG3 cells. Performed a TSS regions. Error bars indicate ±SEM for 4-6 replicates.

6.2 Supplementary Tables

Online Attachment.

6.3 List of Abbreviations

Abbreviations	Description
5-EdU	5-ethynyl-2'-deoxyuridine
5hmC	5-hydroxymethylcytosine
AEBP2	AE binding protein 2
ASH2L	Absent, small, or homeotic 2-like
ATAC	Assay for transposase-accessible chromatin with sequencing
BAF	BRG1/BRM-associated factor
BAH	Bromo-adjacent homology
BAHD1	Bromo adjacent homology domain-containing protein 1
BPTF	Bromodomain PHD finger transcription factor
BRD4	Bromodomain-containing protein 4
CBP	CREB-binding protein
Cbx7	Chromobox protein homolog 7
Cbx8	Chromobox protein homolog 8
CFP1	CpG-binding CXXC zinc finger protein 1
CGI	CpG-rich islands
CHD1	Chromodomain helicase dna binding protein 1
ChIP	Chromatin immunoprecipitation
ChIP-seq	Chromatin immunoprecipitation sequencing
Click-seq	Click nascnet RNA sequencing
COMPASS	Complex proteins associated with set1
CoREST	Co-repressor of repressor element-1 silencing transcription
CRBN	Cereblon
CRL	Cullin-RING ligase
CTD	C-terminal domain
DMEM	Dulbecco’s modified eagle medium
DNMT	DNA methyltransferases
EBS	Early bolting in short day
EGR1	Early growth response protein 1
EHMT2	Euchromatic histone-lysine N-methyltransferase 2
EMF1	Embryonic flower 1
ER	Endoplasmic reticulum
ERCC	External rna control consortium
ESC	Embryonic stem cells
EZH2	Enhancer of zeste homolog 2
FACS	Fluorescence-activated cell sorting
FBS	Fetal bovine serum
FDR	False discovery rate
FKBP	Fk506-binding protein
GNAT	GCN5-related n acetyltransferases
GO	Gene ontology
GW	Genome-wide

H3K4me	Histone 3 lysine 4 methylation
HAT	Histone acetyl transferase
HDAC	Histone deacetylase
HECT	Homologous to the e6ap carboxyl terminus
HMT	Histone methyltransferase
HOT	4-hydroxytamoxifen
IDR	Intrinsically disordered regions
iMEF	Immortalized mouse embryonic fibroblasts
IMiDs	Immunomodulatory imide drugs
ING2	Inhibitor of growth family member 2
INTS11	Integrator complex subunit 11
ISWI	Imitation switch
JARID1	Jumonji at-rich interactive domain-1
JMJD3	Jumonji domain-containing protein-3
KAT	Lysine acetyltransferases
KD	Knock down
KDM	Lysine demethylases
KMT2	Lysine methyltransferase 2
KO	Knock out
LB	Luria-bertani
Log2FC	Log2 fold change
LSD1	Lysine-specific histone demethylase 1a
MAPJD	Ribosomal oxygenase 1-No66, Riox1
MBT	Malignant brain tumor
MEF	Mouse embryonic fibroblasts
mESC	Mouse embryonic stem cells
MLL	Mixed-lineage leukemia
MORC	Microrchidia family of proteins
NFR	Nucleosome-free region
NGS	Next generation sequencing
NSD1	Nuclear receptor-binding set domain protein 1
NURF	Nucleosome-remodeling factor
OD	Optical density
OSN	Oct4, Sox2 and Nanog
PBS	Phosphate buffered saline
PcG	Polycomb group of proteins
PFA	Paraformaldehyde
PHD	Plant homoedomain
PHF2	PHD finger protein 2
PHF8	PHD finger protein 8
PIC	Preinitiation complex
PNUTS/PP1	Phosphatase 1 nuclear targeting subunit
POI	Protein of interest
PRC2	Polycomb repressor complex 2
PROTAC	Proteolysis targeting chimera
PTM	Histone post-translational modifications
PWM	Position weight matrix
qPCR	Quantitative polymerase chain reaction

RBBP5	Retinoblastoma-binding protein 5
RBR	RING-between-RING
RING	Really interesting new gene
RNA Pol II	RNA polymerase II
RNAi	RNA interfrence
RPM	Round per minute
SAGA	Spt-Ada-Gcn5 acetyltransferase
SDI	Sdc1 DPY30 interaction
SDS-PAGE	Sodium dodecyl-sulfate poly-acrylamide gel electrophoresis
SET3C	SET domain-containing protein 3
SGF29	SAGA complex associated factor 29
SHL	Short life
Shld1	Shield-1
SOB	Super optimal broth
SOC	SOB with catabolite repression
SPRY	Spla and the ryanodine receptor
SWI/SNF	SWItch/Sucrose Non-Fermentable
TAD	Transcactivation domain
TAF3	TATA-box binding protein associated factor 3
TET1	TET methylcytosine dioxygenase 1
TF	Transcription factor
TPD	Targeted protein degredation
TrxG	Trithorax-group proteins
TSS	Transcription start sites
Ub	Ubiquitin protein
UPS	Ubiquitin-proteasome system
WDR5	WD repeat-containing protein 5
WDR82	WD repeat-containing protein 82
WH	Winged helix domain
WT	Wild-type

6.4 List of Figures

6.5 List of Tables

6.6 Curriculum Vitae

Personal Information

Surname, name	Sayadi Boroujeni, Roksaneh
LinkedIn	www.linkedin.com/in/roksanehsayadi

Education

05.2020- 06.2023	Ph.D. Studies_ Biology Institute of Biochemistry, RWTH Aachen University Supervisors: Prof. Bernhard Lüscher & Prof. Ivan Costa Thesis Title: "Exploring Cellular and Molecular Consequences of PROTAC-Mediated Epigenetic Regulation in Mouse Embryo Fibroblast Cells"
09.2014- 07.2017	M.Sc. Studies_ Biology- Molecular Genetics Departments of Genetics, Shahre'kord University Thesis Title: "Design and Cloning of a DNA-Vaccine for Prevention of Viral Hemorrhagic Septicemia (VHS) Disease Using Saccharomyces cerevisiae"
09.2010- 07.2014	B.Sc. Studies_ Biology- Biotechnology Department of Chemistry, Kashan University Thesis Title: "Synthesize of Biocompatible and Biodegradable Poly-Lactic co Glycolic acid copolymerized with Vitamin D"
09.2006- 07.2010	High School Diploma- Mathematics and Physics

Professional Experience

12.2023- Present	Co-leader_ Global Postdoc Community (EMERGE), Bayer AG
06.2023- Present	Postdoctoral Associate- Molecular Biologist Resistance Management, Crop Science, Bayer AG Supervisor: Distinguished Fellow Dr. Ralf Nauen
09.2019- 12.2019	Research Assistant- Biology University of Würzburg
08.2019- 03.2019	Lab Assistant- Molecular Geneticist Emad Pathobiology Diagnostic Lab

6.7 Scientific Contributions

Barsoum M.*, **Sayadi-Boroujeni R.***, Stenzel A. T., Bussmann P., Lüscher-Firzlaff J., Lüscher B. (2023) Sequential deregulation of histone marks, chromatin accessibility and gene expression in response to PROTAC-induced degradation of ASH2L. Scientific Reports 13(1), 22565.

Bochyńska A.*, Stenzel A. T.*, **Sayadi-Boroujeni R.***, Kuo C.-C., Barsoum M., Liang W., Bussmann P., Costa I. G., Lüscher-Firzlaff J., & Lüscher B. (2022). Induction of senescence upon loss of the Ash2l core subunit of H3K4 methyltransferase complexes. Nucleic Acids Research, 50(14), 7889-7905.

Barsoum M.*, Stenzel A.T.*, Bochynska A.*, Kuo C.-C.*, **Sayadi-Boroujeni R.**, Bussmann P., Lüscher-Firzlaff J., Costa I. G., Lüscher B. (2022). Loss of the Ash2l subunit of H3K4 methyltransferase complexes promotes chromtin compaction at promoters, Scientific Reports 12(1), 21506.

Sayadi Boroujeni, R., Papizadeh, M., Talebi, M., & Pourshafie, M. R. (2019). Simultaneous Comparison of Serological and Molecular Results of HBV Test in Patients Referring to the Pathobiology Laboratory. Infection Epidemiology and Microbiology, 5(2), 53-58.

6.8 Eidesstattliche Erklärung

Declaration of Authorship

I, Roksaneh Sayadi Boroujeni, declare that this thesis and the work presented in it are my own and has been generated by me as the result of my own original research. Hiermit erkläre ich an Eides statt / I do solemnely swear that:

1. This work was done wholly or mainly while in candidature for the doctoral degree at this faculty and university;

2. Where any part of this thesis has previously been submitted for a degree or any other qualification at this university or any other institution, this has been clearly stated;

3. Where I have consulted the published work of others or myself, this is always clearly attributed;

4. Where I have quoted from the work of others or myself, the source is always given. This thesis is entirely my own work, with the exception of such quotations;

5. I have acknowledged all major sources of assistance;

6. Where the thesis is based on work done by myself jointly with others, I have made clear exactly what was done by others and what I have contributed myself;

7. Parts of this work have been published before as:

Barsoum M.*, **Sayadi-Boroujeni R.***, Stenzel A. T., Bussmann P., Lüscher-Firzlaff J., Lüscher B. (2023) Sequential deregulation of histone marks, chromatin accessibility and gene expression in response to PROTAC-induced degradation of ASH2L. Scientific Reports 13(1), 22565.

Bochyńska A.*, Stenzel A. T.*, **Sayadi-Boroujeni R.***, Kuo C.-C., Barsoum M., Liang W., Bussmann P., Costa I. G., Lüscher-Firzlaff J., & Lüscher B. (2022). Induction of senescence upon loss of the Ash2l core subunit of H3K4 methyltransferase complexes. Nucleic Acids Research, 50(14), 7889-7905.

Barsoum M.*, Stenzel A.T.*, Bochynska A.*, Kuo C.-C.*, **Sayadi-Boroujeni R.**, Bussmann P., Lüscher-Firzlaff J., Costa I. G., Lüscher B. (2022). Loss of the Ash2l subunit of H3K4 methyltransferase complexes promotes chromtin compaction at promoters, Scientific Reports 12(1), 21506.

*Authors contributed equally as a first author

Monheim am Rhein, 2024.11.20

Roksaneh Sayadi Boroujeni

6.9 Acknowledgment/Danksagung

When it is time to say thank you, so many faces come to mind. Some I am grateful to for samples and help with experiments, and others I am grateful to for the many life lessons they have taught me.

First and foremost, I would like to thank my dad and mom, who kept their worries in their hearts and warmly sent me thousands of kilometers away to pursue my childhood dream. No words, sentences, or text will ever be enough to express how much I owe them and how much I love them.

Second, I want to truly thank Bernhard Lüscher, my doctoral supervisor, who became like a father to me during the difficult times of my immigration to Germany. He never stopped supporting me in so many aspects of life. I consider myself lucky to have had the chance to come to another country and have Bernhard as my PhD project supervisor, guide, and inspiration for many life lessons.

I would also like to thank Juliane Lüscher for her warm demeanor, support with experimental issues, and patience in helping me understand the topic and improve my English.

I want to thank Mirna Barsoum, who was initially a great colleague and became like an older sister to me. She comforted me during very difficult moments, and I could trust her and cry on her shoulder. These are the most valuable memories from my time with the ASH team, that I will never forget.

I am grateful to Alexander Stenzel for being an intelligent and supportive colleague. I learned a lot from him, gaining different perspectives on scientific and non-scientific subjects.

I would also like to thank Philip Bussmann, who initially seemed like a serious technician but later warmly supported me.

The ASH team may never be replicated in my life, but I have learned a lot and will take these lessons with me to create a similar atmosphere in my future career.

Of course, I have not forgotten to thank all the smiling faces and helpful older and newer colleagues at the Institute of Biochemistry. I spent three years of my 30-year life with them, which was one-tenth of my lifetime at the time.

I also want to thank Ivan Costa for agreeing to be my second supervisor and providing different insights on my PhD project. Additionally, I would like to thank Ivan's lab for their great cooperation in previous collaborations.

A very big thank you to the IZKF team, who I enjoyed working with so much and who unconditionally supported my sequencing experiments.

I want to thank my friends in Aachen, who have become like a family to me and with whom I found a second home for myself in Germany.

I also want to thank my leader at Bayer, Ralf Nauen, who genuinely supported and encouraged me to do all my best to graduate from PhD studies, along with the amazing team I am working with.

Last but not least, I want to thank all the challenges I have faced, and even the people who caused these challenges, as they have contributed to making me the person I am today and feeling happy about my life so far.

I wish all of us to feel safe, happy, and successful, and to be as kind to each other as we can in our one chance of a lifetime.